THEORETICAL AND EXPERIMENTAL INVESTIGATION OF VIBRATION DAMPING BY VORTICITY PRODUCTION

M. S. Howe
Boston University, College of Engineering
110 Cummington Street, Boston MA 02215

1 July, 1998

Report AM-98-029

REPORT DOCUMENTATION PAGE

AFRL-SR-BL-TR-98-
0572

1. AGENCY USE ONLY (Leave blank)	2. REPORT DATE	3. REPORT TYPE AND DATES COVERED
	1 July 1998	Final. 1 Apr. 1996 - 31 May 1998

4. TITLE AND SUBTITLE
Theoretical and experimental investigation of vibration damping by vorticity production

5. FUNDING NUMBERS
F49620-96-1-0098

6. AUTHOR(S)
Michael S. Howe

7. PERFORMING ORGANIZATION NAME(S) AND ADDRESS(ES)
Boston University
College of Engineering
110 Cummington Street
Boston MA 02215

8. PERFORMING ORGANIZATION REPORT NUMBER
AM-98-029

9. SPONSORING/MONITORING AGENCY NAME(S) AND ADDRESS(ES)
Major Brian Sanders
Air Force Office of Scientific Research
110 Duncan Ave, Suite B115,
Bolling AFB, DC 20332-8080

10. SPONSORING/MONITORING AGENCY REPORT NUMBER

11. SUPPLEMENTARY NOTES

12a. DISTRIBUTION/AVAILABILITY STATEMENT
Approved for public release;
distribution unlimited.

12b. DISTRIBUTION CODE
F49620-96-1-0098

13. ABSTRACT (Maximum 200 words)

Analytical models are formulated and solved to determine the energy transfer between a vibrating perforated plate of finite thickness and a mean shear flow over one or both sides of the plate. Energy transferred to the flow appears as the kinetic energy of vorticity produced in the perforates and swept downstream by the flow. Regions of positive and negative damping are identified as functions of the vibration frequency, and a new, analytic determination is made of the operating stages of self-sustained oscillations of shear flow over apertures (including wall cavities) and validated by comparison with experiment. Numerical predictions are also given that extend the analysis to perforates of arbitrary shape. A water channel experiment has been performed to measure the damping by vorticity production of a vibrating, perforated elastic plate at zero mean angle of attack. An outline description is given of experiments currently in progress in which a porous flap is excited by a large scale vortex flow in a wind tunnel; measurements are being made of the vibration damping achieved by vorticity production stimulated by blowing through surface apertures.

14. SUBJECT TERMS
Damping, sound, structural vibrations, vorticity, bias flow and grazing flow perforated screen, Rayleigh conductivity, Kutta condition.

15. NUMBER OF PAGES
178 + iv

16. PRICE CODE

17. SECURITY CLASSIFICATION OF REPORT	18. SECURITY CLASSIFICATION OF THIS PAGE	19. SECURITY CLASSIFICATION OF ABSTRACT	20. LIMITATION OF ABSTRACT
Unclassified	Unclassified	Unclassified	UL

THEORETICAL AND EXPERIMENTAL INVESTIGATION OF VIBRATION DAMPING BY VORTICITY PRODUCTION

M. S. Howe
Boston University, College of Engineering
110 Cummington Street, Boston MA 02215
1 July, 1998

Report AM-98-029

Final Technical Report

AFOSR Grant F49620-96-1-0098
Period of Performance: 1 April 1996 - 31 May 1998

Prepared for Major Brian Sanders
Program Manager, Structural Mechanics
Air Force Office of Scientific Research
110 Duncan Ave, Suite B115, Bolling AFB, DC 20332-8080

CONTENTS

CONTENTS continued

CONTENTS continued

PREFACE

The research documented in this report was sponsored by the Air Force Office of Scientific Research under Grant No. F49620-96-1-0098, administered by Major Brian Sanders.

The theoretical investigations described in Chapters 1 - 3 were conducted by the Principal Investigator (PI). The numerical analysis described in Chapter 4 formed the basis of the MS thesis of Ms. Kelly P. Horan; the numerical work of Chapter 5 is the outcome of an assignment undertaken by Mr. T. H. Wood as part of the Boston University graduate level course *Waves in Fluids* given by the PI in the Spring of 1997. Professor Sheryl M. Grace provided the detailed guidance and assistance necessary to ensure the successful completion of this graduate student contribution to the research project.

Mr. P. M. Maung is conducting the experiment described in Chapter 6 and that currently underway and outlined in Chapter 7 in partial fulfillment of the requirements for a doctoral degree. Both experiments are performed using facilities made available by the Division of Applied Sciences at Harvard University, with the kind permission of Professors Albert Gore and Frederick H. Abernathy. Professor G. H. McKinley (formerly of Harvard University) provided invaluable assistance in the water channel experiment (Chapter 6), and in the formulation of the wind tunnel test currently in progress.

The following articles also document aspects of the research conducted under the present grant:

1. M. S. Howe *Influence of wall thickness on Rayleigh conductivity and flow-induced aperture tones.* Journal of Fluids and Structures **11**, 351 - 366, 1997.
2. M. S. Howe *Influence of cross-sectional shape on the conductivity of a wall aperture in mean flow.* Journal of Sound and Vibration **207**, 601 - 616, 1997.
3. M. S. Howe *Rayleigh conductivity and self-sustained oscillations.* Theoretical and Computational Fluid Dynamics **10**, 187 - 200, 1998.
4. S. M. Grace, K. P. Horan and M. S. Howe *The influence of shape on the Rayleigh conductivity of a wall aperture in the presence of grazing flow.* Journal of Fluids and Structures (in press) 1998.
5. S. M. Grace, T. H. Wood and M. S. Howe *On the stability of high Reynolds number flow over a circular aperture.* Submitted to the Proceedings of the Royal Society, Series A, 1998.
6. P. M. Maung, M. S. Howe and G. McKinley *Experimental investigation of the damping of structural vibrations by vorticity production.* Submitted to the Journal of Sound and Vibration, 1997.
7. P. M. Maung and M. S. Howe *Vibration damping of jet nozzle flaps by vorticity production.* AIAA Paper 97-0576, 1997.

M. S. Howe
Principal Investigator

CHAPTER 1

INFLUENCE OF WALL THICKNESS ON RAYLEIGH CONDUCTIVITY

M. S. Howe

SUMMARY

A theoretical investigation is made of the effect of finite wall thickness on the interaction of a pressure perturbation, produced by sound or large scale structural vibration, with a wall aperture in the presence of a tangential mean flow. Previous analyses for a wall of infinitesimal thickness (Howe, Scott & Sipcic 1996) indicate that the perturbation is damped during the interaction if the Strouhal number based on aperture diameter and mean velocity is small. The damping is caused by the transfer of energy to the mean flow via the production of vorticity in the aperture. We show that the damping at low Strouhal numbers is unchanged when the wall has small, but finite thickness, characteristic of real structures. However, wall thickness has a substantial influence on flow stability and on the excitation of self-sustained oscillations of fluid in the aperture. Instabilities exist when the Rayleigh conductivity $K_R(\omega)$ of the aperture at frequency ω possesses poles in the upper ω-plane (an instability frequency being equal to the real part of ω at a pole); increasing wall thickness exacerbates the tendency towards instability by causing poles initially in the lower half plane to cross the real axis. Detailed results are given for two-sided flow which (for an ideal fluid) is stable for a wall of zero thickness when the flow speed is the same on both sides, and for one-sided flow over an aperture, which is unstable for arbitrary wall thickness. In both cases the instability frequencies are shown to progressively decrease as the wall thickness increases, but externally forced motion at low Strouhal numbers is always damped.

1. INTRODUCTION

Narrow band acoustic tones are frequently generated by nominally steady, high Reynolds number flow over cavities and wall apertures (Rockwell 1983). The tones are associated with distinct "operating stages", each of which corresponds to a continuous range of Strouhal numbers governed by a *feedback* mechanism involving the periodic shedding of vorticity and its convection over the aperture or cavity opening (Rossiter 1962). Feedback occurs via impulsive pressures produced by the impingement of the vorticity on a downstream edge. The tonal amplitude varies with flow speed and exhibits abrupt, hysteretic jumps between stages. Empirical formulae for the different stages and their Strouhal number ranges are well known (Rossiter 1962; East 1966; Heller and Bliss 1975; Komerath *et al* 1987; Ahuja and Mendoza 1995), although a general theory valid at arbitrary Mach number is still lacking (Tam and Block 1978; Bruggeman 1987; Bruggeman *et al* 1989; Peters 1993; Hardin and Pope 1995; Kriesels *et al* 1995).

A deductive theory of the resonance stages has been proposed by Howe (1997) for low Mach number, high Reynolds number flows, in situations where the wavelength of the generated sound is always large compared to the cavity or aperture diameter. This theory identifies the Strouhal numbers of the operating stages with the real parts of poles in the (upper) complex frequency plane of a certain impulse response function, which is equal to the Rayleigh conductivity for wall apertures and to an unsteady drag coefficient for shallow wall cavities. The response function is calculated on the basis of perturbation theory, in which the shear layer over the aperture or cavity is modeled by a *linearly* disturbed vortex sheet. Nonlinear factors must be invoked to limit the growth of instabilities predicted by this approach, but it is argued that finite amplitude motion of the shear layer does not significantly change the linear theory prediction of the resonance frequencies, which depend on the convection velocity U_c of disturbances within the shear layer. This hypothesis appears to be justified by experiments, which suggest that U_c is effectively independent of amplitude (Powell 1961; Holger *et al* 1977; Blake and Powell 1986). Indeed, Howe (1997) obtains excellent agreement between predictions of this type of linear theory and published data for edge and cavity tones.

The analysis of Howe (1997) of the stability of flow over a rectangular aperture is applicable only for a wall of infinitesimal thickness, and was an extension of earlier, numerical studies for a circular aperture in a thin wall (Scott 1995; Howe, Scott and Sipcic 1996). In applications involving, say, sound waves incident on a perforated screen in the presence of mean flow, the wall thickness is not necessarily negligible compared to the aperture diameter. The zero-thickness approximation predicts that acoustic energy is always absorbed during such interactions (by transformation to the kinetic energy of vorticity generated at aperture edges) provided the Strouhal number based on aperture dimension and the mean flow speed is small. Vibrational energy can be absorbed by the same mechanism during tangential flow over a vibrating perforated plate (see Chapter 6 and Maung and Howe 1997). In all such cases it is clearly desirable to incorporate the influence of finite wall thickness directly into the damping prediction scheme.

In this chapter we do this for a rectangular aperture in a wall of small, but finite thickness by generalizing the method of Howe (1997). Predictions are given for cases involving mean flow on one or both sides of the wall at very high Reynolds number, when free shear layers may be modeled by vortex sheets. For an infinitely thin wall the flow is stable when the mean flow is the same on both sides (such that, for an ideal fluid, the mean vorticity vanishes in the steady state; see Howe, Scott and Sipcic 1996); we demonstrate how this flow is destabilized by finite wall thickness by tracing the motions of poles of the Rayleigh conductivity from the lower to the upper halves of the complex frequency plane as wall thickness increases from zero. For one-sided flow (when the aperture is spanned by a plane vortex sheet in the undisturbed state), increasing wall thickness ultimately causes the Strouhal numbers of different instability stages to decrease to a common value, although the hypotheses of our thin wall approximation are strictly invalid when the wall thickness becomes comparable to the aperture diameter.

The analytical model for a wall of small, but finite thickness is formulated in §2 for a rectangular aperture in the presence of an arbitrary, two-sided, low Mach number, high Reynolds number flow. Specific results are given in §§3, 4 respectively for two-sided uniform flow and one sided flow.

2. THE GOVERNING EQUATIONS

2.1 The Rayleigh conductivity

Consider high Reynolds number grazing flow at infinitesimal Mach number of fluid of uniform mean density ρ_o over both sides of a rectangular aperture in a plane, rigid wall of thickness d. The midplane of the wall is taken to coincide with the plane $x_2 = 0$ of the rectangular coordinate system (x_1, x_2, x_3), whose origin is at the geometrical center of the aperture. The mean flow is parallel to the x_1-axis with mean stream velocities U_+ and U_- in the "upper" and "lower" regions $x_2 \gtrless \pm\frac{1}{2}d$ respectively (see Figure 1). The aperture is aligned with sides of length L parallel to the mean flow and of length b in the transverse (x_3-) direction, so that the upper and lower openings occupy $|x_1| < s \equiv \frac{1}{2}L$, $x_2 = \pm\frac{1}{2}d$, $|x_3| < \frac{1}{2}b$. The shear layer over each opening is modeled by a vortex sheet, and the fluid within the volume of the aperture (in $|x_2| < \frac{1}{2}d$) is assumed to be in a mean state of rest.

Let uniform, small amplitude, time-dependent pressures $p_\pm(t)$ be applied in the vicinity of the aperture respectively in the upper and lower regions, and suppose the resulting motion of the vortex sheets is adequately described by linear perturbation theory. The motion produces a volume flux Q(t) through the aperture that is related to the applied pressure jump

$$[p_o(t)] \equiv p_+(t) - p_-(t)$$

by

$$\rho_o \partial Q(t)/\partial t = -\int_{-\infty}^{\infty} K_R(\omega)[p_o(\omega)]e^{-i\omega t}\, d\omega, \qquad (2.1)$$

where $K_R(\omega)$ is the Rayleigh conductivity (Rayleigh 1945), which is a function of the radian frequency ω with the dimensions of length, and

$$[p_o(\omega)] \equiv (1/2\pi)\int_{-\infty}^{\infty} [p_o(t)]e^{i\omega t}\, dt$$

is the Fourier transform of $[p_o(t)]$.

The instantaneous rate at which energy is dissipated at the aperture by the applied pressure field is $\Pi \equiv -Q(t)[p_o(t)]$, which is just the net rate of working of the applied pressure forces on the aperture. For time-harmonic fluctuations, where $[p_o(t)] \equiv \mathrm{Re}\{[p_o(\omega)]e^{-i\omega t}\}$, equation (2.1) enables Π to be expressed in the time-averaged form

$$\Pi(\omega) = -|[p_o]|^2 \mathrm{Im}\{K_R(\omega)\}/2\rho_o\omega \quad (\omega > 0). \qquad (2.2)$$

At high Reynolds number, when thermo-viscous losses are negligible, dissipation is the result of the direct transfer of energy from the applied pressure (an incident sound wave, say) to the kinetic energy of the mean flow. According to (2.2) this is the case provided $\mathrm{Im}\{K_R(\omega)\} < 0$ (for $\omega > 0$). Negative damping occurs if $\mathrm{Im}\{K_R(\omega)\} > 0$, when energy is *extracted* from the mean flow. For a compressible fluid Q represents the effective acoustic monopole source strength of the aperture, and a net gain in perturbation energy would be radiated as sound on either side of the wall.

These conclusions are applicable strictly for real values of the radian frequency ω. Equation (2.1) determines the volume flux resulting from the applied pressure differential $[p_o(t)]$, and a strictly causal evaluation of the integral demands that the path of integration from $\omega = \pm\infty$ should pass *above* all singularities of the integrand in the complex frequency plane. Since the applied pressure may be assumed to vanish prior to some finite time in the past, $[p_o(\omega)]$ is regular in $\mathrm{Im}\{\omega\} > 0$, and any singularities are associated with the conductivity $K_R(\omega)$. According to Howe (1997), these singularities are simple poles for one-sided mean flow (when $U_- \equiv 0$) over a rectangular aperture in a thin wall ($d = 0$); a comparison with experiment indicated that the real parts of the poles correspond to the various operating frequencies of self-sustained oscillations of the aperture shear layer. For uniform grazing flow ($U_+ \equiv U_-$) $K_R(\omega)$ is regular in $\mathrm{Im}(\omega) > 0$ for $d = 0$ (Howe, Scott and Sipcic 1996); in this case there is no vortex sheet across the aperture in the undisturbed state, and linear theory predicts that there are no self-sustained oscillations.

2.2 The thin wall approximation

The equations of motion of the vortex sheets spanning the aperture openings of Figure 1 ($d \neq 0$) are similar to that discussed by Howe, Scott and Sipcic (1996) for circular and rectangular apertures in a wall of infinitesimal thickness, and only a brief outline of the derivation is needed here.

Consider time-harmonic excitation of the aperture by a uniform pressure differential $[p_o(\omega)]e^{-i\omega t}$. Let $\zeta_\pm(x_1, x_3)e^{-i\omega t}$ respectively denote the displacement (in the x_2-direction) of the upper and lower vortex sheets from

their undisturbed positions $x_2 = \pm\frac{1}{2}d$. At low Mach numbers the local motion may be regarded as incompressible, and linearized representations of the perturbation pressures above and below the wall have the forms

$$\left.\begin{aligned} p &= p_+ - \rho_o\left(\omega+iU_+\frac{\partial}{\partial x_1}\right)^2\int_S \frac{\zeta_+(y_1,y_3)}{2\pi|x-y|}\,dy_1dy_3, \quad x_2 > \tfrac{1}{2}d \\ &= p_- + \rho_o\left(\omega+iU_-\frac{\partial}{\partial x_1}\right)^2\int_S \frac{\zeta_-(y_1,y_3)}{2\pi|x-y|}\,dy_1dy_3, \quad x_2 < -\tfrac{1}{2}d, \end{aligned}\right\} \tag{2.3}$$

where respectively $y = (y_1, \pm\frac{1}{2}d, y_3)$, the integration is over the aperture cross-section S, and the exponential time factor $e^{-i\omega t}$ is here and hereinafter suppressed. Note that, according to linear theory, vorticity impinging on the downstream edge of the aperture remains in the plane of the (upper or lower) surface of the wall, where its subsequent influence on the unsteady flow is annulled by image vorticity in the wall.

In the thin wall approximation the wavelength of motions of the vortex sheets is assumed to be large compared to the wall thickness d. In these circumstances the fluid displacement ζ in the x_2-direction within the aperture may be assumed to be independent of x_2, i.e., we can take

$$\zeta \equiv \zeta(x_1,x_3) = \zeta_+(x_1,x_3) = \zeta_-(x_1,x_3). \tag{2.4}$$

Then the equation of motion of a "column" of fluid within the aperture is just

$$\rho_o d\partial^2\zeta/\partial t^2 = -[p], \quad |x_1| < s, \ |x_3| < \tfrac{1}{2}b,$$

where [p] is the difference in the pressures applied to the upper and lower ends of the column at $x_2 = \pm\frac{1}{2}d$. For time-harmonic motion, equations (2.3) accordingly imply that

$$\left[\left(\omega+iU_+\frac{\partial}{\partial x_1}\right)^2 + \left(\omega+iU_-\frac{\partial}{\partial x_1}\right)^2\right]\frac{1}{2\pi}\int_S \frac{\zeta(y_1,y_3)dy_1dy_3}{\sqrt{(x_1-y_1)^2+(x_3-y_3)^2}} + d\omega^2\zeta(x_1,x_3) = \frac{[p_o]}{\rho_o} \tag{2.5}$$

This equation is simplified by means of the hypothesis that vortex shedding from the straight end $x_1 = -s$ of the aperture produces strongly correlated motions of the vortex sheets at different transverse locations x_3, so that ζ may assumed to be independent of x_3. Equation (2.5) may then be explicitly integrated over the transverse span of the aperture with respect to both y_3 and x_3 and the result cast in the form

$$\left[\left(\sigma+i\frac{\partial}{\partial\xi}\right)^2+\left(\sigma+i\mu\frac{\partial}{\partial\xi}\right)^2\right]\int_{-1}^{1}\zeta(\eta)\{\ln|\xi-\eta|+\mathcal{L}(\xi,\eta)\}d\eta$$

$$-2\pi\left(\frac{d}{L}\right)\sigma^2\zeta(\xi)=-\pi s[p_o]/\rho_o U_+^2,\quad |\xi|<1, \tag{2.6}$$

where

$$\left.\begin{aligned}&\sigma=\omega s/U_+,\ \mu=U_-/U_+,\ \xi=x_1/s,\ \eta=y_1/s,\\ &\mathcal{L}(\xi,\eta)=-\ln\{b/s+\sqrt{[(b/s)^2+(\xi-\eta)^2]}\}+\sqrt{[1+(s/b)^2(\xi-\eta)^2]}-(s/b)|\xi-\eta|.\end{aligned}\right\} \tag{2.7}$$

Equation (2.6) is next integrated with respect to the second order differential operator on the left hand side by introducing the Green's function

$$G(\xi,\eta)=\frac{1}{2\sigma(1-\mu)}\left(H(\xi-\eta)e^{i\sigma_+(\xi-\eta)}+H(\eta-\xi)e^{i\sigma_-(\xi-\eta)}\right), \tag{2.8}$$

which is a particular solution of

$$\left[\left(\sigma+i\frac{\partial}{\partial\xi}\right)^2+\left(\sigma+i\mu\frac{\partial}{\partial\xi}\right)^2\right]G(\xi,\eta)=\delta(\xi-\eta).$$

In these formulae, H(x) is the Heaviside unit function (= 0, 1 according as $x \lessgtr 0$), and $\sigma_\pm$ are the Kelvin-Helmholtz wavenumbers (Lamb 1932)

$$\sigma_\pm=\sigma\left(\frac{1\pm i}{1\pm i\mu}\right). \tag{2.9}$$

The dimensionless displacement

$$Z(\xi)\equiv\frac{-2\rho_o\omega^2 s}{\pi[p_o]}\zeta(\xi), \tag{2.10}$$

then satisfies the following integrated form of equation (2.6)

$$\int_{-1}^{1}Z(\eta)\{\ln|\xi-\eta|+\mathcal{L}(\xi,\eta)\}d\eta-2\pi\sigma^2(d/L)\int_{-1}^{1}Z(\eta)G(\xi,\eta)d\eta+\lambda_+e^{i\sigma_+\xi}+\lambda_-e^{i\sigma_-\xi}=1,\quad |\xi|<1, \tag{2.11}$$

where $\lambda_\pm$ are constants of integration.

The integral equation (2.11) is readily solved by collocation, by the procedure described by Scott (1995) for a vortex sheet over a circular

aperture. The values of $\lambda_\pm$ are fixed by imposing the Kutta condition that the vortex sheets should leave the upstream edges of the aperture smoothly, i.e., by requiring that $\zeta = \partial\zeta/\partial\xi = 0$ as $\xi \to -1$ (Crighton 1985). No further conditions can be imposed at the trailing edge ($\xi = 1$), where the displacement must be permitted to develop a mild, yet integrable potential flow singularity proportional to the inverse square-root of the distance from the edge. This singularity is the linear theory representation of the large amplitude edge motion observed in experiments.

The aperture volume flux $Q(\omega) = -i\omega b\int_{-s}^{s} \zeta(x_1)dx_1$, from which relation it is readily deduced that the Rayleigh conductivity is given in terms of Z by

$$K_R = -\tfrac{\pi}{2}b\int_{-1}^{1} Z(\eta)\ d\eta. \qquad (2.12)$$

The conductivity is generally a complex valued function of the frequency ω, but also depends on the aperture aspect ratio b/L, the wall thickness ratio d/L, and the mean velocity ratio $\mu = U_-/U_+$.

In the special case of uniform, two sided mean flow, where $U_- = U_+ \equiv U$, the wavenumbers σ_+ and σ_- are both equal to $\sigma = \omega s/U$, and it is convenient to take Green's function (2.8) in the degenerate form

$$G(\xi,\eta) = -H(\xi-\eta)(\xi-\eta)e^{i\sigma(\xi-\eta)}.$$

The terms in $\lambda_\pm$ in equation (2.11) should then be replaced by $(\lambda_1 + \lambda_2\xi)e^{i\sigma\xi}$, where λ_1, λ_2 are constants determined by the Kutta condition.

3. UNIFORM, TWO-SIDED FLOW OVER A RECTANGULAR APERTURE

Equations (2.11), (2.12) are first applied to investigate the stability of nominally steady flow over an aperture in a uniform grazing mean flow, where $U_- = U_+ \equiv U$ (Figure 2). Linear theory predicts this flow to be stable when $d = 0$.

3.1 Dependence of Rayleigh conductivity on wall thickness

Representative plots are shown in Figure 3 of the real and imaginary parts of the dimensionless conductivity

$$K_R(\omega)/b = \Gamma_R(\omega) - i\Delta_R(\omega), \tag{3.1}$$

for real values of $\sigma = \omega s/U$, when the aspect ratio $b/L = 2$ and for a range of values of $d/L < 1$. These results are typical of all aspect ratios. K_R has been calculated from the numerical solution of equation (2.11) modified as described in the last paragraph of §2. According to (2.2), perturbation energy is dissipated at the aperture at those frequencies where $\Delta_R(\omega) > 0$. Figure 3 shows that Δ_R is positive and effectively invariant with changing d/L in the low frequency region $\omega s/U < 2.4$, where energy is always dissipated. This conclusion is important because it suggests that the effectiveness of perforated, grazing flow screens used to absorb low Strouhal number sound and vibration is not significantly dependent on screen thickness.

According to Figure 3a, $K_R(\omega)$ varies periodically when $\omega s/U > 2$ and $d/L = 0$. However, the influence of small, but finite wall thickness is always felt at sufficiently high frequencies, when the second integral on the left of (2.11), which represents the inertia of fluid in the aperture, becomes important. This causes the oscillations in the real and imaginary parts of $K_R(\omega)$ ultimately to die out as σ becomes large. We shall demonstrate below that the aperture motion is absolutely unstable when $d/L \neq 0$; indeed, when d/L exceeds about 0.1 (Figure 3e) $\Gamma_R(\omega)$ and $\Delta_R(\omega)$ vary with frequency in qualitatively the same way as for an aperture in the presence of an unstable, one-sided mean flow (Howe, Scott and Sipcic 1995; see also §4). In Figure 3g ($d/L = 0.5$) the imaginary component $\Delta_R > 0$ for all $\omega > 0$, which implies that

forced motion at the real frequency ω is always damped; this conclusion should be treated with caution, however, since the present thin wall theory may not be strictly valid for such a large value of d/L.

3.2 Poles of the conductivity

An understanding of the changes in $\Gamma_R(\omega)$ and $\Delta_R(\omega)$ with increasing values of d/L can be obtained from the asymptotic approximation given by Howe, Scott and Sipcic (1996, §3) for d/L = 0 and b/L ≫ 1, namely

$$K_R \approx \frac{\pi b}{2\{F(\sigma) + \ln(8b/eL)\}}, \tag{3.2}$$

where $e \approx 2.718$ is the exponential constant, and

$$F(\sigma) = \frac{i\sigma J_0(J_0 - iJ_1) - [J_0 - 2i\sigma(J_0 - iJ_1)][J_0 - i\sigma(J_0 + iJ_1)]}{\sigma[J_0 J_1 + \sigma\{J_1^2 + (J_0 - 2iJ_1)^2\}]}, \tag{3.3}$$

$J_{0,1} \equiv J_{0,1}(\sigma)$ being Bessel functions. The variations with σ of Γ_R and Δ_R predicted by this formula are similar to those shown in Figure 3a (d/L = 0) for b/L = 2, becoming periodic when σ exceeds about 2, where

$$F \approx -2/\{1 - ie^{-2i\sigma}\},$$

so that $K_R(\omega)$ has simple poles at

$$\sigma \equiv \frac{\omega s}{U} \approx (n + \tfrac{1}{4})\pi + \frac{i}{2}\ln\left(\frac{1}{2} - \frac{1}{\ln\{8b/eL\}}\right), \quad n = \pm 1, \pm 2, \ldots \tag{3.4}$$

These poles lie in the lower half, $\mathrm{Im}(\omega) < 0$, of the frequency plane provided $b/L > e^3/8 \approx 2.51$, which is always satisfied when the asymptotic formula (3.2) is applicable. Numerical computation indicates the presence of an additional pole, not given by this formula, on the negative imaginary axis.

The asymptotic formula (3.2) supplies a qualitative picture of the behavior of $K_R(\omega)$ also for b/L = 2 and d/L = 0 (the case considered in Figure 3a); the motion is stable and poles of K_R are all in the lower frequency plane. The real parts of these poles are close to those defined by (3.4), and correspond approximately to the locations of successive *minima* of $\Gamma_R(\omega)$ in Figure 3a near $\omega s/U = 3.9, 7.1, 10.2$, etc. An indication of what happens to these poles as d/L increases from zero can be surmised from Figure 3.

Consider, in particular, the pole whose real part is near $\sigma_o = 3.9$ at d/L = 0. The rapid variations near this frequency exhibited by $\Gamma_R(\omega)$ and $\Delta_R(\omega)$ in Figures 3c and 3d implies that the pole is close to the real axis for $0.03 < d/L < 0.065$. If the location of the pole is approximated by

$$\sigma \equiv \sigma_o + i\epsilon,$$

where ϵ is real, then the curves in Figure 3c are consistent with a local variation in the neighborhood of $\sigma = \sigma_o$ defined by

$$\Gamma_R - i\Delta_R \approx \text{constant} - \frac{i\alpha}{\sigma-\sigma_o - i\epsilon}, \quad \text{where } \alpha > 0,$$

i.e.

$$\Gamma_R \approx \text{constant} + \frac{\alpha\epsilon}{(\sigma-\sigma_o)^2+\epsilon^2}, \quad \Delta_R \approx \frac{\alpha(\sigma-\sigma_o)}{(\sigma-\sigma_o)^2+\epsilon^2}.$$

When $\alpha > 0$ and ϵ is small and *negative* (the pole being just below the real axis), Γ_R exhibits a deep negative minimum at $\sigma \equiv \omega s/U = \sigma_o$, as in Figure 3c near $\sigma = 3.9$. When d/L increases to 0.065, Figure 3d shows that the negative minimum has been transformed into a sharp maximum. Since the inflexional behavior of Δ_R is the same in each of these cases, this change must have occurred because of a reversal in the sign of ϵ, i.e., because the pole has crossed the real axis into the upper half plane.

The Newton-Raphson procedure and numerical predictions of $1/K_R(\omega)$ supplied by (2.12) can be used to track the motion of poles into the upper half-plane as d/L increases from zero, by starting from initial trial values given by (3.4) for a given value of n. Poles in the upper frequency plane correspond to spontaneously excited instabilities. Figure 4 illustrates pole loci for the first four "operating stages" n = 1 - 4 when the aspect ratio b/L = 2, and reveals that high frequency, high order instabilities (n large) are the first to be excited as d/L becomes finite. All instability modes are possible when d/L exceeds about 0.05. When d/L *decreases* from this value, the poles corresponding to n = 1, 2, 3, etc, successively cross into the lower half plane; the first four stages are stable when d/L is less than about 10^{-3}. This figure also shows that the various poles converge onto the imaginary axis when d/L becomes large, and that their real parts become approximately equal,

although the present thin wall approximation is probably not applicable for $d/L \geq 0.5$. The results are presented differently in Figure 5, where the dependence of the Strouhal number fL/U on d/L (where $f = \mathrm{Re}(\omega)/2\pi$ for the pole at ω) is shown for the first four operating stages. Each curve starts on the left at that finite, non-zero value of d/L at which the corresponding pole crosses into the upper frequency plane.

These predictions are for $b/L = 2$. However, similar results are obtained for arbitrary values of the aspect ratio b/L. This is illustrated by the example of Figure 6, which gives the Strouhal number dependence on d/L for $b/L = 500$, i.e., for an aperture in the form of a long, transverse slot.

4. ONE-SIDED FLOW OVER A RECTANGULAR APERTURE

4.1 Instability of one-sided flow

Let the mean flow be confined to the upper region of Figure 1 (i.e., $U_- \equiv 0$). In the steady state a vortex sheet separates the uniform flow at speed $U_+ \equiv U$ from the stagnant fluid within and below the aperture. The sheet is unstable for arbitrary wall thickness, and $K_R(\omega)$ must therefore have poles in the upper frequency plane. This may be contrasted with the uniform, two-sided flow of §3, which is stable when $d = 0$. However, two-sided flow is also unstable for $d = 0$ when the aperture supports a mean shear ($U_+ \neq U_-$). The manner in which this instability arises can be illustrated in terms of the analytical approximation (3.2) for $K_R(\omega)$ for $b/L \gg 1$; when $U_+ \neq U_-$, the definition (3.3) is replaced by (Howe, Scott and Sipcic 1996)

$$F(\sigma) = \frac{-\sigma_+ J_0(\sigma_-)[J_0(\sigma_+)-2W(\sigma_+)] + \sigma_- J_0(\sigma_+)[J_0(\sigma_-)-2W(\sigma_-)]}{\sigma_+ W(\sigma_-)[J_0(\sigma_+)-2W(\sigma_+)] - \sigma_- W(\sigma_+)[J_0(\sigma_-)-2W(\sigma_-)]}, \qquad (4.1)$$

where $W(x) = ix[J_0(x) - iJ_1(x)]$ and $\sigma_\pm$ are defined as in (2.9).

This formula can be used to calculate the loci of the poles from their initial locations in $\mathrm{Im}(\omega) < 0$, given by (3.4), as $\mu \equiv U_-/U_+$ decreases from 1 to 0. The result is depicted in Figure 7 for the first four operating stages. As for the case of destabilization by increasing wall thickness (§3.2), higher order poles are the first to cross into the upper half plane as U_-/U_+ decreases; all of the poles lie in $\mathrm{Im}(\omega) > 0$ when $U_-/U_+ < 0.47$. These plots are for the quasi-two-dimensional aspect ratio $b/L = 500$, but are typical of the behavior for arbitrary values of b/L. Ultimately, when $U_- = 0$, the poles for large values of n lie along a ray making an angle of 45° with the positive real axis (a related set of poles, corresponding to $n < 0$ in (3.4) lies asymptotically along the image of this ray in the imaginary axis). According to (3.4), when $U_-/U_+ = 1$ the real parts of successive poles differ by about π. As U_-/U_+ decreases this difference gradually diminishes, until when $U_- = 0$ both their real *and* imaginary parts differ by about $\pi/2$. This means that the jump in Strouhal number fL/U between successive stages of the aperture tones is about $\frac{1}{2}$ when $d = 0$ (Howe 1997).

4.2 Conductivity for finite wall thickness

The conductivity $K_R(\omega)$ for one-sided flow and real ω is calculated from equations (2.11) and (2.12), and does not vary significantly with d/L except when d/L is greater than about 0.2. This is illustrated in Figure 8 for an aspect ratio b/L = 2. The real part $\Gamma_R(\omega)$ hardly changes at all with increasing d/L, and (as in the case of two-sided uniform flow) $\Delta_R(\omega) > 0$ when $\omega s/U$ is small (less than about 1.5), at which frequencies forced motion of the shear layer by the applied pressure load $[p_o]$ is always damped; the variation of $\Delta_R(\omega)$ with ω is effectively independent of d/L in this frequency range. For larger values of $\omega s/U$ energy is extracted from the flow and supplied to the perturbing field where $\Delta_R(\omega) < 0$.

In Figure 3, for two-sided uniform flow, the rapid changes in the form of $K_R(\omega)$ with varying d/L are produced by poles crossing the real axis. In the present case the poles are already in the upper half-plane when $U_- = 0$ and d = 0, and their subsequent motions when d/L increases from zero causes relatively minor changes in $K_R(\omega)$. These motions (from initial positions indicated in Figure 7 at $U_-/U_+ = 0$) are plotted in Figure 9 for the first four operating stages when b/L = 500. $\mathrm{Re}(\omega s/U)$ becomes approximately the same for the poles shown in the Figure when d/L is larger than about 0.4, i.e., the Strouhal numbers of the operating stages become equal. One-sided flow is unstable for all values of d/L; Figure 10 shows how the Strouhal numbers $fL/U = \mathrm{Re}(\omega s/\pi U)$ change with d/L for b/L = 500. Results for smaller aspect ratios are qualitatively and quantitatively similar, and will not be given here.

5. CONCLUSION

Vortex shedding in wall apertures in the presence of grazing mean flow is responsible for an exchange of energy between the mean flow and an applied pressure, associated, for example, with a sound wave incident on the wall or with pressures generated by structural vibrations. Previous analytical treatments of such interactions for an infinitely thin wall have predicted that the applied perturbation is damped (energy being transferred to the mean flow) provided the Strouhal number is sufficiently small. In this chapter the magnitude of this low Strouhal number damping has been shown to be effectively unchanged when the wall has small, but finite thickness, characteristic of real structures. In all cases, however, finite thickness *does* modify the stability of the motion. For high Reynolds number two-sided flow, when the mean velocity is the same on both sides, the aperture flow is linearly stable for a wall of zero thickness. The mean shear layers introduced by finite wall thickness destabilize the flow, mathematically because increasing thickness is responsible for the migration of poles of the Rayleigh conductivity into the upper half of the complex frequency plane. The instabilities are here interpreted as tonal, self-sustained oscillations of the flow, whose frequencies occur in discrete bands (or "stages") as the wall thickness varies, at values equal to the real parts of the instability poles. The absence of experimental data for aperture flows of this type precludes a direct experimental validation of this hypothesis. However, Howe (1997) has reported excellent agreement with published data for frequency predictions of the same theory applied to edge-tones and shallow wall-cavity tones. The amplitudes of the oscillations are controlled by nonlinear mechanisms not discussed in this paper, and are typically independent of the presence of any other applied pressure perturbation.

One-sided flow over an aperture is unstable for arbitrary wall thickness. As the wall thickness increases from zero, for either one or two-sided flow, the frequencies of the instability modes progressively decrease, and ultimately approach a common value, although it is uncertain whether the approximation of this paper remains valid in this limit. At low Strouhal numbers, forced motion of an aperture by an applied pressure is always damped.

REFERENCES

Ahuja, K. K. & Mendoza, J. 1995 *Effects of cavity dimensions, boundary layer, and temperature on cavity noise with emphasis on benchmark data to validate computational aeroacoustic codes*. NASA Contractor Report: Final Report Contract NAS1-19061, Task 13.

Blake, W. K. and Powell, A. 1986 *The development of contemporary views of flow-tone generation*, pp 247 - 325 in *Recent Advances in Aeroacoustics* (edited by A. Krothapali and C. A. Smith), New York: Springer.

Bruggeman, J. C. 1987 *Flow induced pulsations in pipe systems*, PhD. Thesis, Eindhoven University of Technology.

Bruggeman, J. C., Hirschberg, A., van Dongen, M. E. H., Wijnands, A. P. J. and Gorter, J. 1989 Flow induced pulsations in gas transport systems: analysis of the influence of closed side branches. *Journal of Fluids Engineering* 111, 484 - 491.

Crighton, D. G. 1985 The Kutta condition in unsteady flow. *Annual Reviews of Fluid Mechanics* 17, 411 - 445.

East, L. F. 1966 Aerodynamically induced resonance in rectangular cavities. *Journal of Sound and Vibration* 3, 277 - 287.

Hardin, J. C. and Pope, D. S. 1995 Sound generation by flow over a two-dimensional cavity. *American Institute of Aeronautics and Astronautics Journal* 33, 407 - 412.

Heller, H. H. and Bliss, D. B. 1975 The physical mechanism of flow-induced pressure fluctuations in cavities and concepts for their suppression. *American Institute of Aeronautics and Astronautics Paper 75-491.*

Holger, D. K., Wilson, T. A. and Beavers, G. S. 1977 Fluid mechanics of the edgetone. *Journal of the Acoustical Society of America* 62, 1116 - 1128.

Howe, M. S. 1997 Edge, cavity and aperture tones at very low Mach numbers. *Journal of Fluid Mechanics* 330, 61 - 84.

Howe, M. S., Scott, M. I. and Sipcic, S. R. 1996 The influence of tangential mean flow on the Rayleigh conductivity of an aperture. *Proceedings of the Royal Society of London* A452, 2303 - 2317.

Komerath, N. M., Ahuja, K. K. and Chambers, F. W. 1987 Prediction and measurement of flows over cavities - a survey. *American Institute of Aeronautics and Astronautics Paper 87-022.*

Kriesels, P. C., Peters, M. C. A. M., Hirschberg, A., Wijnands, A. P. J., Iafrati, A., Riccardi, G., Piva, R. and Bruggeman, J. C. 1995 High amplitude vortex induced pulsations in gas transport systems. *Journal of Sound and Vibration* **184**, 343 - 368.

Lamb, H. 1932 *Hydrodynamics* (6th. ed., reprinted 1994) Cambridge University Press.

Maung, P. and Howe, M. S. 1997 Vibration damping of jet nozzle flaps by vorticity production. *American Institute of Aeronautics and Astronautics Paper 97-0576*.

Peters, M. C. A. M. 1993 *Aeroacoustic sources in internal flows*. PhD Thesis, Eindhoven University of Technology

Powell, A. 1961 On the edgetone. *Journal of the Acoustical Society of America* **33**, 395 - 409.

Rayleigh, Lord 1945 *Theory of Sound*, Vol 2. New York: Dover.

Rockwell, D. 1983 Oscillations of impinging shear layers. *American Institute of Aeronautics and Astronautics Journal*. **21**, 645 - 664.

Rossiter, J. E. 1962 *The effect of cavities on the buffeting of aircraft*. Royal Aircraft Establishment Technical Memorandum 754.

Scott, M. I. 1995 *The Rayleigh conductivity of a circular aperture in the presence of a grazing flow*. Master's thesis, Boston University.

Tam, C. K. W. and Block, P. J. W. 1978 On the tones and pressure oscillations induced by flow over rectangular cavities. *Journal of Fluid Mechanics* **89**, 373 - 399.

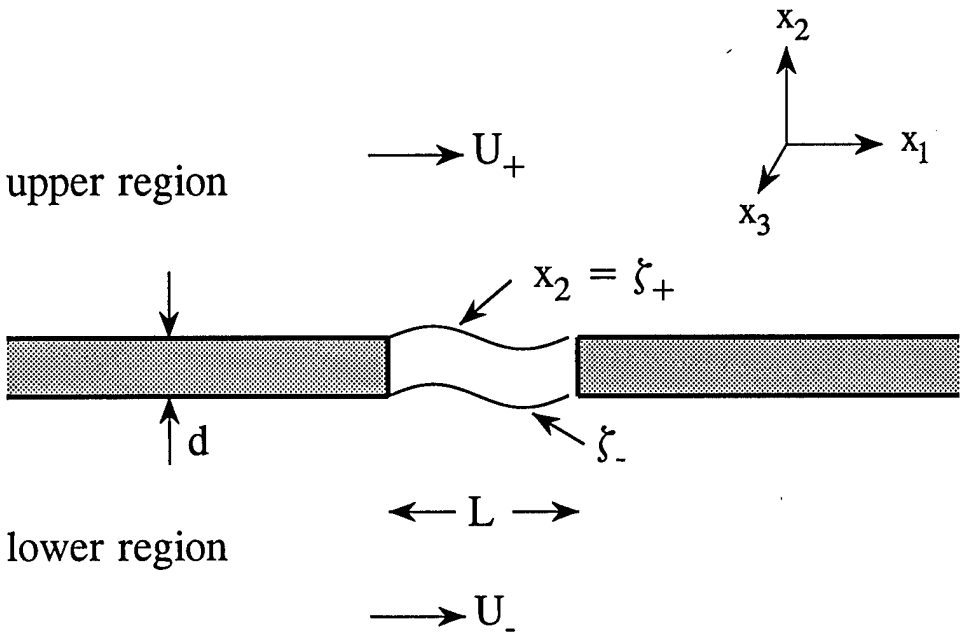

Figure 1. Idealized model of two-sided mean flow over a rectangular aperture in a wall of thickness d; the transverse length (out of the plane of the paper) of the aperture is b.

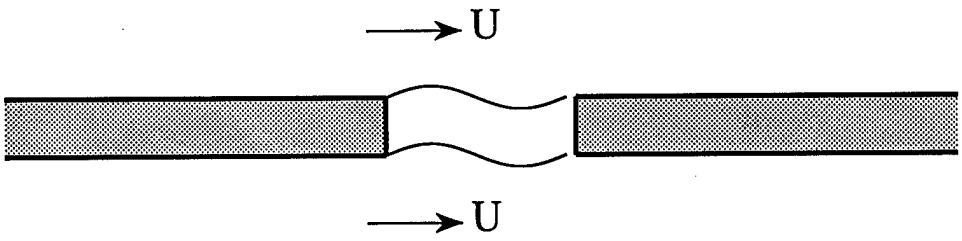

Figure 2. Uniform grazing mean flow over a rectangular aperture.

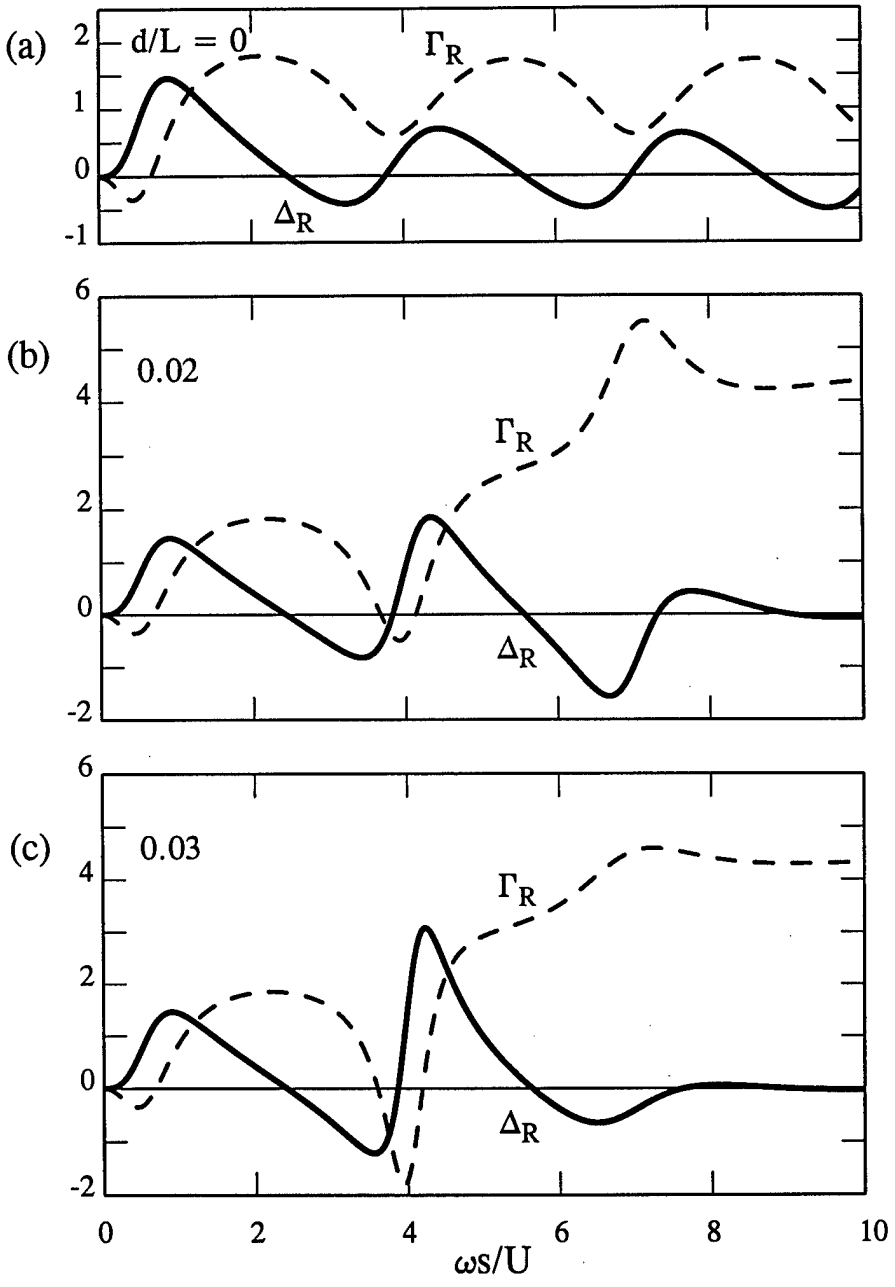

Figure 3. Illustrating the dependence of $K_R(\omega)/b = \Gamma_R(\omega) - i\Delta_R(\omega)$ on frequency when $U_- = U_+ \equiv U$ for b/L = 2 and for (a) d/L = 0, (b) 0.02, (c) 0.03.

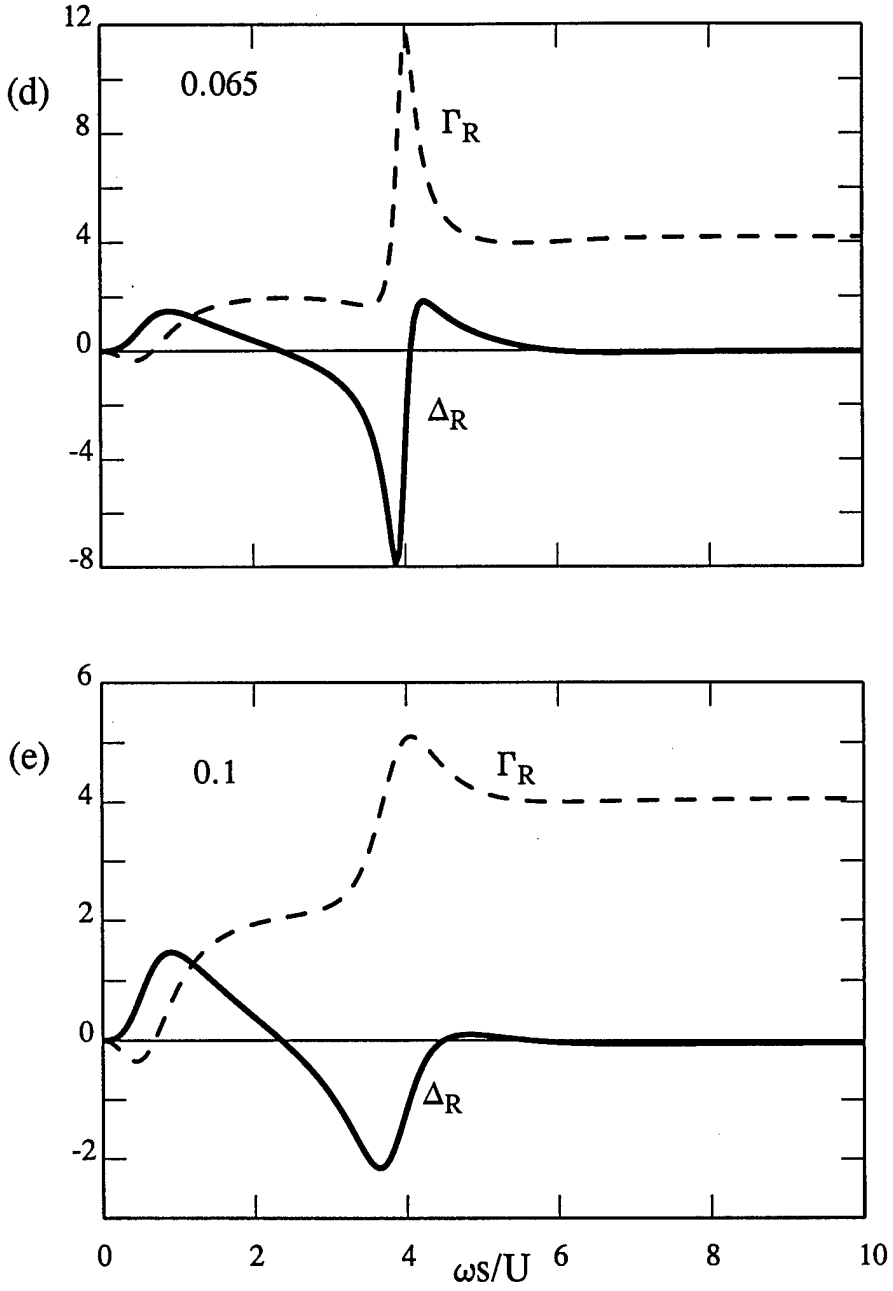

Figure 3. Illustrating the dependence of $K_R(\omega)/b = \Gamma_R(\omega) - i\Delta_R(\omega)$ on frequency when $U_- = U_+ \equiv U$ for b/L = 2 and for (d) 0.065, (e) 0.1.

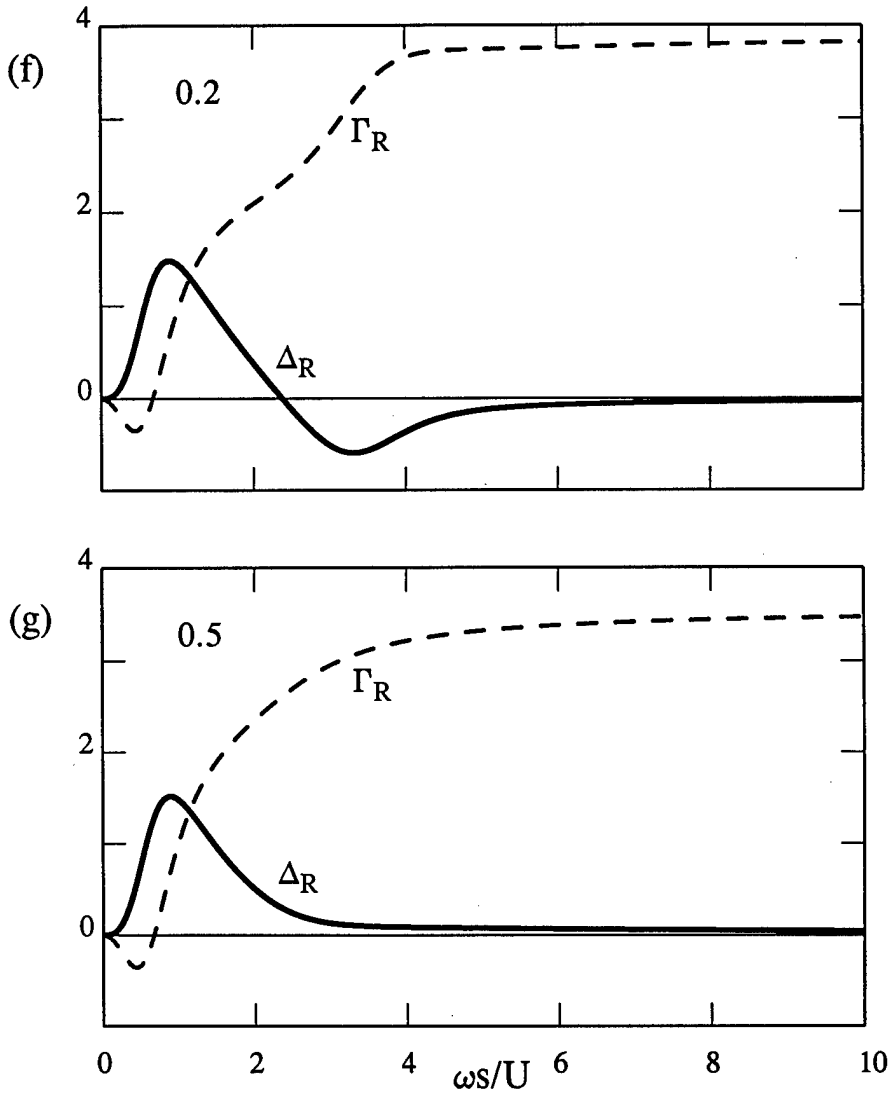

Figure 3. Illustrating the dependence of $K_R(\omega)/b = \Gamma_R(\omega) - i\Delta_R(\omega)$ on frequency when $U_- = U_+ \equiv U$ for b/L = 2 and for (f) 0.2, (g) 0.5.

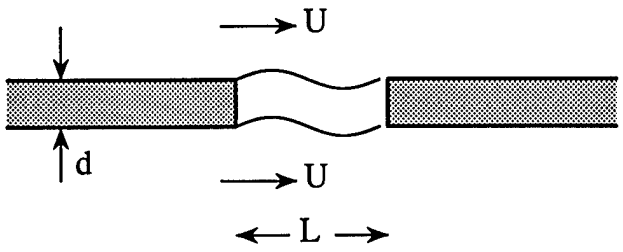

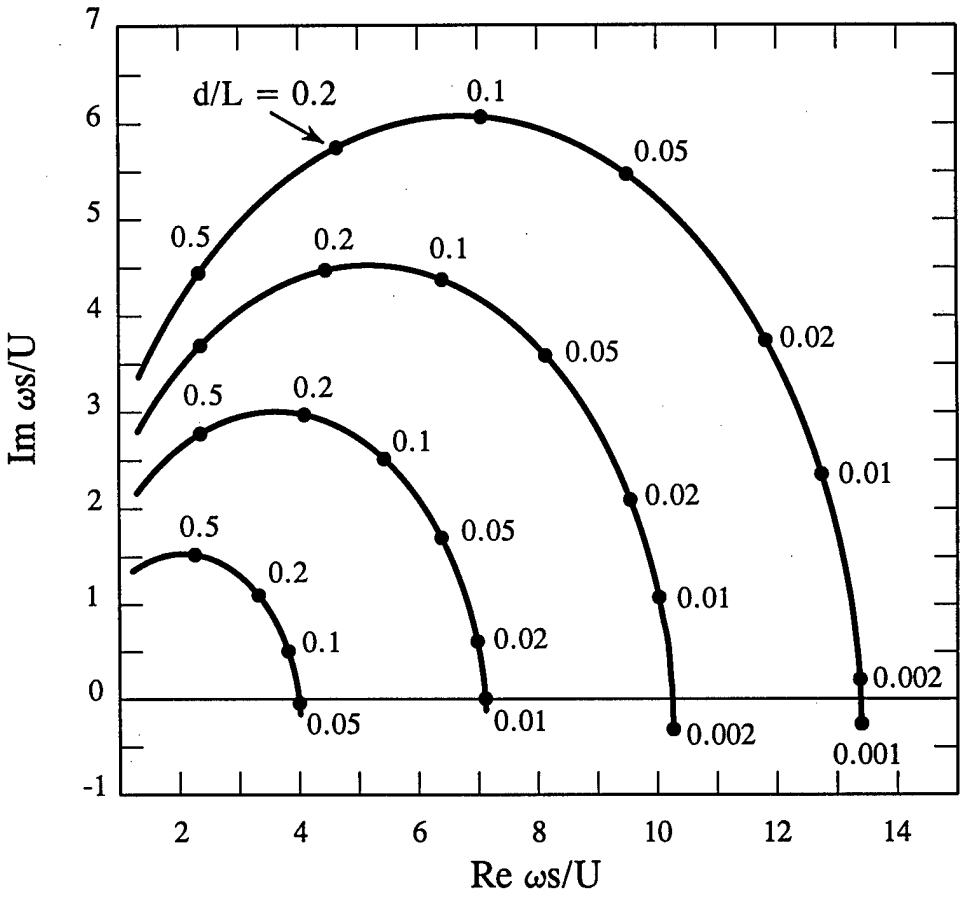

Figure 4. Loci of poles of $K_R(\omega)$ in the complex frequency plane for $U_+ = U_- \equiv U$ for the first four operating stages n = 1 - 4 when b/L = 2.

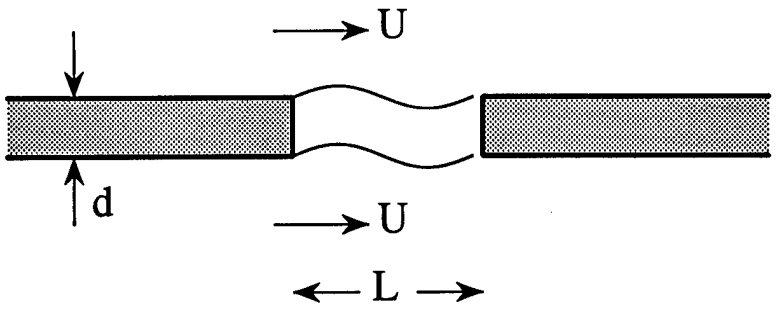

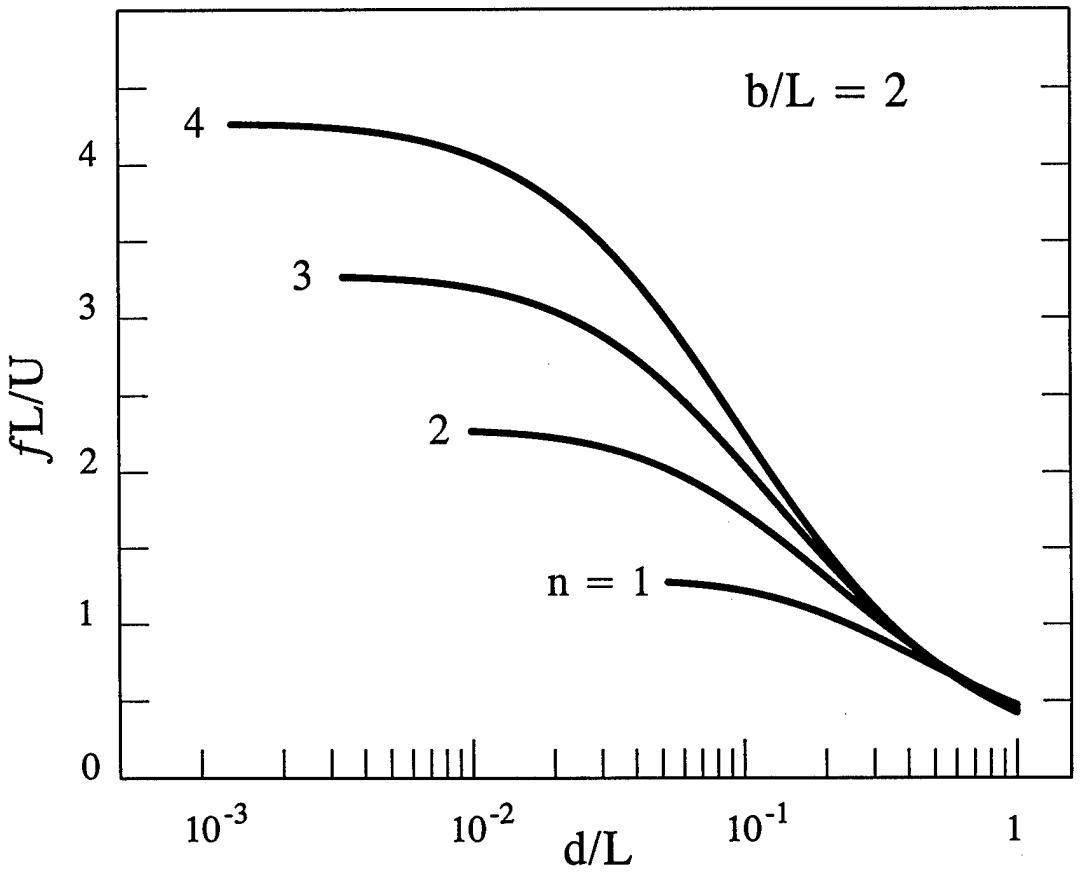

Figure 5. Strouhal number dependence on wall thickness for two-sided uniform flow ($U_+ = U_- \equiv U$) when b/L = 2.

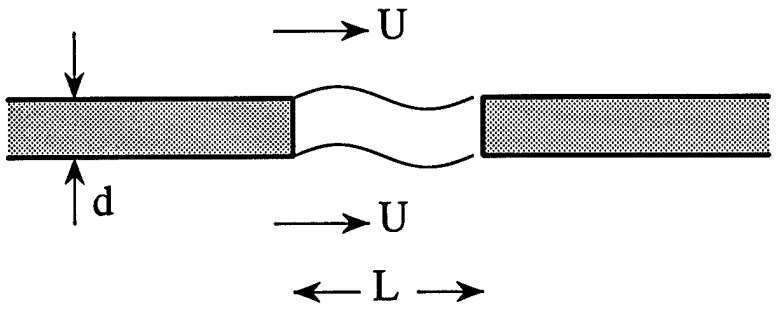

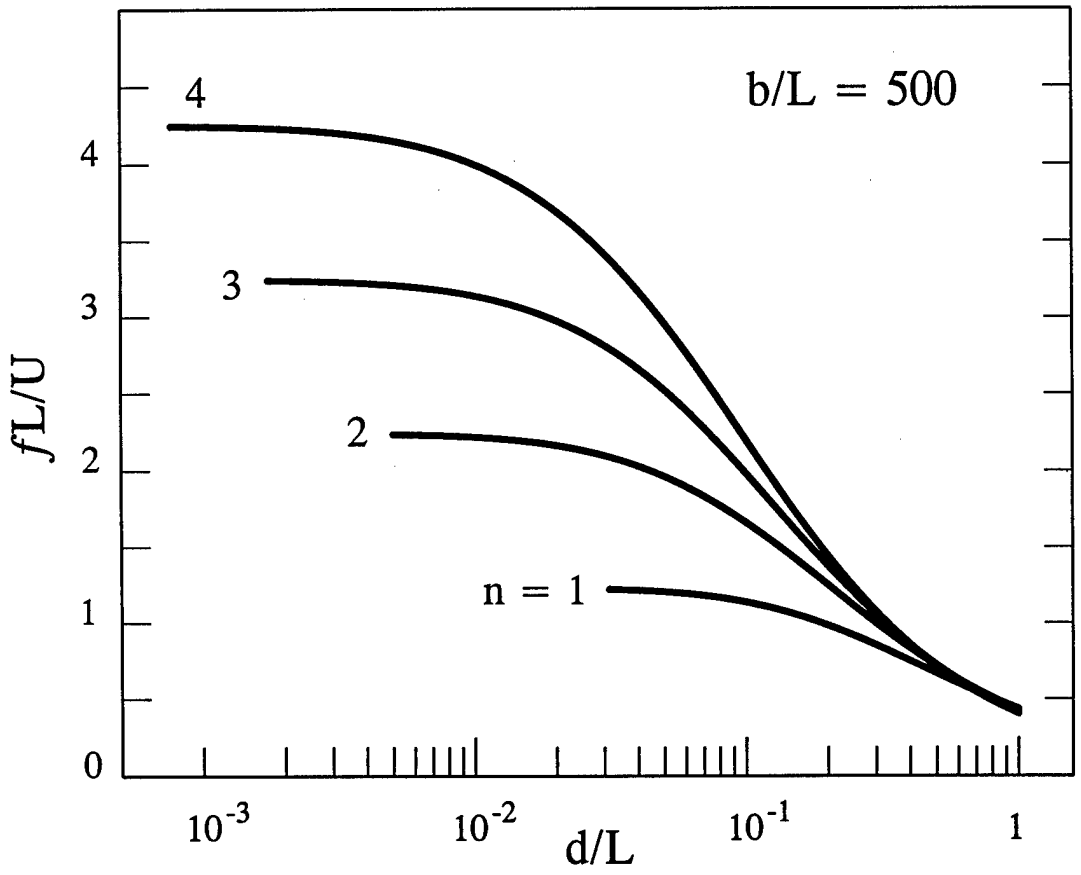

Figure 6. Strouhal number dependence on wall thickness for two-sided uniform flow ($U_+ = U_- \equiv U$) when b/L = 500.

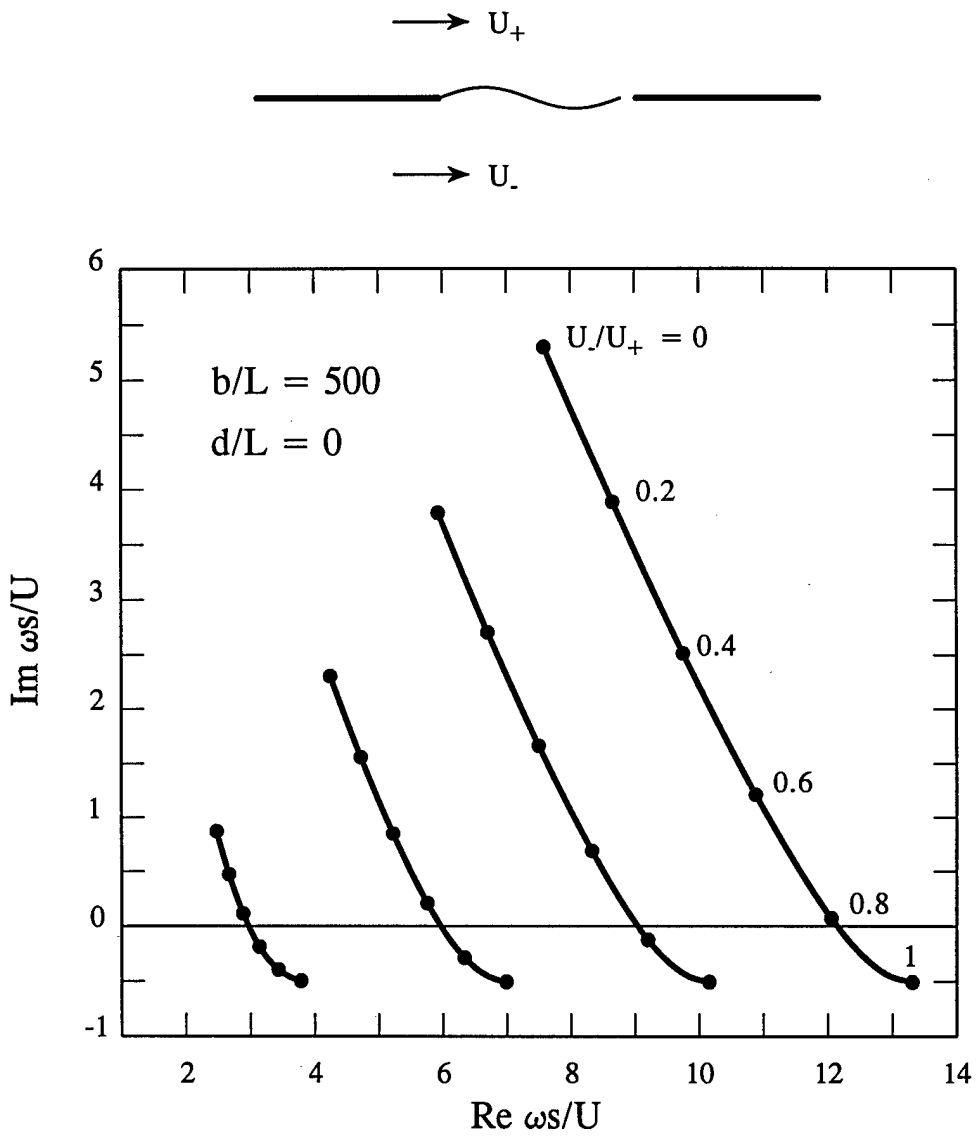

Figure 7. Loci of poles of $K_R(\omega)$ in the complex frequency plane for d/L = 0, b/L = 500 and $0 \leq U_-/U_+ \leq 1$ for the first four operating stages n = 1 - 4.

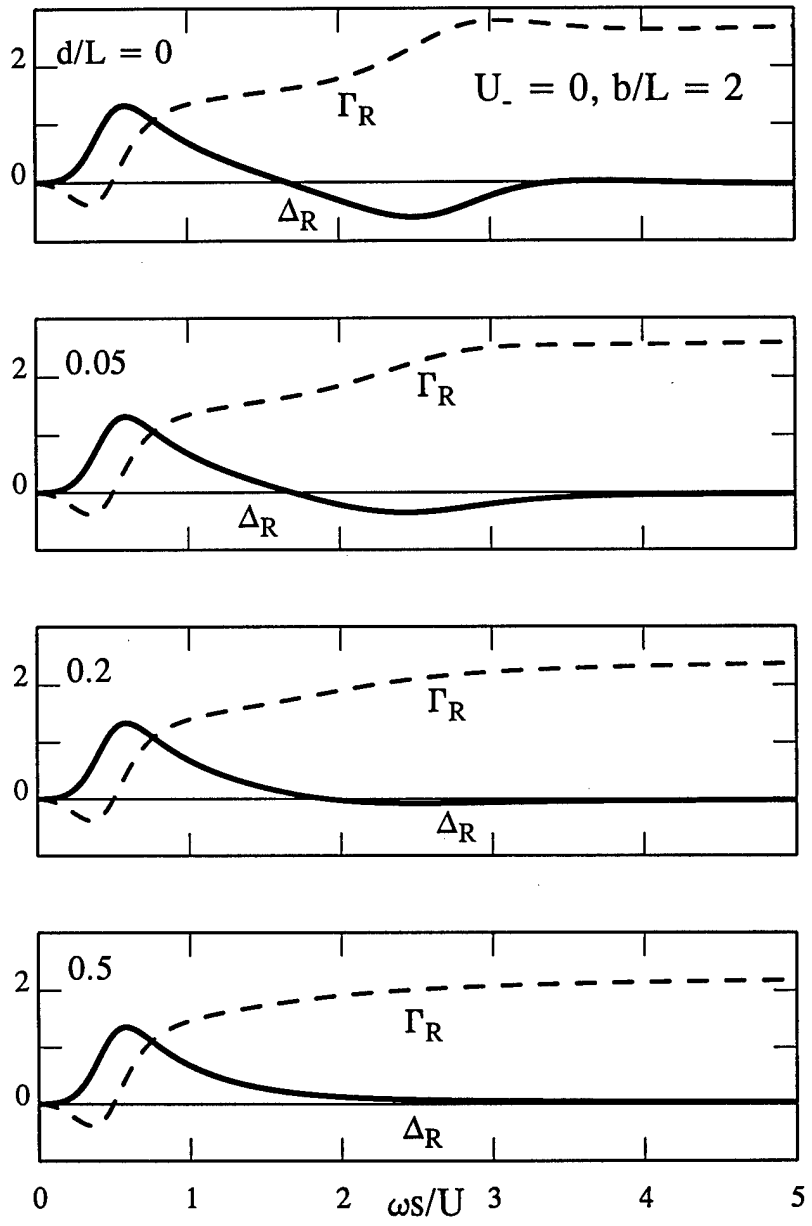

Figure 8. The dependence of $K_R(\omega)/b = \Gamma_R(\omega) - i\Delta_R(\omega)$ on frequency when $U_- = 0$ for b/L = 2 and for d/L = 0, 0.05, 0.2, 0.5.

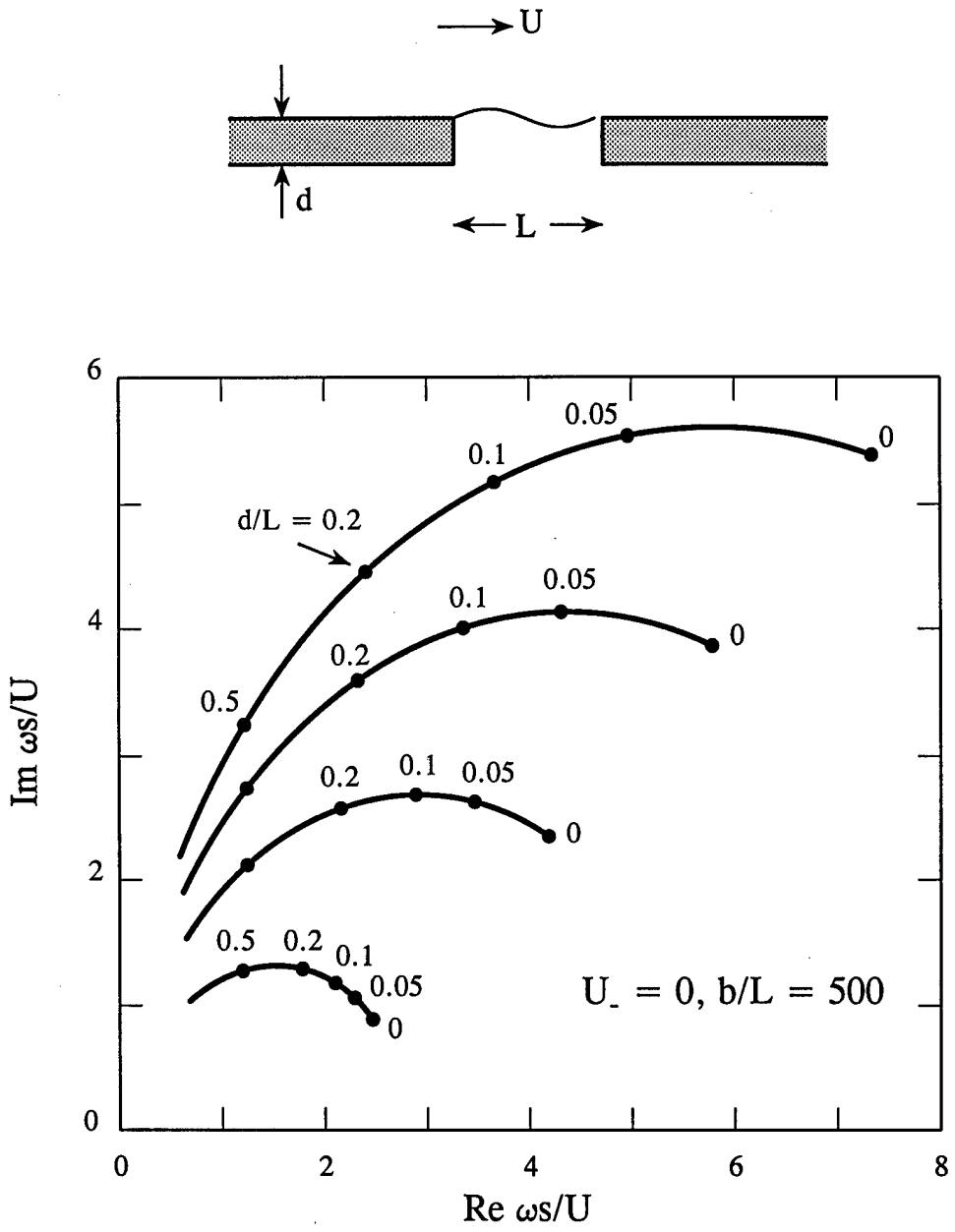

Figure 9. Loci of poles of $K_R(\omega)$ in the complex frequency plane for $U_- = 0$ for the first four operating stages n = 1 - 4 when b/L = 500.

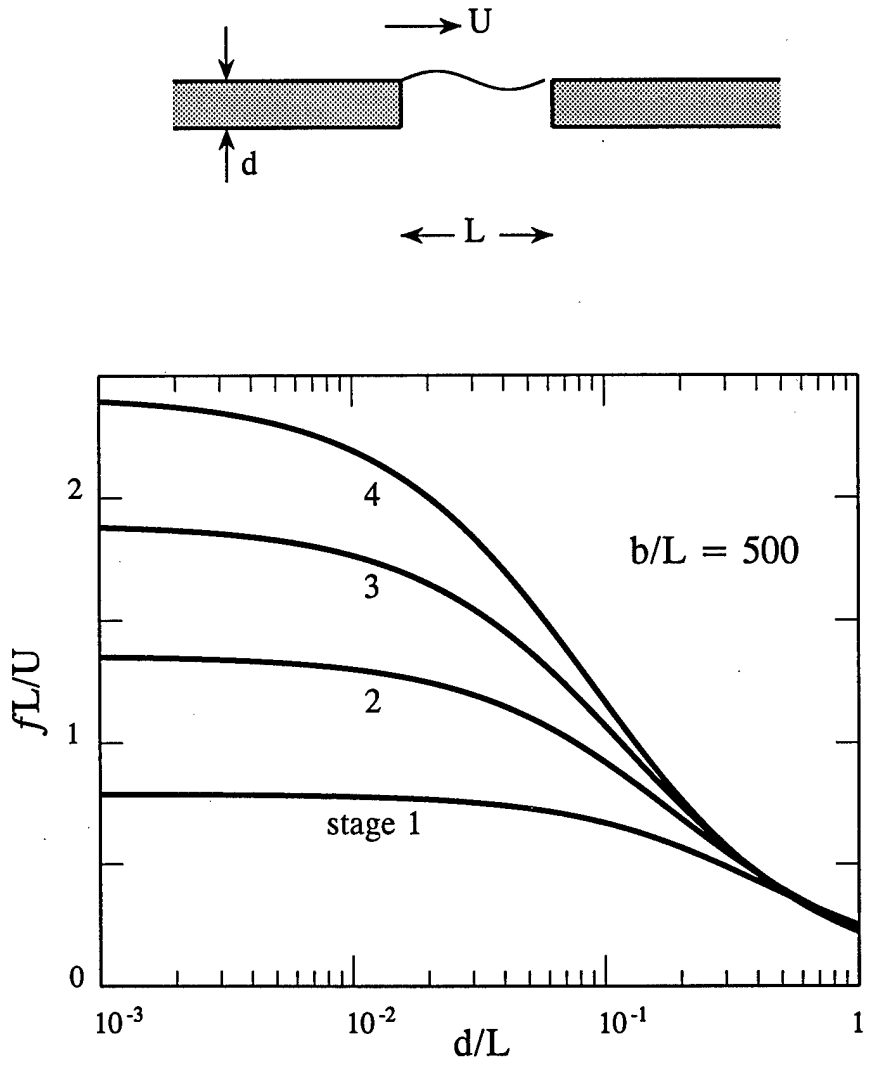

Figure 10. Strouhal number dependence on wall thickness for one-sided flow ($U_- = 0$) when b/L = 500 for the first four operating stages.

CHAPTER 2

INFLUENCE OF CROSS-SECTIONAL SHAPE ON THE CONDUCTIVITY OF A WALL APERTURE

M. S. Howe

SUMMARY

An analysis is made of the effect of cross-sectional shape on the motion induced in a wall aperture by a pressure perturbation in the presence of high Reynolds number tangential flow. Previous studies for circular and rectangular apertures indicate that there is a transfer of energy from the applied perturbation to the mean flow (via the production of vorticity in the aperture) provided the Strouhal number based on aperture diameter and mean velocity is small. In this chapter we consider apertures whose cross-sections are symmetrically tapered in a direction parallel to the mean flow. For highly tapered apertures of trapezoidal cross-section, it is found that low Strouhal number damping is confined to a smaller range of frequencies. Self-sustaining oscillations of the shear layers spanning the aperture can occur at certain discrete frequencies, which correspond to the real parts of complex eigenfrequencies of the aperture motion having *positive* imaginary parts. The eigenfrequencies are poles of the Rayleigh conductivity, and are found to vary in proportion to U/L, where U is mean flow speed and L is the maximum streamwise length of the aperture, but to be only weakly dependent on aperture shape.

1. INTRODUCTION

Sound incident on small apertures in the presence of mean flow is frequently dissipated via the production of vortical kinetic energy that is swept away by the flow [1]. The absorption can be enhanced over well defined ranges of frequencies when the apertures are backed by resonant cavities [2, 3]. Under certain conditions, narrow band acoustic tones may be generated spontaneously at the aperture, even when the mean flow is nominally steady and there is no applied pressure [4]. The tones are often heard over distinct "operating stages" within which the Strouhal number based on aperture dimension and mean flow velocity varies over a finite range controlled by an acoustic or hydrodynamic *feedback*. The feedback is related to the periodic shedding of vorticity from an edge, its convection over the aperture, and the subsequent production of impulsive pressures when the vorticity impinges on a downstream edge [5]. The tonal amplitude varies with flow speed and exhibits discontinuous changes in frequency as the system jumps between different operating stages, in accordance with various well known empirical laws [5 - 9].

There is no general theory of feedback controlled by vortex shedding at arbitrary Mach number (particular approximations are discussed in [10 - 15]), but a deductive theory of the resonance stages has been proposed by the author [16] for cases of low Mach number, high Reynolds number flow over an acoustically compact aperture in a plane wall. The Strouhal number of an operating stage is identified with the real part of a pole in the upper half of the complex frequency plane of the Rayleigh conductivity of the aperture [17]. The conductivity is calculated according to linear perturbation theory, by approximating the shear layer over the aperture by a *linearly* disturbed vortex sheet. Nonlinearity must limit the growth of instabilities predicted by this approach, but it is argued that the finite amplitude of the real motion will not significantly change Strouhal number predictions of linear theory, because feedback is controlled by the convection velocity U_c of disturbances across the aperture, which experiments suggest to be effectively independent of amplitude [18 - 20]. Further justification is given in [16],

where predictions (based on the same theory) of the operating stages of jet-edge interactions and shallow wall cavities are shown to be in excellent agreement with experiment.

The theory of reference [16] is applicable to rectangular apertures in a wall of infinitesimal thickness, and is an extension of a numerical investigation of the conductivity of a circular aperture in the presence of flow performed by Scott [21, 22]. The influence of small, but finite wall thickness is considered in [23]. In applying idealized models of this kind to practical problems involving, say, the interaction of sound waves with a sparsely perforated screen in a mean flow, it is also desirable to know the likely effects of varying the shape of the aperture cross-section (for shapes other than circular or rectangular). It would then be possible to ascertain, for example, whether it is possible to optimize the attenuation of sound by the screen by a suitable adjustment of aperture shape and dimensions. Similar considerations are important for vortex shedding devices used to absorb structural vibrations [24], examples of which are discussed in Chapters 6 and 7.

In this chapter we investigate the influence of cross-sectional shape for a class of "tapering" apertures that have one straight edge normal to the flow, and an axis of symmetry parallel to the mean flow direction. Predictions are given for cases involving flow on one or both sides of the wall at very high Reynolds number, when free shear layers may be modeled by vortex sheets. The motion is stable when the mean flow is the same on both sides of the wall and the wall has negligible thickness (when, for an ideal fluid, the mean vorticity vanishes in the steady state [22]), but becomes unstable at finite thickness, giving rise to self-sustaining aperture oscillations and sound generation. One-sided flow over the aperture (which is then spanned by a plane vortex sheet in the undisturbed state) is always unstable, and finite wall thickness merely changes the Strouhal numbers of the self-sustained oscillations. Reverse flow reciprocity can be invoked to argue that the conductivity and instability Strouhal numbers are unchanged when the direction of the mean flow is reversed. We present detailed results for an aperture of trapezoidal cross-section that is symmetric with respect to the direction of the mean flow. It is concluded that permissible Strouhal numbers

of self-sustained oscillations for symmetric shapes of this kind scale with the maximum aperture dimension in the streamwise direction, but that the damping of an incident pressure field at low Strouhal numbers is confined to progressively smaller frequencies as the tapering increases.

The analytical model is formulated in §2 for a general symmetric, tapering aperture in the presence of an arbitrary, two-sided, low Mach number, high Reynolds number flow. Specific results are given in §§3, 4 respectively for two-sided uniform flow and one sided flow past an aperture of trapezoidal cross-section.

2. THE GOVERNING EQUATIONS

2.1 The Rayleigh conductivity

Consider fluid of uniform mean density ρ_o in nominally steady, low Mach number, high Reynolds number flow over both sides of an aperture in a plane, rigid wall of thickness d. The midplane of the wall coincides with the plane $x_2 = 0$ of the rectangular coordinate system (x_1, x_2, x_3). The mean flow is parallel to the x_1-axis with main stream velocities U_+ and U_- in the "upper" and "lower" regions $x_2 \gtrless \pm\frac{1}{2}d$ respectively. Attention is confined to the set of tapering apertures of the type illustrated schematically in Figure 1. The "leading edge" of the aperture is assumed to be straight, and to occupy the interval $x_1 = -s \equiv -L/2$, $|x_3| < b_o/2$, where L denotes the maximum length of the aperture in the streamwise direction, and b_o is the maximum spanwise dimension (at the leading edge). Over the interval $-s < x_1 < s$ of length L, the aperture is symmetric about the x_1-axis, with side edges defined in the x_1x_3-plane by $x_3 = \pm b(x_1)/2$, where $b(x_1)$ is required to be either constant or to decrease monotonically with x_1. The shear layers over the upper and lower faces of the aperture are modeled by vortex sheets, and the fluid within the volume of the aperture (in $|x_2| < \frac{1}{2}d$) is taken to be in a mean state of rest.

Uniform, small amplitude, time-dependent pressures $p_\pm(t)$ are applied in the vicinity of the aperture respectively in the upper and lower regions. The resulting disturbances of the vortex sheets are assumed to be governed by linearized equations of motion. The aperture volume flux Q(t) produced by the pressure differential

$$[p_o(t)] \equiv p_+(t) - p_-(t)$$

can be expressed in the form

$$\rho_o \partial Q(t)/\partial t = -\int_{-\infty}^{\infty} K_R(\omega)\,[p_o(\omega)]\,e^{-i\omega t}\,d\omega, \qquad (1)$$

where $K_R(\omega)$ is the Rayleigh conductivity [17], which is a function of the radian frequency ω with the dimensions of length, and

$$[p_o(\omega)] \equiv (1/2\pi)\int_{-\infty}^{\infty} [p_o(t)]\,e^{i\omega t}\,dt$$

is the Fourier transform of $[p_o(t)]$.

For time-harmonic fluctuations, where $[p_o(t)] \equiv \mathrm{Re}\{[p_o(\omega)]e^{-i\omega t}\}$, the power $\Pi(\omega)$ dissipated at the aperture by the applied pressure field can be expressed in terms of the conductivity by making use of the formula

$$\Pi \equiv -\langle Q(t)[p_o(t)]\rangle,$$

where the angle brackets denote a time average. This yields (for $\omega > 0$)

$$\Pi(\omega) = -|[p_o]|^2 \mathrm{Im}\{K_R(\omega)\}/2\rho_o\omega. \qquad (2)$$

Direct thermo-viscous losses are usually negligible at high Reynolds numbers, when most of the dissipation is caused by the transfer of energy from the applied pressure (an incident sound wave, say) to the kinetic energy of vorticity generated in the aperture. Equation (2) shows that this occurs provided $\mathrm{Im}\{K_R(\omega)\} < 0$ (when $\omega > 0$). The damping is *negative* if $\mathrm{Im}\{K_R(\omega)\} > 0$, in which case energy is *extracted* from the mean flow. When the fluid is compressible Q determines the amplitude of an effective acoustic monopole source at the aperture, and a net gain in perturbation energy would result in increased levels of radiation from the aperture on either side of the wall.

In practice an arbitrary flow disturbance can trigger instabilities of the aperture flow, and result in oscillations and acoustic radiation at one or more preferred frequencies. These instabilities are associated with singularities of the conductivity $K_R(\omega)$ in the upper half of the complex frequency plane [16]. Indeed, although equation (1) determines Q(t) in terms of the applied pressure differential $[p_o(t)]$, a strictly *causal* evaluation of the integral requires the path of integration from $\omega = \pm\infty$ to pass *above* the singularities of the integrand in the ω-plane. Since $p_\pm(t)$ may be assumed to vanish prior to some finite time in the past, $[p_o(\omega)]$ is regular in $\mathrm{Im}\{\omega\} > 0$, and any singularities are associated with the conductivity $K_R(\omega)$. These singularities are simple poles for circular and rectangular apertures [16, 21 - 23], and will be shown to be poles also for the set of apertures discussed in this chapter. Experiments on jet-edge interactions and shallow wall cavities, for which the same type of theory is applicable, indicate [16] that the real part of the complex frequency at these poles, determined according to idealized, linear perturbation theory, may be identified with the frequency of an operating stage of the self-sustained oscillations of the aperture flow for the real, nonlinear system.

2.2 The thin wall approximation

The equations of motion of the vortex sheets spanning the aperture openings of Figure 1 are similar to those discussed in [16, 22] for circular and rectangular apertures in a wall of zero thickness, and only a brief outline of the derivation is needed here.

Let the aperture be excited by a time-harmonic, uniform pressure differential $[p_o(\omega)]e^{-i\omega t}$, and denote respectively by $\zeta_\pm(x_1,x_3)e^{-i\omega t}$ the displacement (in the x_2-direction) of the upper and lower vortex sheets from their undisturbed positions $x_2 = \pm\frac{1}{2}d$. The flow Mach numbers are assumed to be sufficiently small that the motion in the neighborhood of the aperture may be treated as incompressible, so that the following linearized formulae for the perturbation pressures above and below the wall are applicable

$$\left.\begin{aligned} p &= p_+ - \rho_o\left(\omega+iU_+\frac{\partial}{\partial x_1}\right)^2\int_S \frac{\zeta_+(y_1,y_3)}{2\pi|x-y|}\,dy_1dy_3, \quad x_2 > \tfrac{1}{2}d \\ &= p_- + \rho_o\left(\omega+iU_-\frac{\partial}{\partial x_1}\right)^2\int_S \frac{\zeta_-(y_1,y_3)}{2\pi|x-y|}\,dy_1dy_3, \quad x_2 < -\tfrac{1}{2}d, \end{aligned}\right\} \tag{3}$$

where respectively $y = (y_1,\pm\frac{1}{2}d,y_3)$, the integration is over the aperture cross-section S, and the exponential time factor $e^{-i\omega t}$ is here and henceforth suppressed.

We now introduce the *thin wall* approximation, in which the wavelength of vortex sheet motions is restricted to be large compared to the wall thickness d. The x_2-component ζ of the fluid displacement within the aperture may then be regarded as independent of x_2, i.e.

$$\zeta \equiv \zeta(x_1,x_3) = \zeta_+(x_1,x_3) = \zeta_-(x_1,x_3), \tag{4}$$

and the equation of motion of a "column" of fluid within the aperture is

$$\rho_o d\partial^2\zeta/\partial t^2 = -[p], \quad |x_1| < s, \ |x_3| < \tfrac{1}{2}b(x_1), \tag{5}$$

where [p] is the difference in the pressures applied to the upper and lower ends of the column at $x_2 = \pm\frac{1}{2}d$, determined by equations (3). Thus, substituting from (3) into (5) we find, for time-harmonic motion,

$$\left[\left(\omega+iU_+\frac{\partial}{\partial x_1}\right)^2+\left(\omega+iU_-\frac{\partial}{\partial x_1}\right)^2\right]\frac{1}{2\pi}\int_S \frac{\zeta(y_1,y_3)dy_1dy_3}{\sqrt{(x_1-y_1)^2+(x_3-y_3)^2}} + d\omega^2\zeta(x_1,x_3) = \frac{[p_o]}{\rho_o}. \tag{6}$$

According to Figure 1 the aperture motion involves the unsteady shedding of vorticity from the straight leading edge $x_1 = -s$ of the aperture. Equation (6) is considerably simplified by means of the hypothesis that this shedding produces strongly correlated motions of the vortex sheets at different transverse locations x_3, and that ζ may therefore be assumed to be independent of x_3. To be sure, observations [11 - 13, 15] suggest that, although the laterally uniform shed vorticity interacts with different parts of the downstream edge at different times, the aggregate back reaction on the leading edge is equivalent to an average back reaction that causes the stability characteristics to be the same as those of a rectangular aperture of intermediate length. By explicitly performing the integration in (6) with respect to y_3 over the interval $-\frac{1}{2}b(y_1) < y_3 < \frac{1}{2}b(y_1)$, and also integrating the equation with respect to x_3 (over $-\frac{1}{2}b(x_1) < x_3 < \frac{1}{2}b(x_1)$), we can then re-cast (6) in the following dimensionless form:

$$\left[\left(\sigma+i\frac{\partial}{\partial\xi}\right)^2+\left(\sigma+i\mu\frac{\partial}{\partial\xi}\right)^2\right]\int_{-1}^{1} Z(\eta)\{\ln|\xi-\eta| + \mathcal{L}(\xi,\eta)\}d\eta - \pi\left(\frac{d}{s}\right)\sigma^2 Z(\xi) = 2\sigma^2\bar{\beta}(\xi),$$

$$|\xi| < 1, \tag{7}$$

where Z is an effective dimensionless displacement defined by

$$Z(\xi) = \frac{-2\rho_o\omega^2 s}{\pi[p_o]b_o}\, b(\xi)\zeta(\xi), \tag{8}$$

and

$$\sigma = \omega s/U_+,\ \mu = U_-/U_+,\ \xi = x_1/s,\ \eta = y_1/s, \tag{9}$$

$$\mathcal{L}(\xi,\eta) = \frac{1}{2\beta(\eta)}\Big\{[\beta(\xi)-\beta(\eta)]\ln\Big[\beta(\xi)-\beta(\eta) + \sqrt{(\xi-\eta)^2+\{\beta(\xi)-\beta(\eta)\}^2}\Big]$$

$$- [\beta(\xi)+\beta(\eta)]\ln\Big[\beta(\xi)+\beta(\eta) + \sqrt{(\xi-\eta)^2+\{\beta(\xi)+\beta(\eta)\}^2}\Big]$$

$$- \sqrt{(\xi-\eta)^2+\{\beta(\xi)-\beta(\eta)\}^2} + \sqrt{(\xi-\eta)^2+\{\beta(\xi)+\beta(\eta)\}^2}\Big\}, \tag{10}$$

$$\beta(\xi) = b(x_1)/2s,\ \bar{\beta}(\xi) = b(x_1)/b_o \equiv (2s/b_o)\beta(\xi). \tag{11}$$

We next integrate equation (7) with respect to the second order differential operator on the left hand side by introducing the Green's function

$$G(\xi,\eta) = \frac{1}{2\sigma(1-\mu)}\left\{H(\xi-\eta)e^{i\sigma_+(\xi-\eta)} + H(\eta-\xi)e^{i\sigma_-(\xi-\eta)}\right\}, \tag{12}$$

which is a particular solution of

$$\left[\left(\sigma+i\frac{\partial}{\partial\xi}\right)^2 + \left(\sigma+i\mu\frac{\partial}{\partial\xi}\right)^2\right]G(\xi,\eta) = \delta(\xi-\eta).$$

In these formulae, H(x) is the Heaviside unit function (= 0, 1 according as $x \lessgtr 0$), and $\sigma_\pm$ are the Kelvin-Helmholtz wavenumbers [25]

$$\sigma_\pm = \sigma\left(\frac{1\pm i}{1\pm i\mu}\right). \tag{13}$$

By this means the effective displacement Z is found to satisfy

$$\int_{-1}^{1} Z(\eta)\{\ln|\xi-\eta|+\mathcal{L}(\xi,\eta)\}d\eta - \pi\sigma^2(d/s)\int_{-1}^{1} Z(\eta)G(\xi,\eta)d\eta$$

$$+ \lambda_+ e^{i\sigma_+\xi} + \lambda_- e^{i\sigma_-\xi} = F(\sigma,\xi), \quad |\xi| < 1, \tag{14}$$

where $\lambda_\pm$ are constants of integration, and $F(\sigma,\xi)$ is a particular integral of the term $2\sigma^2\overline{\beta}(\xi)$ on the right of (7) with respect to the second order differential operator.

The integral equation (14) is solved by collocation, by the procedure described by Scott [21] for a vortex sheet over a circular aperture. The values of $\lambda_\pm$ are fixed by imposing the Kutta condition that the vortex sheets should leave the upstream edge of the aperture smoothly, i.e., by requiring that $\zeta = \partial\zeta/\partial\xi = 0$ as $\xi \to -1$ [26], which is equivalent to

$$Z = \partial Z/\partial\xi = 0 \text{ at } \xi = -1. \tag{15}$$

Potential theory implies that the displacement has a mild, yet integrable singularity where the vortex sheet impinges on the downstream curvilinear aperture edge, at the worst proportional to the inverse square-root of the distance from that edge. This singularity is the linear theory representation of the large amplitude edge motion observed in practice.

The aperture volume flux is calculated from

$$Q(\omega) = -i\omega\int_{-s}^{s} b(x_1)\zeta(x_1)dx_1,$$

from which it follows that the Rayleigh conductivity is given in terms of Z by

$$K_R = -\tfrac{\pi}{2}b_o\int_{-1}^{1} Z(\eta)d\eta. \tag{16}$$

The conductivity is a complex valued function of the frequency ω, and also depends on the aperture shape, the wall thickness ratio d/L, and the mean velocity ratio $\mu = U_-/U_+$.

In the special case of uniform, two sided mean flow, where $U_- = U_+ \equiv U$, the wavenumbers σ_+ and σ_- are both equal to $\sigma = \omega s/U$, and Green's function (12) may be taken in the form

$$G(\xi,\eta) = -H(\xi-\eta)(\xi-\eta)e^{i\sigma(\xi-\eta)}. \tag{17}$$

The terms in $\lambda_\pm$ in equation (14) are now replaced by $(\lambda_1 + \lambda_2\xi)e^{i\sigma\xi}$, where λ_1, λ_2 are constants determined by the Kutta condition.

2.3 Reciprocity

A simple extension of the reverse flow reciprocal theorem [28, 29] can be used to show (see [22]) that the conductivity $K_R(\omega)$ determined by (16) for the aperture of Figure 1 is unchanged when the mean flow directions above and below the wall are reversed. The reciprocal theorem for an ideal fluid of uniform mean density, implies that $\varphi(\mathbf{x}_B,\mathbf{x}_A,\omega) \equiv \varphi^R(\mathbf{x}_A,\mathbf{x}_B,\omega)$, where $\varphi(\mathbf{x},\mathbf{x}_A,\omega)$, $\varphi^R(\mathbf{x},\mathbf{x}_B,\omega)$ are the perturbation velocity potentials produced by equal volume point sources located respectively at $\mathbf{x}_A$ in the direct problem and at $\mathbf{x}_B$ in the reciprocal problem, provided the mean flow is reversed in the reciprocal problem. The theorem remains valid in the presence of vortex sheets spanning the wall aperture provided that, in both the direct and reciprocal problems, the sheets are *linearly* disturbed from their equilibrium positions, and the Kutta condition is satisfied at the appropriate "leading edge". In the reciprocal flow illustrated in Figure 2, the Kutta condition must be imposed at the curvilinear edge of the aperture, and this is precisely the case that defines the conductivity when the mean flow is reversed. The theorem has been confirmed by recent numerical studies [30] that do not invoke the lateral averaging approximation introduced above to simplify equation (6).

3. UNIFORM, TWO-SIDED FLOW OVER A TRAPEZOIDAL APERTURE

Equations (14), (15) are now applied to the trapezoidal aperture depicted in planform in Figure 3a. The aperture is symmetric with respect to the x_1-axis, with transverse ends at $x_1 = \pm s$ of lengths b_o and b_1 ($\leq b_o$) respectively, in terms of which

$$\bar{\beta}(\xi) = 1 + \tfrac{1}{2}\left(\frac{b_1}{b_o} - 1\right)\xi, \qquad F(\sigma,\xi) = \bar{\beta}(\xi) - i\left(\frac{b_1}{b_o} - 1\right)\frac{(1+\mu)}{\sigma} . \tag{18}$$

In this section we consider the particular case in which the mean flows have equal speeds $U_+ = U_- \equiv U$ above and below the aperture.

3.1 Dependence of Rayleigh conductivity on b_1/b_o

In Figures 3b and 3c the real and imaginary components Γ_R, Δ_R of the dimensionless conductivity, defined by

$$K_R(\omega)/\sqrt{A} = \Gamma_R(\omega) - i\Delta_R(\omega), \tag{19}$$

are plotted against real values of $\sigma = \omega s/U$, for $b_o/L = 1$ and $d \equiv 0$, for the two characteristic cases $b_1/b_o = 1$ and 0.1 respectively, where

$$A = s(b_o+b_1) \equiv \tfrac{1}{2}L(b_o+b_1)$$

is the area of the aperture. The first of these corresponds to a square aperture and the second approximates to a triangular profile with apex angle close to 50°. K_R is calculated from the numerical solution of (14) modified as described at the end of §2.2 by using the degenerate Green's function (17). According to Figure 3b, Γ_R and Δ_R are periodic functions when $\omega s/U$ exceeds about 2. The particular results shown in Figure 3c are typical of all values of $b_1/b_o < 1$. The real and imaginary parts of K_R again exhibit wavelike variations with frequency, but the waveforms are now sharper than for the square aperture, essentially because singularities (poles) of $K_R(\omega)$ occurring at complex frequencies tend to be closer to the real axis (cf. [23]). Equation (2) implies that perturbation energy is dissipated in the aperture when $\Delta_R(\omega) > 0$, and Figure 3 shows that the intervals where this is the case

are effectively the same for the square and tapered apertures, except for the first, low frequency interval, where tapering reduces the width of the dissipative zone by about a half. Figure 3c also exhibits a gradual decrease with increasing frequency in the amplitude of the oscillations of Γ_R and Δ_R; this is similar to the results given in [21, 22] for the circular aperture, but does not occur for the square aperture.

3.2 Flow instability for finite wall thickness

When the wall has zero thickness (d = 0) and the flow is the same on both sides ($U_+ = U_-$), the unsteady aperture motion is stable, in the sense that self-sustaining oscillations cannot be maintained by the extraction of energy from the mean flow. According to (2), energy is extracted from the flow at those excitation frequencies in Figure 3 where $\Delta_R(\omega) < 0$. But this instability is *conditional*, inasmuch as the oscillations do not persist once the exciting pressure $[p_o]e^{-i\omega t}$ is removed. On the basis of linear theory, absolute instabilities are associated with singularities of the conductivity $K_R(\omega)$ in $\mathrm{Im}(\omega) > 0$. These singularities are typically simple poles of $K_R(\omega)$; they are eigenvalues of equation (14), and are independent of both $F(\sigma,\xi)$ and the assumption that the driving pressures $p_\pm$ are uniform.

To see this, the integrals over (-1,+1) on the left of equation (14) are discretized by using a convenient Gauss integration formula that expresses them in terms of the integrands evaluated at N lattice points ξ_i $(1 \le i \le N)$. For such a scheme $\xi_1 = -1 + \delta$, $\xi_N = +1 - \delta$, where $\delta \to +0$ as N becomes large. The Kutta condition (15) is applied by requiring $Z_1 = Z_2 = 0$, where $Z_i \equiv Z(\xi_i)$. The discretized form of equation (14) may then written

$$\sum_{j=1}^{N} \mathfrak{C}_{ij} \bar{Z}_j = F(\sigma,\xi_i), \quad i = 1 \text{ to } N, \tag{20}$$

where

$$\bar{Z}_1 = \lambda_+, \ \bar{Z}_2 = \lambda_-, \text{ and } \bar{Z}_i \equiv Z_i \text{ for } i \ge 3.$$

For each fixed value of i,

$$\mathfrak{C}_{i1} = e^{i\sigma_+\xi_i}, \quad \mathfrak{C}_{i2} = e^{i\sigma_-\xi_i},$$

and $\mathfrak{C}_{ij}$ $(j \ge 3)$ depends only on the integration scheme used to approximate

the integrals in (14). The eigenvalues $\sigma_n = \omega_n s/U$ of (20) are the (generally complex) roots of the equation

$$\det(\mathfrak{C}_{ij}) = 0. \tag{21}$$

Cramer's rule [27] and (16) now imply that the singularities of $K_R(\omega)$ are poles and coincide with the roots of (21). When $U_+ = U_-$ and $d = 0$, they all lie in the lower half of the frequency plane ($\mathrm{Im}\{\omega\} < 0$). The first four (n = 1 to 4, defined such that their positive real parts *increase* with n) have been determined from (21) by Newton-Raphson iteration, and are shown by the points labeled "0" in Figure 4 for the case $b_1/b_o = 0.1$ and $b_o/L = 1$. The real parts ω_r of these successive zeros differ by about π, and comparison with Figure 3c reveals that they correspond approximately to the real frequencies of the successive minima of $\Gamma_R(\omega)$.

When the wall thickness $d \neq 0$, vortex sheets span the upper and lower faces of the aperture in the absence of external excitation, and the aperture motion must be expected to be unstable. This suggests that the roots of equation (21) cross the real axis into the upper frequency plane, and the curves in Figure 4 show how this occurs for the first four operating stages. High order instabilities (n large) are excited first when d/L increases from zero, and all modes are unstable when d/L exceeds about 0.02. When d/L *decreases* from this value, the poles corresponding to n = 1, 2, 3, etc, successively cross into the lower half plane; the first four stages are stable when d/L is less than about 7.5×10^{-4}. As d/L increases the complex operating frequencies are seen to converge towards the imaginary axis, their real parts becoming approximately equal; however, the thin wall approximation requires d/L to be small, and probably breaks down before this limiting behavior is realized. According to the experimental results discussed in [16], the real parts of the complex operating frequencies correspond to the Strouhal numbers of self-sustaining oscillations of fluid in the aperture. The dependence of these Strouhal numbers fL/U on d/L (where $f = \mathrm{Re}(\omega)/2\pi$ for a root ω of equation (21)) is illustrated by the solid curves in Figure 5 for the first four operating stages (for $b_o/L = 1$, $b_1/b_o = 0.1$) Each curve starts on the left at that non-zero value of d/L at which the corresponding root of (21) crosses into the upper frequency plane. The dotted curves are analogous predictions for the square aperture ($b_o = b_1$); corresponding modes are seen to become unstable at larger values of d/L. These results imply that the

Strouhal numbers of different trapezoidal apertures are approximately the same when based on the *total aperture length* in the streamwise direction.

It is also instructive to examine the structural changes in $K_R(\omega)$ for real frequencies when d/L increases from zero. The real and imaginary components $\Gamma_R(\omega)$, $\Delta_R(\omega)$ have the near periodic forms shown in Figure 3c when d = 0 and $b_1/b_o = 0.1$, $b_o/L = 1$. The influence of small, but finite wall thickness is always felt at sufficiently high frequencies, when the second integral on the left of equation (14), which represents the *inertia* of fluid in the aperture, becomes important. This causes the oscillations in the real and imaginary parts of $K_R(\omega)$ ultimately to die out as σ becomes large. The variations of Γ_R and Δ_R for the four different wall thicknesses d/L = 0.007, 0.01, 0.03 and 0.1 are depicted respectively in Figures 6a - 6c. In Figure 6a the second stage pole of $K_R(\omega)$ (i.e., the n = 2 root of (21)) is close to the real axis in the upper frequency plane. When d/L increases to 0.01 the first stage pole is approaching the real axis from below, and this is reflected in Figure 6b by the more rapid variations of Γ_R and Δ_R near $\omega R/U = 4$; this pole has crossed the real axis in Figure 6c, where the former deep minimum of Γ_R is replaced by a sharp maximum, and the variations in Γ_R and Δ_R at higher frequencies are smoother because higher order poles are now further from the real axis. When d/L has increased to 0.1 all of the poles are far from the real axis and the conductivity assumes the characteristic form shown in Figure 6d, which is very similar to that for *one-sided* flow over the same aperture (see §4).

4. ONE-SIDED FLOW OVER A TRAPEZOIDAL APERTURE

4.1 The conductivity for zero wall thickness

Let the mean flow be confined to the upper region $x_2 > \frac{1}{2}d$, over the trapezoidal aperture of Figure 3a (so that $U_- \equiv 0$). In the undisturbed state a vortex sheet separates the uniform flow at speed $U_+ \equiv U$ from the stagnant fluid within and below the aperture. The sheet is unstable for arbitrary wall thickness d, and $K_R(\omega)$ has poles in $\mathrm{Im}(\omega) > 0$. Representative plots of $K_R(\omega)/\sqrt{A}$ for real frequencies are given in Figure 7 for d = 0, when $b_o/L = 1$ and $b_1/b_o = 0.01$, 0.1 and 1. All of these plots are structurally similar, and exhibit damping of the applied disturbance by vorticity production when ω is smaller than a critical frequency ω_c, say (where $\Delta_R(\omega) > 0$) which, however, becomes progressively smaller as b_1/b_o decreases.

They are also similar in form to the conductivity illustrated in Figure 6d for two sided, uniform flow ($U_- = U_+$) over a wall of finite thickness d/L = 0.1, and indeed the conductivity $K_R(\omega)$ for one sided flow over a thin wall also has a similar distribution of instability poles in the upper frequency plane. The variations in the positions of these poles with the ratio b_1/b_o for the first four stages (n = 1 to 4) are shown in Figure 8 for the case $b_o/L = 1$, d/L = 0. By means of the identification $f = \mathrm{Re}(\omega)/2\pi$, the dependence on b_1/b_o of the corresponding Strouhal numbers fL/U may be calculated; Figure 9 reveals that the Strouhal number changes by about $\frac{1}{2}$ between neighboring stages and, in particular (as in the case of two sided flow over a wall of finite thickness, see Figure 5), is only weakly dependent on the shape of the aperture.

4.2 Influence of finite wall thickness

For real values of ω the conductivities $K_R(\omega)$ displayed in Figure 7 do not vary significantly with the trapezoidal shape ratio b_1/b_o. Changes with variations in wall thickness are also small, unlike the case of uniform, two-sided flow discussed in §3, where $K_R(\omega)$ changes rapidly with d/L because of the passage of poles across the real axis. For one-sided flow, the instability poles are already in $\mathrm{Im}(\omega) > 0$ when d = 0, and their subsequent

motions in the complex plane when d/L increases from zero produce relatively minor changes in $K_R(\omega)$. The particular case in which $b_o/L = 1$, $b_1/b_o = 0.1$ is illustrated in Figure 10, where the poles of the first four operating stages are tracked (from initial positions given in Figure 8 for $b_1/b_o = 0.1$) in the complex plane as d/L increases over the range 0 - 0.5. $Re(\omega s/U)$ is approximately the same for these poles when d/L exceeds about 0.4, implying that the Strouhal numbers fL/U of the operating stages become equal, although, as already stressed in §3, the present thin wall theory may not be strictly applicable for such large values of d/L.

5. CONCLUSION

The properties of unsteady flow induced in a wall aperture by an applied, fluctuating pressure (such as an acoustic disturbance) are significantly affected by the presence of mean flow. At the high Reynolds numbers characteristic of many practical situations, vortex shedding from the aperture edges results in an exchange of energy between the mean flow and the applied pressure. In this chapter we have investigated these interactions for a class of apertures whose cross-sections are symmetric with respect to an axis in the mean stream direction and for a wall of small, but finite thickness. Detailed predictions have been given for apertures with tapering (trapezoidal) cross-sections. For two-sided flow, when the mean velocity is the same on both sides of the wall, the motion in the aperture is linearly stable when the wall has zero thickness, but is de-stabilized by finite thickness, when complex eigenfrequencies acquire positive imaginary parts. These eigenfrequencies are poles of the Rayleigh conductivity of the aperture; their values vary in proportion to U/L, where U is mean flow speed and L is the maximum streamwise length of the aperture, but are only weakly dependent on aperture shape (i.e., on the degree of tapering). A comparison with experiment reported in [16] for related physical systems (edge and cavity tones) indicates that the real parts of the complex eigenfrequencies correspond to the tonal frequencies of possible self-sustaining oscillations of the aperture shear layers, the amplitudes of which are controlled by nonlinear mechanisms not considered in this paper.

The motion is always unstable for one-sided flow over a wall aperture. In both this case and also for uniform, two-sided flow, increasing the wall thickness causes the eigenfrequencies to progressively decrease, apparently towards a common limiting value for their real parts, although the approximations made in this paper become invalid before this limit is reached. At sufficiently low Strouhal numbers, forced motion of an aperture by an applied pressure is always damped.

REFERENCES

1. I. L. Vér 1990 *Noise Control Engineering Journal* 35 (Nov/Dec issue) 115 - 125. Practical examples of noise and vibration control: case history of consulting projects.
2. F. P. Mechel and I. L. Vér, I. L. 1992 *Sound absorbing materials and sound absorbers*. Chapter 8 of *Noise and Vibration Control Engineering* (eds. L. E. Beranek and I. L. Vér); New York: John Wiley.
3. I. J. Hughes and A. P. Dowling 1990 *Journal of Fluid Mechanics* 218, 299 - 336. The absorption of sound by perforated linings.
4. D. Rockwell 1983 *American Institute of Aeronautics and Astronautics Journal* 21, 645 - 664. Oscillations of impinging shear layers.
5. J. E. Rossiter 1962 Royal Aircraft Establishment Technical Memorandum 754: *The effect of cavities on the buffeting of aircraft.*
6. L. F. East 1966 *Journal of Sound and Vibration* 3, 277 - 287. Aerodynamically induced resonance in rectangular cavities.
7. H. H. Heller and D. B. Bliss 1975 *American Institute of Aeronautics and Astronautics Paper 75-491*. The physical mechanism of flow-induced pressure fluctuations in cavities and concepts for their suppression.
8. N. M. Komerath, K. K. Ahuja and F. W. Chambers 1987 *American Institute of Aeronautics and Astronautics Paper 87-022*. Prediction and measurement of flows over cavities - a survey.
9. K. K. Ahuja and J. Mendoza 1995 NASA Contractor Report: Final Report Contract NAS1-19061, Task 13. *Effects of cavity dimensions, boundary layer, and temperature on cavity noise with emphasis on benchmark data to validate computational aeroacoustic codes.*
10. C. K. W. Tam and P. J. W. Block 1978 *Journal of Fluid Mechanics* 89, 373 - 399. On the tones and pressure oscillations induced by flow over rectangular cavities.
11. J. C. Bruggeman 1987 PhD. Thesis: *Flow induced pulsations in pipe systems*, Eindhoven University of Technology.
12. J. C. Bruggeman, A. Hirschberg, M. E. H. van Dongen, A. P. J. Wijnands and J. Gorter 1989 *Journal of Fluids Engineering* 111, 484 - 491. Flow induced pulsations in gas transport systems: analysis of the influence of closed side branches.

13. M. C. A. M. Peters 1993 PhD Thesis: *Aeroacoustic sources in internal flows*, Eindhoven University of Technology
14. J. C. Hardin and D. S. Pope 1995 *American Institute of Aeronautics and Astronautics Journal* 33, 407 - 412. Sound generation by flow over a two-dimensional cavity.
15. P. C. Kriesels, M. C. A. M. Peters, A. Hirschberg, A. P. J. Wijnands, A. Iafrati, G. Riccardi, R. Piva and J. C. Bruggeman 1995 *Journal of Sound and Vibration* 184, 343 - 368. High amplitude vortex induced pulsations in gas transport systems.
16. M. S. Howe 1997 *Journal of Fluid Mechanics* 330, 61 - 84. Edge, cavity and aperture tones at very low Mach numbers.
17. Lord Rayleigh 1945 *Theory of Sound*, Vol 2. New York: Dover.
18. A. Powell 1961 *Journal of the Acoustical Society of America* 33, 395 - 409. On the edgetone.
19. D. K. Holger, T. A. Wilson and G. S. Beavers 1977 *Journal of the Acoustical Society of America* 62, 1116 - 1128. Fluid mechanics of the edgetone.
20. W. K. Blake and A. Powell 1986 *The development of contemporary views of flow-tone generation*, pp 247 - 325 in *Recent Advances in Aeroacoustics* (edited by A. Krothapali and C. A. Smith), New York: Springer.
21. M. I. Scott 1995 Master's thesis: *The Rayleigh conductivity of a circular aperture in the presence of a grazing flow*, Boston University.
22. M. S. Howe, M. I. Scott and S. R. Sipcic 1996 *Proceedings of the Royal Society of London* A452, 2303 - 2317. The influence of tangential mean flow on the Rayleigh conductivity of an aperture,
23. Chapter 1 of this report.
24. P. Maung, M. S. Howe and S. I. Madanshetty 1996 *Vibration damping of a perforated flap by vorticity production*. Boston University, College of Engineering Report No. AM96-016.
25. H. Lamb 1932 *Hydrodynamics* (6th. ed., reprinted 1994) Cambridge University Press.
26. D. G. Crighton 1985 *Annual Reviews of Fluid Mechanics*. 17, 411 - 445. The Kutta condition in unsteady flow.

27. G. Dahlquist and Å Björck 1974 *Numerical Methods*. Englewood Cliffs, NJ: Prentice-Hall inc.

28. M. S. Howe 1975 *Journal of Fluid Mechanics* 67, 579 - 610. The generation of sound by aerodynamic sources in an inhomogeneous steady flow.

29. W. Möhring 1979 *Modelling low Mach number noise*, pp 85 - 96, *Proceedings of the Symposium of Mechanics of Sound Generation in Flows*, Göttingen, August 28 - 31 (editor E.-A. Müller: Springer, Berlin, 1979).

30. Chapter 4 of this report.

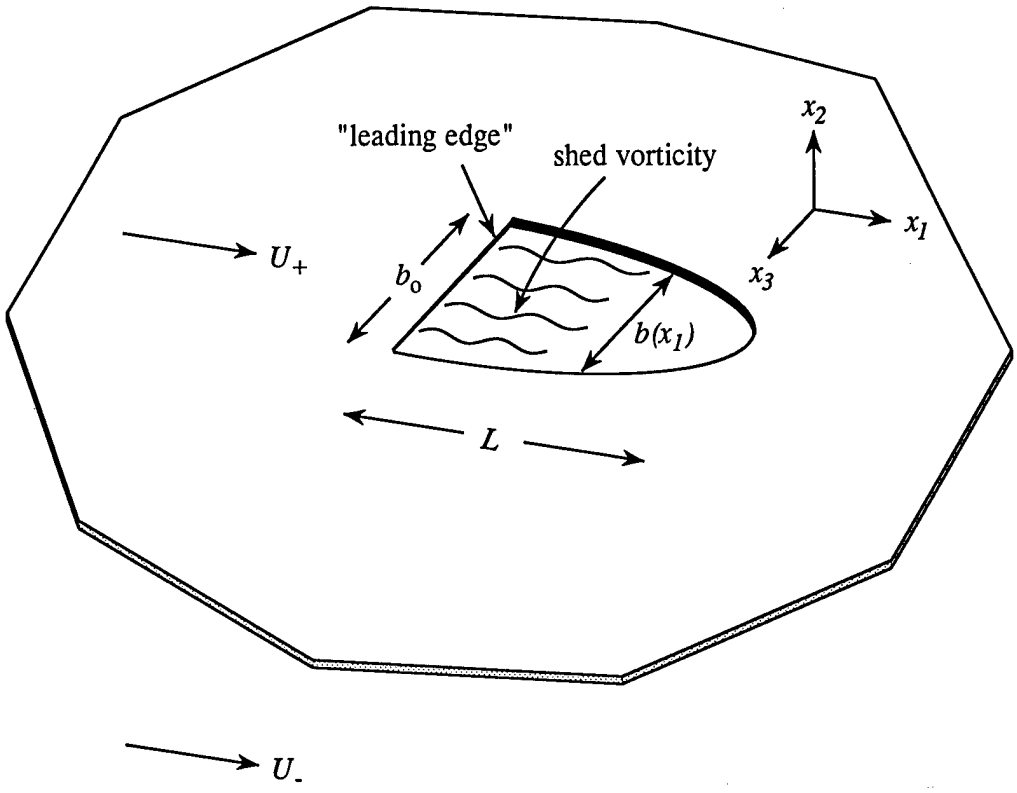

Figure 1. Two-sided flow over a symmetric, tapered aperture with a straight leading edge in a wall of thickness d.

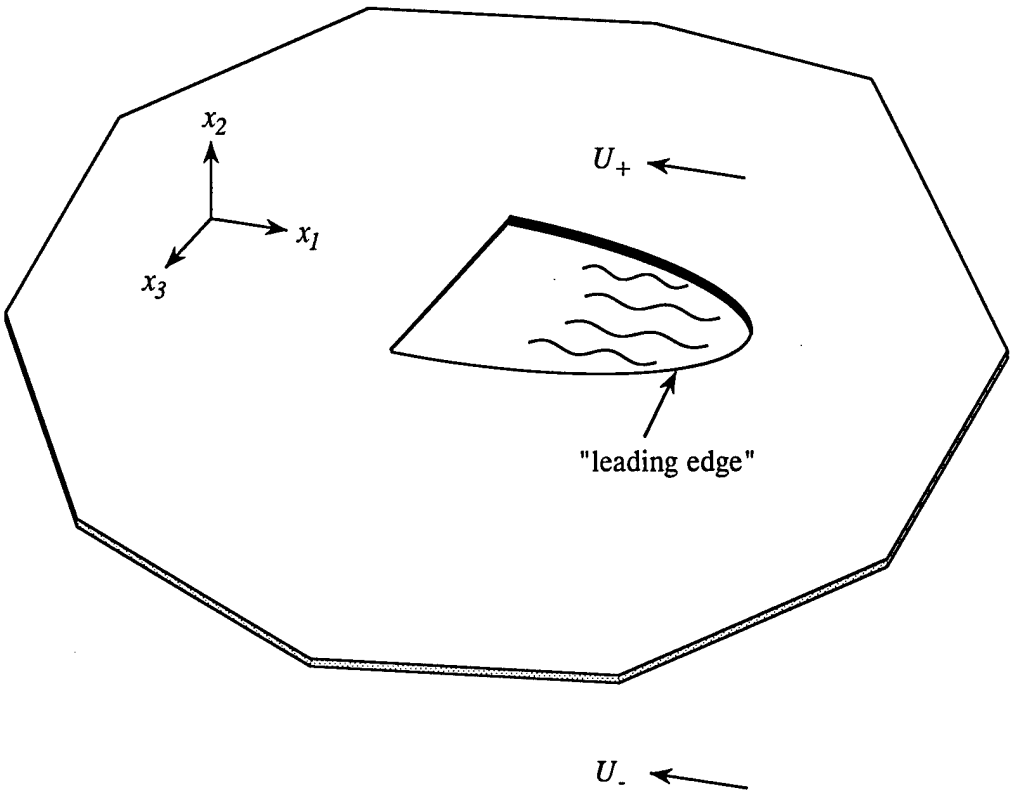

Figure 2. The reciprocal problem.

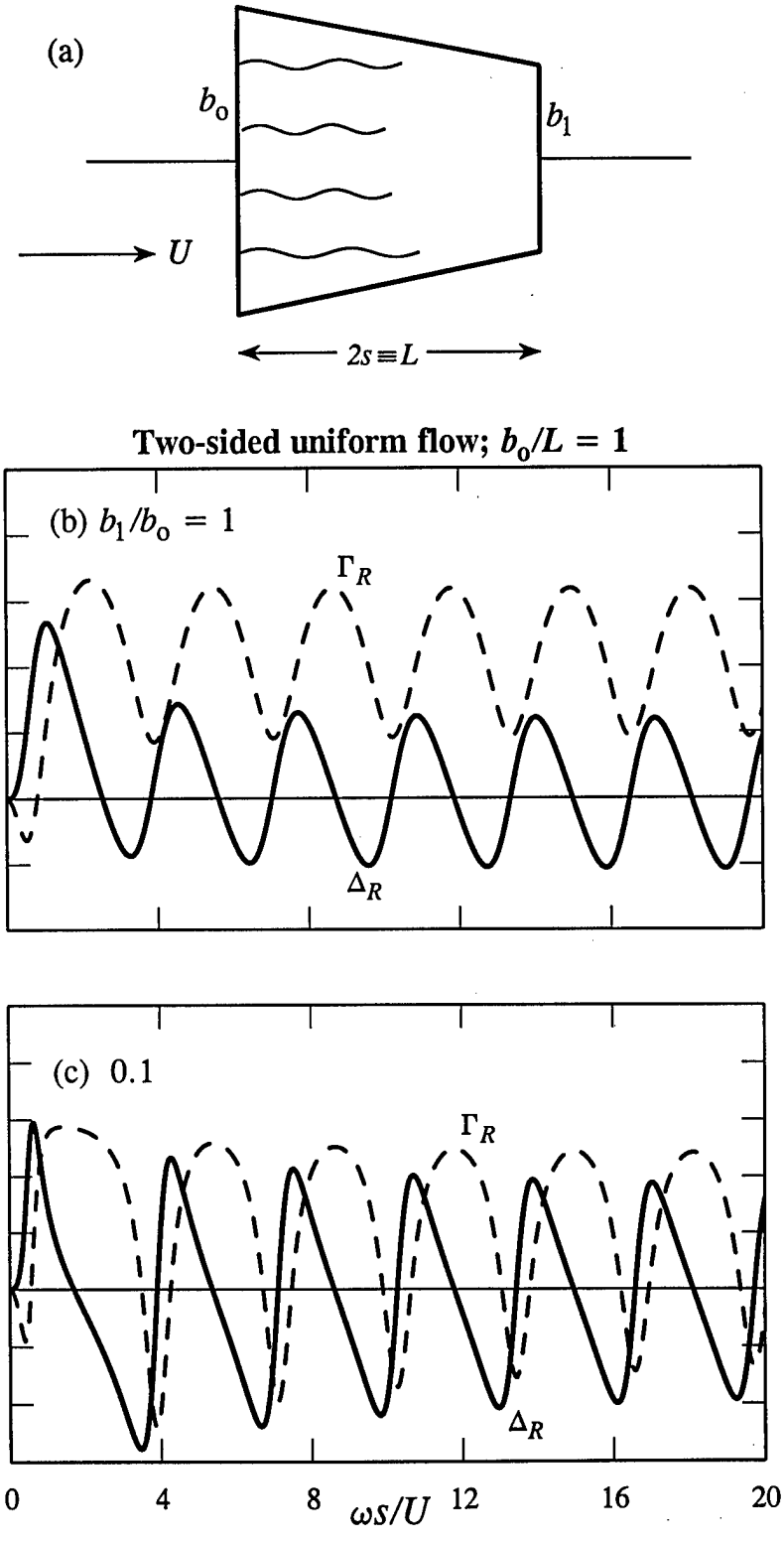

Figure 3. (a) Trapezoidal aperture; (b) The conductivity $K_R(\omega)/\sqrt{A} \equiv \Gamma_R(\omega) - i\Delta_R(\omega)$ for $U_- = U_+$ and $d/L = 0$ for a square aperture, $b_o/L = 1$, $b_1/b_o = 1$; (c) conductivity for $b_o/L = 1$, $b_1/b_o = 0.1$.

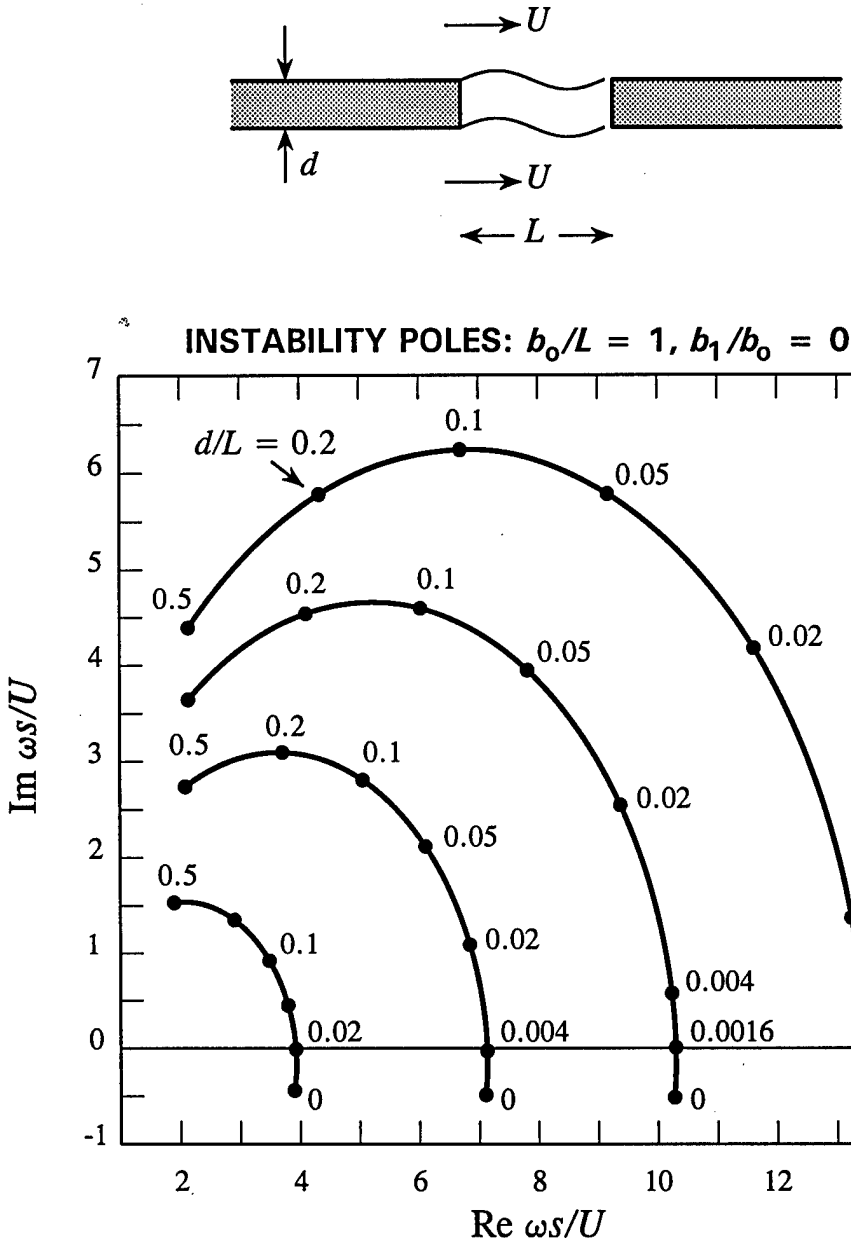

Figure 4. Loci of the complex eigenvalues (zeros of $\det(\mathfrak{C}_{ij})$, poles of K_R) for varying d/L, for the first four operating stages when $U_+ = U_- \equiv U$, $b_o/L = 1$, $b_1/b_o = 0.1$.

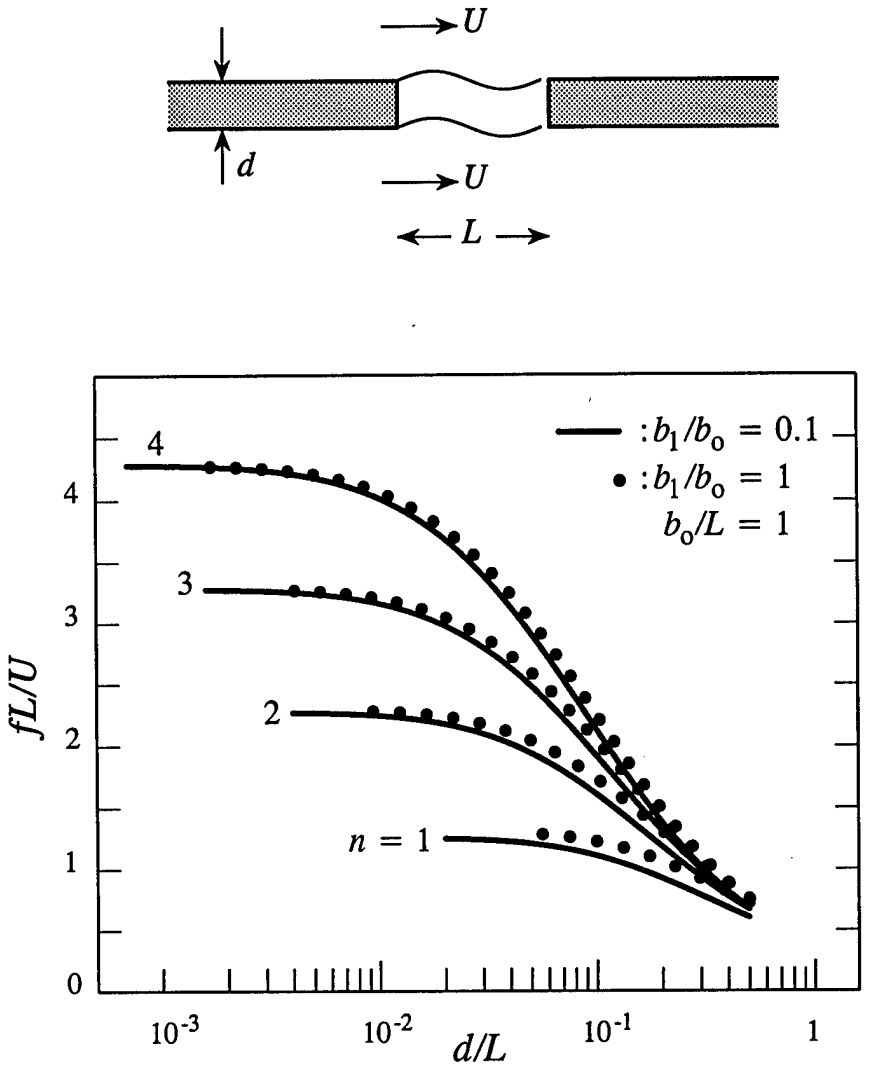

Figure 5. Strouhal number dependence on wall thickness for two-sided uniform flow ($U_+ = U_- \equiv U$) for $b_o/L = 1$: ———, $b_1/b_o = 0.1$; ••••, $b_1/b_o = 1$.

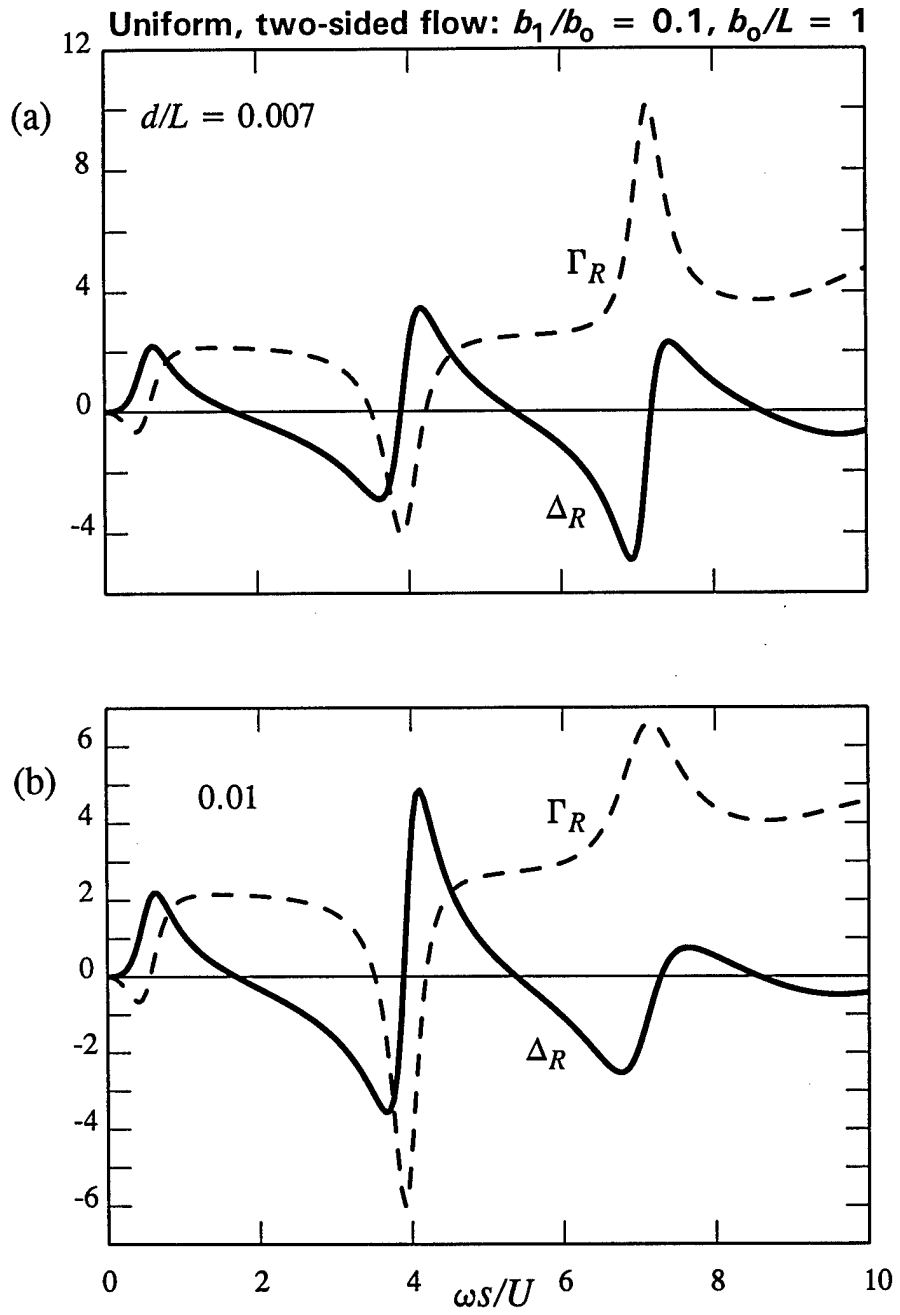

Figure 6. The dependence of $K_R(\omega)/\sqrt{A} = \Gamma_R(\omega) - i\Delta_R(\omega)$ on frequency when $U_- = U_+ \equiv U$, $b_o/L = 1$, $b_1/b_o = 0.1$ and for $d/L = 0.007$, 0.01.

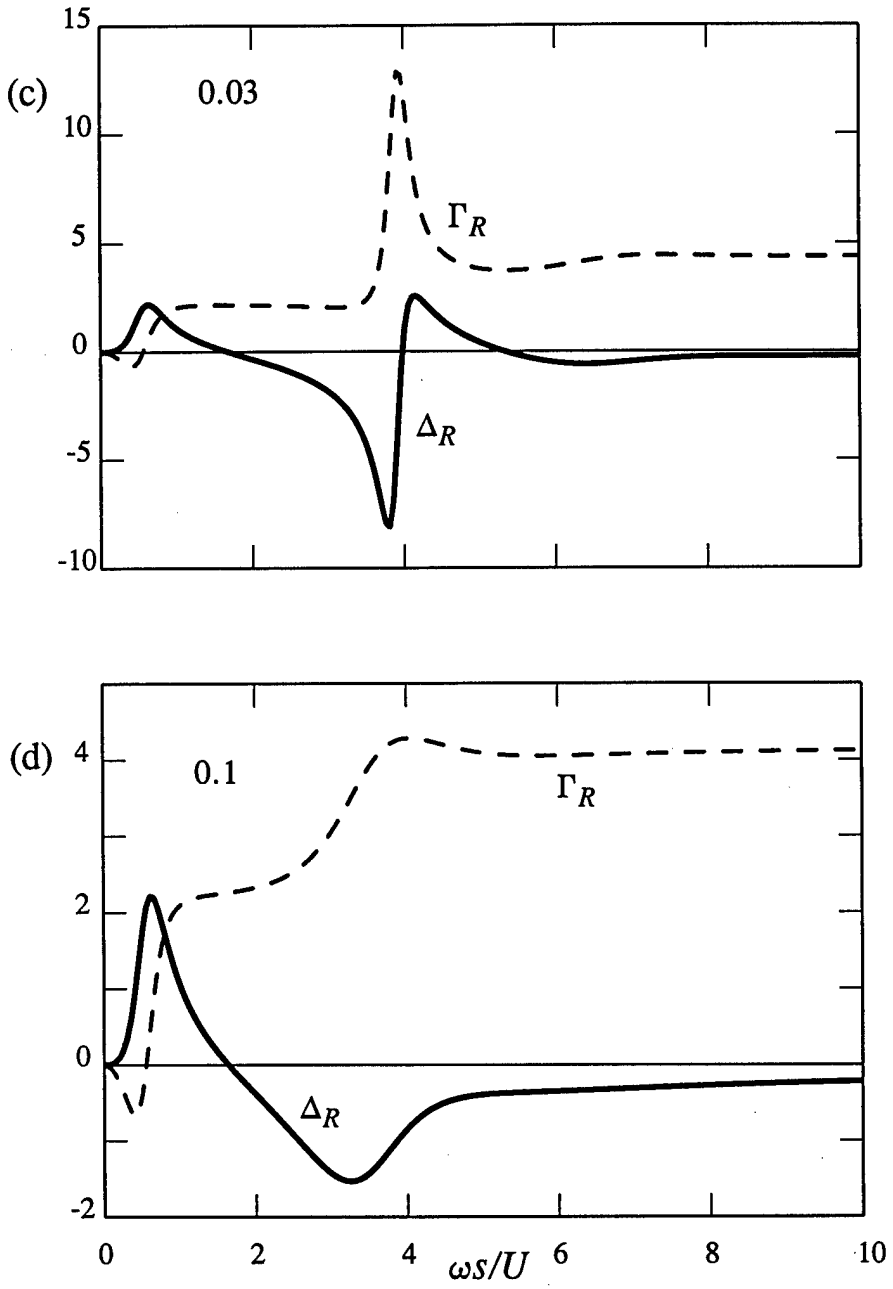

Figure 6. The dependence of $K_R(\omega)/\sqrt{A} = \Gamma_R(\omega) - i\Delta_R(\omega)$ on frequency when $U_- = U_+ \equiv U$, $b_o/L = 1$, $b_1/b_o = 0.1$ and for $d/L = 0.03$, 0.1.

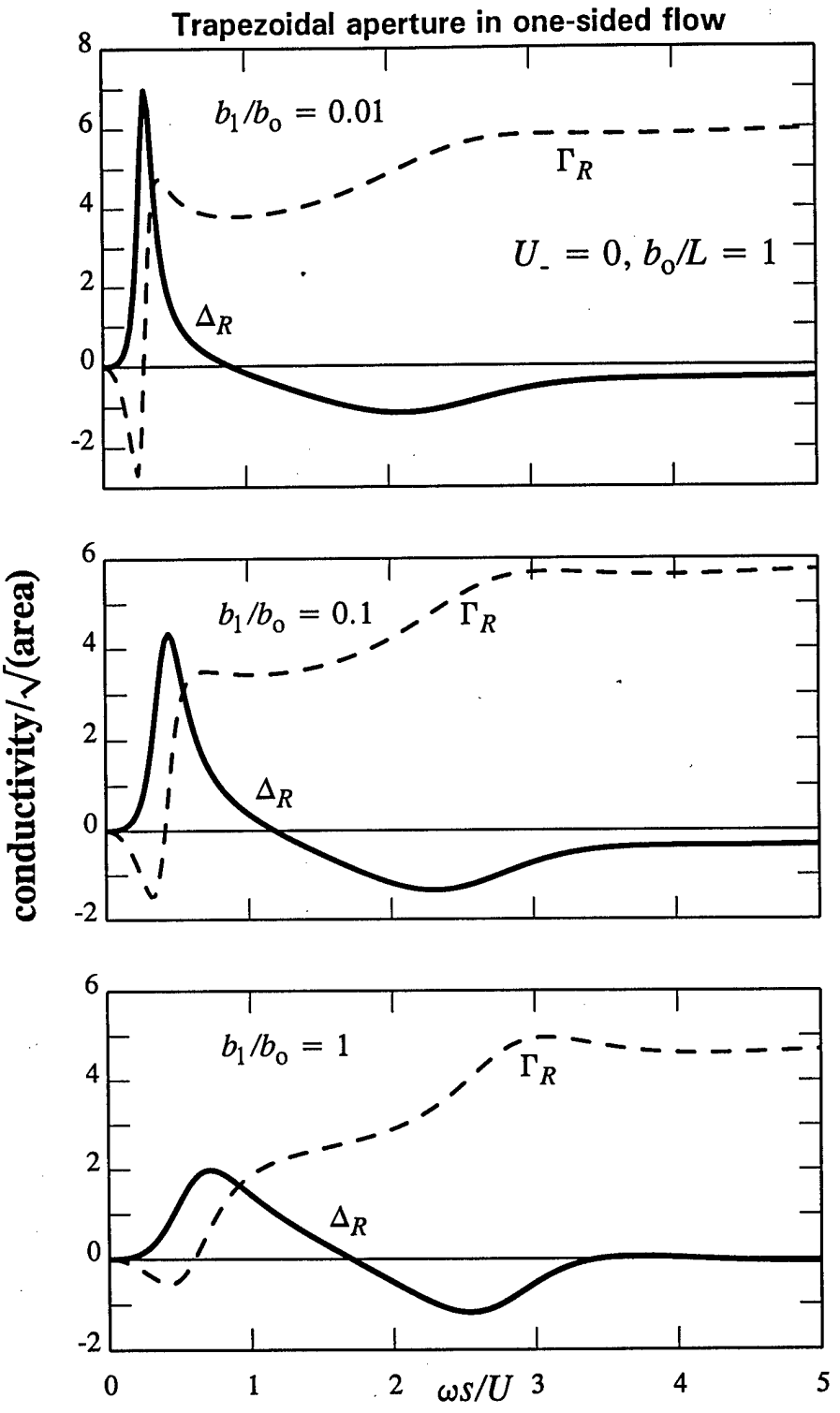

Figure 7. The conductivity $K_R(\omega)/\sqrt{A} \equiv \Gamma_R(\omega) - i\Delta_R(\omega)$ for one-sided flow ($U_+ \equiv U$, $U_- = 0$) over a trapezoidal aperture when $d/L = 0$, $b_o/L = 1$ and for $b_1/b_o = 0.01$, 0.1 and 1.

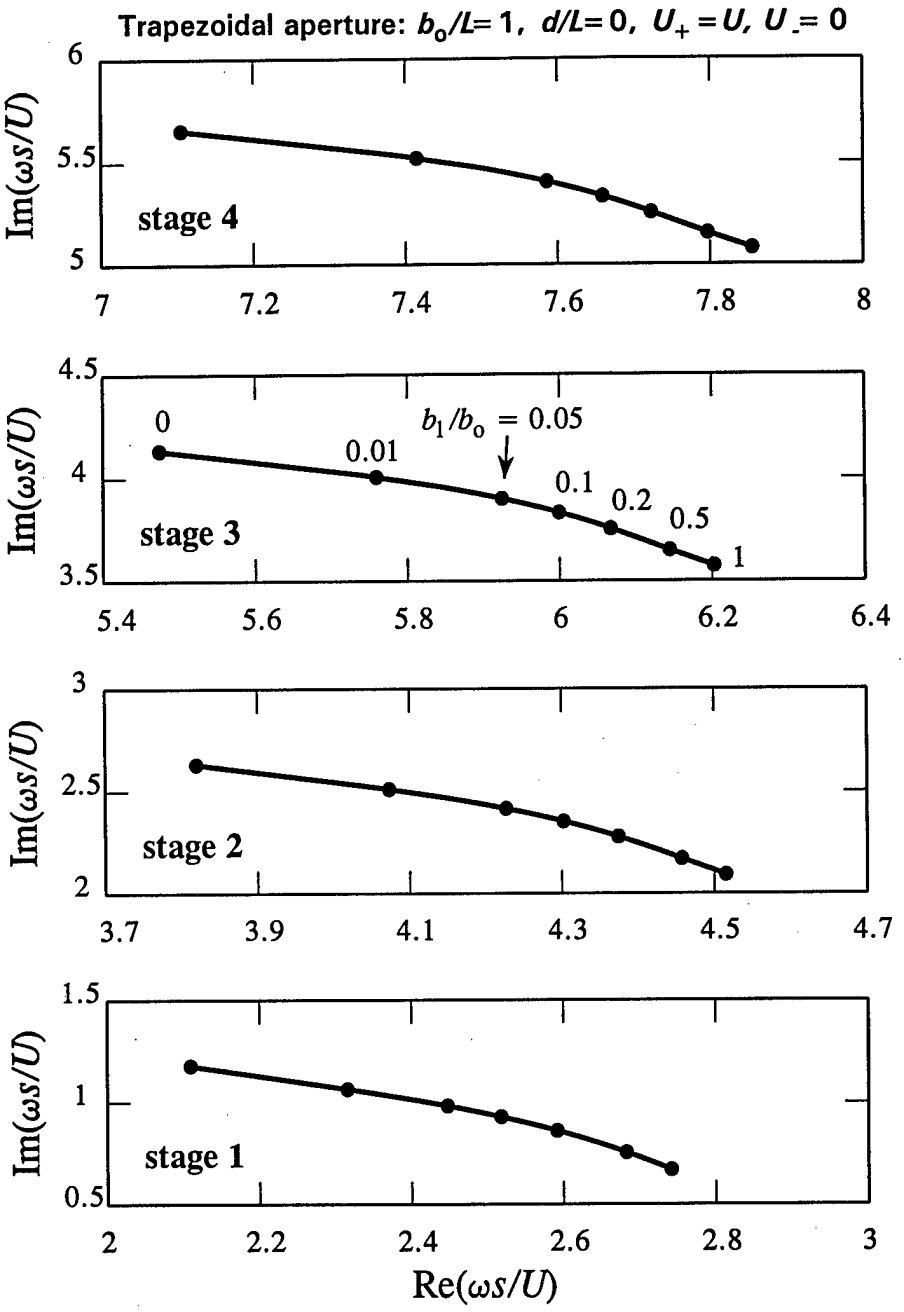

Figure 8. Complex eigenvalues (zeros of $\det(\mathfrak{C}_{ij})$, poles of K_R) for the first four operating stages of one-sided flow ($U_+ = U$, $U_- \equiv 0$) over a trapezoidal aperture when $d/L = 0$ and $b_o/L = 1$, and for $0 < b_1/b_o < 1$.

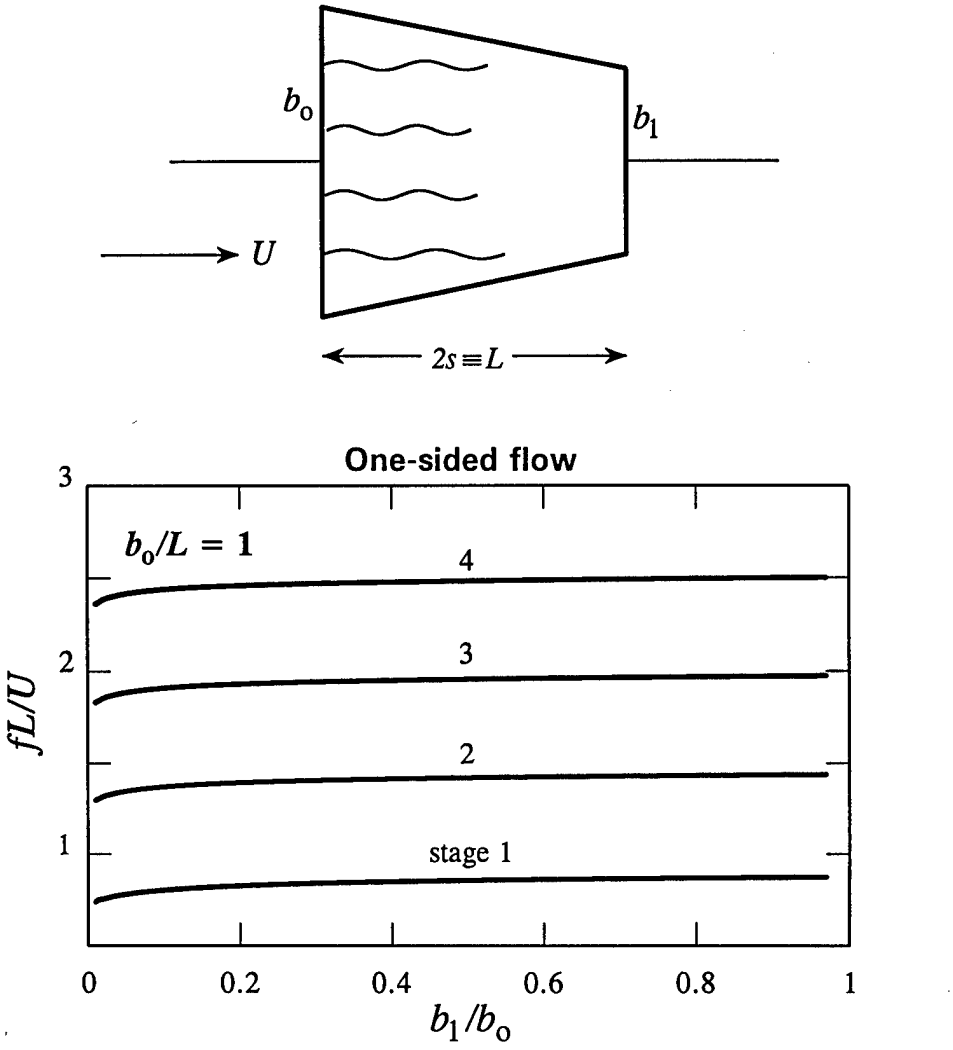

Figure 9. Strouhal number dependence on b_1/b_o for one-sided flow ($U_+ = U$, $U_- \equiv 0$) over a trapezoidal aperture when $d/L = 0$ and $b_o/L = 1$.

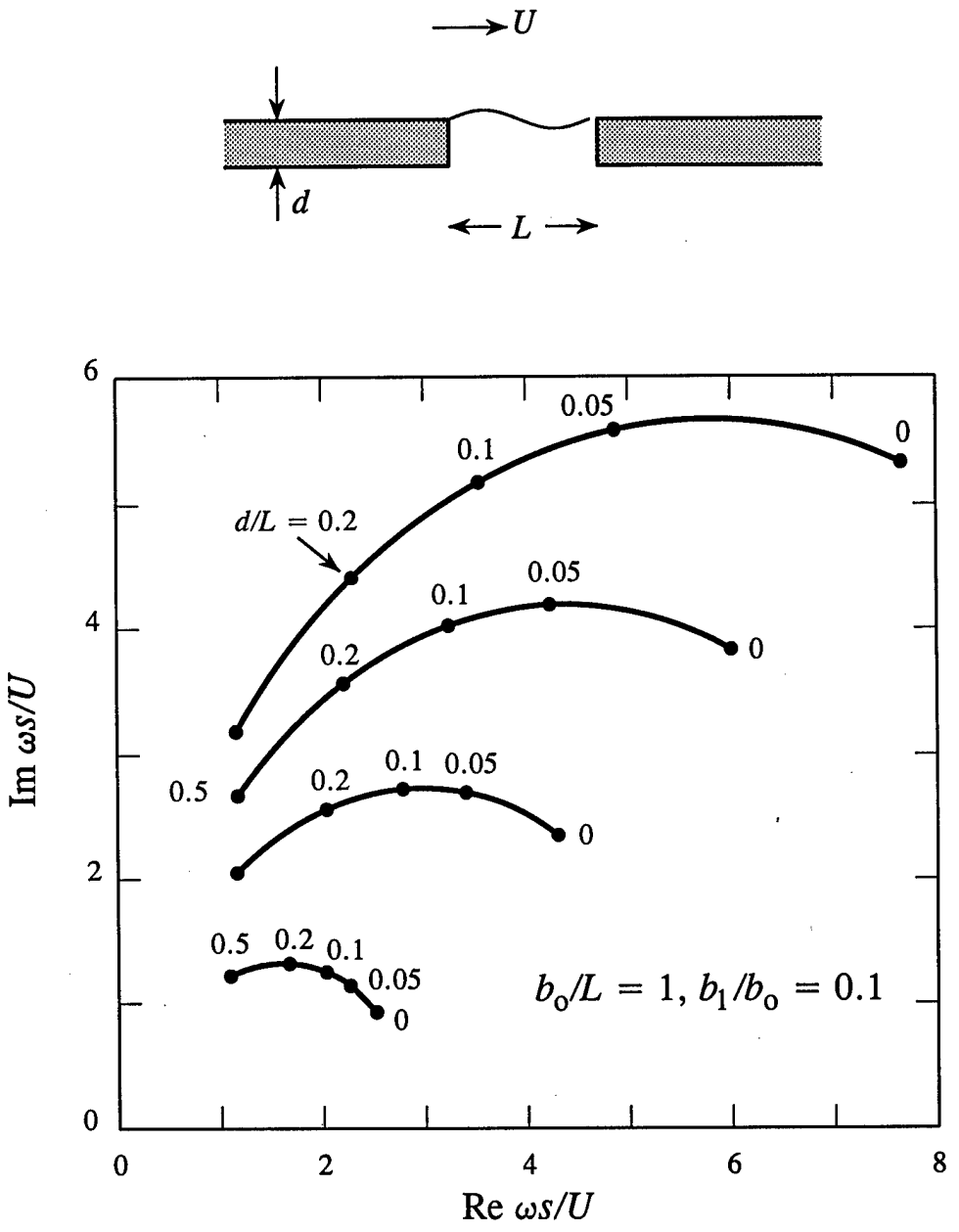

Figure 10. Loci of the complex eigenvalues (zeros of $\det(\mathfrak{C}_{ij})$, poles of K_R) for varying d/L, for the first four operating stages of one sided flow ($U_+ = U$, $U_- = 0$) when $b_o/L = 1$ and $b_1/b_o = 0.1$.

CHAPTER 3

RAYLEIGH CONDUCTIVITY AND SELF-SUSTAINED OSCILLATIONS

M. S. Howe

SUMMARY

The theory of self-sustaining oscillations of low Mach number, high Reynolds number shear layers and jets impinging on edges and corners is discussed. Such oscillations generate narrow band sound, and are usually attributed to the formation of discrete vortices whose interactions with the edge or corner produce impulsive pressures that trigger the cyclic formation of new vorticity. A linearized analysis of these interactions is described in which free shear layers are treated as vortex sheets. Details are given for shear flow over wall apertures and shallow cavities, and for jet-edge interactions. The *operating stages* of the oscillations are determined by complex eigenvalues of the linear theory: for wall apertures and edge tones they can be identified with poles in the upper half of the complex frequency plane of the Rayleigh conductivity of the "window" spanned by the shear flow; for shallow wall cavities they correspond to poles of a frequency dependent drag coefficient. It is argued that the frequencies defined by the real parts of the complex frequencies at these poles determine the operating stage Strouhal numbers observed experimentally. Strouhal number predictions for a shallow wall cavity are found to be in good agreement with data extrapolated to zero Mach number from measurements in air; edge tone predictions are in excellent accord with data from various sources in the literature.

1. INTRODUCTION

Consider a uniform time-harmonic pressure load $[p_o] = (p_+ - p_-)e^{-i\omega t}$ applied across an aperture in a flat, rigid wall. The "upper" and "lower" faces of the wall are respectively the planes $x_2 = \pm\frac{1}{2}d$ defined relative to the rectangular axes (x_1, x_2, x_3), and p_+, p_- are the respective pressures above and below the wall. In practice the fluctuating load may be caused by an incident sound wave, or by a large scale disturbance convected past the aperture in a mean flow. The frequency of the motion is sufficiently small that the reciprocating flow through the aperture may be regarded as incompressible.

The *Rayleigh conductivity* of the aperture is defined in terms of the aperture volume flux $Qe^{-i\omega t}$ (in the positive x_2-direction) and the pressure differential $p_+ - p_-$ by the relation [1]

$$K_R(\omega) = \frac{i\omega\rho_o Q}{p_+ - p_-} \tag{1.2}$$

where ρ_o is the fluid density. K_R has the dimensions of length. In the absence of mean flow, and when dissipation within the fluid and at boundaries is ignored, its value is a constant determined by the aperture shape (it is equal to $2R$ for a circular aperture of radius R in a wall of negligible thickness, and equal roughly to $2 \times \sqrt{(\text{aperture area}/\pi)}$ for a non-elongated aperture). When thermo-viscous losses are important the conductivity is complex, and the power Π dissipated in the aperture is given (for $\omega > 0$) by

$$\Pi = -\frac{1}{2}\mathrm{Re}\big(Q^*[p_o]\big) \equiv -\frac{\mathrm{Im}\{K_R(\omega)\}}{2\rho_o\omega}|[p_o]|^2\,, \tag{1.3}$$

where the asterisk denotes complex conjugate. Π is positive provided $\mathrm{Im}\{K_R(\omega)\} < 0$.

K_R becomes strongly frequency-dependent in the presence of mean flow. Large increases can occur in the dissipation, because the kinetic energy of vorticity generated by the fluctuating pressure at the aperture edges is swept away by the flow, although this may be offset by the negative damping associated with instabilities of a mean shear layer adjacent to the aperture, which causes perturbations to grow by extracting energy from the mean flow.

When $[p_o] = [p_o(t)]$ has arbitrary time dependence, equation (1.1) assumes the more general form

$$\rho_o\frac{\partial Q}{\partial t}(t) = -\int_{-\infty}^{\infty} K_R(\omega)[p_o(\omega)]e^{-i\omega t}\,d\omega, \tag{1.4}$$

where $[p_o(\omega)] \equiv \frac{1}{2\pi}\int_{-\infty}^{\infty}[p_o(t)]e^{i\omega t}\,dt$ is the Fourier transform of $[p_o(t)]$. The applied pressure $[p_o(t)]$ may be assumed to vanish prior to some initial instant $t = t_o$, say, and to be non-zero only within some subsequent finite interval. Then $[p_o(\omega)]$ is regular in the whole of the complex ω-plane and vanishes as $|\omega| \to \infty$. A strictly *causal* determination of $Q(t)$ from (1.3) requires the path of integration to lie in Im $\omega > 0$, above all of the singularities of $K_R(\omega)$. For $t > t_o$ the integral is evaluated by displacing the path downwards towards the real axis, thereby capturing contributions from any singularities in the upper half-plane, which would grow exponentially with $t - t_o$. Unlimited exponential growth cannot occur for a real flow, but may be a mathematical artifact of a linearized approximation that neglects the nonlinear mechanisms that curtail unlimited growth.

Linearized treatments of this kind are the subject of this chapter for flows of the type illustrated schematically in Figure 1, involving self-sustaining oscillations of a mean flow over a rectangular aperture in a wall. There is currently no general prediction scheme for these flows, and only very limited progress has been made in their direct numerical simulation at finite Reynolds number [2 - 7]. We shall assume the Reynolds number to be sufficiently large that turbulence-free mean streams above and below the wall may be taken to be uniform, and the mean shear layer over the aperture may be treated as a vortex sheet that is *linearly* disturbed from an undisturbed, nominally planar form. In these circumstances we find that $K_R(\omega)$ has simple poles in Im $\omega > 0$.

Each pole initiates oscillatory motions of fixed frequency whose amplitudes increase exponentially with time. Nonlinear mechanisms that in practice cut-off unlimited growth do not necessarily alter the frequency of the oscillations, since this is determined in both the linear and nonlinear regimes by the convection velocity of vortical disturbances across the aperture which, according to experiment [9 - 12], is hardly influenced by vortex strength. This suggests that linear theory may be used with advantage to identify the Strouhal numbers of self-sustaining oscillations with the real parts of the complex frequencies defining the poles of $K_R(\omega)$ in the upper frequency plane. The oscillations are sources of narrow band sound, and are usually associated with a sequence of four or more "operating stages". For each stage the fundamental frequency is controlled by a feedback mechanism involving the formation of discrete vortices near the leading (upstream) edge of the aperture, whose interactions with a downstream edge produce impulsive pressures that trigger the cyclic release of new vorticity [13, 14]. The amplitudes of the oscillations depend on flow speed, and usually vary discontinuously as the system jumps to an adjacent higher or lower stage

respectively as the flow speed increases or decreases [13 - 17]. The transitions typically exhibit hysteresis, a downward jump being delayed to a lower speed than the corresponding upward transition.

In this chapter this general linearized approach to the determination of the operating stages is discussed for mean flow at very low Mach number over an aperture in a thin wall and over a shallow wall-cavity, and also for the "edge tones" produced when a thin blade of air impinges on a sharp edge [4, 18]. In all cases the complex frequencies actually correspond to eigenvalues of an integro-differential equation that describes (in the linearized approximation) the motion of the shear layer when approximated by one or more vortex sheets. For wall apertures and edge-tones the eigenvalues coincide with the poles of the Rayleigh conductivity of the structural "window" spanned by the shear layer or jet. The theory of self-sustained oscillations of the flow over an open, shallow wall cavity has received relatively little attention at low Mach number; it is of special interest because feedback to the cavity leading edge from vorticity interacting with the trailing edge effectively occurs instantaneously, and the motion within the cavity can be regarded as incompressible, thereby excluding an association of the periodic motion with an acoustic mode of the cavity. Evidently, we must then have $Q \equiv 0$, so that the conductivity of the cavity mouth vanishes identically. In this case the eigenvalues are poles of the cavity *drag coefficient.*

The theory is described in detail §2 for the simplest case of flow over a rectangular wall aperture. Edge-tones are investigated in §3, where the predicted operating stages are shown to be in excellent accord with experimental data from several sources. In §4 predictions are made of the operating stages of a shallow wall cavity at infinitesimal Mach number, and shown to be in good agreement with experimental data for cavities in air extrapolated to zero Mach number.

2. APERTURE IN A THIN WALL

2.1 The equations of motion Consider low Mach number flow at high Reynolds number over both sides of the rectangular aperture of Figure 1 in a plane, rigid wall. The mean flow is parallel to the x_1-axis with main stream velocities U_+ and U_- in the "upper" and "lower" regions $x_2 \gtrless \pm \frac{1}{2}d$ respectively. The aperture is aligned with sides of length L parallel to the mean flows and of length b in the transverse (x_3-) direction, so that the upper and lower mouths of the aperture occupy the regions $|x_1| < s \equiv L/2$, $x_2 = \pm\frac{1}{2}d$, $|x_3| < \frac{1}{2}b$. The shear layers over each mouth are modeled by vortex sheets, and the fluid within the aperture (in $|x_2| < \frac{1}{2}d$) is assumed to be in a mean state of rest.

Let the aperture be excited by a uniform, time-harmonic pressure differential $[p_o(\omega)]e^{-i\omega t}$, and denote by $\zeta_\pm(x_1, x_3)e^{-i\omega t}$ the respective displacements (in the x_2-direction) of the upper and lower vortex sheets from their undisturbed positions $x_2 = \pm\frac{1}{2}d$. The Mach number is small enough that the motion in the neighborhood of the aperture may be treated as incompressible, so that the following linearized approximations for the perturbation pressures above and below the wall are applicable [19]

$$\begin{aligned} p &= p_+ - \rho_o\left(\omega + iU_+\frac{\partial}{\partial x_1}\right)^2 \int \frac{\zeta_+(y_1, y_3)}{2\pi|\mathbf{x}-\mathbf{y}|}\, dy_1 dy_3\ ,\ x_2 > d/2 \\ &= p_- + \rho_o\left(\omega + iU_-\frac{\partial}{\partial x_1}\right)^2 \int \frac{\zeta_-(y_1, y_3)}{2\pi|\mathbf{x}-\mathbf{y}|}\, dy_1 dy_3\ ,\ x_2 < -d/2 \end{aligned} \tag{2.1}$$

where respectively $\mathbf{y} = (y_1, \pm\frac{1}{2}d, y_3)$, the integration is over the aperture cross-section, and the exponential time factor $e^{-i\omega t}$ is here and henceforth suppressed.

For a *thin* wall, and when the wavelength of disturbances on the vortex sheets are large compared to d, the vertical displacement of fluid in the aperture is independent of x_2, i.e. $\zeta \equiv \zeta(x_1, x_3) = \zeta_\pm(x_1, x_3)$, and the equation of motion of a "column" of fluid is

$$\rho_o d\frac{\partial^2\zeta}{\partial t^2} = -[p],\ |x_1| < s,\ |x_3| < b/2,$$

where $[p]$ is the difference in the pressures applied to the upper and lower ends of the column at $x_2 = \pm\frac{1}{2}d$. Using (2.1) this equation becomes

$$\left[\left(\omega + iU_+\frac{\partial}{\partial x_1}\right)^2 + \left(\omega + iU_-\frac{\partial}{\partial x_1}\right)^2\right]\frac{1}{2\pi}\int \frac{\zeta(y_1,y_3)dy_1dy_3}{\sqrt{(x_1-y_1)^2+(x_3-y_3)^2}} + d\omega^2\zeta(x_1,x_3) = \frac{[p_o]}{\rho_o}. \tag{2.2}$$

Vortex shedding from the straight leading edges of the aperture (at $x_1 = -s$) tends to produce strongly correlated motions of the vortex sheets at different transverse locations x_3, so that in a first approximation ζ may be regarded as independent of x_3. The integration in (2.2) with respect to y_3 may then be performed explicitly; if the equation is also integrated over $-b/2 < x_3 < b/2$, it can be re-cast in the dimensionless form:

$$\left[\left(\sigma + i\frac{\partial}{\partial \xi}\right)^2 + \left(\sigma + i\mu\frac{\partial}{\partial \xi}\right)^2\right]\int_{-1}^{1} Z(\eta)\{\ln|\xi-\eta| + \mathcal{L}(\xi,\eta)\}\,d\eta - \frac{2\pi\sigma^2 d}{L}Z(\eta) = 2\sigma^2 \tag{2.3}$$

where

$$Z(\xi) = \frac{-2\rho_o\omega^2 s\zeta(\xi)}{\pi[p_o]}, \tag{2.4}$$

is dimensionless, and

$$\sigma = \omega s/U_+,\ \mu = U_-/U_+,\ \xi = x_1/s,\ \eta = y_1/s, \tag{2.5}$$

$$\mathcal{L}(\xi,\eta) = -\ln\{b/s + \sqrt{[(b/s)^2 + (\xi-\eta)^2]}\} + \sqrt{\{1 + (s/b)^2(\xi-\eta)^2\}} - (s/b)|\xi-\eta|. \tag{2.6}$$

Equation (2.3) can be integrated with respect to the second order differential operator on the left by using the Green's function

$$G(\xi,\eta) = \frac{1}{2\sigma(1-\mu)}\left(H(\xi-\eta)e^{i\sigma_+(\xi-\eta)} + H(\eta-\xi)e^{i\sigma_-(\xi-\eta)}\right), \tag{2.7}$$

which is a particular solution of

$$\left[\left(\sigma + i\frac{\partial}{\partial \xi}\right)^2 + \left(\sigma + i\mu\frac{\partial}{\partial \xi}\right)^2\right]G(\xi,\eta) = \delta(\xi-\eta).$$

In these formulae, $H(x)$ is the Heaviside unit function ($= 0$, 1 according as $x \gtrless 0$), and $\sigma_\pm$ are the Kelvin-Helmholtz wavenumbers [8]

$$\sigma_\pm = \sigma \left(\frac{1 \pm i}{1 \pm i\mu} \right). \tag{2.8}$$

Hence, Z is found to satisfy the integral equation

$$\int_{-1}^{1} Z(\eta) \left[\ln|\xi - \eta| + \mathcal{L}(\xi, \eta) - 2\pi\sigma^2 \frac{d}{L} G(\xi, \eta) \right] d\eta + \lambda_+ e^{i\sigma+\xi} + \lambda_- e^{i\sigma-\xi} = 1, \ |\xi| < 1, \tag{2.9}$$

where $\lambda_\pm$ are constants of integration.

This equation is readily solved by the collocation procedure described by Scott [20] for a vortex sheet over a circular aperture. The values of $\lambda_\pm$ are fixed by imposing the Kutta condition that the vortex sheets leave the upstream edges smoothly, i.e. by requiring that $\zeta = \partial\zeta/\partial\xi = 0$ as $\xi \to -1$ [21]. Potential theory then implies that the displacement has a mild, but integrable singularity at the downstream edge ($\xi = 1$), which is the linear theory representation of the large amplitude edge motion observed in practice.

2.2 The Rayleigh conductivity The volume flux is calculated from $Q(\omega) = -i\omega b \int_{-s}^{s} \zeta(x_1)\, dx_1$. The definition (1.1) and equation (2.4) therefore supply the following expression for the Rayleigh conductivity in terms of the solution Z of (2.9).

$$K_R = -\frac{\pi b}{2} \int_{-1}^{1} Z(\eta)\, d\eta. \tag{2.10}$$

K_R is a complex valued function of ω that also depends on the wall thickness ratio d/L, the aspect ratio b/L, and the velocity ratio $\mu = U_-/U_+$.

It is convenient to set

$$K_R(\omega)/b = \Gamma_R(\omega) - i\Delta_R(\omega)\,, \tag{2.11}$$

where $\Gamma_R(\omega)$, $\Delta_R(\omega)$ are real. Figure 2 illustrates their dependence on $\omega s/U$ for the case of one-sided flow where $U_+ \equiv U$, $U_- = 0$, when $b/L = 2$ and for different wall thicknesses. The changes with d/L are relatively insignificant until d/L exceeds about 0.2. The real part $\Gamma_R(\omega)$ determines the *reactive* response of the aperture to an applied pressure $[p_o]$, and

hardly varies with increasing d/L; the imaginary component $\Delta_R(\omega)$ is positive when $\omega s/U$ is less than about 1.5 where, according to equation (1.2), the forced motion in the aperture is damped by vorticity production [19]. At larger values of $\omega s/U$, where $\Delta_R(\omega) < 0$, energy is extracted from the mean flow and the perturbations grow. Figure 2 suggests that the magnitude of this negative damping at higher frequencies decreases as the wall thickness increases. However, this instability is only conditional, in that oscillations of frequency ω do not persist and continue to grow once the exciting pressure $[p_o]e^{-i\omega t}$ is removed. Absolute instabilities of the aperture flow are governed by the singularities of $K_R(\omega)$ in $\mathrm{Im}(\omega) > 0$.

These singularities are simple poles, and correspond to eigenvalues of the integral equation (2.9); they are a fundamental attribute of the shear layer, being independent of the assumption that the driving pressures $p_\pm$ are uniform (when $[p_o]$ is an arbitrary function of the streamwise coordinate ξ the right of (2.9) is replaced by a function of ξ). To see this, consider the limiting process whereby the integral in (2.9) is first discretized by using, for example, a Gauss integration formula that expresses it as a sum of terms evaluated at N lattice points ξ_i $(1 \le i \le N)$, where $\xi_1 = -1 + \delta$, $\xi_N = +1 - \delta$, and $\delta \to +0$ as $N \to \infty$. The Kutta condition is imposed by setting $Z_1 = Z_2 = 0$, where $Z_i \equiv Z(\xi_i)$. The discrete form of (2.9) can then be written form

$$\sum_{j=1}^{N} \mathcal{A}_{ij} \mathcal{Z}_j = 1 \tag{2.12}$$

where $\mathcal{Z}_1 = \lambda_+$, $\mathcal{Z}_2 = \lambda_-$, and $\mathcal{Z}_i = Z_i$ for $i \ge 3$. For each fixed i,

$$\mathcal{A}_{i1} = e^{i\sigma + \xi_i}, \ \mathcal{A}_{i2} = e^{i\sigma - \xi_i},$$

and the coefficients $\mathcal{A}_{ij}$ $(j \ge 3)$ include similar terms, but depend on the integration scheme used to approximate the integral. The eigenvalues of (2.12) are the (generally complex) roots $\omega s/U_+$ of

$$\det(\mathcal{A}_{ij}) = 0. \tag{2.13}$$

Since the integral (2.10) defining $K_R(\omega)$ may be approximated by the same Gaussian integration formula, it follows from Cramer's rule [22], as N becomes large, that $K_R(\omega)$ is regular except for simple poles at the roots of (2.13).

This conclusion can be verified directly when $b/L \gg 1$ and $d = 0$. In this case equation (2.9) can be solved analytically, and the conductivity determined in the form [19]

$$K_R \approx \frac{\pi b}{2\{F(\sigma) + \ln(8b/eL)\}}, \tag{2.14}$$

where

$$F(\sigma) = \frac{-\sigma_+ J_0(\sigma_-)[J_0(\sigma_+) - 2W(\sigma_+)] + \sigma_- J_0(\sigma_+)[J_0(\sigma_-) - 2W(\sigma_-)]}{\sigma_+ W(\sigma_-)[J_0(\sigma_+) - 2W(\sigma_+)] - \sigma_- W(\sigma_+)[J_0(\sigma_-) - 2W(\sigma_-)]}, \tag{2.15}$$

$W(x) = ix[J_0(x) - iJ_1(x)]$, J_0 and J_1 are Bessel functions, and $e \approx 2.718$ is the exponential constant.

The approximation (2.14) is applicable when b/L exceeds about 10. Because of the logarithm in the denominator the positions of the poles do not vary rapidly with the aspect ratio. Figure 3 illustrates how the the first four instability poles of (2.14) (that determine the first four operating stages) vary with the velocity ratio $\mu = U_-/U_+$ for the "two-dimensional" case $b/L = 500$. For one-sided flow (when $U_- \equiv 0$) the poles lie roughly along a ray making an angle of about 45° with the real axis (a related set of poles, with equal and opposite real parts lie along the image of this ray in the imaginary axis). As U_-/U_+ increases the poles approach the real axis, and ultimately, when $U_-/U_+ = 1$, they have all crossed into the lower half plane. In this limit the mean velocities are the same on both sides of the wall, there is no mean vortex sheet across the aperture in the undisturbed state; the motion is then absolutely stable.

The effect on the poles of finite wall thickness ($d/L \neq 0$) can be determined by solving equation (2.13). Confining attention to one-sided flow ($U_+ = U$, $U_- = 0$) it is found [23] that, as d/L increases from zero the poles labelled $U_-/U_+ = 0$ in Figure 3 move towards the imaginary axis, and that their real parts become approximately equal when d/L exceeds about 0.4. However, the thin wall approximation requires d/L to be small, and probably breaks down before this limiting behavior is attained. If the real part $\mathrm{Re}(\omega) = 2\pi f$ of the pole at ω is identified with the frequency f of a possible self-sustaining oscillation, these results determine the dependence of the operating stage Strouhal numbers fL/U on wall thickness, as shown in Figure 4 for $b/L = 500$. When d/L is very small successive Strouhal numbers differ by about 0.5, but this difference rapidly decreases when $d/L > 0.1$. Predictions for smaller aspect ratios b/L are qualitatively and quantitatively similar, and will not be given here.

3. EDGE TONES

3.1 Thin jet approximation Edge tones are generated by a low Mach number stream of air issuing at velocity U from a thin-walled rectangular duct of height d and width b, where $b \gg d$ (see Figure 5). The duct is assumed to be symmetrically located within a semi-infinite rectangular slot of equal width in the rigid plane $x_2 = 0$, with its open end a distance $L \equiv 2s$ from the end of the slot, upon which the jet impinges. Take the origin of coordinates on the centerline of the jet, midway between the orifice and the edge, with the x_1-axis in the flow direction, so that the edge is at $x_1 = s$, $|x_3| < b/2$.

The edge tone frequencies correspond to poles of the Rayleigh conductivity of the "window" $x_1 = s$, $|x_3| < b/2$ connecting the "upper" and "lower" fluid regions. These poles are the eigenvalues of the equation of motion of the jet. In the thin jet approximation (which is analogous to the thin wall theory of §2) the wavelengths of disturbances are assumed to be much larger than the jet thickness d, and the equation determining the vertical displacement ζ of the jet (in the x_2-direction) is approximated by

$$\rho_o d \left(\frac{\partial}{\partial t} + U \frac{\partial}{\partial x_1} \right)^2 \zeta = -[p], \ |x_1| < s, \ |x_3| < b/2, \tag{3.1}$$

where [p] is the net pressure difference between the upper and lower surfaces ($x_2 \approx \pm \frac{1}{2} d$) of the jet. In this equation it is assumed that the mean jet velocity U is uniform across the jet, and the gradual increase in jet thickness across the window is ignored.

When the motion in the immediate neighborhood of the window is regarded as incompressible (and in the absence of external forcing), the pressure perturbations in $x_2 \gtrless \pm \frac{1}{2} d$, just above and below the jet, can be expressed in the forms given in equation (2.1) with $U_+ = U_- = 0$ and $p_\pm = 0$ where now the integrations are over the planes $y_2 = \pm \frac{1}{2} d$, including the sections $|y_3| > \frac{1}{2} b$ of these planes to the sides of the main jet stream. When d is much smaller than either b or L the pressures on the upper and lower surfaces of the jet can be approximated by setting $\zeta \equiv 0$ outside the window. If the spanwise variation of ζ is neglected (as in §2), transverse motions of the jet are then governed by the equation

$$\left(\sigma + i \frac{\partial}{\partial \xi} \right)^2 \zeta - \frac{2\sigma^2 s}{\pi d} \int_{-1}^{1} \zeta(\eta) \Big(\ln |\xi - \eta| + \mathcal{L}(\xi, \eta) \Big) \, d\eta = 0, \tag{3.2}$$

where $\sigma = \omega s / U$, $\xi = x_1/s$, $\eta = y_1/s$, and $\mathcal{L}(\xi, \eta)$ is defined as in (2.6).

A first integral of this equation is

$$\zeta(\xi) + \int_{-1}^{1} \mathcal{K}(\xi,\eta)\zeta(\eta)\,d\eta + (\lambda_1 + \xi\lambda_2)e^{i\sigma\xi} = 0, \tag{3.3}$$

where

$$\mathcal{K}(\xi,\eta) = \frac{2\sigma^2 s}{\pi d}\int_{-1}^{\xi}(\xi-\lambda)\Big(\ln|\lambda-\eta| + \mathcal{L}(\lambda-\eta)\Big)e^{i\sigma(\xi-\lambda)}\,d\lambda,$$

and λ_1, λ_2 are constants of integration which are determined by the thin jet approximation to the Kutta condition: $\zeta = \partial\zeta/\partial\xi = 0$ as $\xi \to -1$.

3.2 The edge tone frequencies The eigenvalues $\omega s/U$ of equation (3.3) are given by the roots of equation (2.13) as $N \to \infty$, where the matrix $\mathcal{A}_{ij}$ is defined by the procedure described in §2 for the wall aperture, with $\mathcal{A}_{i1} = e^{i\sigma\xi_i}$ and $\mathcal{A}_{i2} = \xi_i e^{i\sigma\xi_i}$. The calculation has been performed for $5 < L/d < 50$, for different fixed values of the "window" aspect ratio b/L. The real part of a root in $\mathrm{Im}(\omega) > 0$ is interpreted as the frequency $f = \mathrm{Re}(\omega)/2\pi$ of a possible edge tone. As L/d varies for each fixed value of b/L, the roots are found to lie along a succession of discrete bands in the complex plane [18], illustrated in Figure 6 for the quasi-two-dimensional case $b/L = 500$. Successive bands correspond to the edge tone operating stages, in each of which the Strouhal number fL/U is a smoothly varying function of L/d. The solid circles in Figure 7 represent calculated values of the first stage Strouhal number plotted against L/d for the two aspect ratios $b/L = 0.5$ and 10. For fixed b/L, the points are collinear when L/d is large, and the solid lines in the figure are rectilinear approximations defined by

$$\frac{fL}{U} = \alpha\sqrt{\frac{d}{L}}, \quad L/d \gg 1, \tag{3.4}$$

where values of the constant α are given in the figure.

Similar asymptotic approximations have been derived by Holger et al [10] and Crighton [24] from two-dimensional models of the jet-edge interaction (i.e., for $b/L \to \infty$). The corresponding limiting behavior in our case is depicted by the broken straight line in Figure 7 (calculated from (2.13) by setting $b/L = 500$), for which $\alpha \approx 1.76$.

Measurements of the Strouhal number dependence on L/d for the first four operating stages (the only ones observed in practice) have been compiled by Holger et al [10]

from several different investigations of nominally two-dimensional jet-edge interactions. Representative averages of this data are plotted as solid circles and squares in Figure 8; any significant spread about the average is indicated by a vertical bar through a data point. The solid curves are the variations of $fL/U \equiv \mathrm{Re}(\omega s/\pi U)$ predicted by equation (2.13) for $b/L = 500$; these are in excellent agreement with experiment except for the first stage, where most data points are confined principally to the region $L/d < 10$, where thin jet theory is not applicable.

The following generalization of (3.4) (derived in [18] from a nonlinear model of the jet-edge interaction)

$$fL/U \approx 0.92(d/L)^{1/2}(n + 0.54)^{3/2}, \tag{3.5}$$

agrees with the calculated and measured Strouhal numbers for all of the edge tone operating stages. It is plotted as the dashed lines in Figure 8 for the operating stages $n = 1$ to 4, and is in exact agreement with linear theory for $L/d \gg 1$.

4. THE SHALLOW WALL-CAVITY

Acoustic tones generated by high speed flow over a rectangular wall cavity have been studied extensively, principally for cases where the mean flow Mach number $M = U/c_o > 0.2$ (where c_o denotes the free stream sound speed) because of its relevance to vibration problems experienced by exposed aircraft structures [2, 7, 13 - 17, 25 - 27]. Theoretical progress has been limited, however, and none of the existing models is applicable at very low Mach number when the cavity depth ℓ (see Figure 9a) is very much smaller than the acoustic wavelength [28].

Suppose the cavity is of length L ($\equiv 2s$) in the streamwise direction, let b denote its transverse dimension (out of the plane of the paper in Figure 9a), and take the coordinate origin in the centre of the cavity mouth. At very small Mach numbers, when the convection of sound by the mean flow can be ignored, the acoustic pressure at large distances from the cavity can be expressed in the form

$$p(\mathbf{x},t) \approx \frac{\rho_o}{2\pi|\mathbf{x}|}\frac{\partial}{\partial t}\int v_2(\mathbf{y}, t-|\mathbf{x}-\mathbf{y}|/c_o)\,dy_1dy_3, \text{ as } |\mathbf{x}|\to\infty, \tag{4.1}$$

where v_2 is the fluid velocity in the x_2-direction normal to the wall, and the integration is extended over any section of the plane $y_2 = 0$ spanning the mouth. When the acoustic wavelength $\gg L$ or b, this expression would normally be representative of a monopole source of sound, whose strength is the volume flux $Q \approx \int v_2(\mathbf{y},[t])\,dy_1dy_3$ evaluated at the retarded time $[t] = t - |\mathbf{x}|/c_o$. However, at very low frequencies (smaller than the Helmholtz resonance frequency [29]), the motion within the cavity becomes indistinguishable from that of an incompressible fluid, and there can be no net flux through the mouth ($Q \equiv 0$). The cavity then radiates as a dipole whose pressure field is determined by the first non-zero term obtained by expanding the integrand of (4.1) in powers of $\mathbf{y}/c_o$:

$$\begin{aligned} p(\mathbf{x},t) &\approx \frac{x_j}{2\pi c_o|\mathbf{x}|^2}\frac{\partial F_j}{\partial t}(t-|\mathbf{x}|/c_o) \quad |\mathbf{x}|\to\infty, \\ F_j &= \rho_o\int y_j\frac{\partial v_2}{\partial t}(\mathbf{y},t)\,dy_1dy_3 \quad (j=1 \text{ or } 3), \end{aligned} \tag{4.2}$$

where the integration is over the cavity mouth. The axis of the dipole is parallel to the wall, and its strength $\mathbf{F}$ is the unsteady *drag* exerted on the fluid by the cavity.

When $Q = 0$ a uniform pressure $p_o(t)$ applied (in $x_2 > 0$) in the vicinity of the cavity cannot exert a drag force, nor any motion of an initially undisturbed shear layer over the mouth. The simplest disturbance that can induce drag is a tangential pressure force $-\partial p_o/\partial x_j$. Consider, in particular, a *uniform* pressure force applied in the direction of the mean flow (the x_1-direction); then $\mathbf{F} \equiv (F_1, 0, 0)$, and by analogy with equation (1.3) a drag coefficient $D(\omega)$ can be defined by

$$F_1(t) = -\int_{-\infty}^{\infty} D(\omega) p_o'(\omega) e^{-i\omega t}\, d\omega, \tag{4.3}$$

where $p_o'(\omega) \equiv \partial p_o(\omega)/\partial x_1$ is independent of $\mathbf{x}$. When the shear layer is approximated by a linearly disturbed vortex sheet, the frequencies of self-sustained radiation from the cavity are determined by the poles of $D(\omega)$ in Im $\omega > 0$.

The motion of the vortex sheet can be investigated by the method of §2. When its displacement from $x_2 = 0$ is regarded as independent of the spanwise coordinate x_3, equations (4.2) and (4.3) imply that

$$D(\omega) = \frac{\rho_o \omega^2 b}{p_o'(\omega)} \int_{-s}^{s} y_1 \zeta(y_1)\, dy_1, \tag{4.4}$$

where $\zeta(y_1)$ is the displacement produced by the uniform pressure gradient $p_o'(\omega)$.

To simplify the calculation the direct influence of the cavity base (at $x_2 = -\ell$) on the motion of the vortex sheet is neglected by assuming that $\ell \gg L$. This is done by considering first *compressible* motion within the cavity (for which $Q \neq 0$) and subsequently obtaining the solution for incompressible cavity motion by taking the limit $\omega\ell/c_o \to 0$. When $\omega\ell/c_o$ is small, the motion of the sheet will excite acoustic depth modes in the cavity, which vary only with x_2. The condition that the normal velocity must vanish at $x_2 = -\ell$, implies that the pressure p_- just below the cavity mouth produced by a depth mode of frequency ω is given by [29]

$$p_- = \frac{-i\rho_o c_o Q}{A} \cot(\kappa_o \ell), \tag{4.5}$$

where $A = bL$ is the cross-sectional area and, provided thermo-viscous losses at the interior acoustic boundary layers are ignored, $\kappa_o = \omega/c_o$ is the acoustic wavenumber. If the motion near the vortex sheet is regarded as incompressible (as in §§2, 3), the small influence of

damping by the radiation of sound into the exterior fluid can be included by taking the mean pressure above the cavity to consist of the applied component p_o (which is assumed above to be a linear function of x_1) together with a uniform pressure $\omega\kappa_o\rho_o Q/2\pi$, which vanishes as $c_o \to \infty$ (the incompressible limit), and actually corresponds to the first compressible term in the expansion of (4.1) in powers of $\omega|\mathbf{x}|/c_o$. By taking $p_o = 0$ at $x_1 = 0$, we can then write

$$p_+ = x_1 p_o' + \omega\kappa_o\rho_o Q/2\pi. \tag{4.6}$$

The fluctuating pressure above the vortex sheet, near the mouth is given by the first of equations (2.1). When ζ is independent y_3 the pressure on the upper surface of the vortex sheet, averaged over the span, therefore becomes

$$p = p_+ + \frac{\rho_o U^2}{\pi s}\left(\sigma + i\frac{\partial}{\partial\xi}\right)^2 \int_{-1}^{1} \zeta(\eta)\big(\ln|\xi-\eta| + \mathcal{L}(\xi,\eta)\big)\,d\eta, \quad |\xi| \equiv |x_1/s| < 1, \tag{4.7}$$

where the notation is the same as in §§2, 3 and $\mathcal{L}(\xi,\eta)$ is defined as in (2.6).

Similarly, because ζ does not depend on x_3, the motion close to the mouth just below the vortex sheet can be calculated by conformal transformation, by expressing it as an integral involving the potential of a line source injecting fluid into a semi-infinite, uniform duct. This procedure yields the following expression for pressure on the lower surface of the sheet:

$$p = p_- - \frac{\rho_o U^2\sigma^2}{\pi s}\int_{-1}^{1} \zeta(\eta)\big(\ln|\xi-\eta| + \mathcal{L}_c(\xi,\eta)\big)\,d\eta, \quad |\xi| < 1, \tag{4.8}$$

where

$$\mathcal{L}_c(\xi,\eta) = \ln\left[\frac{4\sin\{\pi(\xi-\eta)/4\}\cos\{\pi(\xi+\eta)/4\}}{\xi-\eta}\right].$$

The equation of motion of the sheet now follows by equating the pressures (4.7) and (4.8), and can be cast in the form

$$\left[\sigma^2 + \left(\sigma + i\frac{\partial}{\partial\xi}\right)^2\right]\int_{-1}^{1}\zeta(\eta)\big(\ln|\xi-\eta| + \mathcal{L}(\xi,\eta)\big)\,d\eta$$

$$+\,\sigma^2\int_{-1}^{1}\zeta(\eta)\big(\mathcal{L}_c(\xi,\eta) - \mathcal{L}(\xi,\eta)\big)\,d\eta \;=\; \frac{-\pi s(p_+ - p_-)}{\rho_o U^2}, \quad |\xi| < 1. \tag{4.9}$$

Integrating with respect to the differential operator in the square brackets (using the Green's function (2.7) with $\mu = 0$), we find

$$\int_{-1}^{1} \zeta(\eta)\Big(\ln|\xi-\eta| + \mathcal{L}(\xi,\eta) + \mathcal{C}(\xi,\eta)\Big)\,d\eta + \lambda_+ e^{i\sigma_+\xi} + \lambda_- e^{i\sigma_-\xi} = \mathcal{F}(\xi),\ |\xi|<1, \qquad (4.10)$$

where $\mathcal{F}(\xi)$ is a known linear function of ξ which is a particular integral of the right hand side of equation (4.9), $\lambda_\pm$ are constants of integration, $\sigma_\pm$ are Kelvin-Helmholtz wavenumbers defined by (2.8) with $\mu = 0$, and

$$\mathcal{C}(\xi,\eta) = \frac{\sigma}{2}\int_{-1}^{1}\Big(\mathcal{L}_c(\lambda,\eta) - (\mathcal{L}(\lambda,\eta)\Big)\exp\Big\{i\sigma(\xi-\lambda) - \sigma|\xi-\lambda|\Big\}\,d\lambda.$$

To solve equation (4.10) we set

$$\zeta = \frac{i\pi Q\mathcal{R}_A}{2\omega s}Z_1 - \frac{\pi p_o'}{2\rho_o\omega^2}Z_2 \qquad (4.11)$$

where $\mathcal{R}_A \equiv i\kappa_o/2\pi - \cot(\kappa_o\ell)/\kappa_o A$ is the acoustic impedance of the cavity mouth in the absence of flow [29]. The dimensionless displacement Z_1 is the solution of (4.10) satisfying the Kutta condition at $\xi = -1$ when $\mathcal{F} \equiv 1$, and Z_2 is the corresponding solution when $\mathcal{F} \equiv \xi - i/\sigma$. These solutions can be used to evaluate the drag coefficient $D(\omega)$ from the definition (4.3) and the volume flux $Q = -i\omega b\int_{-s}^{s}\zeta(y_1)\,dy_1$ in the forms

$$D = \frac{\pi bs}{2}\frac{(\pi b/2)\mathcal{R}_A[I_1M_2 - I_2M_1] - M_2}{1-(\pi b/2)\mathcal{R}_A I_1}, \quad Q = \frac{(i\pi bsp_o'/2\rho_o\omega)I_2}{1-(\pi b/2)\mathcal{R}_A I_1} \qquad (4.12)$$

where

$$I_\alpha = \int_{-1}^{1} Z_\alpha(\eta)\,d\eta, \quad M_\alpha = \int_{-1}^{1}\eta Z_\alpha\,d\eta, \quad \alpha = 1 \text{ or } 2.$$

The values of the moments I_α, M_α depend on the shape of the cavity and on the hydrodynamic flow in the mouth, but are independent of fluid compressibility (i.e., of $\kappa_o\ell$). Hence, since the acoustic impedance $\mathcal{R}_A \to \infty$ in the limit $\kappa_o\ell \to 0$ of incompressible cavity flow, it follows that $Q \to 0$, as expected, and that the drag coefficient D approaches the limiting value given by

$$\frac{D}{(\pi bs^2/2)} = \frac{M_1I_2 - M_2I_1}{I_1} \equiv \Gamma_D(\omega) - i\Delta_D(\omega), \qquad (4.13)$$

where Γ_D and $-\Delta_D$ are nondimensional real and imaginary parts of $D(\omega)$.

The calculated variations of $\Gamma_D(\omega)$ and $\Delta_D(\omega)$ with real values of $\omega s/U$ are shown in Figure 9b for a cavity of aspect ratio $b/L = 1$. It follows easily from the definition of the drag coefficient D that the cavity absorbs energy from the applied pressure gradient p'_o when $\Delta(\omega) > 0$, i.e. when $\omega s/U$ is less than about 2.8. The motion is unstable, however, since $D(\omega)$ has poles in $\mathrm{Im}(\omega) > 0$ which occur in a sequence of bands (analogous to those shown in Figure 6 for the edge tone) as b/L varies. The corresponding variations of the Strouhal number $fL/U \equiv \mathrm{Re}(\omega s/\pi)$ are illustrated in Figure 10 for the first four operating stages. fL/U increases very slowly with the aspect ratio, in broad agreement with observations reported by Ahuja and Mendoza [17], and jumps in value by about $\frac{1}{2}$ between adjacent operating stages. Table 1 reveals further an excellent numerical correspondence with Strouhal number estimates (in the third column) obtained by extrapolating to zero Mach number experimental results for shallow cavities presented by Ahuja and Mendoza in their Figure 2.2.

stage n	Theory: $b/L = 5$ fL/U	Ahuja & Mendoza [17] fL/U
1	0.78	0.7
2	1.37	1.1
3	1.92	1.7
4	2.45	2.5

Table 1.

5. CONCLUSION

The incidence of unstable shear layers or jets on edges and corners is frequently a source of narrow band sound, the production of which is associated with the formation of discrete vortices whose interaction with the structure produces impulsive pressures that trigger the formation of new vortices and complete a self-sustaining feedback cycle. In this chapter a review has been given of the linear theory of these oscillations for shear flows over wall apertures and cavities, and for the jet-edge interaction. The feedback operating stages are determined by complex eigenvalues of the equation of motion of the shear layer or jet. For wall apertures and jet-edge interactions, these eigenvalues coincide with the poles in the upper half of the complex frequency plane of the Rayleigh conductivity of the "window" spanned by the shear flow; for shallow wall cavities (where there is no net volume flux through the mouth of the cavity) they are poles of the cavity drag coefficient.

It is argued that the correct interpretation of linear theory is that the frequency of a possible self-sustained oscillation of the real system is equal to the real part of the complex frequency at a pole. This is because nonlinear mechanisms that control the amplitude of the oscillations do not significantly affect their frequencies, which are determined by the convection velocity of the vortices, and experiment shows this to be effectively independent of amplitude. Indeed, the linear theory predictions given in this chapter of the Strouhal numbers of a shallow wall cavity in flow at infinitesimal Mach number are in excellent accord with extrapolations to zero Mach number of data from measurements in air. Our predictions for the edge tone agree with data from several independent experimental investigations.

REFERENCES

1. Rayleigh, Lord (1945). *Theory of Sound*, Vol 2. New York: Dover.
2. Tam, C. K. W. and Block, P. J. W. (1978). On the tones and pressure oscillations induced by flow over rectangular cavities. *J. Fluid Mech.* **89**, 373 - 399.
3. Bruggeman, J. C. (1987). PhD. Thesis, *Flow induced pulsations in pipe systems*, Eindhoven University of Technology.
4. Bruggeman, J. C., Hirschberg, A., van Dongen, M. E. H., Wijnands, A. P. J. and Gorter, J. (1989). Flow induced pulsations in gas transport systems: analysis of the influence of closed side branches. *J. Fluids Eng.* **111**, 484 - 491.
5. Peters, M. C. A. M. (1993). PhD Thesis, *Aeroacoustic sources in internal flows*, Eindhoven University of Technology.
6. Kriesels, P. C., Peters, M. C. A. M., Hirschberg, A., Wijnands, A. P. J., Iafrati, A., Riccardi, G., Piva, R, and Bruggeman. J. C. (1995). High amplitude vortex induced pulsations in gas transport systems. *J. Sound Vib.* **184**, 343 - 368.
7. Hardin, J. C. and Pope, D. S. (1995). Sound generation by flow over a two-dimensional cavity. *AIAA J.* **33**, 407 - 412.
8. Lamb, Horace (1932). *Hydrodynamics* (6th. ed., reprinted 1994). Cambridge University Press.
9. Powell, A. (1961). On the edgetone. *J. Acoust. Soc. Am.* **33**, 395 - 409.
10. Holger, D. K., Wilson, T. A. and Beavers, G. S. (1977). Fluid mechanics of the edgetone. *J. Acoust. Soc. Am.* **62**, 1116 - 1128.
11. Rockwell, D. (1983). Oscillations of impinging shear layers. *AIAA J.* **21**, 645 - 664.
12. Blake, W. K. and Powell, A. (1986). The development of contemporary views of flow-tone generation, pp 247 - 325 of *Recent Advances in Aeroacoustics* (edited by A. Krothapali and C. A. Smith). Springer.
13. Rossiter, J. E. (1962). The effect of cavities on the buffeting of aircraft. *Royal Aircraft Establishment Tech. Memo.* **754**.
14. Heller, H. H. and Bliss, D. B. (1975). The physical mechanim of flow-induced pressure fluctuations in cavities and concepts for their suppression. *AIAA* Paper 75-491.

15. East, L. F. (1966). Aerodynamically induced resonance in rectangular cavities. *J. Sound Vib.* **3**, 277 - 287.

16. Komerath, N. M., Ahuja, K. K. and Chambers, F. W. (1987). Prediction and measurement of flows over cavities - a survey. *AIAA* Paper 87-022.

17. Ahuja, K. K. and Mendoza, J. (1995). NASA Contractor Report: Final Report Contract NAS1-19061, Task 13. *Effects of cavity dimensions, boundary layer, and temperature on cavity noise with emphasis on benchmark data to validate computational aeroacoustic codes.*

18. Howe, M. S. (1997). Edge, cavity and aperture tones at very low Mach numbers. *J. Fluid Mech.* **330**, 61 - 84.

19. Howe, M. S., Scott, M. I. and Sipcic, S. R. (1996). The influence of tangential mean flow on the Rayleigh conductivity of an aperture. *Proc. Roy. Soc. Lond.* **A452**, 2303 - 2317.

20. Scott, M. I. (1995) MS Thesis, *The Rayleigh conductivity of a circular aperture in the presence of a grazing flow.* Boston University, College of Engineering.

21. Crighton, D. G. (1985) The Kutta condition in unsteady flow. *Ann. Rev. Fluid Mech.* **17**, 411 - 445.

22. Dahlquist, G. and Björck, Å. (1974). *Numerical Methods.* Englewood Cliffs, NJ: Prentice-Hall inc.

23. Howe, M. S. (1996) Influence of wall thickness on Rayleigh conductivity and flow-induced aperture tones. Submitted to *J. Fluids and Structures.*

24. Crighton, D. G. (1992). The jet edge-tone feedback cycle; linear theory for the operating stages. *J. Fluid Mech.* **234**, 361 - 392.

25. Covert, E. E. (1970). An approximate calculation of the onset velocity of cavity oscillations. *AIAA J.* **12**, 2189 - 2194.

26. Heller, H. H., Holmes, D. G. and Covert, E. E. (1971). Flow induced pressure oscillations in shallow cavities. *J. Sound Vib.* **18**, 545 - 553.

27. Bilanin, A. J. and Covert, E. E. (1973). Estimation of possible excitation frequencies for shallow rectangular cavities. *AIAA J.* **11**, 347 - 351.

28. Burroughs, C. B. and Stinebring, D. R. (1994). Cavity flow tones in water. *J. Acoust. Soc. Am.* **95**, 1256 - 1263.

29. Pierce, A. D. (1989) *Acoustics, An introduction to its principles and applications.* American Institute of Physics.

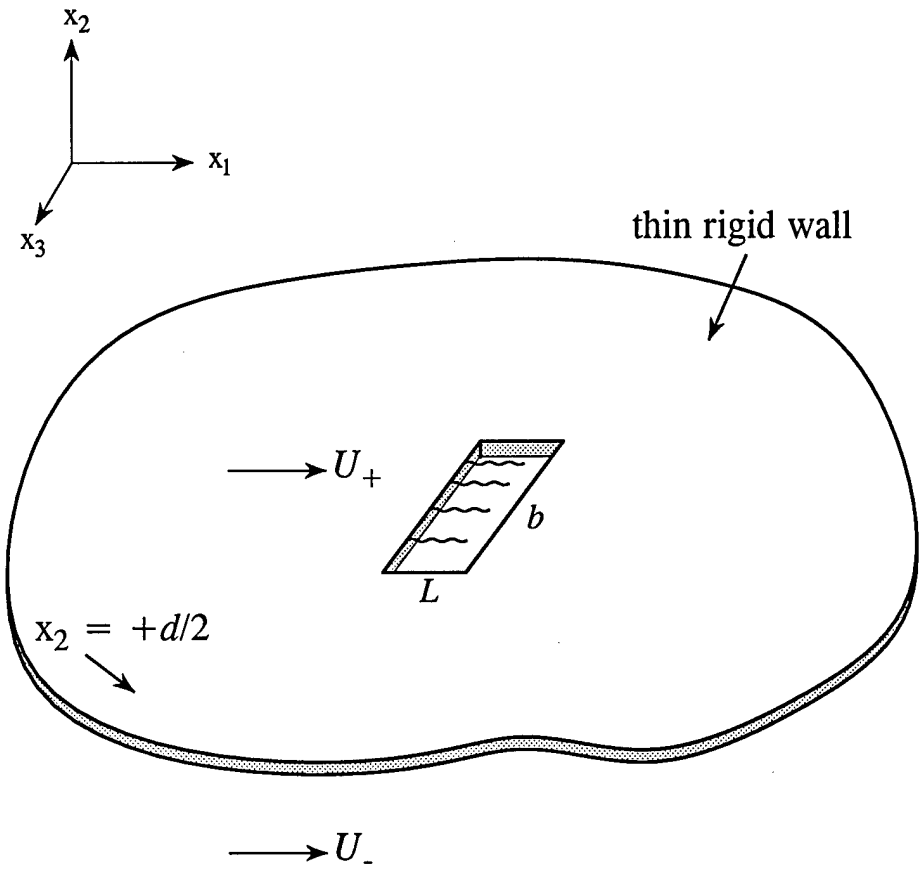

Figure 1. Two-sided flow past a rectangular aperture in a rigid plate of thickness d.

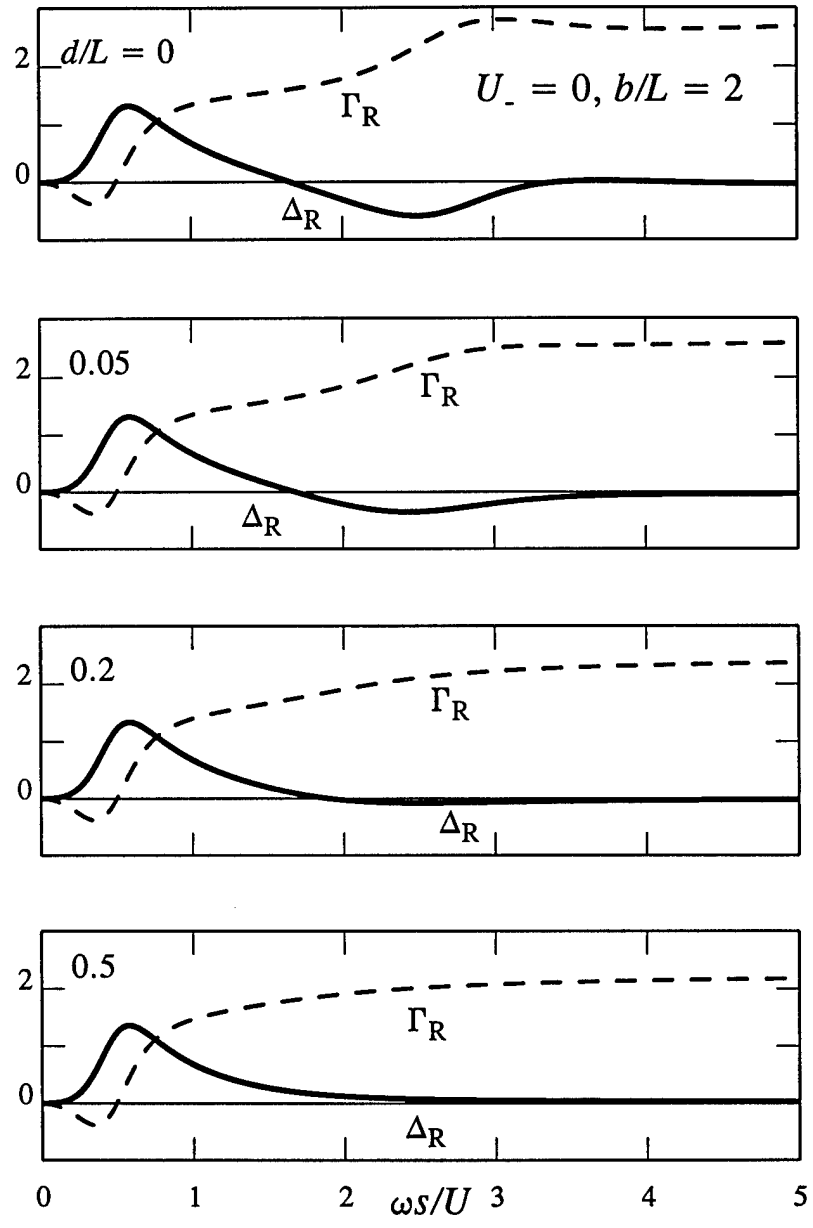

Figure 2. The dependence of $K_R(\omega)/b = \Gamma_R(\omega) - i\Delta_R(\omega)$ on frequency when $U_- = 0$, for $b/L = 2$ and for $d/L = 0,\ 0.05,\ 0.2,\ 0.5$.

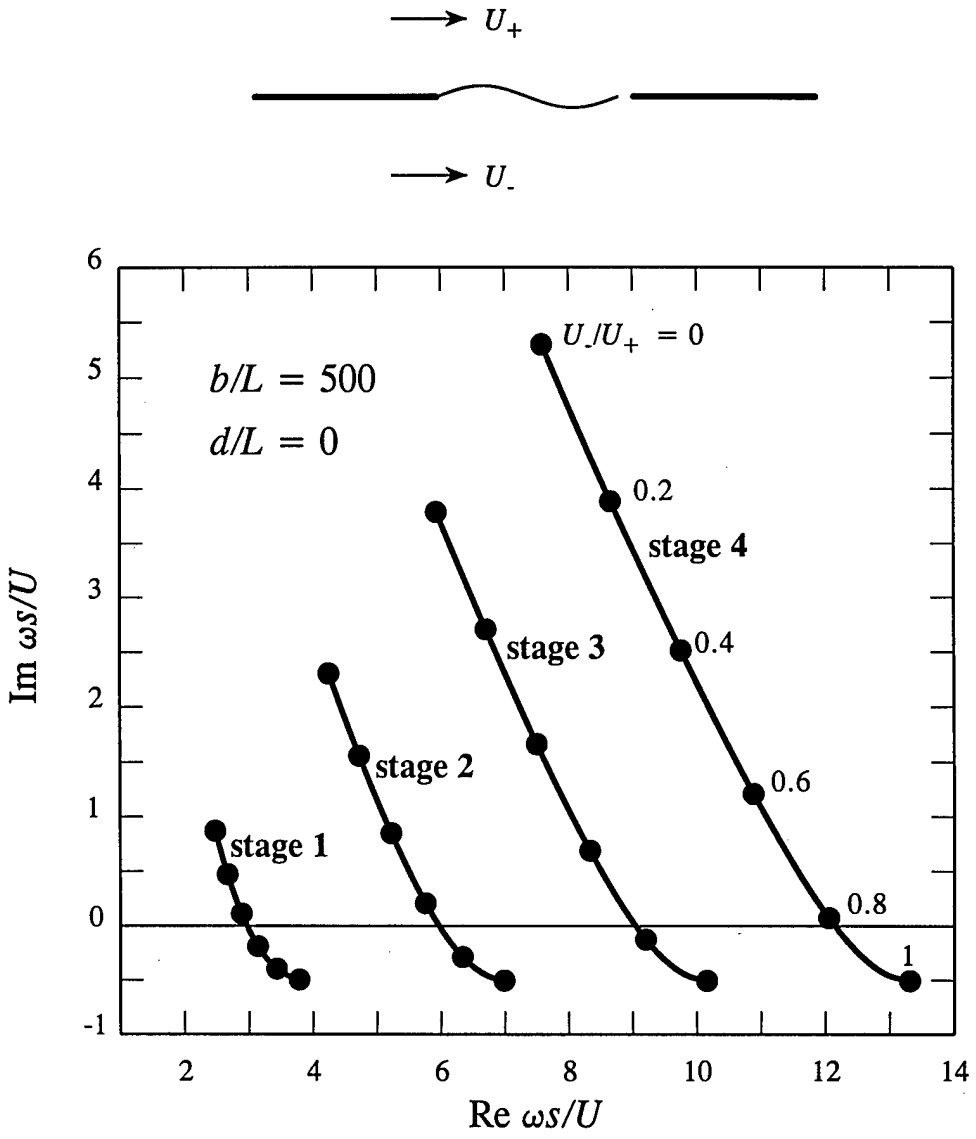

Figure 3. Poles of $K_R(\omega)$ in the complex frequency plane for $d/L = 0$, $b/L = 500$ and $0 \leq U_-/U_+ \leq 1$.

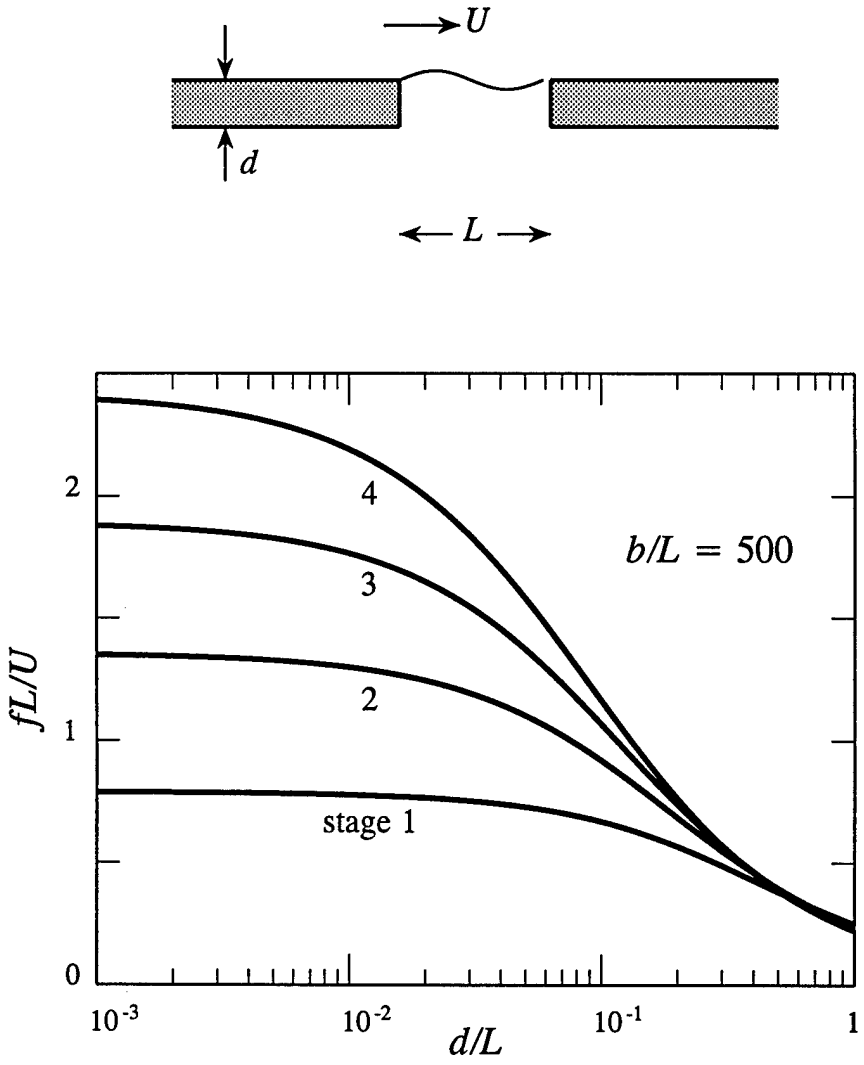

Figure 4. Strouhal number dependence on wall thickness for one-sided flow ($U_- = 0$) when $b/L = 500$.

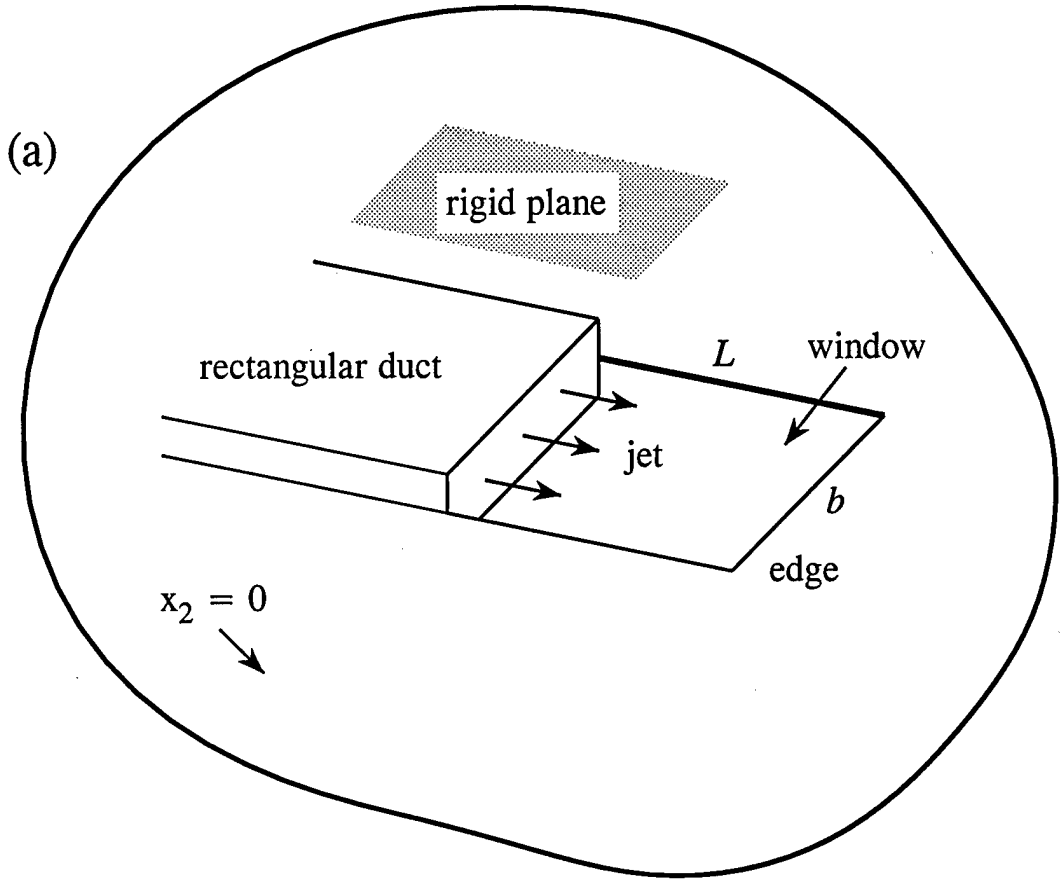

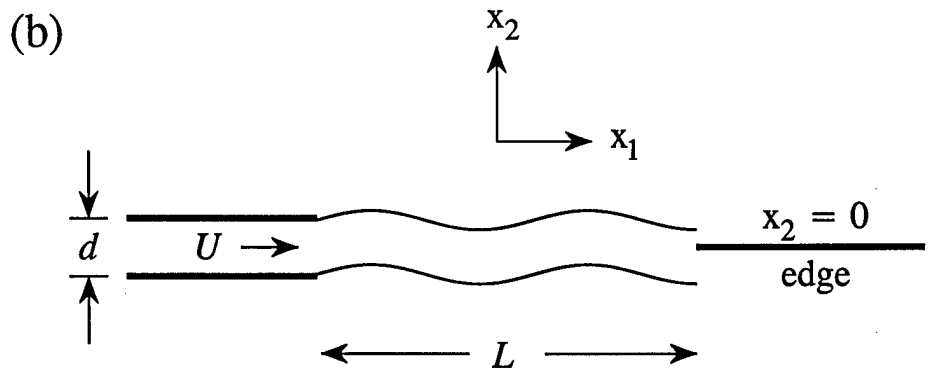

Figure 5. Jet-edge interaction.

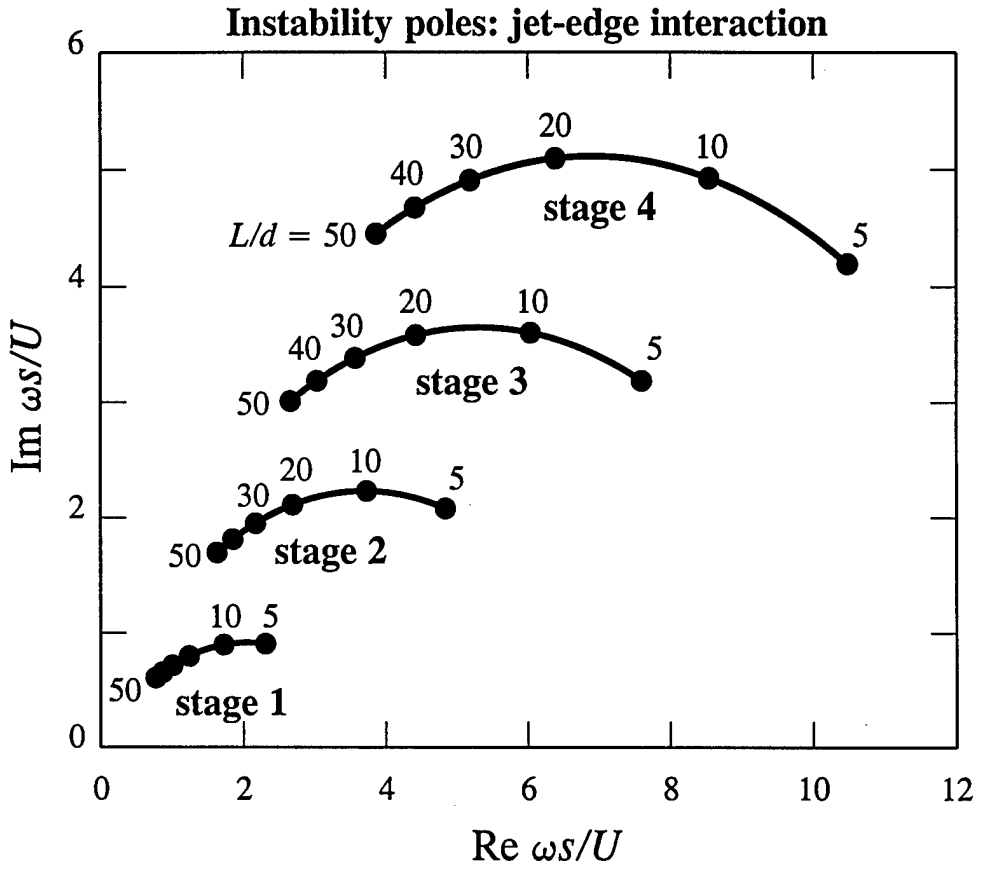

Figure 6. Two-dimensional edge tone poles.

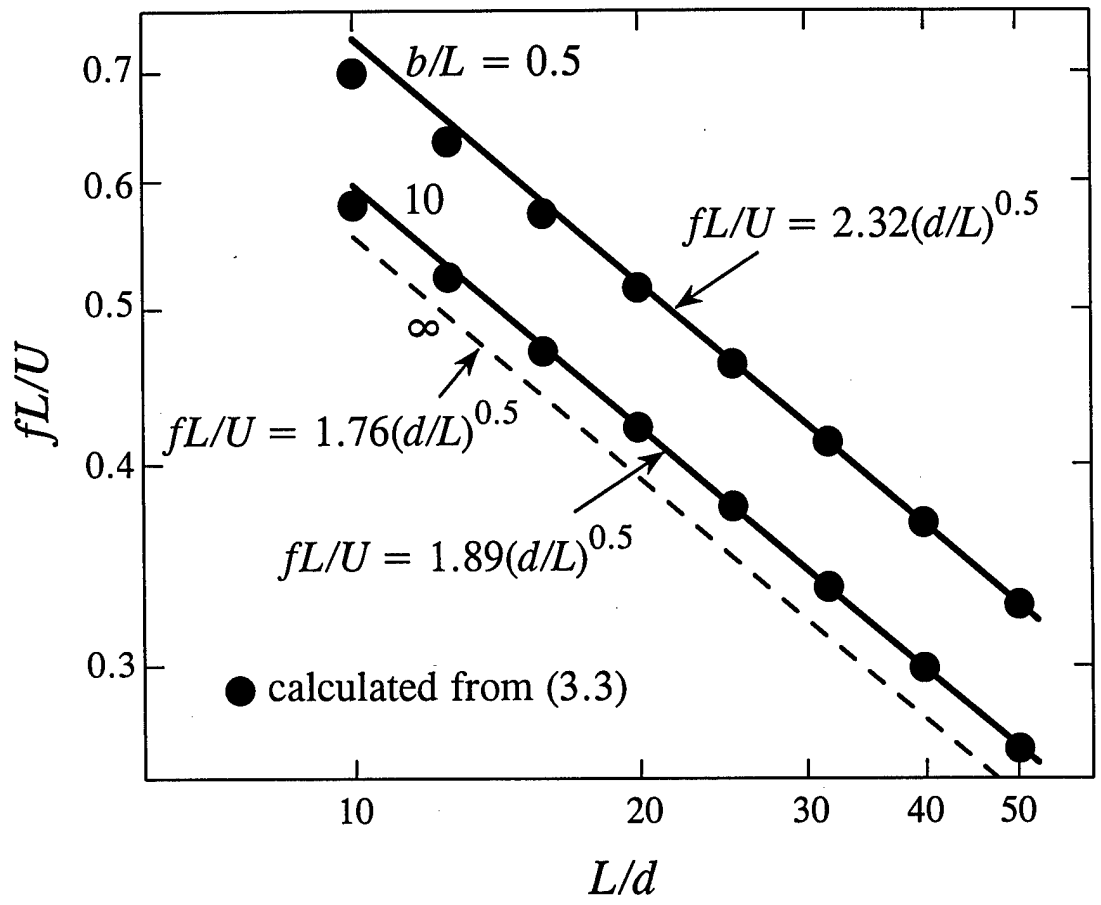

Figure 7. Strouhal number dependence on L/d for the first edge tone operating stage for different values of b/L: •••••, prediction of equation (3.3); the straight lines are best fits of the formula (3.4) for $L/d > 20$.

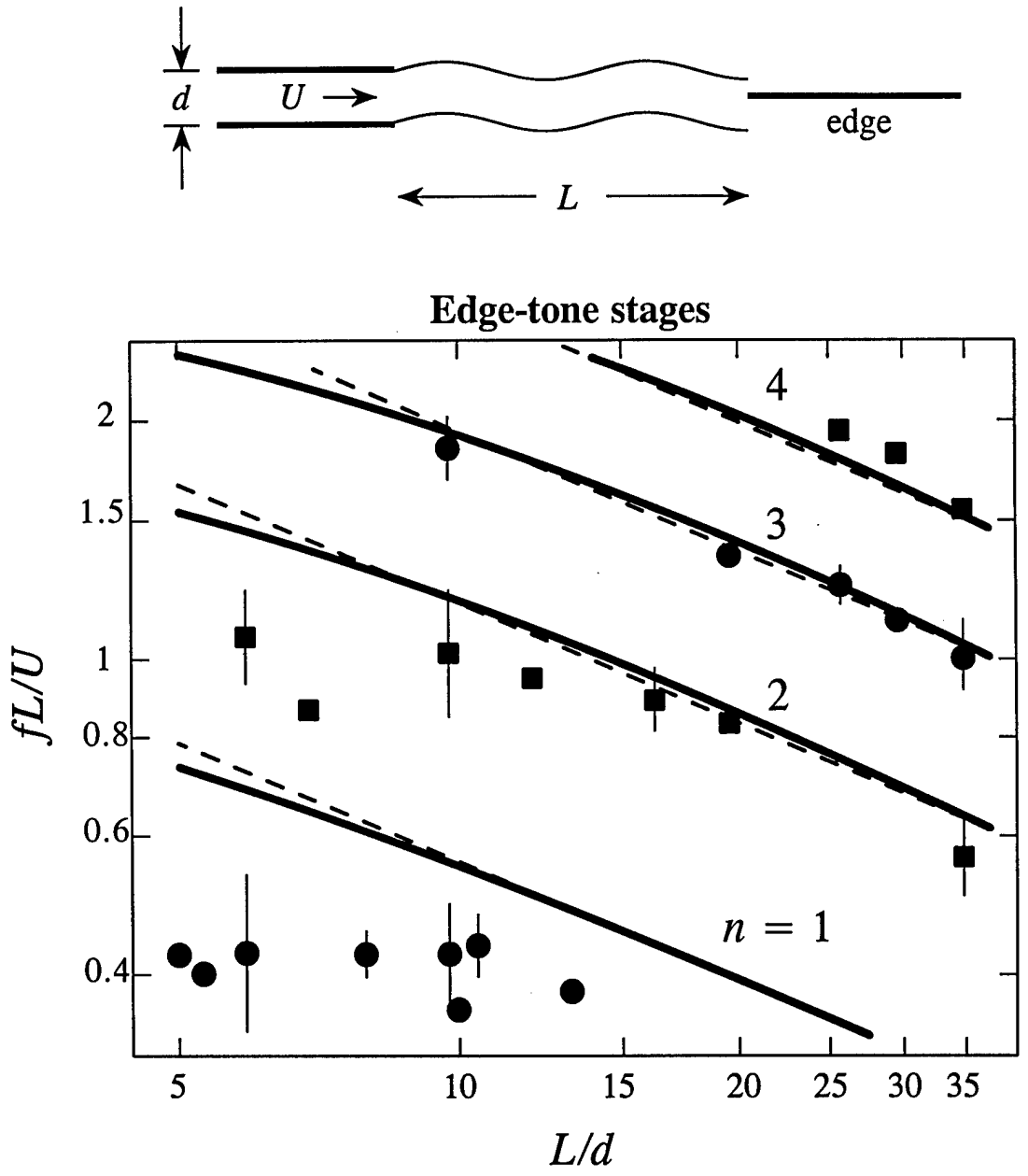

Figure 8. Comparison of edge tone Strouhal numbers predicted by equation (3.3) for $b/L = 500$ (———) with representative averages of data from Holger et al [17]. The broken lines are predictions of (3.5).

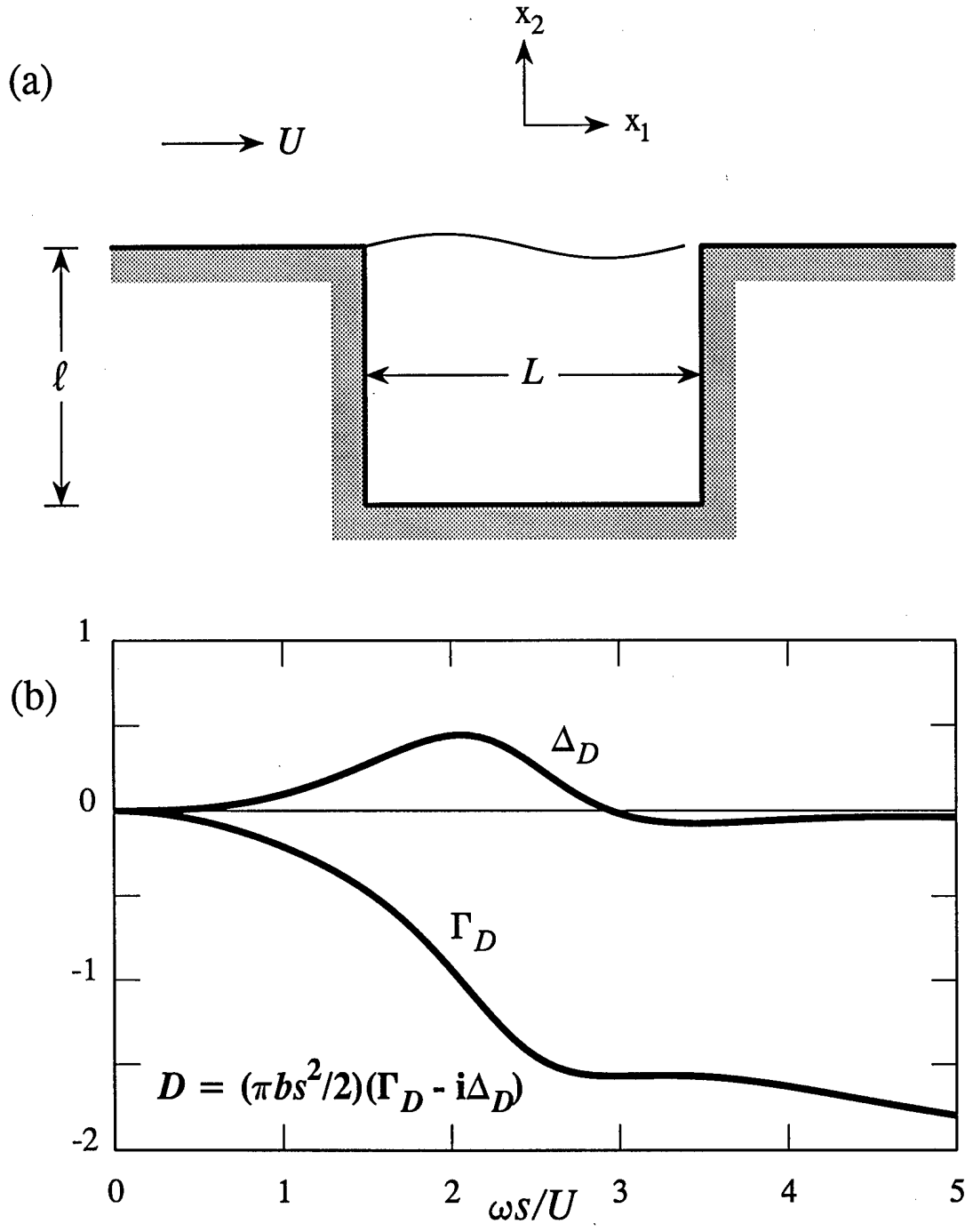

Figure 9. (a) Rectangular wall cavity. (b) Real and imaginary parts of the drag coefficient $D(\omega)$ for real ω when the cavity aspect ratio $b/L = 1$.

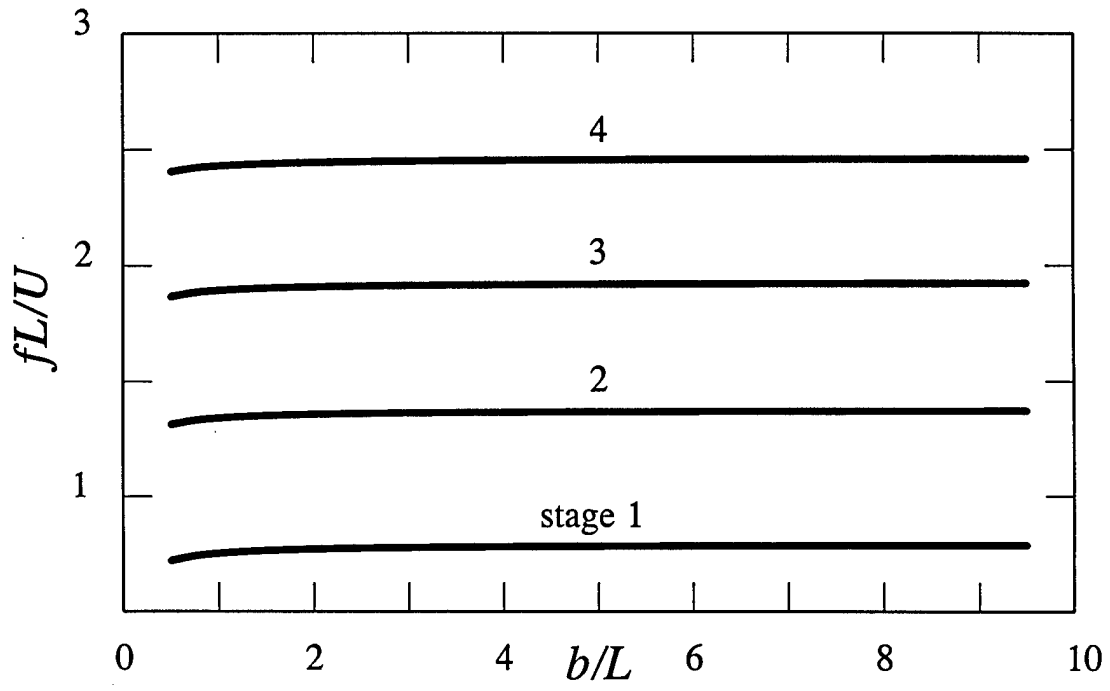

Figure 10. Predicted dependence of the shallow cavity Strouhal number on the aspect ratio b/L at infinitesimal mean flow Mach number.

CHAPTER 4

THE INFLUENCE OF SHAPE ON THE RAYLEIGH CONDUCTIVITY OF A WALL APERTURE IN THE PRESENCE OF GRAZING FLOW

Sheryl M. Grace, Kelly P. Horan
and M. S. Howe

SUMMARY

A numerical investigation is made of the influence of grazing flow on the Rayleigh conductivity K_R of an aperture in a thin rigid wall. The Mach number is sufficiently small for the local motion near the aperture to be regarded as incompressible, and the Reynolds number is taken to be large enough for the aperture shear layer to be modeled by a vortex sheet. The vortex sheet is assumed to be linearly perturbed from its equilibrium position by a small amplitude, time-harmonic pressure, and K_R is determined from the ratio of the resulting aperture volume flux to the applied pressure. The frequency dependence of K_R is computed for a variety of aperture shapes for both one-sided and two-sided flows. For apertures of equal maximum streamwise dimension in one-sided flow, the Strouhal number range within which perturbation energy is extracted from the mean flow (where Im $K_R > 0$) is found to be effectively independent of the aperture shape. The frequency of the first "operating stage" of self-sustained (*unforced*) oscillations of the aperture shear layer lies approximately in the center of this range, and is the minimum frequency at which narrow band sound is generated by nominally steady flow over the aperture. The numerical predictions are shown to satisfy the reverse flow reciprocal theorem (Howe et al. 1996), according to which K_R is unchanged when the mean flow directions on both sides of the wall are reversed (when vortex shedding occurs from the "opposite" edge of the aperture).

1. INTRODUCTION

A time harmonic pressure load $(p_o^+ - p_o^-)e^{-i\omega t}$ is applied across an aperture in a thin rigid wall, which coincides with the plane $x_2 = 0$ of the rectangular coordinate system (x_1, x_2, x_3) (see Figure 1). The pressures p_o^+, p_o^- are uniform respectively in $x_2 \gtrless 0$, and produce a volume flux through aperture in the positive x_2-direction equal to $Qe^{-i\omega t}$.

The *Rayleigh conductivity* is defined in terms of these quantities by the ratio (Rayleigh 1945)

$$K_R(\omega) = \frac{i\omega\rho_o Q}{p_o^+ - p_o^-} \tag{1.1}$$

where ρ_o is the mean fluid density, which is assumed to be constant. Conductivity has the dimensions of length; for an ideal, incompressible fluid (in the absence of mean flow) its value is entirely determined by the geometric shape of the aperture, being equal to $2R$ for a circular aperture of radius R, and approximately equal to $2 \times \sqrt{(\text{aperture area}/\pi)}$ for an arbitrary, non-elongated aperture. In a real fluid K_R is generally a complex function of the frequency ω, and energy of the applied pressure field (an incident sound wave, for example) is dissipated in the aperture at a rate

$$\Pi = -\frac{1}{2}\mathrm{Re}\big(Q^*[p_o^+ - p_o^-]\big) \equiv -\frac{\mathrm{Im}\{K_R(\omega)\}}{2\rho_o\omega}|p_o^+ - p_o^-|^2\,, \tag{1.2}$$

where the asterisk denotes complex conjugate (Pierce 1989). The damping is *negative* ($\Pi < 0$) if $\mathrm{Im}\{K_R(\omega)\} > 0$ (for $\omega > 0$), which can happen in the presence of mean flow over one or both sides of the wall. The forced motion in the aperture then grows at the expense of mean flow kinetic energy (Howe et al. 1996) via coupling facilitated by unsteady vortex shedding from the aperture leading edge. The phase of the interaction of this vorticity with the trailing edge (after convection across the aperture) determines whether or not perturbation energy is extracted from or ceded to the mean flow.

The negative damping of forced motion in the presence of flow is related to the instability of the mean shear layer in the aperture (Lamb 1932) and to the possible occurrence of self-sustained oscillations that produce narrow band sound (Rossiter 1964; Howe et al. 1996; Rockwell 1983; Blake & Powell 1986). Such oscillations are maintained by feedback,

involving the periodic generation of pressure "waves" at the trailing edge by interaction with shed vorticity, which triggers the cyclic formation of new vorticity at the leading edge. The oscillations are reinforced and sustained for a set of discrete values of the *Strouhal* number based on the streamwise length of the aperture and the mean flow velocity (Powell 1961; Rossiter 1964; Blake & Powell 1986). A quantitative understanding of the feedback mechanism is desirable because of its importance in a diverse range of physical systems including, for example, perforated baffles in heat exchangers, depressions in submarine and ship hulls, computer boards with closely spaced chip carriers, aircraft control surfaces and fuselage openings, and flow-through resonators of automobile mufflers.

To obtain a complete picture of the motion produced by the applied pressure, or of the frequency and amplitude of the self-sustaining oscillations, it is necessary to solve the nonlinear Navier-Stokes equations. However, an accurate first approximation to the forced motion and to the *frequencies* of self-sustained oscillations is furnished by a *linearized* treatment of the shear layer motion (Howe 1997a). This is because both the feedback and non-resonant energy transfers are governed primarily by the convection speed of vorticity across the aperture, which experiment shows to be essentially independent of the amplitude of the shear layer motion (Powell 1961; Holger, Wilson, & Beavers 1977; Rockwell 1983; Blake & Powell 1986).

Approximations of this kind have been considered by Howe (1981a,1981b) for slot-type apertures of very large aspect ratio. The Reynolds number was taken to be sufficiently large that turbulence-free mean streams over the wall could be regarded as uniform, and the mean shear layer in the aperture was modeled by a vortex sheet that is *linearly* disturbed from its mean position. The same method was applied by Scott (1995) (see also Howe et al. (1996)) to a circular aperture, and by Howe (1997a, 1997b,1997c) to rectangular apertures of arbitrary aspect ratio. The mean flow Mach number was assumed to be small enough for the aperture motion to be regarded as incompressible. Viscosity was ignored, except for its role in shedding vorticity from the leading edge of the aperture, which was incorporated by application of the Kutta condition. Howe (1997a) showed that linear theory predicts that $K_R(\omega)$ has simple poles in $\mathrm{Im}\,\omega > 0$, and that the real part of the complex frequency at a pole corresponds to the frequency of an "operating stage" of the self-sustained oscillations.

In this paper the numerical method of Scott (1995) is extended to determine the ef-

fect of shape on the conductivity of an aperture in a thin wall in the presence of grazing flow. Detailed comparisons are made of the conductivities for shapes including the circle, square, triangle, "cross", and a square whose leading or trailing edge has triangular serrations ("crown"). When the Strouhal number $\omega L/U$ is defined in terms of the maximum streamwise dimension $2L$ of the aperture and a mean flow velocity U, it is shown that aperture shape has effectively no influence on the Strouhal number ranges in which forced oscillations are unstable (i.e., where $\Pi(\omega)$ of (1.2) is *negative*). According to Howe (1997c) this indicates that the minimum Strouhal number of self sustained oscillations (i.e., of the first operating stage) does not vary significantly with geometry. The calculations also furnish direct numerical confirmation of *reverse flow reciprocity* (Howe et al. 1996), namely, that the value of $K_R(\omega)$ is unchanged when the direction of the mean flow is reversed. This remarkable theorem implies, for example, that the conductivity of a square aperture with a serrated leading edge is unchanged when the flow is reversed, such that shed vorticity from a straight leading edge now *impinges* on the serrations. This result could be important in assessing the efficiency of "spoilers" intended to reduce the coherence of sound generated by vortex shedding.

The numerical problem is formulated in §2, and applied in §3 to determine the conductivities of apertures of various shapes in the presence of mean flow over one or both sides of the wall. A comparison is also made with the approximate theory of Howe (1997a). Reverse flow reciprocity is discussed in §4.

2. THE GOVERNING EQUATIONS

2.1 Equation of motion of the vortex sheet

The motion on either side of the aperture induced by the perturbed motion of the vortex sheet is regarded as incompressible and irrotational, and is expressed in terms of velocity potentials $\Phi^{\pm}$ respectively in the regions $x_2 \gtrless 0$ "above" and "below" the wall. The potentials satisfy Laplace's equation

$$\nabla^2 \Phi^{\pm} = 0, \quad x_2 \gtrless 0, \tag{2.3}$$

and the associated pressure fluctuations $p^{\pm}$ are given by the linearized Euler equation in the form

$$p^{+} = i\rho_0(\omega + iU^{+}\frac{\partial}{\partial x_1})\Phi^{+}, \quad x_2 > 0 \tag{2.4}$$

$$p^{-} = i\rho_0(\omega + iU^{-}\frac{\partial}{\partial x_1})\Phi^{-}, \quad x_2 < 0. \tag{2.5}$$

The equation of motion of the vortex sheet is obtained by equating the net pressures on opposite sides at the undisturbed position of the sheet, i.e.,

$$p_o^{+} + i\rho_0(\omega + iU^{+}\frac{\partial}{\partial x_1})\Phi^{+} = p_o^{-} + i\rho_0(\omega + iU^{-}\frac{\partial}{\partial x_1})\Phi^{-}, \quad x_2 = 0, \tag{2.6}$$

where the field point $(x_1, 0, x_3)$ lies within the aperture.

The solution of Laplace's equation (2.3) can be written

$$\Phi^{\pm}(\mathbf{x}) = \mp\frac{1}{2\pi}\int_{-\infty}^{\infty}\int_{-\infty}^{\infty}\frac{\partial\Phi^{\pm}/\partial y_2}{|\mathbf{x}-\mathbf{y}|}\,dy_1 dy_2, \qquad \mathbf{y} = (y_1, 0, y_3), \quad x_2 \gtrless 0, \tag{2.7}$$

where the normal derivatives $\partial\Phi^{\pm}/\partial y_2$ are evaluated on $y_2 = \pm 0$ (Hildebrand 1976). These derivatives are related to the displacement ζ of the vortex sheet (in the y_2 direction) by

$$\frac{\partial\Phi^{\pm}}{\partial y_2} = -i(\omega + iU^{\pm}\frac{\partial}{\partial y_1})\zeta\ , \quad y_2 = \pm 0,$$

which permits equation (2.6) to be cast in the form

$$\frac{p_o^+ - p_o^-}{\rho_0} = \frac{1}{2\pi}\left[(\omega + iU^-\frac{\partial}{\partial x_1})^2 + (\omega + iU^+\frac{\partial}{\partial x_1})^2\right]\int_S \frac{\zeta(y_1, y_3)}{|\mathbf{x}-\mathbf{y}|}\, dy_1 dy_3 \qquad (2.8)$$

where the integration is now restricted to the aperture opening S.

This equation is simplified by introducing the nondimensional notation

$$\mathbf{X}, \mathbf{Y} = \mathbf{x}/L, \mathbf{y}/L \qquad (2.9)$$

$$\sigma = \omega L/U^+ \qquad (2.10)$$

$$Z = \frac{\zeta \rho_0 \sigma^2 U^{+2}}{\pi L(p_o^+ - p_o^-)} \qquad (2.11)$$

where σ is the Strouhal number and $2L$ is the maximum streamwise length of the aperture. By integrating (2.8) with respect to the second order differential operator in x_1 on the right hand side, we can then write

$$\int_{S} \frac{Z(Y_1, Y_3)}{|\mathbf{X}-\mathbf{Y}|}\, dY_1 dY_3 = 1 + \alpha(X_3)e^{i\sigma_1 X_1} + \beta(X_3)e^{i\sigma_2 X_1}, \quad X_2 = 0. \qquad (2.12)$$

Here, $\sigma_{1,2}$ are the nondimensional Kelvin-Helmholtz wavenumbers (Lamb 1932)

$$\sigma_1 = \frac{\omega L(1+i)}{U^+ + iU^-}, \qquad \sigma_2 = \frac{\omega L(1-i)}{U^+ - iU^-}. \qquad (2.13)$$

$\alpha(X_3)$ and $\beta(X_3)$ are "constants" of integration that depend on the spanwise coordinate X_3. They may be interpreted as the amplitudes of instability waves of wavenumbers $\sigma_{1,2}$ propagating across the aperture, their values being fixed by application of the Kutta condition at the leading edge (Howe et al. 1996; Scott 1995).

When the mean velocities are the same on both sides of the wall ($U^+ = U^-$) the wavenumbers σ_1 and σ_2 are both equal to σ, and the right hand side of equation (2.12) may be replaced by

$$1 + \alpha(X_3)e^{i\sigma X_1} + \beta(X_3)X_1 e^{i\sigma X_1}\,.$$

2.2 The numerical procedure

Equation (2.12) is solved for the nondimensional displacement Z by introducing the Cartesian grid shown schematically in Figure 2 and discretizing the integration over the aperture. The displacement $Z(Y_1, Y_3)$ is taken to be constant and equal to Z_{ij} on the grid cell centered on (Y_{1i}, Y_{3j}), but the kernel function $1/|\mathbf{X} - \mathbf{Y}|$ is integrated analytically. The Kutta condition is imposed by setting $Z = 0$ on the first two grid cells in each grid row of constant Y_3 (indicated in the figure by the asterisks), i.e., by demanding that $Z_{1j} = Z_{2j} = 0$; this is equivalent to requiring that the displacement and streamwise derivative of the vortex sheet vanish at the aperture leading edge. When this is done, Z_{1j} and Z_{2j} may be discarded from the discretized equation of motion and their respective roles in the vector of unknowns assumed by the corresponding instability wave amplitudes $\alpha(Y_{3j})$ and $\beta(Y_{3j})$. The equation is then solved for the Z_{ij} by collocation, by requiring it to be satisfied at each lattice point of the grid.

The definition (1.1) and the solution array Z_{ij} then determine the Rayleigh conductivity by

$$\begin{aligned} K_R(\omega) &= \pi L \int\int_S Z(Y_1, Y_3)\, dY_1 dY_3 \\ &\approx \pi L \sum_{i \neq 1,2;j} Z_{ij} W_{ij}, \end{aligned} \tag{2.14}$$

where W_{ij} denotes the area of the grid element centered on (Y_{1i}, Y_{3j}).

3. NUMERICAL RESULTS

The set of aperture shapes considered in this investigation is illustrated in Figure 3, and includes the circle, square, cross, two different forward (upstream pointing) and backward (downstream pointing) facing triangles, and a "crown" (square with triangular serrated leading or trailing edge). For each aperture the conductivity is calculated in the normalized form

$$K_R(\omega)/2L = \Gamma - i\Delta,$$

for both one-sided flow (where $U^- = 0$), and for two-sided flow when $U^+ = U^-$.

The circular aperture was treated by Scott (1995), and his results have been used as one method to validate the integration procedure. Chanaud (1994) discussed the cross-shaped aperture in the absence of flow. The "crown" is examined because of its relevance to applications in which it is desirable to create incoherent streams of vorticity by shedding from a serrated edge. The computations are performed in single precision using a square mesh discretization of equation (2.12). The validity of using single precision was tested by calculating the conductivity for two-sided flow past a square aperture using both single and double precision and comparing the results. The absolute difference between the real part of the conductivity from the two calculations and the absolute difference between the imaginary part from the two calculations are plotted in Figure 4. The maximum difference is 7×10^{-4} and the average absolute difference is approximately 2×10^{-4}. Because this difference is so small, there is no loss of information when performing the calculation using single precision.

The size of the square mesh elements is set by choosing the number of mesh elements stretching between the leading and trailing edges along the centerline of the aperture. Figures 5 and 6 show the effect of increasing the mesh density on the calculations of the conductivity for one and two sided grazing flow past a square aperture. (When the number of elements increases from 30 to 60, this decreases the grid element nondimensional area from 4.4×10^{-2} to 1.1×10^{-2}.) In these figures the calculated real and imaginary components, Γ and Δ, of the conductivities for one-sided and two-sided flow are plotted against Strouhal number $\sigma = \omega L/U$. Figure 5 shows that for the Strouhal numbers of interest in the one-sided flow case the numerical results become completely grid independent at a grid corresponding to 50

mesh elements in the streamwise direction. The two-sided flow case, which can be calculated out to higher Strouhal number becomes grid independent when the grid has 60 elements in the streamwise direction.

For the cases of both one-sided and two-sided flow, the difference between the discretizations of 40, 50, and 60 elements are very small. Past this Strouhal number, a grid of more than 70 elements must be used as the finer grids shift the results for the higher Strouhal number to the left slightly. Because it was the point of this research to compare the conductivity for several aperture shapes, we have used a discretization 40. The slight shift that exists at the higher Strouhal numbers will be the same for all of the calculations and was a small trade-off for a large speed up computationally. If a discretization higher than 40 was used for a specific case, it will be noted.

3.1 One-sided mean flow

The real and imaginary components, Γ and Δ, of the conductivities for one-sided flow past the different aperture shapes are plotted against Strouhal number ω in Figure 7. All of these plots are qualitatively the same. In particular $\Delta > 0$ at low frequencies, so that forced motion of the aperture at such frequencies is always damped (see equation (1.2)), the energy of the applied pressure force (produced by an incident sound wave, for example) being lost to the mean flow. The damping is negative ($\Delta < 0$) over a band of higher frequencies, wherein the mean flow releases kinetic energy when shed vorticity interacts with the aperture trailing edge. In this case there would be a net gain in acoustic energy when the shear layer is excited by sound. By invoking function theoretic arguments it can be shown (Howe 1997c) that $K_R(\omega)$ has a simple pole at a complex frequency in the upper half-plane whose real part is approximately equal the real frequency at which $\Delta(\omega)$ is a minimum. The real part of the frequency at this pole corresponds to the Strouhal number of the first operating stage of self-sustained oscillations of the aperture shear layer (Howe 1997a). It is only weakly dependent on aperture shape, since all of the minima in Figure 7 lie within the interval $2.5 < \omega L/U < 3.2$. In particular, the conductivity of the square aperture with a serrated leading edge (the "crown") is practically the same as that for the straight-edged square. A comparison of the conductivities for the forward and backward facing triangles indicates that $K_R(\omega)$ is unchanged when the flow direction is reversed. This reverse flow reciprocity is

discussed further below. The calculation of the conductivity of the smaller triangle required a mesh with 100 elements in the streamwise direction.

In the absence of flow Rayleigh (1945) showed that $K_R/\sqrt{A} \approx$ constant, where A is the aperture area. The result of normalizing $K_R(\omega)$ in the same way in the presence of one-sided flow is shown in Figure 8.

3.2 Uniform two-sided mean flow, $U^+ = U^-$

Figure 10 shows the calculated frequency dependencies of Γ and Δ when the mean flow speed is the same on both sides and equal to U. The quasi-periodic behavior of these functions confirms the earlier prediction of Scott (1995) for the circle. In this case, however, the aperture motions are only conditionally unstable, in the sense that an incident perturbation will grow by extracting energy from the mean flow provided $\Delta < 0$, but there are no poles in Im $\omega > 0$, so that self-sustaining oscillations are not possible, at least in the ideal limit of a vanishingly thin wall (Howe 1997c). The minima of Δ occur at roughly the same values of σ for all of the cases shown in the figures; this is also evident from Figures 11 and 12, where the conductivities are normalized with respect to $\sqrt{A}$. Again the agreement shown in Figure 12 for corresponding forward and backward triangles is in accord with reverse flow reciprocity.

For regularly shaped apertures such as the square, the results indicate that $K_R(\omega)$ is periodic at high enough frequency, and that the magnitudes of successive maxima and minima are effectively constant. For those apertures whose streamwise dimension decreases continuously with distance from the line of symmetry (the circle and triangle), the magnitudes of successive maxima and minima decrease with increasing σ. For the cross-shaped aperture, which has two very different streamwise length scales, successive maxima and minina exhibit two distinct values which recur alternately as the frequency increases. In the case of the "crown" shaped aperture, there are two dominant length scales, which are reflected in the two alternating sets of values for the maxima and minima, in addition however, the magnitudes of the peaks gradually decrease with increasing σ.

3.3 One-dimensional approximation to the aperture motion

Howe (1997b) has estimated the influence of mean flow on the conductivity of *rectangular* apertures (with sides parallel to the mean flow direction) by neglecting the dependence of the vortex sheet displacement on the spanwise coordinate x_3. The integro-differential equation (2.8) can then be simplified by explicitly performing the integration on the right hand side with respect to y_3. When the equation is also integrated with respect to x_3 over the span, the analog of equation (2.12) assumes the one-dimensional form

$$\int_{-1}^{1} Z'(Y_1)\,[\ln|Y_1 - X_1| + \mathcal{L}(X_1, Y_1)]\,dY_1 + \lambda_1 e^{i\sigma_1 X_1} + \lambda_2 e^{i\sigma_2 X_1} = 1,\ |X_1| < 1, \qquad (3.15)$$

where

$$Z' = \frac{-2\zeta\rho_o\sigma^2 U^{+2}}{\pi L(p_o^+ - p_o^-)}$$

$$\mathcal{L}(X_1, Y_1) = -\ln\{b/L + \sqrt{[(b/L)^2 + (X_1 - Y_1)^2]}\} + \sqrt{\{1 + (L/b)^2(X_1 - Y_1)^2\}} - (L/b)|X_1 - Y_1|,$$

$\lambda_{1,2}$ are constants to be determined, and b is the span.

Equation (3.15) is solved by collocation; the values of $\lambda_{1,2}$ are determined by imposing the Kutta condition at the upstream edge $X_1 = -1$ as before, and the conductivity is calculated from

$$K_R = -\frac{\pi b}{2}\int_{-1}^{1} Z'(Y_1)\,dY_1.$$

Predictions of $K_R(\omega)$ obtained in this way for a square aperture in one or two-sided grazing flow are plotted as solid curves in Figure 13. The dotted curves in Figure 13 correspond to the numerical solution of the full three-dimensional equation of motion (2.8) obtained with a discretization corresponding to 60 mesh elements in the streamwise direction for the one-sided flow case and 70 for the two-sided flow case. It is clear from the figure that the one-dimensional approximation produces a good prediction to the motion of the vortex sheet

in the mouth of the square aperture. The approximation does not work as well for lower aspect ratio apertures nor for apertures with tapered spans.

4. REVERSE FLOW RECIPROCITY

Reverse flow reciprocity (Howe, Scott, & Sipcic 1996) requires that the Rayleigh conductivity at a given frequency ω be unchanged in value when the directions of the mean flows on both sides of the wall are reversed. The theorem has been verified in §3 for forward and backward facing triangular apertures. In doing this we used a square element numerical grid. It is important that the mesh be sufficiently fine to properly capture the dynamics of shedding from the sloping edges of a triangle. This is clear from divergence of the numerical predictions at the higher Strouhal numbers shown in Figure 9.

More dramatic confirmation of the theorem is exhibited in Figure 14, where the conductivities for a square aperture with either a serrated leading or serrated trailing edge (the "crown") are seen to be identical. This conclusion may be very significant for the design of flow control devices that depend on the use of serrations to 'break up" an organized flow in an attempt to minimize coherent generation of sound and vibration.

5. CONCLUSION

When a sound wave impinges on a wall aperture in the presence of high Reynolds number flow there is generally an exchange of energy between the sound and the flow brought about by acoustically induced vortex shedding. For a small aperture, the motion in its immediate neighborhood can be regarded as incompressible, and the interaction with the sound is conveniently expressed in terms of the Rayleigh conductivity K_R.

In this paper $K_R(\omega)$ has been computed for a variety of apertures in a wall of infinitesimal thickness in the presence of high Reynolds number grazing flow. The shear layer in the aperture is modeled by a linearly disturbed vortex sheet. For one-sided flow over apertures with equal maximum streamwise dimension, the Strouhal number range in which energy is extracted from the mean flow is found not to vary significantly with aperture shape. The center of this range corresponds approximately to the frequency of the lowest order "operating stage" of self-sustained (*unforced*) oscillations of the aperture shear layer, which is therefore effectively independent of aperture shape.

Self-sustaining oscillations cannot occur in the ideal limit of a wall of zero thickness when the flows are the same on both sides, although forced motion by an incident disturbance can still induce vortex shedding and a positive or negative exchange of energy with the mean flow. In such cases $K_R(\omega)$ becomes essentially periodic when the Strouhal number exceeds about 3, and the number of distinct values taken by the maxima or minima of the real and imaginary parts of K_R turns out to be equal to the number of distinct streamwise length scales that characterize aperture geometry.

The reverse flow reciprocal theorem requires the value of $K_R(\omega)$ to be unchanged when the mean flow directions on both sides of the wall are reversed. This is confirmed by our computations, and is remarkable because the edges of the aperture at which vorticity is generated and on which vorticity impinges are reversed in the reciprocal problem, and, the respective geometries of these cases can be markedly different.

REFERENCES

Blake, W. K. & Powell, A. 1986 *The Development of Contemporary Views of Flow-tone Generation*, pp. 247–315. Springer.

Chanaud, R. C. 1994 Effects of geometry on the resonance frequency of Helmholtz resonators. *Journal of Sound and Vibration*, Vol. 178, 337–348.

Hildebrand, F. B. 1976 *Advanced Calculus for Applications*, p. 301. Prentice Hall.

Holger, D. K., Wilson, T. A., & Beavers, G. S. 1977 Fluid mechanics of the edgetone. *Journal of the Acoustical Society of America*, Vol. 62, 1116–1128.

Howe, M. S. 1981a The influence of mean shear on unsteady aperture flow, with application to acoustical diffraction and self-sustained cavity oscillations. *Journal of Fluid Mechanics*, Vol. 109, 125–146.

Howe, M. S. 1981b On the Theory of Unsteady Shearing Flow Over a Slot. *Philosophical Transactions of the Royal Society of London*, Vol. A-303.

Howe, M. S. 1997a Edge, cavity and aperture tones at very low Mach numbers. *Journal of Fluid Mechanics*, Vol. 330, 61–84.

Howe, M. S. 1997b Influence of Wall Thickness on Rayleigh Conductivity and Flow-Induced Aperture Tones. *Journal of Fluids and Structures*, (in press).

Howe, M. S. 1997c Low Strouhal number instabilities of flow over apertures and wall cavities. *Journal of the Acoustical Society of America*, (in press).

Howe, M. S., Scott, M. I., & Sipcic, S. R. 1996 The Influence of Tangential Mean Flow on the Rayleigh Conductivity of an Aperture. *Proceedings of the Royal Society of London*, Vol. A452, 2303–2317.

Lamb, S. H. 1932 *Hydrodynamnics* (6th, reprinted 1995 ed.), p. 373. Cambridge University Press.

Pierce, A. D. 1989 *Acoustics: An Introduction to Its Physical Principles and Applications.* Acoustical Society of America.

Powell, A. 1961 On the edgetone. *Journal of the Acoustical Society of America*, Vol. 33, 395–409.

Rayleigh, J.-W. S. 1945 *The Theory of Sound*, Vol. II, p. 173. Dover Publications.

Rockwell, D. 1983 Oscillations of Impinging Shear Layers. *AIAA Journal*, Vol. 21, 645 – 664.

Rossiter, J. E. 1964 Wind tunnel experiments of the flow over rectangular cavities at subsonic and transonic speeds. Technical Report 3438, Aeronautical Research Council Reports and Memoranda.

Scott, M. I. 1995 The Rayleigh Conductivity of A Circular Aperture in The Presence of A Grazing Flow. Master's thesis, Boston University.

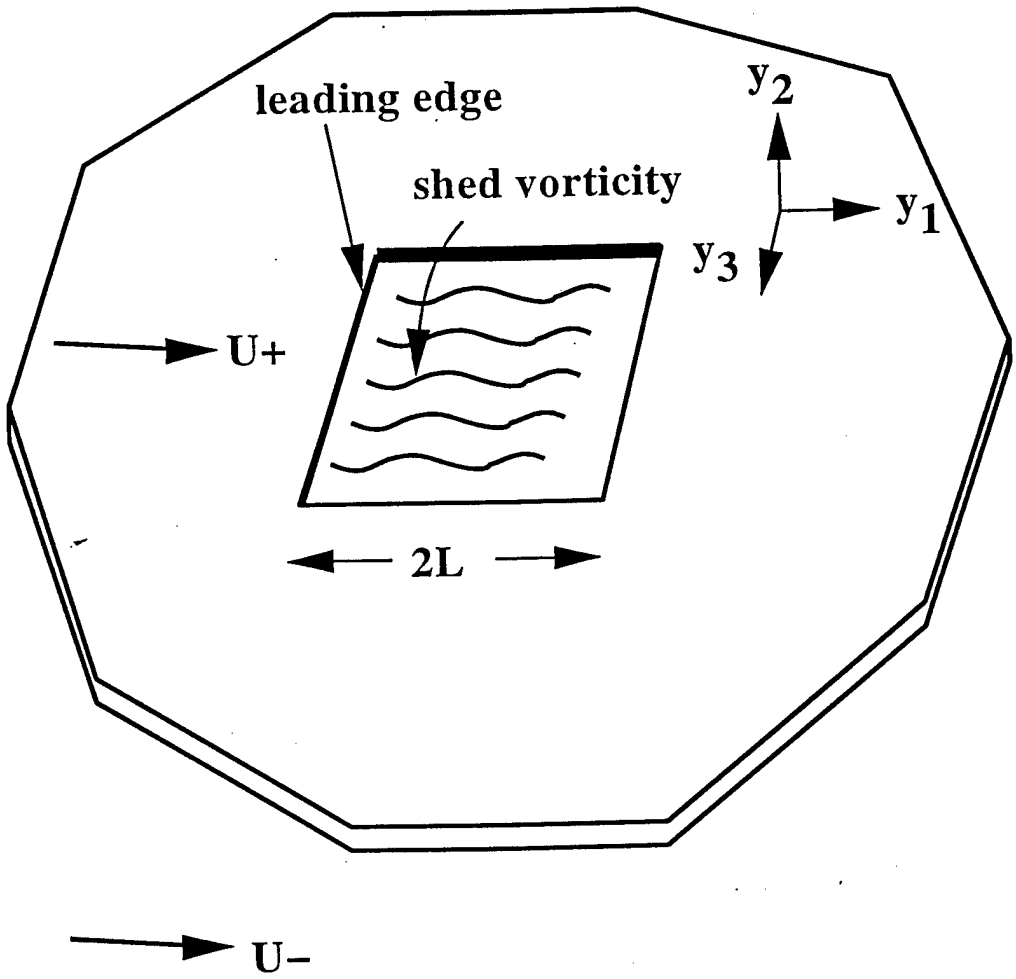

Figure 1: Grazing flow past a wall aperture.

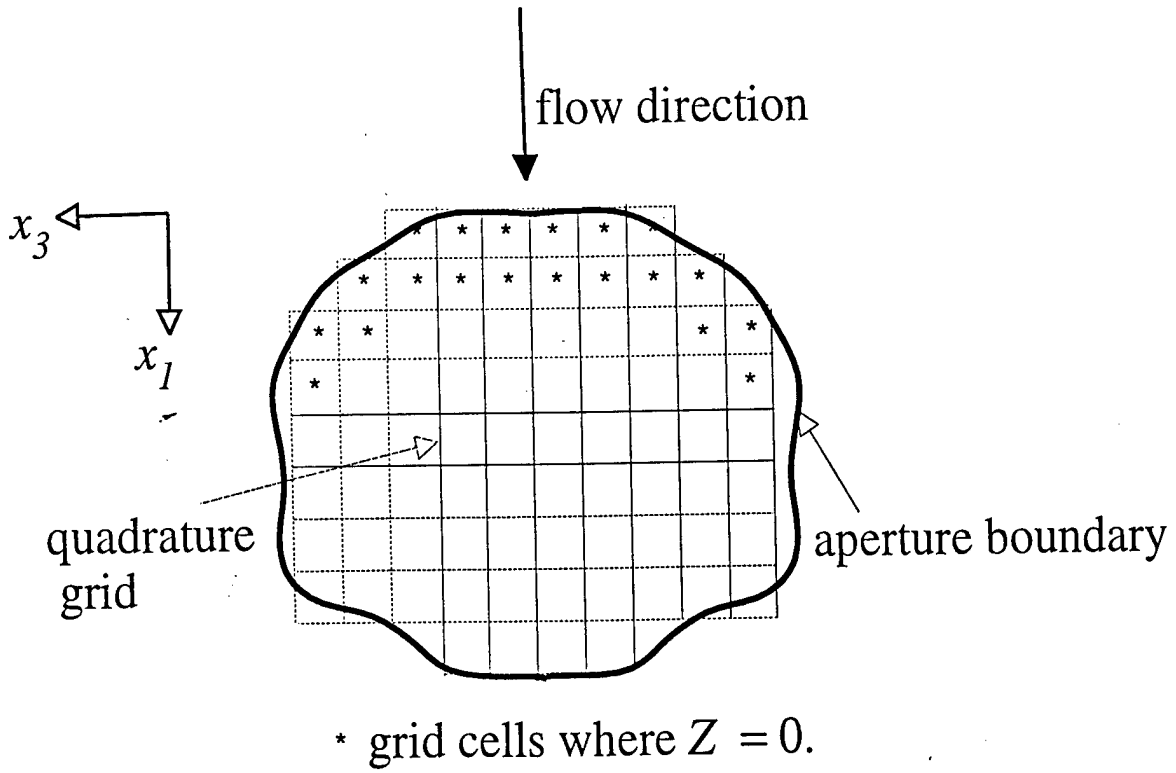

Figure 2: Quadrature grid used to solve the integral equation; asterisks denote the elements used to satisfy the Kutta condition.

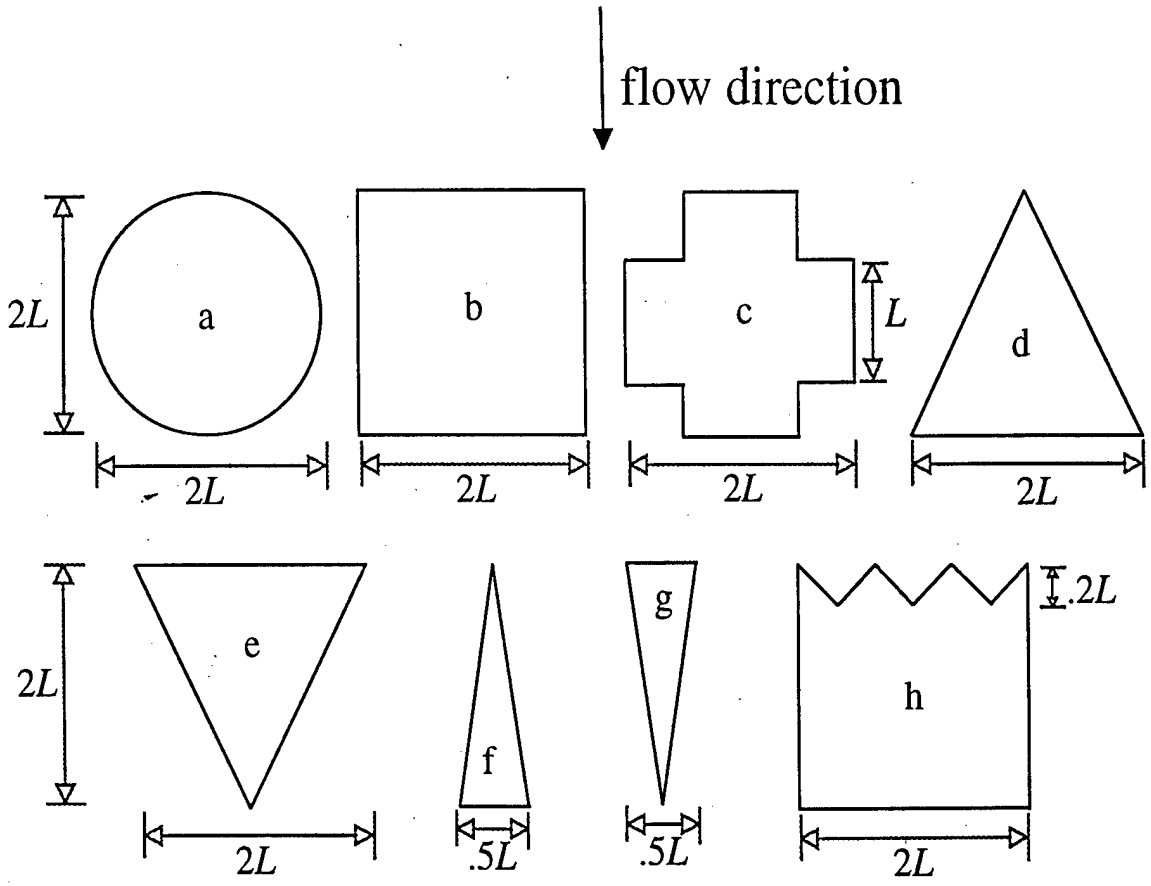

Figure 3: Aperture cross-sections studied. a) circle, b) square, c) cross, d) forward pointing triangle, e) backward pointing triangle, f) smaller forward pointing triangle, g) smaller backward pointing triangle, h) crown.

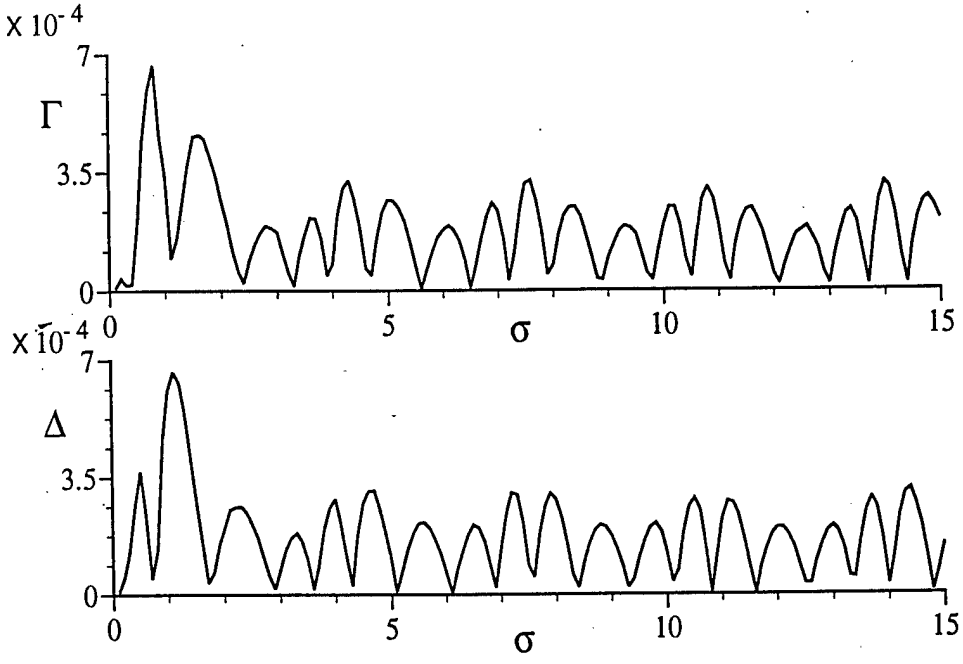

Figure 4: Effect of single precision vs. double precision numerical calculations.

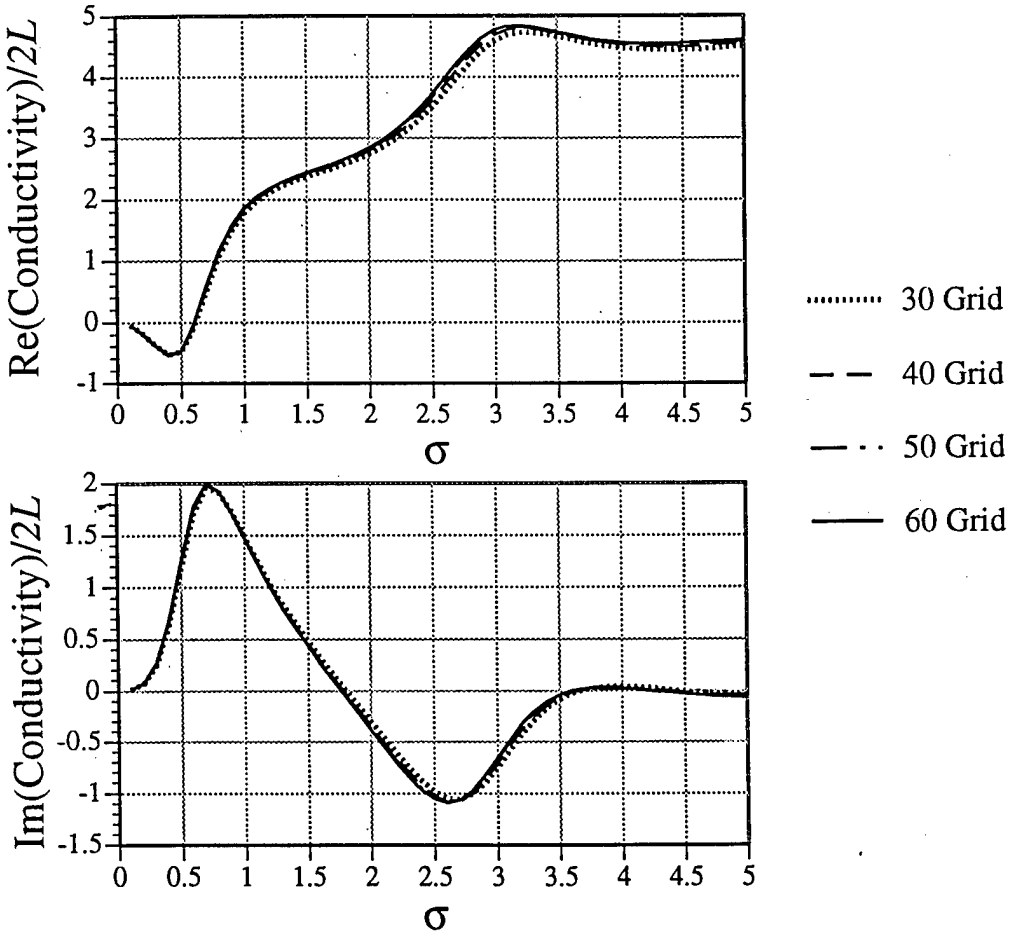

Figure 5: Dependence of Rayleigh conductivity calculation on grid resolution. One-sided grazing flow past a square aperture.

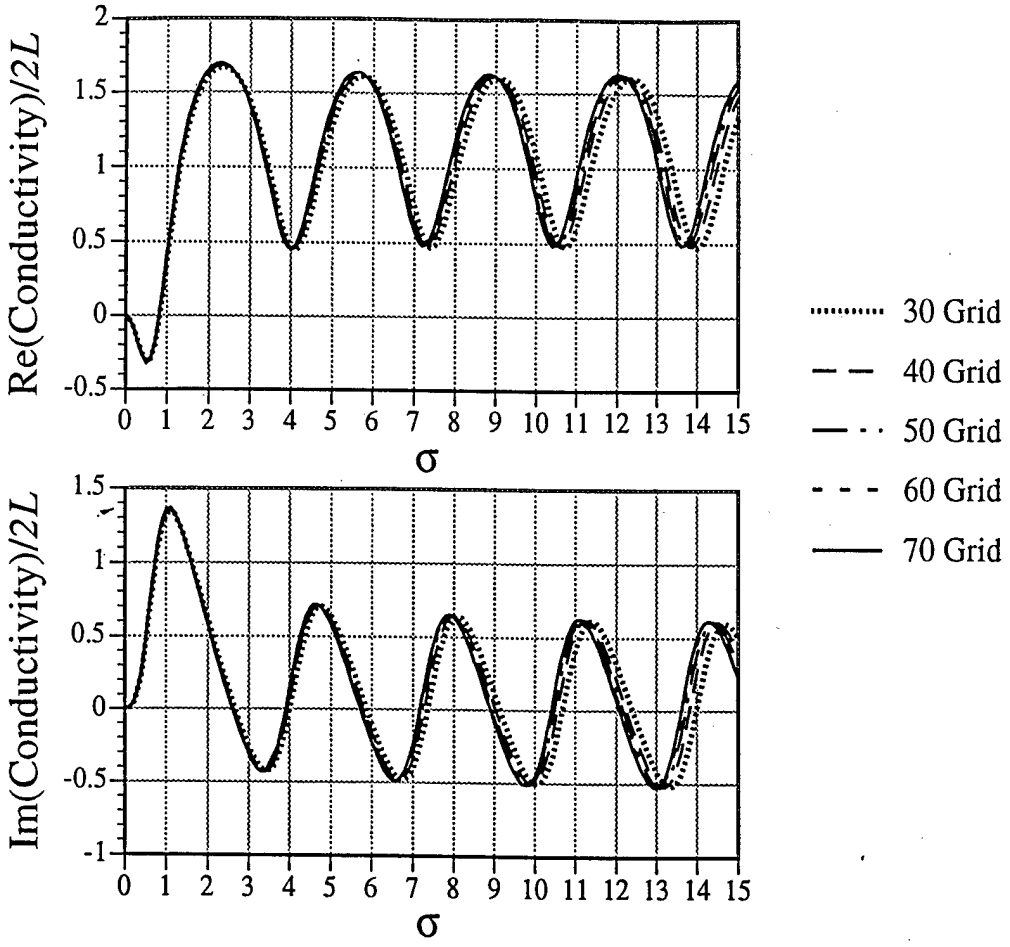

Figure 6: Dependence of Rayleigh conductivity calculation on grid resolution. Two-sided grazing flow past a square aperture.

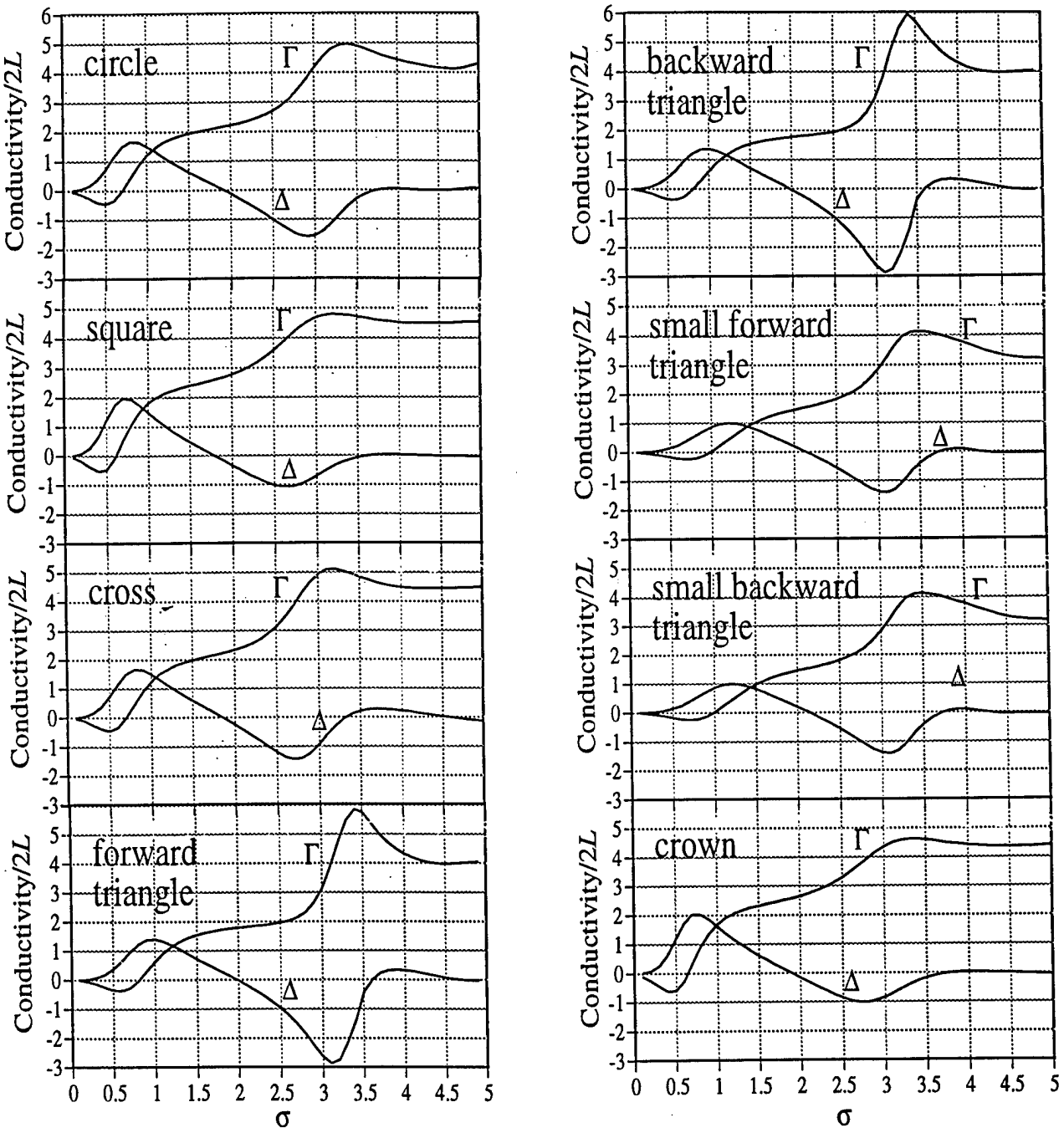

Figure 7: The Rayleigh conductivity for one-sided grazing flow past aperture with shapes circle, square, cross, forward triangle, backward triangle, small forward triangle, small backward triangle, and crown.

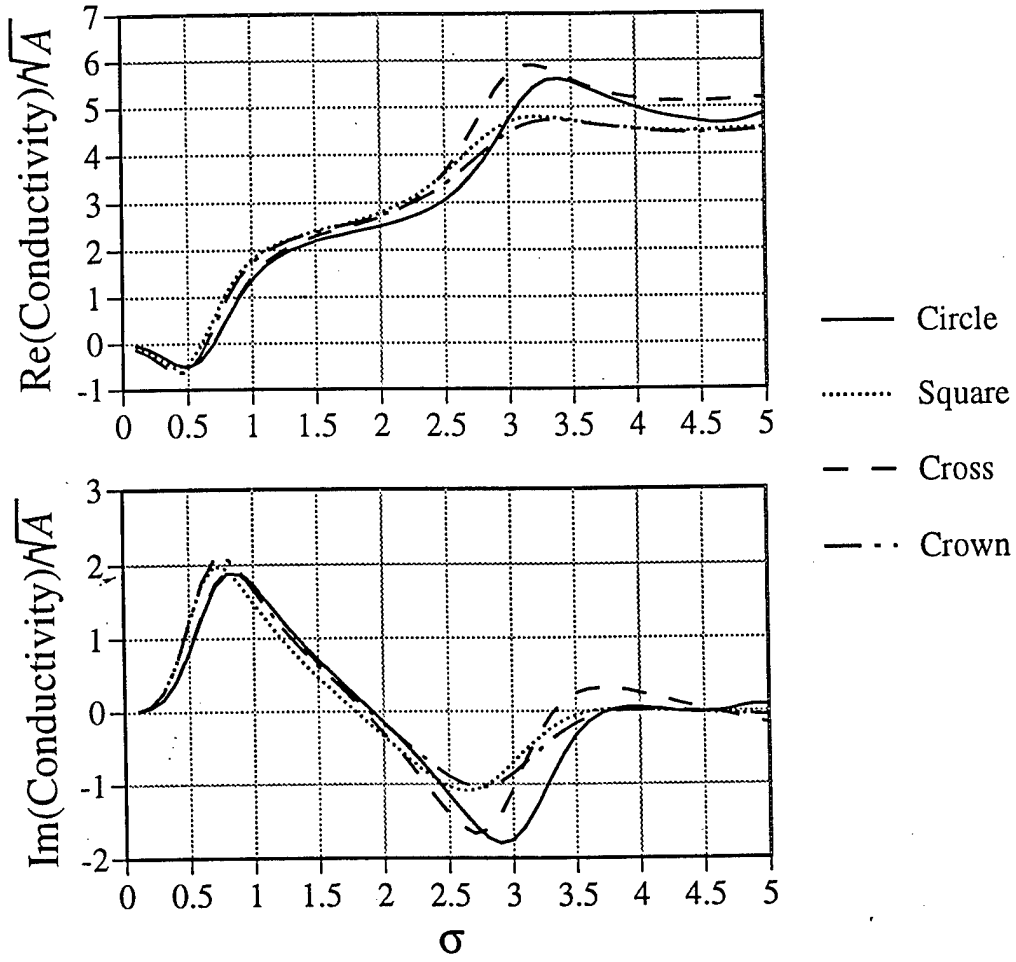

Figure 8: Real part (top) and imaginary part (bottom) of the Rayleigh conductivity normalized by the square root of the area for circle, square, cross, and crown apertures with flow on one side.

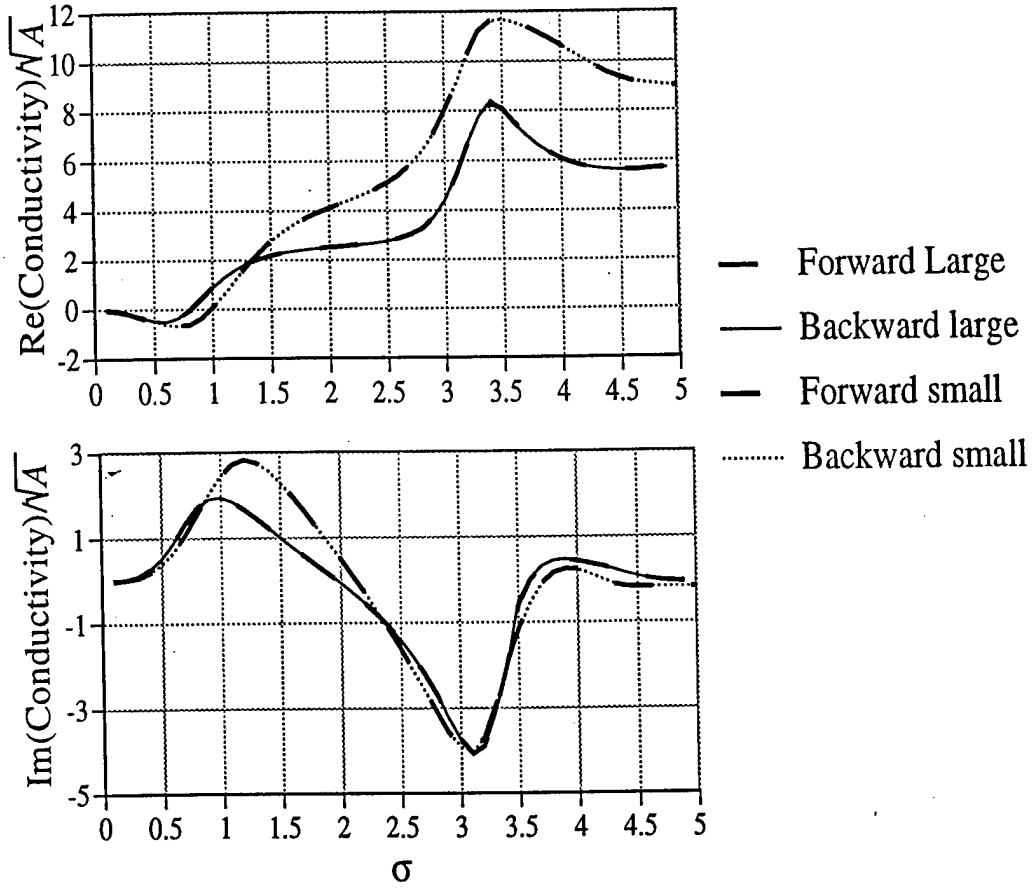

Figure 9: Real part (top) and imaginary part (bottom) of the Rayleigh conductivity normalized by the square root of the area for the large and small, forward and backward facing triangle apertures with flow on one side.

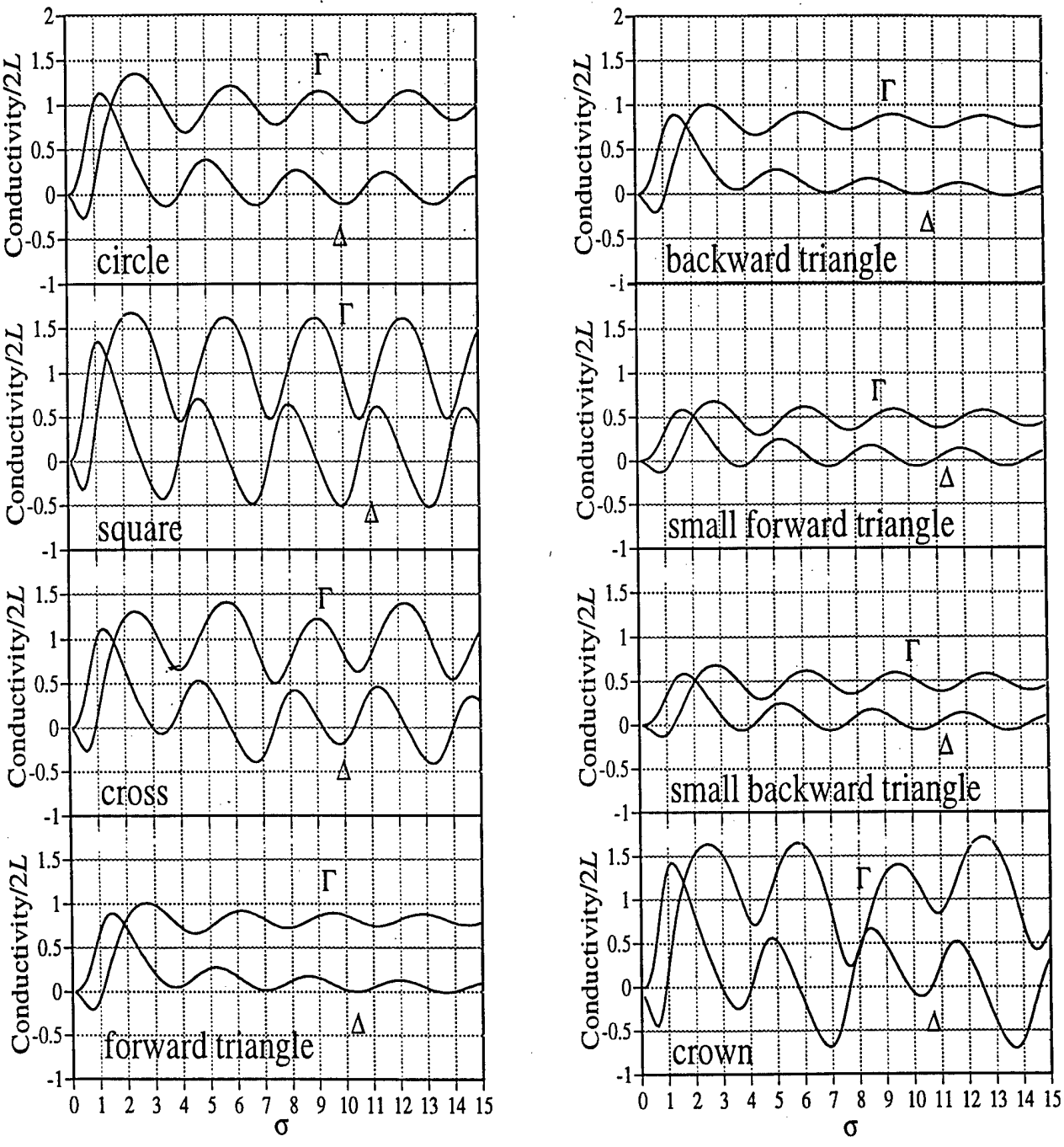

Figure 10: The Rayleigh conductivity for equal two-sided grazing flow past apertures with shapes: circle, square, cross, forward triangle, backward triangle, small forward triangle, small backward triangle and crown.

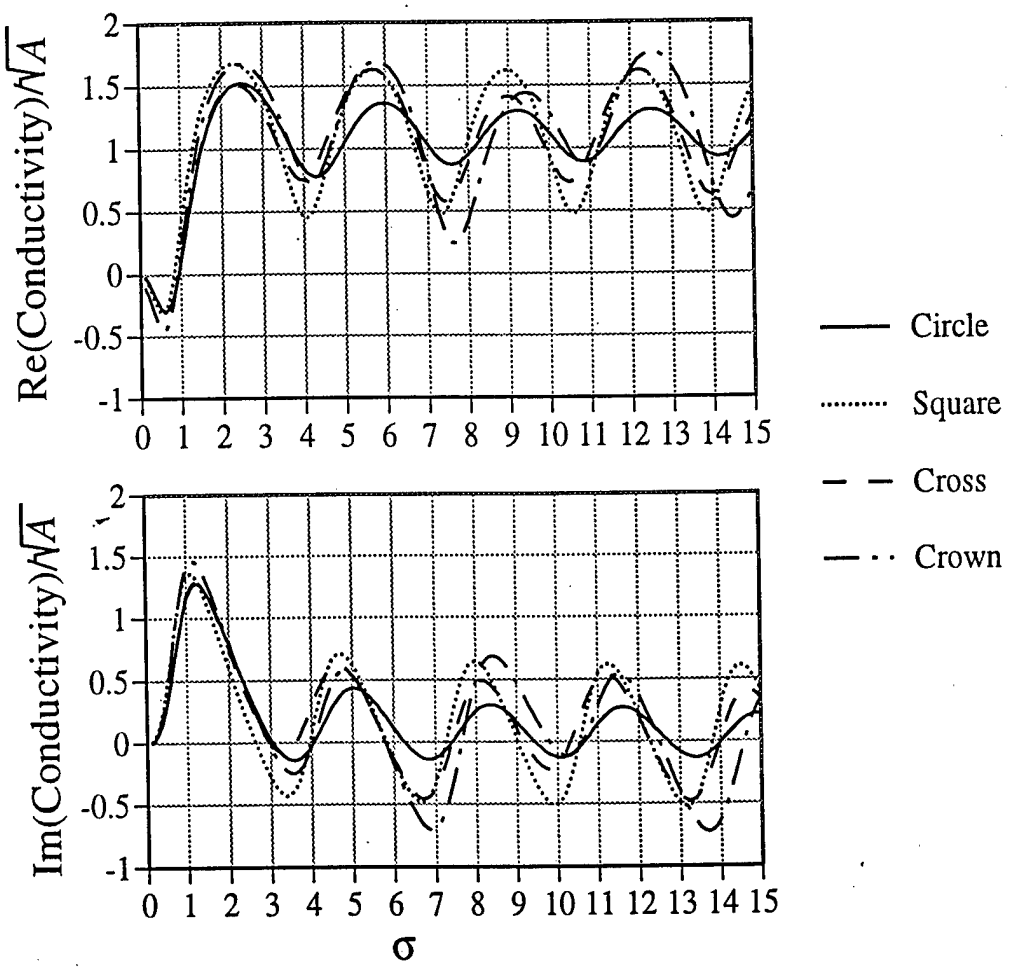

Figure 11: Real part (top) and imaginary part (bottom) of the Rayleigh conductivity normalized by the square root of the area for circle, square, cross, and crown apertures with equal flow on both faces.

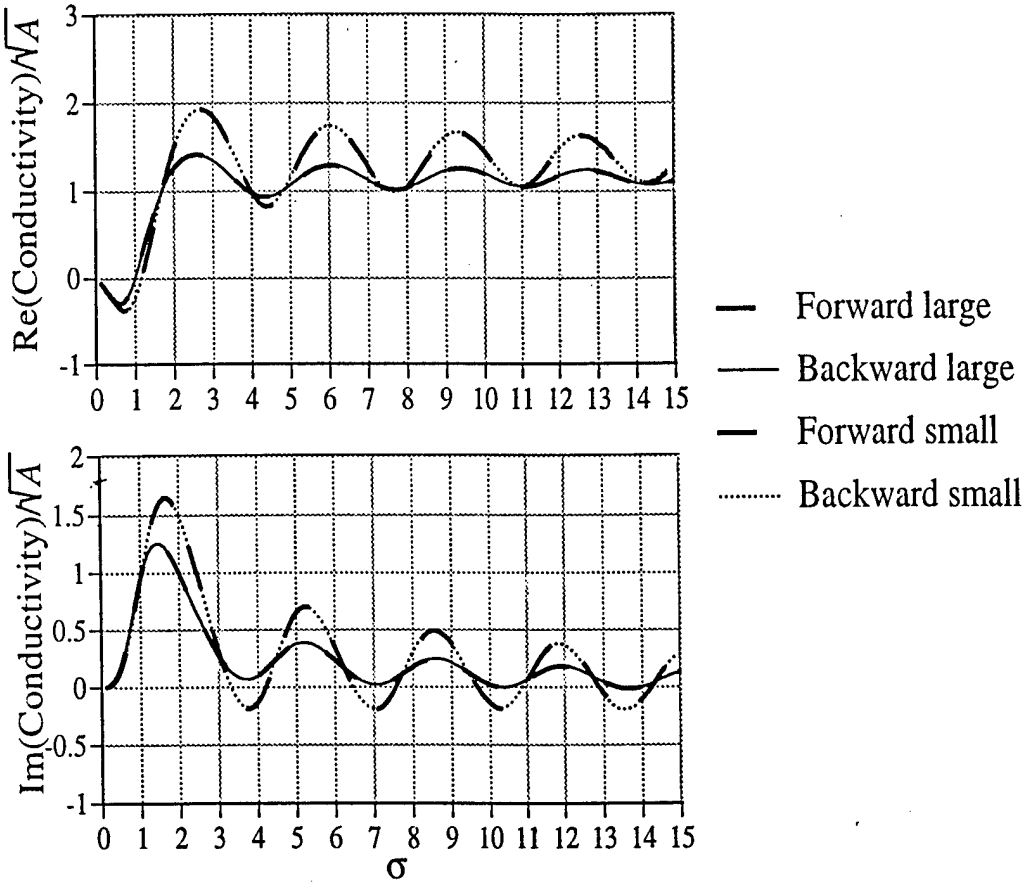

Figure 12: Real part (top) and imaginary part (bottom) of the Rayleigh conductivity normalized by the square root of the area for the large and small, forward and backward facing triangle apertures with equal flow on both faces.

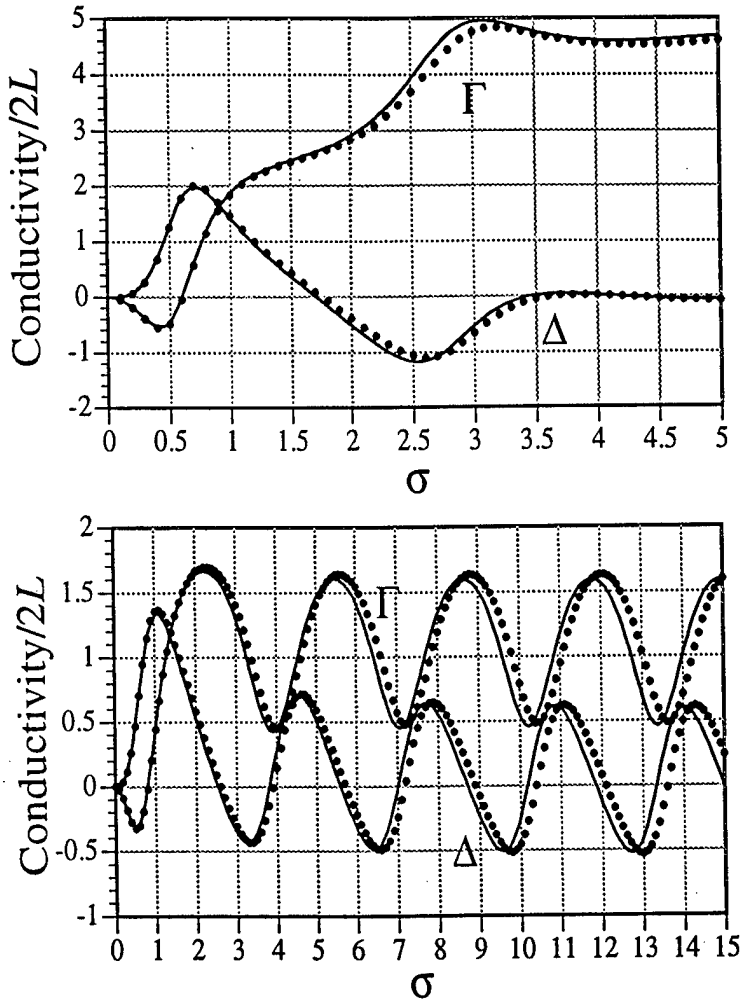

Figure 13: Rayleigh conductivity for a square aperture with one-sided and equal two-sided grazing flow calculated with the three-dimensional numerical method (dotted line) and the approximate theory (solid line).

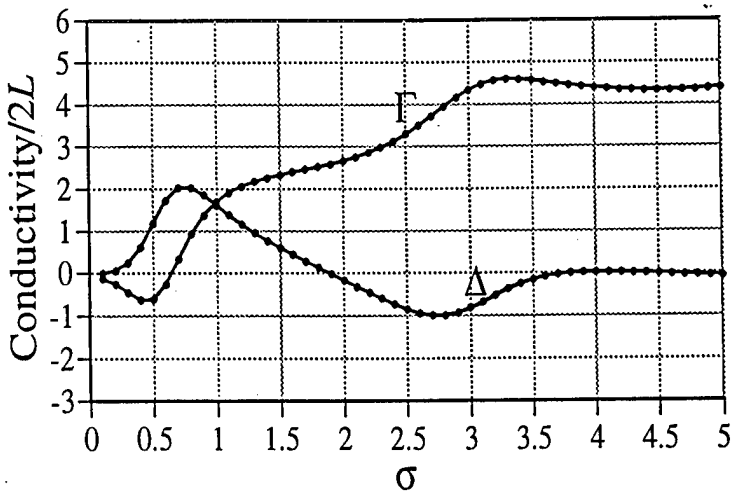

Figure 14: Rayleigh conductivity for one-sided grazing flow past the crown shaped aperture. Comparison of results for serrated edge at the leading edge (solid) and serrated edge at the trailing edge (dots).

CHAPTER 5

STABILITY OF HIGH REYNOLDS NUMBER FLOW PAST A CIRCULAR APERTURE

Sheryl M. Grace, T. H. Wood
and M. S. Howe

SUMMARY

An analysis is made of the canonical problem of flow at very high Reynolds number past a circular aperture in a thin rigid wall. The motion is incompressible, and the shear layer over the aperture is treated as a vortex sheet separating two parallel flows of unequal mean velocities. Viscosity is neglected except for its role in shedding vorticity from the upstream semi-circular edge of the aperture. Nominally steady flow is unstable, and often accompanied by large amplitude self-sustaining oscillations at certain discrete frequencies, whose values are governed by a mechanism involving the periodic shedding of vorticity from the leading edge of the aperture and feedback of pressure disturbances produced by interaction of the vorticity with the downstream edge. Admissible frequencies are identified with the real parts of complex characteristic frequencies of the linearized equation of motion of the vortex sheet. These eigenfrequencies are also poles of the Rayleigh conductivity of the aperture, and their dependence on the mean velocity ratio across the aperture is calculated for the first four 'operating stages' of the motion. Results are presented in both graphical and tabular forms to facilitate their ready incorporation into numerical models of more complicated flow problems. The investigation completes the linearized study of this problem initiated by Scott (1995), which dealt with *forced*, time harmonic oscillations of the shear layer.

1. INTRODUCTION

A^{-1*} At very high Reynolds number the frequencies of sound generated by flow over a wall cavity or aperture depend primarily on the streamwise dimension ℓ of the cavity or aperture and on the mean flow Mach number (Blake and Powell 1986; Rockwell 1983). Discrete tones (and harmonics) are generated within certain 'operating stages', each of which corresponds to a continuous range of the *Strouhal number* $f\ell/U$, where f is the dominant frequency of the sound and U is the free stream speed. A gradual increase or decrease in flow speed is accompanied by discontinuous jumps respectively to a higher or lower Strouhal number at certain critical velocities, which are usually larger for the upward jump than for the corresponding downward jump. Similar abrupt transitions, also exhibiting hysteresis, occur when the length ℓ is caused to vary smoothly.

Rayleigh (1926, §371) gave an explanation of the *feedback* mechanism responsible for the sound that is close to that currently accepted and advanced by Powell (1961) and Rossiter (1962). Vortices are formed within the unstable shear layer that spans the cavity or aperture close to the 'leading' (upstream) edge. A vortex convects across the opening in time $\sim \ell/U_c$, where U_c is about half the free stream speed U; its arrival at the downstream edge excites an impulsive pressure that closes the feedback loop, after travelling back across the opening in time ℓ/c_o, by triggering the formation of a new vortex, c_o being the speed of sound. The permissible frequencies of the operating stages should therefore satisfy a *phase* relation of the form

$$n/f = \ell/U_c + \ell/c_o, \quad n = 1, 2, 3, \ldots .$$

This equation is found to be generally applicable provided n is replaced by $n - \epsilon$, where $\epsilon < 1$ is a suitable empirical coefficient that depends on the detailed geometry of the system (Rossiter 1962; East 1966; Heller and Bliss 1975; Komerath *et al.* 1987; Ahuja and Mendoza 1995). In addition, however, the oscillations must also exhibit no net *gain* of over a complete cycle, which implies that the effects of vortex growth in crossing the opening must be compensated by a corresponding decay of the pressure pulse during its passage from the trailing to the leading edge.

A proper nonlinear numerical treatment of the oscillatory flow based on the full Navier-Stokes equations will automatically satisfy both of these conditions (e.g., Hardin and Pope 1995; Jeng and Payne 1995; Tam *et al.* 1996), although most published results are of limited validity and difficult to interpret. Two-dimensional schemes, in which the

shear layer is modelled by line ('point') vortices, have successfully predicted low Mach number operating stages for deep wall cavities, but the feedback in this case is controlled by the acoustic response of the cavity rather than the hydrodynamic motion in the opening (Bruggeman 1987; Bruggeman *et al.* 1989; Peters 1993; Kriesels *et al.* 1995). The greatest understanding of the role of hydrodynamic instabilities has come from analytical studies of *linearized*, nominally time-harmonic motions of the shear layer. The zero-net-gain condition cannot be satisfied by *real* frequencies when the phase change is calculated from a small amplitude theory that expresses the motion in terms of linear theory eigenfunctions for a uniform shear layer of infinite extent (see, for example, Tam and Block 1978; Crighton 1992; Elder 1992). This is because the linear theory exponential growth of Kelvin-Helmholtz waves on the shear layer is too large to be cancelled by the algebraic decay of the pressure pulse. To obtain linearized predictions of the operating stage Strouhal numbers that agree well with experiment (at least at low Mach numbers, Howe 1997), it is necessary to take a *complex* valued frequency ω, say, in the calculations, and identify the observed oscillation frequency with $\mathrm{Re}\,\omega$. The permissible complex frequencies for a wall aperture satisfy a characteristic equation whose roots are the poles in the complex frequency plane of the Rayleigh conductivity $\mathcal{K}(\omega)$ of the aperture (Rayleigh 1870; 1926, §304; Howe 1997); for a shallow wall cavity the roots correspond to poles of an unsteady drag coefficient.

The characteristic equation for high speed, incompressible flow over a rectangular wall aperture was investigated by Howe (1997). The shear layer was modelled by a vortex sheet, whose integral equation of motion was solved by extension of the method developed for a circular aperture and real frequencies by Scott (1995; see also Howe *et al.* 1996 and Chapter 4). The calculations were done by computing the conductivity $\mathcal{K}(\omega)$ and performing a numerical search for its poles in the complex ω-plane. Those poles in $\mathrm{Im}\,\omega > 0$ were identified with self-sustained oscillations of the shear flow, and the value of $\mathrm{Re}\,\omega$ at the pole was interpreted as the oscillation frequency.

In this chapter we discuss the solution of the characteristic equation for the canonical problem of high speed, incompressible flow past a circular aperture in a thin wall. Scott calculated $\mathcal{K}(\omega)$ for real ω for the two extremes of (a) one-sided grazing flow past the aperture, (b) two-sided flow, where the velocities U_+, U_- on each side of the wall are the same. In case (a) the motion is absolutely unstable, and self-sustained oscillations can occur; in case (b) the poles of $\mathcal{K}(\omega)$ are in $\mathrm{Im}\,\omega < 0$, and the motion is stable. We investigate the destabilization of the motion of case (b) as U_-/U_+ progressively decreases from one to

zero by tracking the motion of poles across the real axis into $\mathrm{Im}\,\omega > 0$. The results should provide a valuable building-block for modelling more complicated systems involving isolated or distributed wall apertures, such as occur, for example, in exhaust mufflers, ventilation ducting systems, combustion chamber linings, etc.

The basis of the present linear theory is outlined in §2. Detailed numerical results for the circular aperture are presented in §3 and briefly compared with the analogous predictions for a square aperture.

2. CONDUCTIVITY IN THE PRESENCE OF GRAZING FLOW

Consider incompressible, uniform mean flow of fluid of density ρ_0 over the upper and lower surfaces of a rigid plane at $x_2 = 0$ containing a circular aperture of radius R whose center is at the origin of the rectangular coordinates (x_1, x_2, x_3). The mean velocities are at speeds $U_\pm$ in the x_1-direction respectively in $x_2 \gtrless 0$, as in Figure 1. The Reynolds number is assumed to be sufficiently large that viscosity can be neglected except for its role in generating vorticity at the sharp edge of the aperture. In the steady state, when $U_+ \neq U_-$, the aperture is spanned by a vortex sheet.

Let $Q(t)$ denote the fluid volume flux through the aperture (in the $+x_2$-direction) produced by the application of uniform, time dependent pressures $p_\pm(t)$ in the vicinity of the aperture in the upper ($x_2 > 0$) and lower ($x_2 < 0$) fluid regions. Then

$$\rho_0 \frac{dQ}{dt} = -\int_{-\infty}^{\infty} \mathcal{K}(\omega)[p_0(\omega)]e^{-i\omega t}d\omega, \quad [p_0(\omega)] \equiv p_-(\omega) - p_+(\omega), \tag{2.1}$$

where $p_\pm(\omega)$ is the Fourier transform $(1/2\pi)\int_{-\infty}^{\infty} p_\pm(t)e^{i\omega t}dt$, and $\mathcal{K}(\omega)$ is the conductivity of the aperture (Rayleigh 1870; 1926; Howe *et al.* 1996).

In a causal representation of the volume flux in terms of $p_\pm$, the path of integration in (2.1) should strictly pass above all singularities of the integrand. The Fourier transform $[p_0(\omega)]$ of an arbitrary pressure load of finite duration is a regular function of ω. In a real fluid $Q(t)$ is finite, and the conductivity $\mathcal{K}(\omega)$ must also be regular. However, when the motion is modelled in terms of a linearly disturbed vortex sheet, the mechanisms that would normally suppress unlimited growth of $Q(t)$ are absent, and the predicted motion is characterized by the appearance of singularities of $\mathcal{K}(\omega)$ in $\mathrm{Im}\,\omega > 0$. To calculate the response when t becomes large and positive, the integration contour must be displaced downwards onto the real axis and indented to pass around these singularities. The contributions from the indentations grow exponentially in time, and represent linear theory instabilities.

$\mathcal{K}(\omega)$ can be calculated in closed analytic form for the special case of a rectangular aperture of large aspect ratio (with its long edges transverse to the mean flow direction), and it is then easy to show that the singularities are simple poles (Howe 1997). More generally, the discretization method that must be used to solve the integral equation satisfied by the vortex sheet displacement strongly suggests that $\mathcal{K}(\omega)$ only has isolated singularities in the form of simple poles, and this is supported by numerical predictions for an arbitrary, rectangular aperture, and also by the results presented in this chapter for the circle. The

residue contributions to (2.1) from poles in $\mathrm{Im}\,\omega > 0$ are associated with disturbances that grow in amplitude as they convect across the aperture in the mean shear layer; their growth is ultimately suppressed by flow nonlinearities, but experiment (Powell 1961; Holger *et al.* 1977; Blake and Powell 1986) indicates that the convection velocity is only very weakly dependent on amplitude, which implies that the value of $\mathrm{Re}\,\omega$ at a pole should be a good approximation to the frequency of a possible self-sustaining periodic motion of finite amplitude.

The unsteady motion above and below the vortex sheet is assumed to be irrotational. The pressures at corresponding points on opposite sides of the sheet must be equal, and the linearized equation satisfied by its displacement ζ (in the x_2-direction) is obtained by equating the potential flow representations of these pressures at the undisturbed position ($x_2 = 0$) of the sheet. When the motion is induced by the time harmonic pressure difference $[p_o(\omega)]\mathrm{e}^{-i\omega t}$, the displacement $\zeta(x_1, x_3, \omega)\mathrm{e}^{-\mathrm{i}\omega t}$ is found to satisfy the following integral equation (Scott 1995; Howe *et al.* 1996)

$$\int_S \frac{Z(\eta_1,\eta_3)d\eta_1 d\eta_3}{\sqrt{(\xi_1-\eta_1)^2+(\xi_3-\eta_3)^2}} + \lambda_1(\xi_3)\mathrm{e}^{i\sigma_1\xi_1} + \lambda_2(\xi_3)\mathrm{e}^{i\sigma_2\xi_1} = 1, \quad \sqrt{\xi_1^2+\xi_3^2} < 1, \tag{2.2}$$

where the integration is over the area S:$\sqrt{\eta_1^2+\eta_3^2} < 1$ of the aperture normalized to unity, and

$$Z(\xi_1,\xi_3) = \frac{\rho_o\omega^2 R\zeta(x_1,x_3,\omega)}{\pi[p_o(\omega)]}, \quad (\xi_1,\xi_3) = \frac{(x_1,x_3)}{R}. \tag{2.3}$$

The functions $\lambda_1(\xi_3)$, $\lambda_2(\xi_3)$ depend only on the transverse coordinate ξ_3, and are the nondimensional amplitudes of the Kelvin-Helmholtz waves of frequency ω excited at the semi-circular, upstream edge of the aperture with complex wavenumbers (Lamb 1932)

$$\sigma_1 = \frac{\omega R(1+i)}{U_+ + iU_-}, \quad \sigma_2 = \frac{\omega R(1-i)}{U_+ - iU_-}. \tag{2.4}$$

The amplitudes are determined by requiring admissible displacements $Z(\xi_1,\xi_3)$ to satisfy the Kutta condition that the pressure must remain finite at a solid trailing edge (Crighton 1985). This is equivalent to requiring the vortex sheet to leave the upstream edge tangentially:

$$Z(\xi_1,\xi_3) \to 0, \quad \frac{\partial Z}{\partial \xi_1}(\xi_1,\xi_3) \to 0 \quad \text{as} \quad \xi_1 \to -\sqrt{1-\xi_3^2}, \quad |\xi_3| < 1. \tag{2.5}$$

The displacement $Z(\xi_1,\xi_3)$ can be calculated from (2.2) and (2.5) for any real or complex value of ω by the collocation procedure originally used by Scott (1995), and refined for

application to more generally shaped apertures in Chapter 4. The aperture is overlaid by a mesh of N rectangular integration elements of equal area $\mathcal{A}$ with sides parallel to the ξ_1 and ξ_3 directions. Within the jth element, Z, λ_1 and λ_2 are assumed to be constant with $Z \equiv Z_j$. The Kutta condition is imposed by requiring Z_j to vanish in those elements that overlap the upstream edge, and in each contiguous element just downstream. The meshes can therefore be labelled such that $Z_j \equiv 0$ for $1 \leq j \leq 2M$ for some positive integer M. The vortex wave amplitudes $\lambda_1(\xi_3)$, $\lambda_2(\xi_3)$ do not vary in the streamwise direction, and there are accordingly precisely $2M$ discretized values of these amplitudes which can be assigned to the first $2M$ components of an N-dimensional vector $\boldsymbol{\mathcal{Z}}$, say. By setting $\mathcal{Z}_j = Z_j$ for $2M < j \leq N$, and requiring the discretized form of equation (2.2) to be satisfied within each of the N mesh elements, the components of $\boldsymbol{\mathcal{Z}}$ can then be found from the system of N linear equations

$$\sum_{j=1}^{N} C_{ij}\mathcal{Z}_j = 1, \quad 1 \leq i \leq N, \tag{2.6}$$

where the $N \times N$ matrix $C_{ij} \equiv C_{ij}(\omega)$ is known as an entire function of ω.

The substitution of the following representation of the time harmonic volume flux

$$Q(\omega) = -i\omega \int_{\text{aperture}} \zeta(x_1, x_3)dx_1dx_3 \equiv \frac{-i\pi R[p_o(\omega)]}{\rho_o \omega} \int_S Z(\xi_1, \xi_3)d\xi_1 d\xi_3$$

into the formula $\mathcal{K}(\omega) = i\rho_o\omega Q(\omega)/[p_o(\omega)]$ then permits the discretized solution to be used to calculate the conductivity from

$$\mathcal{K}(\omega) = \pi R \int_S Z(\eta_1, \eta_3)d\eta_1 d\eta_3 \approx \pi R\mathcal{A} \sum_{j=2M+1}^{N} \mathcal{Z}_j. \tag{2.7}$$

3. NUMERICAL RESULTS

3.1 Conductivity for real frequencies

The conductivity of the circular aperture in an ideal, stationary fluid is equal to twice the aperture radius R. In the presence of flow we write

$$\mathcal{K} = 2R\{\Gamma(\omega) - i\Delta(\omega)\}. \tag{3.1}$$

The imaginary part $\Delta(\omega)$ governs the direction of the energy exchange between the mean flow and the unsteady motion in the aperture. The unsteady motions grow by extracting energy from the mean flow when Im $\Delta(\omega) < 0$, and decay through the production of vorticity in the aperture (which is swept away in the mean flow) when Im $\Delta(\omega) > 0$.

Figures 2a - 2f illustrate how the structure of $\mathcal{K}(\omega)$ as a function of the Strouhal number $\omega R/U_+$ changes as the velocity ratio U_-/U_+ varies between 0 and 1. The curves in Figures 2a and 2f, respectively for one-sided mean flow ($U_- = 0$) and two sided uniform flow ($U_- = U_+$), are identical to those computed by Scott (1995) for these cases. As the velocity ratio U_-/U_+ gradually decreases from 1 to zero, the quasi-periodic behaviors of $\Gamma(\omega)$ and $\Delta(\omega)$ evident in Figure 2f for large values of $\omega R/U_+$ are progressively suppressed. Howe *et al.* (1996) have shown that the motion for $U_- = U_+$ is *conditionally unstable* (Figure 2f) because, for an ideal fluid, there is no mean vortex sheet across the aperture in the undisturbed state, and the conductivity $\mathcal{K}(\omega)$ is regular in Im$(\omega) > 0$, although it has poles in the lower half plane. The real frequency intervals where $\Delta(\omega) < 0$ correspond to *forced instabilities*, where energy is extracted from the mean flow provided the applied pressure load $[p_o(\omega)] \neq 0$. The motion is absolutely unstable when $U_- < U_+$ because the vortex sheet spanning the aperture in the absence of forcing is absolutely unstable. Mathematically, the instability results from the appearance of one or more poles of $\mathcal{K}(\omega)$ in the upper half plane, which cross from Im $\omega < 0$ as U_-/U_+ decreases from unity. If a pole crosses the real axis at $\omega = \omega_r$, the conductivity varies very rapidly for real frequencies near ω_r when the pole is close to ω_r, and in particular, there is an abrupt change in the sign of $\Gamma(\omega)$ near ω_r (from negative to positive) when the pole moves into the upper half plane. Thus, in Figure 2d ($U_-/U_+ = 0.6$) a pole lies just below the real axis near $\omega_r = 9$; the behaviors in Figures 3b and 3c indicate the presence of poles just above the real axis respectively near $\omega_r = 3.2,\ 5.7$. When $U_-/U_+ \to +0$ all of the poles in the upper half-plane with the exception of that with the smallest real part ($\omega_r \sim 3$) are far enough from the real axis to have no significant effect on the behaviors of $\Gamma(\omega)$ and $\Delta(\omega)$ for real ω, which now become essentially constant

for real frequencies when $\omega R/U_+ \geq 5$. These conclusions agree with the investigation in Chapter 1 of the rectangular aperture, but will now be justified by a detailed examination of the poles for the circular aperture.

3.2 Poles of the conductivity

The poles are the eigenvalues of the homogeneous form of the integral equation (2.2), when the right hand side is replaced by zero, and correspond in the discretized approximation (2.6) to the roots of the characteristic equation

$$\det C_{ij}(\omega) = 0. \tag{3.2}$$

However, the calculations were not performed by solving this equation directly, because the determinant varies too rapidly in the region of complex frequencies of interest, and iterative schemes for locating the roots (such as the Newton-Raphson method) are unstable. It turns out to be more convenient to apply Newton-Raphson to determine the complex zeros of $1/\mathcal{K}(\omega)$, which is computed from (2.7). $\mathcal{K}(\omega)$ has no singularities in $\mathrm{Im}\,\omega > 0$ when $U_- = U_+$ (Howe *et al.* 1996), and the search can be automated by first locating the poles for this case in $\mathrm{Im}\,\omega < 0$ and then tracking their motions in the complex plane, across the real axis, by decreasing the value of the velocity ratio U_-/U_+ in small steps. The Argument Principle (Titchmarsh 1952) can be used to obtain rough approximations to the starting positions of the poles (as described by Howe 1997), but this is unnecessary in practice because the poles are initially just below the real axis, and a good approximation to their real parts is obtained by inspection of Figure 2f (for $U_- = U_+$), since the poles are responsible for the oscillatory behavior of $\mathcal{K}(\omega)$, and their respective real parts coincide very approximately with the minima of $\Gamma(\omega)$ on the real axis.

This method was used to determine the trajectories of the first four poles to the right of the imaginary ω-axis as U_-/U_+ decreases from 1 to 0. The marching procedure was sufficiently stable that, typically, only four iterations were necessary to achieve convergence to a pole. The greatest accuracy was obtained with a discretization mesh that used a maximum of 70×70 elements to cover the circular aperture. Because the motion is symmetric about the x_1-axis, the calculations are actually performed using 35 spanwise elements, providing a 70×35 covering of half the aperture. In this case about one hour is required to compute $\mathcal{K}(\omega)$ for a specified complex Strouhal number $\omega R/U_+$. It was therefore necessary to compromise between efficiency of calculation and accuracy. A detailed examination of the convergence of the Newton-Raphson method for different mesh sizes

and several selected values of U_-/U_+ indicated, that when a 60×30 covering was used, the poles could be located to within a relative error that in the worst case (for a fourth stage pole) did not exceed 3%. In this case the time for a single evaluation of $\mathcal{K}(\omega)$ was reduced to about 20 minutes. The trajectories plotted in Figure 3 were obtained using this grid. The poles are also tabulated in Table 1.

	Real and imaginary parts of $\omega R/U_+$			
U_-/U_+	Stage 1	2	3	4
0.00	3.09, 0.56	4.99, 1.98	6.77, 3.47	8.50, 4.98
0.05	3.12, 0.43	5.10, 1.76	6.95, 3.15	8.76, 4.58
0.10	3.15, 0.30	5.20, 1.53	7.12, 2.84	9.01, 4.18
0.15	3.19, 0.17	5.30, 1.31	7.30, 2.53	9.26, 3.78
0.20	3.22, 0.04	5.41, 1.09	7.48, 2.22	9.51, 3.39
0.25	3.26, -0.08	5.51, 0.87	7.66, 1.91	9.77, 2.99
0.30	3.30, -0.21	5.62, 0.65	7.84, 1.61	10.03, 2.60
0.35	3.34, -0.33	5.73, 0.44	8.03, 1.31	10.29, 2.22
0.40	3.39, -0.44	5.85, 0.23	8.21, 1.01	10.55, 1.83
0.45	3.44, -0.55	5.96, 0.03	8.40, 0.72	10.81, 1.45
0.50	3.49, -0.66	6.08, -0.17	8.59, 0.43	11.08, 1.08
0.55	3.54, -0.76	6.20, -0.37	8.79, 0.14	11.35, 0.71
0.60	3.59, -0.86	6.33, -0.55	8.98, -0.13	11.62, 0.35
0.65	3.66, -0.95	6.45, -0.73	9.18, -0.40	11.89, -0.01
0.70	3.72, -1.03	6.58, -0.90	9.38, -0.65	12.17, -0.34
0.75	3.79, -1.11	6.72, -1.05	9.59, -0.89	12.45, -0.67
0.80	3.87, -1.18	6.86, -1.19	9.80, -1.10	12.73, -0.97
0.85	3.95, -1.24	7.01, -1.31	10.02, -1.29	13.03, -1.24
0.90	4.04, -1.29	7.17, -1.40	10.25, -1.45	13.33, -1.46
0.95	4.14, -1.33	7.34, -1.48	10.49, -1.56	13.64, -1.62
1.00	4.24, -1.37	7.52, -1.53	10.75, -1.62	13.98, -1.70

TABLE 1: Poles of $\mathcal{K}(\omega)$ for a circular aperture

According to the interpretation discussed in §2, when $\mathrm{Im}\,\omega > 0$ and $L = 2R$, $fL/U_+ = \mathrm{Re}\,(\omega R/\pi U_+)$ should correspond to the Strouhal number of a possible self-sustaining oscillation of frequency f Hz of the flow over the aperture. This hypothesis appears to be correct for analogous problems of high Reynolds number flow over shallow wall cavities, and for jet-edge interactions (Howe 1997), but experimental data is not available to support the conjecture for the circular aperture. The solid curves in Figure 4 represent the dependence of fL/U_+ on the velocity ratio U_-/U_+ predicted on this basis. The curves represent the first four operating stages and terminate on the right when the corresponding pole crosses into the lower half of the frequency plane.

3.3 Comparison with the square aperture

In the absence of flow Rayleigh (1870) showed that the conductivity of a square aperture of side $2s$ is well approximated by that of a circle of the same area, i.e. of radius $R = 2s/\sqrt{\pi} \approx 1.13s$. In Chapter 4 we have compared of the conductivities of differently shaped apertures in the presence of tangential flow for *real* frequencies. In Figure 5 the pole trajectories $(\omega s/U_+)$ are plotted for $0 < U_-/U_+ < 1$ of the first four operating stages of the square aperture (calculated by the procedure described above for the circle). The open circles in this figure are the corresponding poles $\omega R/U_+$ for a circle of radius $R = s$ at the respective indicated values of the velocity ratio U_-/U_+. By inspection, it is seen that the real part of a pole for the circle is larger than the corresponding real part for the square. An examination of the numerical results reveals that their ratio is almost independent of U_-/U_+ and of the stage number (at least for the first four stages); and that, to a good approximation, the Strouhal numbers fL/U for the circle (where $L = 2R$) are equal to those of a square whose side exceeds the diameter of the circle by about 6%. The open squares in Figure 4 are sample Strouhal numbers for such a square (with $L = 2s$) calculated from the data of Figure 5. The largest Strouhal number shown for the square for each operating stage coincides with the frequency at which the relevant pole crosses into the lower half plane.

4. CONCLUSION

Nominally steady flow past an aperture in a wall is unstable, and under favorable circumstances the instability is accompanied by the emission of sound at certain discrete frequencies. The magnitudes of the frequencies and the amplitudes of the motions are controlled by a feedback loop, whereby periodic shedding of vorticity from the aperture leading edge is maintained by the interaction of that vorticity with the trailing edge, after convection across the aperture, and the formation of new vorticity when a pressure pulse generated by the interaction impinges on the leading edge. The admissible frequencies have been identified with the real parts of those poles in the upper complex frequency plane of the Rayleigh conductivity of the aperture. In this chapter the canonical problem of a circular aperture in a thin rigid wall has been examined in the limit of very high Reynolds number, when the shear layer over the aperture can be modelled by a vortex sheet separating two parallel mean flows of generally unequal velocities. The tabulated values of the poles for the first four operating stages of the aperture instability presented in §3 are expected to be useful in investigations of more complex flow regimes involving flow over a wall containing one or more circular apertures.

REFERENCES

Ahuja, K. K. and Mendoza, J. 1995 NASA Contractor Report 4653: *Effects of cavity dimensions, boundary layer, and temperature on cavity noise with emphasis on benchmark data to validate computational aeroacoustic codes.*

Blake, W. K. and Powell, A. 1986 *The development of contemporary views of flow-tone generation,* pp 247 - 325 of *Recent Advances in Aeroacoustics* (edited by A. Krothapali and C. A. Smith). Springer.

Bruggeman, J. C. 1987 PhD. Thesis: *Flow induced pulsations in pipe systems,* Eindhoven University of Technology.

Bruggeman, J. C., Hirschberg, A., van Dongen, M. E. H., Wijnands, A. P. J. and Gorter, J. 1989 *J. Fluids Eng.* **111**, 484 - 491. Flow induced pulsations in gas transport systems: analysis of the influence of closed side branches.

Crighton, D. G. 1992 *J. Fluid Mech.* **234**, 361 - 392. The jet edge-tone feedback cycle; linear theory for the operating stages.

Crighton, D. G. 1985 *Ann. Rev. Fluid Mech.* **17**, 411 - 445. The Kutta condition in unsteady flow.

East, L. F. 1966 *J. Sound Vib.* **3**, 277 - 287. Aerodynamically induced resonance in rectangular cavities.

Elder, S. A. 1992 *J. Acoust. Soc. Japan* (E) **13**, 11 - 24. The mechanism of sound production in organ pipes and cavity resonators.

Hardin, J. C. and Pope, D. S. 1995 *AIAA J.* **33**, 407 - 412. Sound generation by flow over a two-dimensional cavity.

Heller, H. H. and Bliss, D. B. 1975 *AIAA Paper* 75-491. The physical mechanism of flow-induced pressure fluctuations in cavities and concepts for their suppression.

Holger, D. K., Wilson, T. A. and Beavers, G. S. 1977 *J. Acoust. Soc. Am.* **62**, 1116 - 1128. Fluid mechanics of the edgetone.

Howe, M. S., Scott, M. I. and Sipsic, S. R. 1996 *Proc. Roy. Soc. Lond.* **A452**, 2303 - 2317. The influence of tangential mean flow on the Rayleigh conductivity of an aperture.

Howe, M. S. 1997 *J. Fluid Mech.* **330**, 61 - 84. Edge, cavity and aperture tones at very low Mach numbers.

Jeng, Y. N. and Payne, U. J. 1995 *J. Aircraft* **32**, 363 - 369. Numerical study of a supersonic open cavity flow and pressure oscillation control.

Komerath, N. M., Ahuja, K. K. and Chambers, F. W. 1987 *AIAA Paper* 87-022. Prediction and measurement of flows over cavities - a survey.

Kriesels, P. C., Peters, M. C. A. M., Hirschberg, A., Wijnands, A. P. J., Iafrati, A., Riccardi, G., Piva, R. and Bruggeman, J. C. 1995 *J. Sound Vib.* **184**, 343 - 368. High amplitude vortex induced pulsations in gas transport systems.

Lamb, H. 1932 *Hydrodynamics* (6th. ed., reprinted 1994) Cambridge University Press.

Peters, M. C. A. M. 1993 PhD Thesis: *Aeroacoustic sources in internal flows*, Eindhoven University of Technology.

Powell, A. 1961 *J. Acoust. Soc. Am.* **33**, 395 - 409. On the edgetone.

Rayleigh, Lord 1870 *Phil. Trans. Roy. Soc. Lond.* **161**, 77 - 118. On the theory of resonance.

Rayleigh, Lord 1926 *Theory of Sound*, Vol 2, (Second edition). London: Macmillan and Co.

Rockwell, D. 1983 *AIAA J.* **21**, 645 - 664. Oscillations of impinging shear layers.

Rossiter, J. E. 1962 Royal Aircraft Establishment Technical Memorandum 754. *The effect of cavities on the buffeting of aircraft.*

Scott, M. I. 1995 Master's thesis: *The Rayleigh conductivity of a circular aperture in the presence of a grazing flow*, Boston University.

Tam, C. K. W. and Block, P. J. W. 1978 *J. Fluid Mech.* **89**, 373 - 399. On the tones and pressure oscillations induced by flow over rectangular cavities.

Tam, C.-J., Orkwis, P.D., Disimile, P.J. 1996 *AIAA J.* **34**, 2255 - 2260. Algebraic turbulent model simulations of supersonic open-cavity flow physics.

Titchmarsh, E. C. 1952. *Theory of functions* (2nd corrected edition). Oxford University Press.

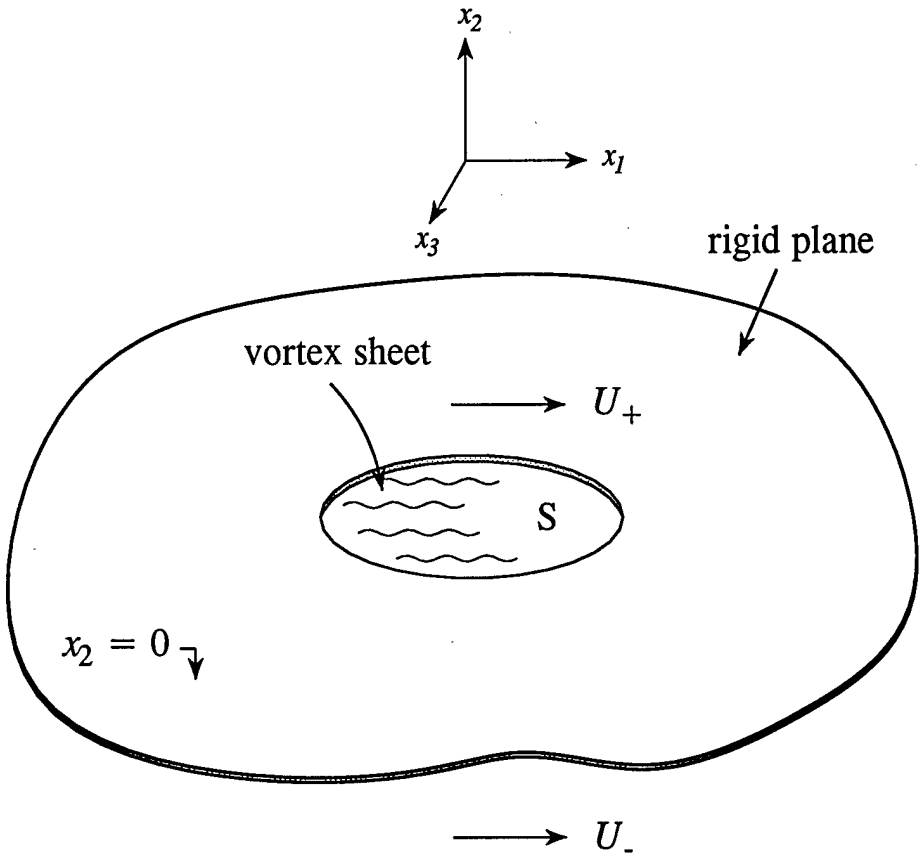

Figure 1. Tangential flow over the upper and lower surfaces of a thin rigid plane with a circular aperture.

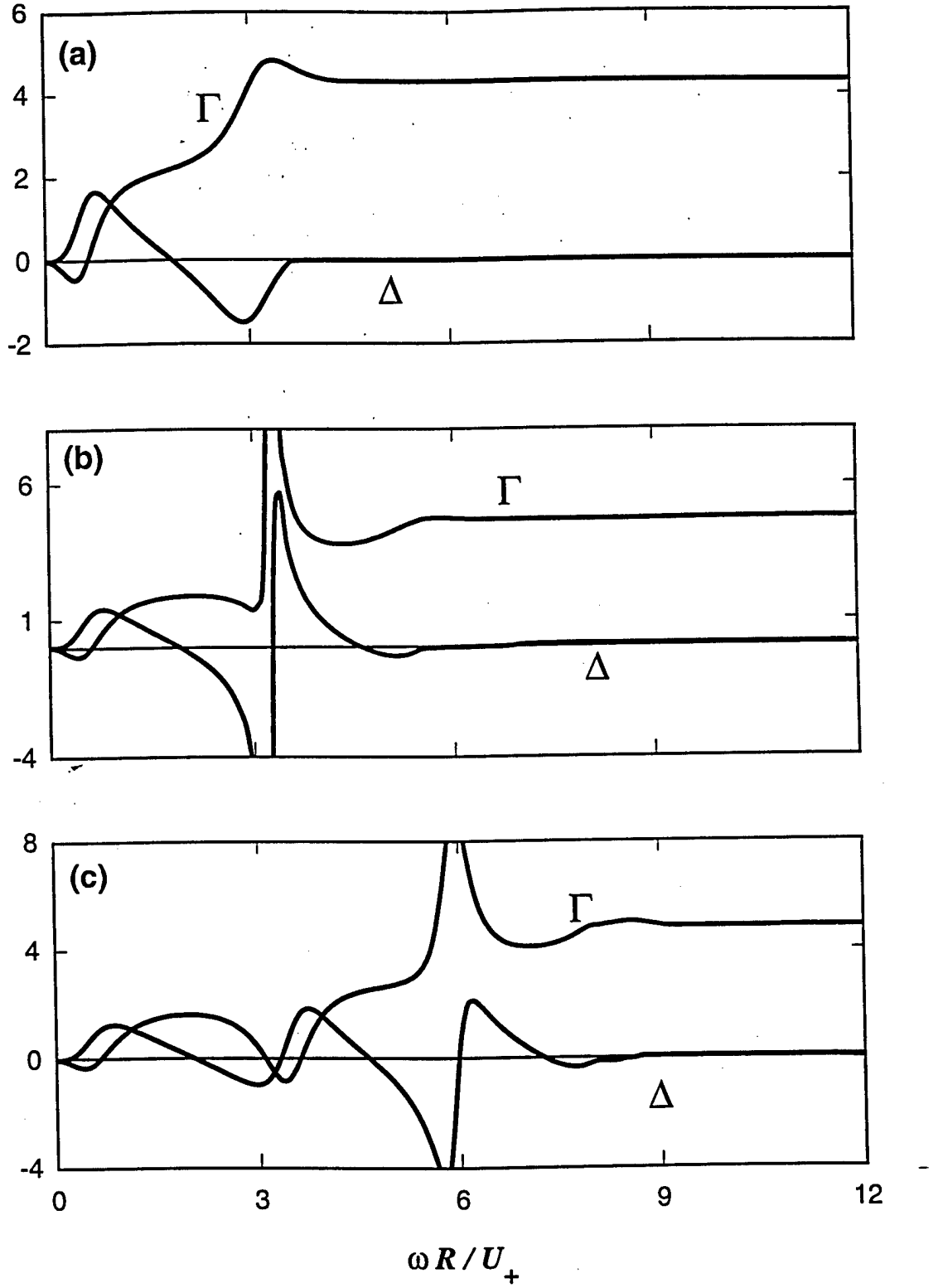

Figure 2. Normalized real and imaginary parts $\mathcal{K}(\omega)/2R = \Gamma(\omega) - i\Delta(\omega)$ of the conductivity of a circular aperture for (a) $U_-/U_+ = 0$, (b) 0.2, (c) 0.4, (d) 0.6, (e) 0.8, (f) 1.0.

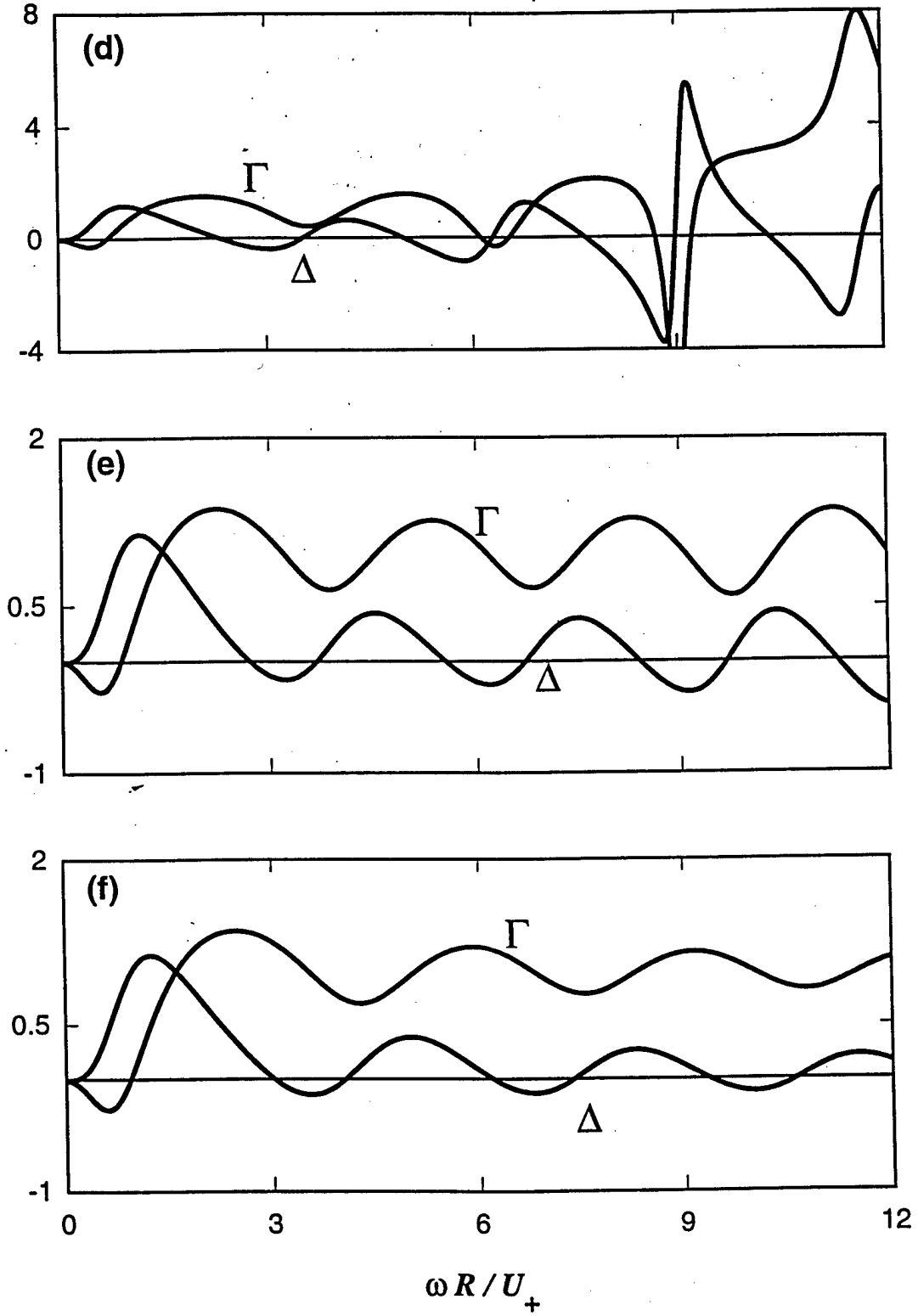

Figure 2. Normalized real and imaginary parts $\mathcal{K}(\omega)/2R = \Gamma(\omega) - i\Delta(\omega)$ of the conductivity of a circular aperture for (a) $U_-/U_+ = 0$, (b) 0.2, (c) 0.4, (d) 0.6, (e) 0.8, (f) 1.0.

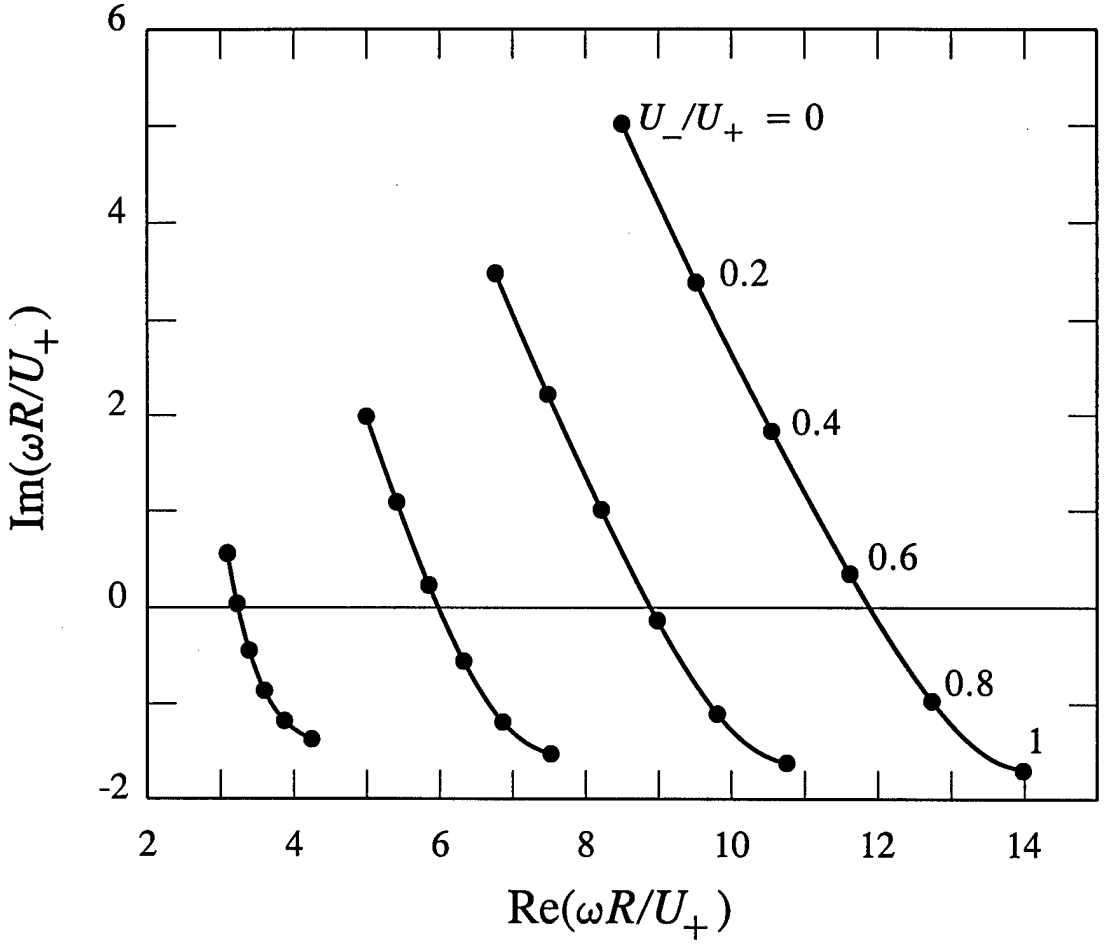

Figure 3. Calculated trajectories of the the first four poles of $K(\omega)$ for a circular aperture for $0 \leq U_-/U_+ \leq 1$.

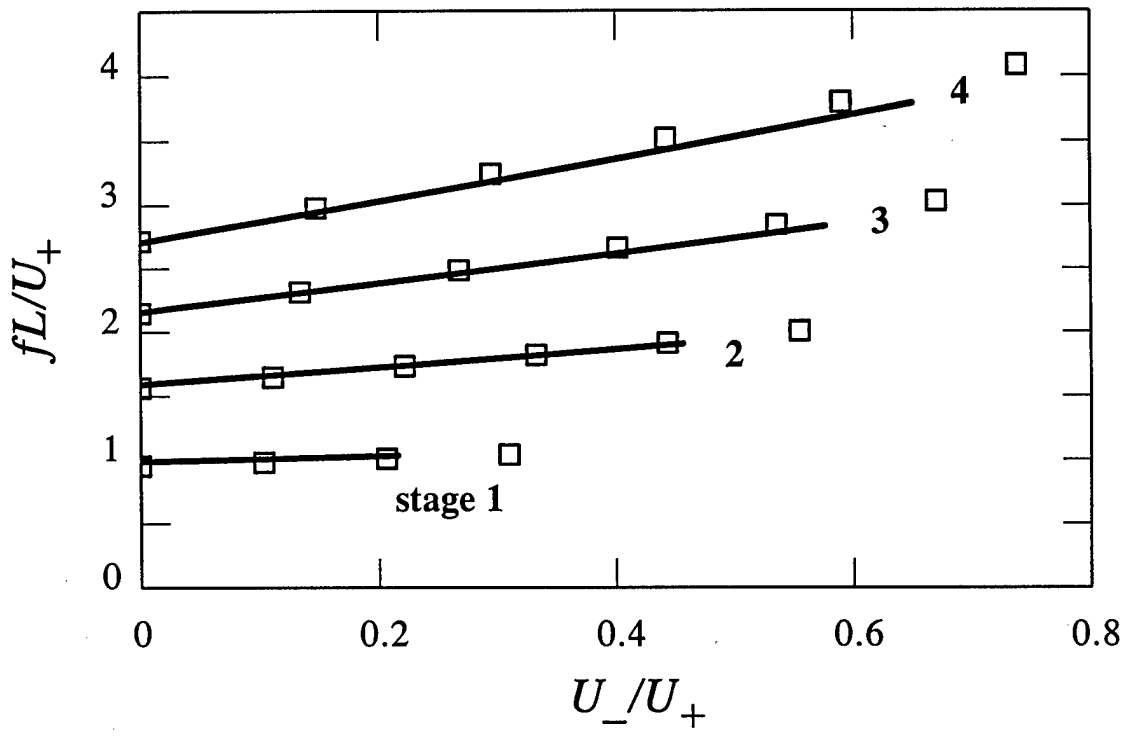

Figure 4. Strouhal numbers $fL/U_+ \equiv \mathrm{Re}(\omega R/\pi U_+)$ of the first four operating stages for a circular aperture; the squares are corresponding predictions for a square aperture whose side is 6% larger than the diameter of the circular aperture.

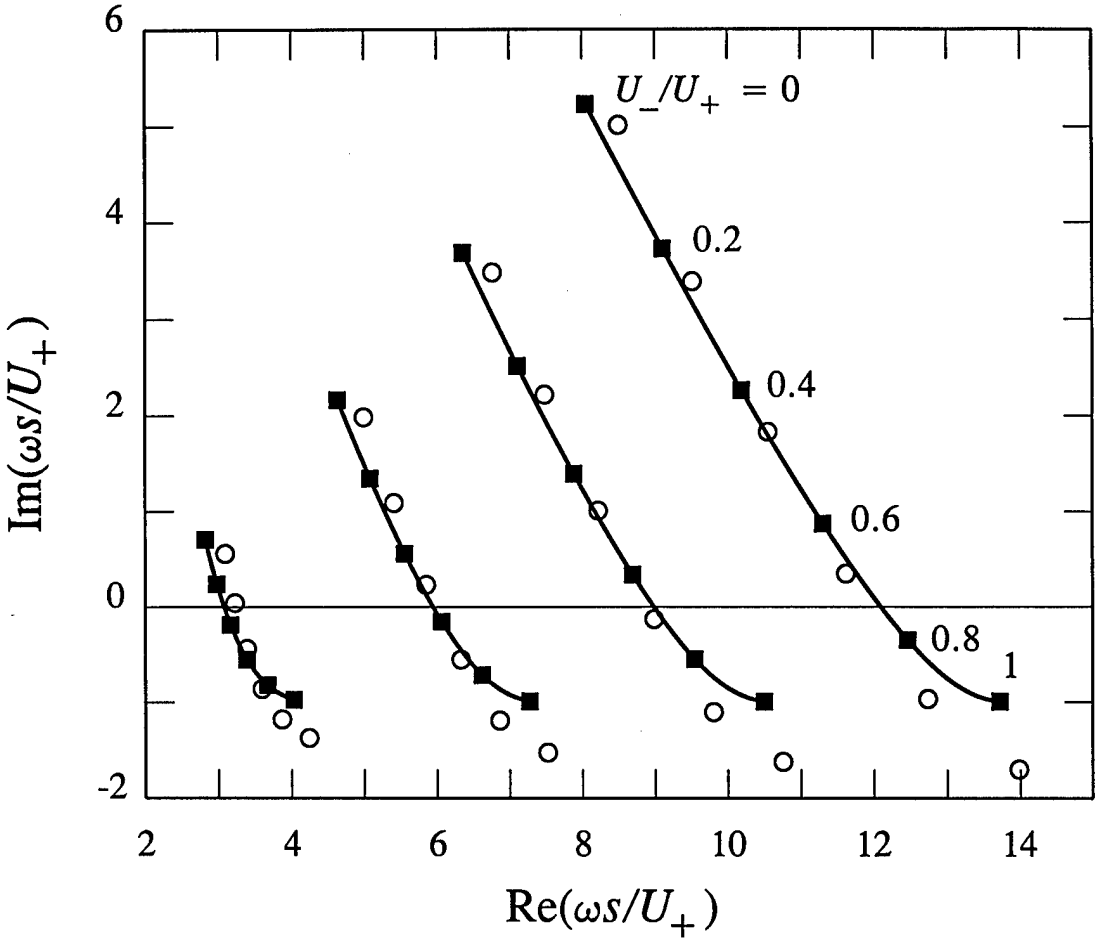

Figure 5. Calculated trajectories of the the first four poles of $\mathcal{K}(\omega)$ for a square aperture of side $2s$ for $0 \leq U_-/U_+ \leq 1$. Each open circle represents the pole for a circular aperture of radius s corresponding to the respective indicated values of U_-/U_+.

CHAPTER 6

EXPERIMENTAL INVESTIGATION OF THE DAMPING OF STRUCTURAL VIBRATIONS BY VORTICITY PRODUCTION

P. M. Maung, M. S. Howe
and G. H. McKinley

SUMMARY

An experimental investigation has been made of the damping of a plate vibrating at zero angle of attack to a nominally steady, high Reynolds number mean flow. The plate is perforated with a distribution of small circular apertures in which vorticity is produced by the unsteady loading of the plate. The kinetic energy of the vorticity is swept downstream by the flow. Damping occurs by the transfer of energy from the plate to the vortex field provided the Strouhal number $\omega R/U$, based on the radian frequency ω of the vibration, the aperture radius R and the mean stream velocity U, lies between about 0.4 and 0.8. The peak attenuation is of the order of 5 dB relative to an identical unperforated plate. The results are interpreted in terms of recent calculations of the unsteady flow through an aperture in the presence of mean flow, and are expected to be relevant to the alleviation of fatigue failure of aerodynamic control surfaces such as jet nozzle flaps.

1. INTRODUCTION

Vorticity is produced by a vibrating solid surface. The rate of production is greatest where the pressure and velocity in the fluid change rapidly, such as at corners and sharp edges. For certain conditions the kinetic energy of the vortex flow is derived from the work done on the fluid by the moving surface, and there is an irreversible transfer of energy to the fluid. The mechanism is very similar to that involved in the conversion of *acoustic* energy into vortical kinetic energy when sound causes vorticity production at an edge: vorticity diffuses from the edge by viscous action and the sound is damped [1 - 3]. If the fluid is at rest relative to the surface the dissipation is caused by the nonlinear convection of vorticity from the surface and subsequent thermoviscous damping, both of which are weak because the growth of vorticity of one sign (and, therefore, of substantial levels of vortical kinetic energy) tends to be inhibited when the motion is periodic. In the acoustic case it is known [4 - 16] that the damping can be greatly increased by the presence of a high Reynolds number mean flow. Viscosity is now important only very close to an edge, where vorticity diffuses from the surface and is then swept away by the flow, its kinetic energy being permanently lost by the sound.

Practical devices for attenuating sound by this means usually involve *bias* or *grazing* flow perforated screens. In the bias flow case a mean pressure difference is maintained across the screen producing a steady flow through the apertures. Damping is caused by the modulation of vorticity production in the mean jet flows through the apertures by impinging sound [6, 7, 12, 14 - 16]. A grazing flow screen works in a similar way: unsteady motion produced by the sound in the apertures generates vorticity which is convected downstream by the tangential flow over the screen. High acoustic intensities are usually accompanied by significant structural vibrations, and since near field (non-acoustic) pressure fluctuations produced by a vibrating body can also modulate vorticity production, it is likely that the vibrations of a perforated structure are also damped by vorticity production. This possibility has been confirmed theoretically [17, 18] for bending waves on a bias flow elastic plate, or when a bending wave impinges on the edge of a plate in the presence of a tangential mean flow. These studies indicated that the damping can be comparable with that normally achieved by heavily coating the vibrating plate with an elastomeric damping material. The efficiency of damping by the bias flow screen can be optimized for any particular frequency by adjusting the bias flow speed in the perforates. This is not generally possible for perforated screens in a tangential flow environment. Either of these

configurations, however, provides a possible mechanism for suppressing the large amplitude vibrations induced in practical flow control devices by large scale flow instabilities, such as those experienced by the jet engine external nozzle flaps of certain military aircraft [19 - 21].

In this chapter we describe the results of an experimental investigation aimed at assessing the likely magnitudes of the structural damping that can be achieved by vorticity production. The case considered here is of damping by the *passive* production of vorticity in the apertures of a perforated plate which vibrates while immersed in a water channel in the presence of a tangential mean flow of speed $U \approx 1$ m/s. Vibration damping measurements were made using several cantilevered, thin steel plates homogeneously perforated with circular apertures of radius $R = \frac{1}{8}$ inch and with respective fractional open areas $\alpha = 0.0135,\ 0.03,\ 0.05$ and 0.1. In all of these cases maximum damping of up to 5 dB (relative to an identical unperforated plate with the same vibrational input power) was obtained at a *Strouhal number* $\omega R/U$ between about 0.4 and 0.8, where ω denotes the radian frequency of vibration. Intervals of *negative* damping were observed at higher Strouhal numbers; in such cases the forced vibrations of the plate are augmented by energy extracted from the mean flow. These conclusions are consistent with elementary analytical models of the hydrodynamics of the unsteady aperture motions in the presence of mean flow [22 - 24], in which the mean shear layer across an aperture is modeled by a vortex sheet, but it is not clear to what extent these models are applicable in the present case.

These simple models are discussed in §2. The experimental set-up and the test procedure are described in §3, and damping measurements are reported in §4. The experimental results are discussed for several fractional open areas, with greatest attention given to the case $\alpha = 0.0135$, which is likely to be the most relevant in applications, where only small fractional open area ratios are likely to be acceptable.

2. THEORETICAL BACKGROUND

Consider a thin plate containing a circular aperture (of radius R) vibrating normal to its surface with small amplitude at radian frequency ω (with time dependence $\propto e^{-i\omega t}$) in the presence of a grazing mean flow in the x_1-direction (Figure 1). In the general case the mean velocities $U_\pm$ respectively above and below the plate will be different, and in the absence of oscillations there will be a mean shear layer across the plane of the aperture. The periodic motion of the plate produces uniform, mean pressures $p_\pm e^{-i\omega t}$ on the upper and lower faces of the plate, as a result of which fluid is forced through the aperture at a volume flux rate $Qe^{-i\omega t}$ (in the positive x_2-direction in the figure) given by

$$Q = \frac{K(\omega)[p_+ - p_-]}{i\rho_o\omega}, \tag{1}$$

where ρ_o is the mean fluid density, and the frequency dependent coefficient K is the *Rayleigh conductivity* of the aperture. In the absence of mean flow in an ideal fluid the value of K depends only on the *shape* of the aperture and the thickness of the plate. For a circular aperture in a plate of infinitesimal thickness $K = 2R$.

Because of the tangential motion, vorticity is shed from the edge of the aperture and carried downstream by the mean flow. This implies that there is an exchange of energy between the fluid and the vibrating plate, and that K is now a *complex* function of the frequency ω, which is usually expressed in the form

$$K(\omega) = 2R\Big(\Gamma(\omega) - i\Delta(\omega)\Big), \tag{2}$$

where Γ and Δ are real. If Π denotes the rate of transfer of energy from the plate to the fluid then [18]

$$\Pi = \frac{-\mathrm{Im}\{K(\omega)\}|p_+ - p_-|^2}{2\rho_o\omega} \equiv \frac{R\Delta(\omega)|p_+ - p_-|^2}{\rho_o\omega}, \tag{3}$$

which is positive provided $\Delta(\omega) > 0$ (for $\omega > 0$).

Figure 2 illustrates the dependencies of Γ and Δ on the *Strouhal number* $\omega R/U$ calculated by Scott [22] for an aperture in a plate of zero thickness in the two extreme cases of (i) one-sided flow, $U_+ = U$, $U_- = 0$, and (ii) two-sided uniform flow, $U_+ = U_- \equiv U$. According to equation (3), in the intervals where $\Delta > 0$ vibrational energy is transferred to the fluid. For one sided flow this occurs at Strouhal numbers less than about 2; for two sided, uniform flow it occurs over a large number of discrete frequency intervals. In obtaining these results, Scott considered the extreme limit of infinite Reynolds number, when the mean shear layer

across the aperture could be modeled by a *vortex sheet* which was linearly perturbed by motion of the plate.

In the experiments considered in this chapter, the vibrating plate is immersed in water at zero mean angle of attack to a nominally uniform mean flow. Thus, it might be expected that case (ii) of Figure 2 would provide an appropriate model for interpreting the exchange of energy between the plate and the flow. However, it turns out that this two sided-flow model is valid only for plates of very small thickness compared to the aperture radius R. Although numerical predictions of $K(\omega)$ for a circular aperture in a thick plate are not available, it was seen in Chapter 1 that, apart from a change of scale on the frequency axis, the results shown Figure 2 are also applicable to a *rectangular* aperture. However, it is also shown in Chapter 1 that for two-sided uniform flow over a rectangular aperture in a plate of moderate thickness, the frequency dependence of the conductivity is actually more like case (i) of Figure 2 (one sided flow). This is illustrated in Figure 3 for a rectangular aperture of length $2s$ and breadth $4s$ (out of the plane of the paper) in a plate of thickness $h = 0.2s$. The reason for this critical dependence on thickness is easily understood. For a plate of zero thickness in a uniform mean flow, there is no mean shear layer (vortex sheet) across the aperture in the limit of infinite Reynolds number, and the undisturbed motion is therefore *stable*. For finite thickness, however, a vortex sheet will span each face of the aperture, as indicated in the upper part of Figure 3, thereby making the aperture motion unstable. Numerical results discussed in Chapter 1 indicate that the unstable motion becomes similar to that for one-sided flow when the plate thickness exceeds about one tenth of the aperture diameter.

3. DESCRIPTION OF THE EXPERIMENT

3.1 Apparatus

The experiment was conducted in the 20 ft long low speed water channel at Harvard University. The channel is 1.5 ft wide and 3 ft high, and the water depth is about 6.75 inches at the maximum flow rate of approximately 100 gallons per minute, corresponding to a mean stream speed $U = 0.8 - 0.85$ m/s. This velocity was measured directly by observation of particle traces on the surface of the water.

The experiments were performed using a set of interchangeable unperforated and perforated rectangular steel plates aligned at zero mean angle of attack to the flow. The plates are of thickness $\frac{1}{32}$ inches and have span 11 inches (transverse to the flow direction) and chord 6 inches. The perforated plates had fractional open areas $\alpha = 0.0135,\ 0.03,\ 0.05\ 0.1$, and were formed by drilling a uniform distribution of circular apertures of radius $R = \frac{1}{8}$ inches. Each test plate is cantilevered about its leading edge, along which it is bolted to a $\frac{1}{8}$ inches thick, horizontal steel bar placed within the water flow at a depth that could be varied between $1.75\ -\ 4.25$ inches, the bar being strong enough to prevent twisting during plate vibration.

A *Ling Dynamic System V203* shaker was mounted on a rigid support above the plate and connected to the midspan of the plate near the trailing edge by a $\frac{1}{4}$ inch diameter vertical aluminum connecting rod. A *Tektronix CFG253* function generator was used to drive the shaker at prescribed values of the radian frequency ω. The connecting rod is rigidly attached to the plate, whose motion at the point of attachment could therefore be measured by means of a high sensitivity accelerometer (*Kistler 863485*) mounted on the rod above the water level. This was checked in the absence of water by operating the shaker at fixed input frequency and amplitude and comparing accelerometer readings when mounted on the connecting rod and when mounted directly on the plate. A PC-based data acquisition system was used to store simultaneous measurements of the accelerometer output $a(t)$, and the voltage $V(t)$ and current $I(t)$ delivered to the shaker. The arrangement is illustrated schematically in Figure 4, and described in greater detail in [21].

3.2 Procedure

The mean flow speed was maintained steady in the range $U = 0.8 - 0.85$ m/s, and the shaker was driven sinusoidally at selected frequencies $f = \omega/2\pi$ between 10 and 90 Hz. Over this range the Strouhal number $S = \omega R/U$ varies from 0.2 to 2.15, where, according to

Figures 2 and 3, vorticity production is expected to provide a significant level of vibration damping.

Spectral analysis of the accelerometer readings indicates that the response of the plate is perfectly sinusoidal except at the lower end of the frequency range and a few other selected points. Even at these exceptional points, however, the signal is nearly sinusoidal with some added noise distortions (see Figures 5 and 6). The plate displacement $u(t)$ as a function of time can be calculated from the accelerometer readings by integration of the formula

$$\frac{d^2u}{dt^2} = a(t). \tag{4}$$

This was done numerically using a trapezoidal procedure and 1024 data points sampled over a three period duration. This time period was found to be large enough to provide a stable frequency spectrum, with adequate low frequency resolution.

The current and voltage delivered to the shaker were analyzed in a similar manner. When conditions vary sinusoidally, the power delivered to the shaker is the product of the voltage $V(t) = v_o \cos(\omega t)$ and current $I(t) = \hat{I}\cos(\omega t + \phi)$, and the average power Π is given by

$$\Pi = v_o \hat{I} \cos\phi. \tag{5}$$

The voltage was measured across the electrical leads coming out of the shaker. The current $I(t)$ was determined from Ohm's law and the measured voltage drop across a $1\,\Omega$ resistor placed in series. Instead of assuming perfectly sinusoidal variations, and using equation (5), the average power was calculated from the actual sampled values of $V(t)$, $I(t)$ over a three period interval by means of the formula

$$\Pi = \frac{\sum_n V(t_n) I(t_n)\, \Delta t}{\sum_n \Delta t}, \tag{6}$$

where Δt is the interval between successive sampling times t_n. This method of computation minimizes the influence of random fluctuations present in the peak to peak measurements.

The plate and the connecting rod to the shaker may be regarded as a linear system executing forced oscillations at frequency ω. The total power dissipated per unit input power to the shaker is proportional to the ratio u_p^2/Π_p, where the subscript p refers to values for the perforated plate, and u_p^2 is the mean square displacement of the plate. The damping of the coupled plate-shaker system afforded by vorticity production in the perforates is therefore determined by

$$10 \times \log_{10}\left(\frac{u_o^2}{u_p^2}\,\frac{\Pi_p}{\Pi_o}\right) \quad \text{dB} \tag{7}$$

where the subscript o refers to the *unperforated* plate.

4. EXPERIMENTAL RESULTS

To assess the importance of vibration amplitude on damping, measurements were made at two different voltage input amplitudes, v_o, to the shaker of 124 mV and 174 mV (corresponding, practically, to a doubling of the input power at the higher voltage), which could be held stable throughout the whole range of test frequencies. It will be seen from the results that the input amplitude has only a minor influence on the measured damping. The input frequency was varied over the range $10 < \omega/2\pi < 90$ Hz in increments of 2 to 5 Hz. Smaller increments were used where significant damping was observed. For each frequency the measured displacement of the plate at the trailing edge (u) and the average input power Π were measured during four different experimental runs to ensure repeatability and consistency of the measurements. The mean values of these results were then used to compute the damping. For a given fractional open area, the shaker input voltage amplitude v_o was constant to within $\pm 3\%$, while the current varied with the driving frequency f. The accuracy of the power measurements was confirmed by direct comparison with performance characteristics supplied by the shaker manufacturer. As an additional precaution to ensure the validity and consistency of the measurements, a second test was conducted after an interval of a few days, and additional checks (described below) were performed for the plate with the smallest fractional open area of 1.35%.

4.1 The 1.35% perforated plate

The most extensive tests were conducted on the 1.35% perforated plate. Four separate tests were performed, each involving the measurement of the displacement and average input power on eight separate occasions with the same flow velocity U, frequency f and input voltage amplitude v_o. The flow velocity and frequency variables were reset before each test, and all of the measurements were performed within a two week time frame. The measured power and displacement signals were stable over the entire frequency range, and spectral analysis revealed that the shaker current and voltage remained sinusoidal at all measurement points. The stability of the signal is demonstrated in Figure 5a and Figure 6a, which show digitized sample readings of $I(t)$ and $V(t)$ for two different frequencies. The accelerometer readings contain a broader spectrum of frequencies, however. The distortion (non-sinusoidal response) of the plate motion was negligible except at very low frequencies. Figure 5a shows conditions at $f = 38$ Hz, where the the input voltage, current and the acceleration are all sinusoidal; the acceleration frequency spectrum shown in Figure 5b is dominated by this frequency. This is the case for the majority of the measured frequencies.

However, at low frequencies, such as that illustrated in Figure 6 for $f = 10$ Hz, the essentially sinusoidal response of the plate is contaminated by high frequency noise. The acceleration spectrum (Figure 6b) is still dominated by the peak at 10 Hz, however, which is about 20 dB above the noise. A comparison of the accelerometer measurements for the perforated and unperforated plates reveals that the noise level in the displacement readings is mainly a function of frequency and is not significantly dependent on the fractional open area.

The damping (calculated from the definition (7)) for $\alpha = 0.0135$ is plotted in Figure 7 as a function of the aperture Strouhal number $\omega R/U$ for the two different peak input voltages $v_o = 124$ and $v_o = 174$ mV. The two results differ in detail, but are similar in overall appearance, confirming that in a first approximation the vibrating system may be treated as a linear oscillator. An error analysis, taking account of both precision and bias errors [24], was conducted on the damping comparison variables and the estimated uncertainties in the measured results are indicated by the error bars in the Figure. Thus, for all practical purposes the results for the two input voltages may be regarded as essentially identical, as expected for a linear system.

Since the ratio plate thickness/aperture diameter $\equiv h/2R = 0.125 > 0.1$, it might be expected that the frequency dependence of the attenuation would be similar to that shown in Figure 3. However, the results of Figure 7 are more like those shown in Figure 2ii for two-sided flow past an aperture in a plate of infinitesimal thickness. But the similarity is only qualitative, the observed frequency intervals of positive damping being much smaller. In the Strouhal number $0.4 < S < 0.8$ the attenuation is typically about 3 dB, and attains a maximum of 5.7 dB at $S \approx 0.7$.

The anomalously large damping which occurs in Figure 7 near $S = 2$ is believed to be associated with a resonance of the structural support at $f \approx 85$ Hz, since it occurs where the plate displacement is very small. To check this the test was repeated after first sealing the apertures with tape. If the tape can be regarded as effectively rigid there should be no damping due to the presence of the apertures, but any anomalies at a structural resonance are still likely to be present. Figure 8 compares the measured attenuations for the perforated and taped plates. Taping the apertures is seen to effectively eliminate the measured damping over most of the frequency range, except at the high frequencies. The small, but finite damping at lower frequencies for the taped plate can be attributed to the interaction of flexural motions of the tape over the apertures with the flow. It may therefore

be concluded that, except for high frequencies, say $f > 50$ Hz, vorticity production in the perforates is the major source of damping when comparing the measured responses of the perforated and unperforated plate.

4.2 Dependence of damping on fractional open area

Figures 9 - 11 illustrate the damping measured for plates with fractional open areas $\alpha = 0.03,\ 0.05$ and 0.10 respectively. The results are quantitatively similar to those discussed above for $\alpha = 0.0135$, however the low Strouhal number interval of significant damping progressively decreases in width as α increases, and the system exhibits "negative damping" over most of the low frequency domain, i.e., the oscillations are amplified by vorticity production.

The average damping for the 3% perforated plate is about 3 dB and occurs over the range $0.7 < S < 0.9$, which is much narrower that for the 1.35% plate. In this interval a peak attenuation of about 5.5 dB occurs at $S \approx 0.8$, corresponding to $f = 33$ Hz. The very large measured damping in the region $S > 1.5$ must again be attributed to a structural resonance. Similar comments apply to the 5% perforated plate. The low frequency region of damping occurs in the range $0.5 < S < 0.8$, with a maximum of 5.2dB at $S \approx 0.7$.

For the plate with the highest open area ratio of 10%, figure 11 shows that the low Strouhal number interval of positive damping is now confined to the very small range $0.7 < S < 0.8$, and the maximum damping is 4 dB. For most frequencies the plate is negatively damped. This suggests that the large fractional open area the plate has a significant influence on the mechanical stiffness of the plate, causing it to exhibit a complex mode of deflection that is basically destabilized by the presence of the apertures. When the fractional open area is as large as 10% the plate no longer behaves as a simple forced oscillator with one degree of freedom. A progressive increase in open area causes a gradual reduction in plate stiffness, which ultimately allows the plate to vibrate in more complex manner than the envisaged simple cantilever mode discussed above, thereby introducing phase differences between the fluid structure interactions at different apertures.

5. CONCLUSION

In this chapter we have described an experiment in which the production of vorticity within the apertures of a vibrating plate immersed in a mean flow has resulted in a net exchange of energy between the flow and the vibrating plate. When vibration damping occurs the kinetic energy of the vorticity is supplied by the plate and swept away by the mean flow. The present experiment relies on the *passive* production of vorticity, and accordingly exhibits ranges of Strouhal numbers (based on mean flow velocity and aperture radius) where the damping can be negative.

Our results for vibrating steel plates in a water channel show that passive vorticity production in the perforates of a vibrating perforated plate can cause significant vibration damping (5 dB or more) for Strouhal numbers in the range 0.4 to 0.8. The width of this Strouhal number range decreases with increasing fractional open area; for the perforated plates studied here the broadest band of attenuation frequencies was obtained for an fractional open area of 1.35%. The solid curve in Figure 12 represents a "best fit" approximation to all of the data in this low Strouhal number range for this plate configuration.

The results give encouraging support to the possibility of controlling or suppressing unwanted vibrations of a structure in a mean flow by introducing a modest degree of surface perforations where vorticity production can occur. The passive vorticity generation configuration examined in this chapter provides little or no control of the frequency at which the damping is maximal. However, the same mechanism is responsible for damping by vorticity production in the apertures through which a mean flow is maintained by "blowing" or "suction". For such an arrangement the "bias flow" velocity within an aperture can be adjusted to optimize damping at any desired frequency. Non-passive devices of this kind are known to be very effective in the damping of sound.

REFERENCES

1. B. T. Zinn 1970 *Journal of Sound and Vibration* **13**, 347 - 356. A theoretical study of nonlinear damping by Helmholtz resonators.
2. T. H. Melling 1973 *Journal of Sound and Vibration* **29**, 1 - 65. The acoustic impedance of perforates at medium and high sound pressure levels.
3. A. Cummings 1983 *American Institute of Aeronautics and Astronautics Paper* 83-0739. Acoustic nonlinearities and power losses at orifices.
4. P. D. Dean and B. J. Tester 1975 *National Aeronautics and Space Administration Contractor Report* CR-134998. Duct wall impedance control as an advanced concept for acoustic suppression.
5. D. Bechert, U. Michel and E. Pfizenmaier 1977 *American Institute of Aeronautics and Astronautics Paper* 77-1278. Experiments on the transmission of sound through jets.
6. D. W. Bechert 1979 *American Institute of Aeronautics and Astronautics Paper* 79-0575. Sound absorption caused by vorticity shedding, demonstrated with a jet flow.
7. M. S. Howe 1980 *Journal of Sound and Vibration* **70**, 407 - 411. The dissipation of sound at an edge.
8. M. S. Howe 1979 *Proceedings of the Royal Society of London* **A366**, 205 - 233. On the theory of unsteady high Reynolds number flow through a circular aperture.
9. M. S. Howe 1980 *Proceedings of the Royal Society of London* **A370**, 523 - 544. On the diffraction of sound by a screen with circular apertures in the presence of a low Mach number grazing flow.
10. I. L. Vér 1982 *Perforated baffles prevent flow-induced acoustic resonances in heat exchangers.* Paper presented at 1982 meeting of the Federation of the Acoustical Societies of Europe; Göttingen, September 1982.
11. A. M. Cargill 1982 *Journal of Fluid Mechanics* **121**, 59 - 105. Low frequency sound radiation and generation due to the interaction of unsteady flow with a jet pipe.
12. M. S. Howe 1984 *Institute of Mathematics and its Applications, Journal of Applied Mathematics* **32**, 187 - 209. On the absorption of sound by turbulence and other hydrodynamic flows.

13. I. L. Vér 1990 *Noise Control Engineering Journal* **35** (Nov/Dec issue) pp. 115 - 125. Practical examples of noise and vibration control: case history of consulting projects.

14. I. J. Hughes and A. P. Dowling 1990 *Journal of Fluid Mechanics* **218**, 299 - 336. The absorption of sound by perforated linings.

15. Y. Fukumoto and M. Takayama 1991 *Physics of Fluids* **A3**, 3080 - 3082. Vorticity production at the edge of a slit by sound waves in the presence of a low Mach number bias flow.

16. A. P. Dowling and I. J. Hughes 1992 *Journal of Sound and Vibration* **156**, 387 - 405. Sound absorption by a screen with a regular array of slits.

17. M. S. Howe 1992 *Journal d'Acoustique* **5**, 603 - 620. On the damping of structural vibrations by vortex shedding.

18. M. S. Howe 1995 *European Journal of Applied Mathematics* **6**, 307 - 328. The damping of flexural and acoustic waves by a bias-flow perforated elastic plate.

19. J. M. Seiner, M. K. Ponton, O. C. Pendergraft Jr., J. C. Manning and M. L. Mason 1990 *American Institute of Aeronautics and Astronautics Paper* 90-1910. External nozzle flap dynamic load measurements on F-15 S/MTD mode.

20. J. M. Seiner, J. C. Manning, F. J. Capone and O. C. Pendergraft Jr 1992 *American Society of Mechanical Engineers Journal of Engineering for Gas Turbines and Power* **114**, 816-829. Study of external dynamic flap loads on a 6 percent B-1B model.

21. P. Maung and M. S. Howe 1997 *American Institute of Aeronautics and Astronautics Paper* 97-0576. Vibration damping of jet nozzle flaps by vorticity production.

22. M. I. Scott 1994 *The Rayleigh conductivity of a circular aperture in the presence of grazing flow.* M.Sc. Thesis, Boston University.

23. M. S. Howe, M. I. Scott and S. R. Sipcic 1996 *Proceedings of the Royal Society of London* **A452**, 2303 - 2317. The influence of tangential mean flow on the Rayleigh conductivity of an aperture.

24. T. G. Bechwith, R. D. Maragoni and J. H. Lienhard 1993 *Mechanical Measurements* (5th edition). Addison-Wesley, Reading MA.

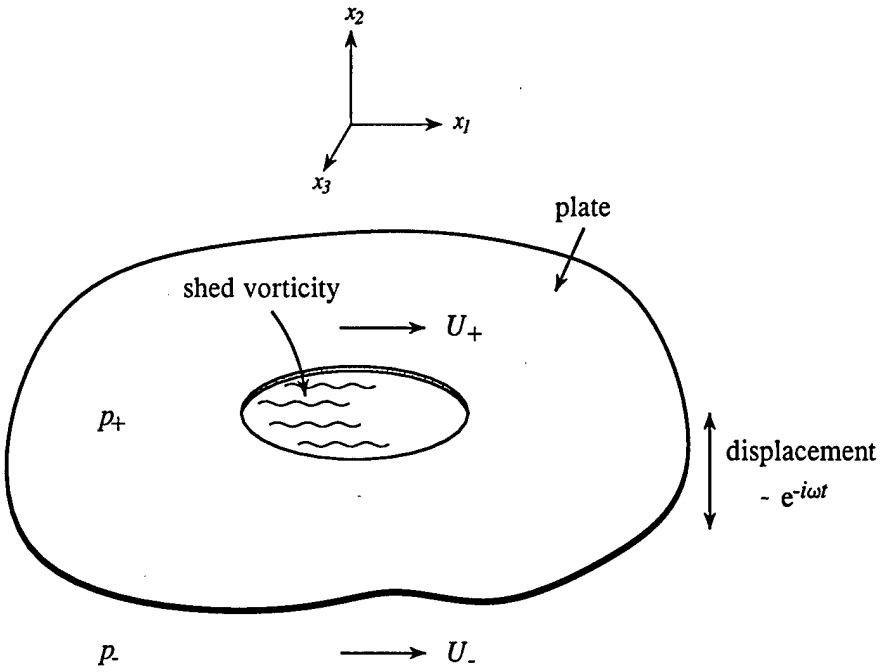

Figure 1. Tangential mean flow past a circular aperture in a vibrating plate.

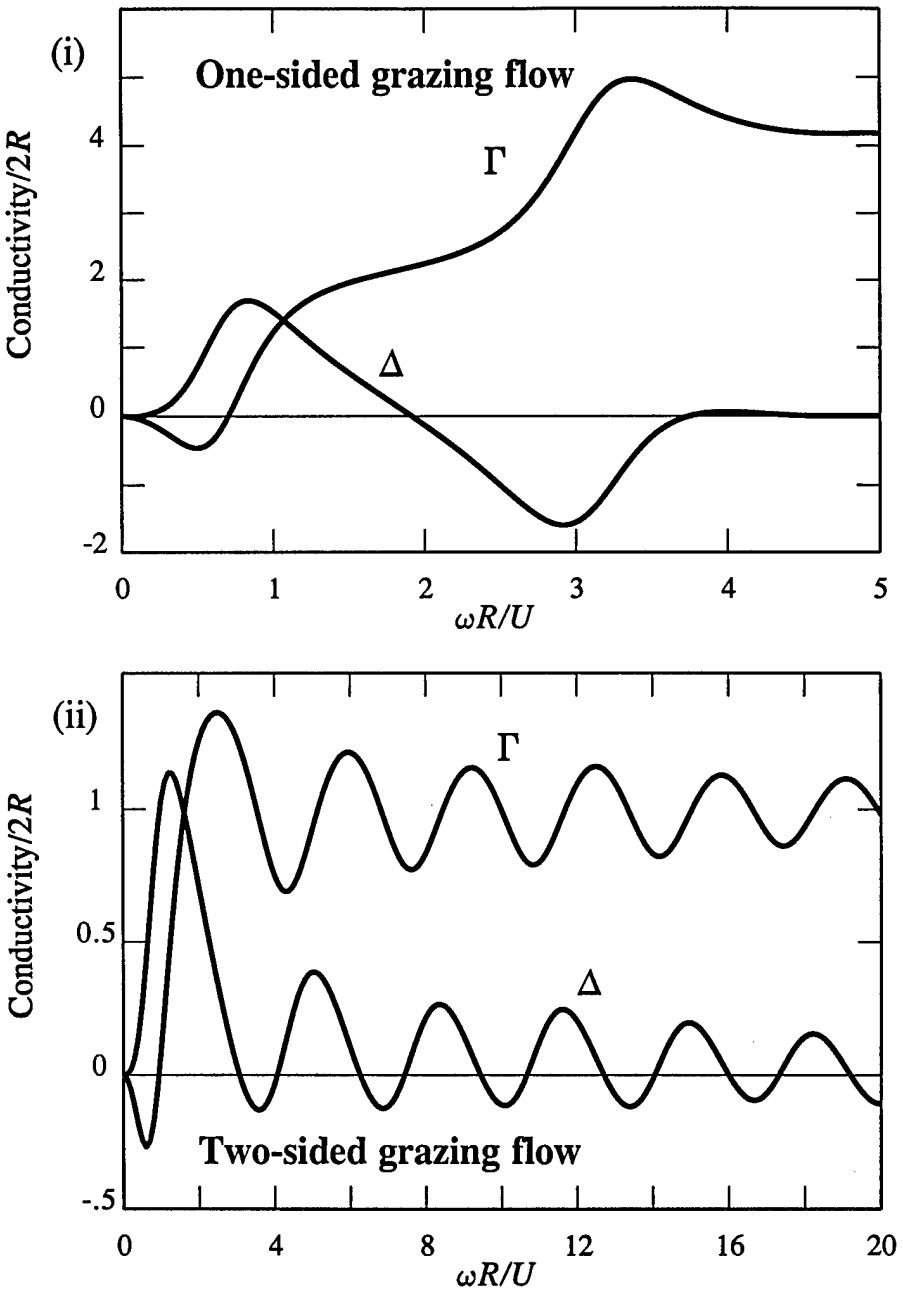

Figure 2. Conductivity of a circular aperture in grazing flow (i) $U_+ = U$, $U_- = 0$; (ii) $U_+ = U_- = U$.

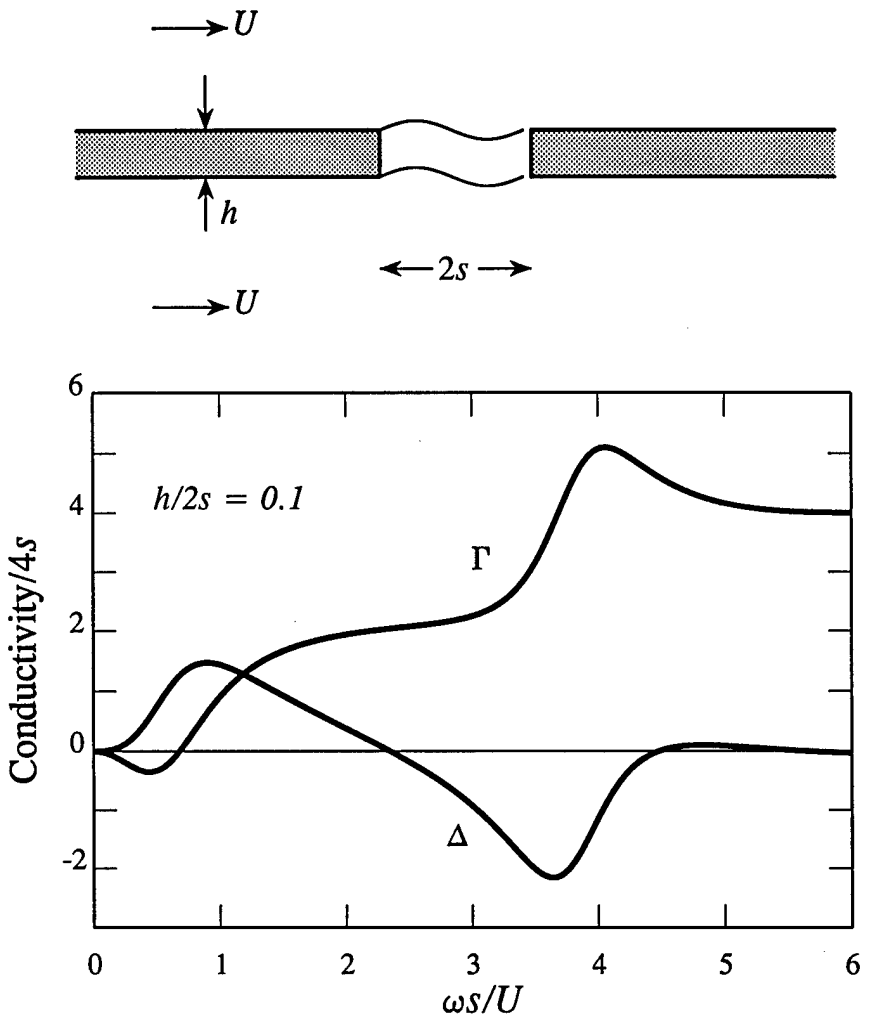

Figure 3. The conductivity of a rectangular aperture of streamwise length $2s$ and breadth $4s$ (out of the paper) in a plate of thickness $h = 0.2s$ in the presence of two-sided uniform flow at speed U.

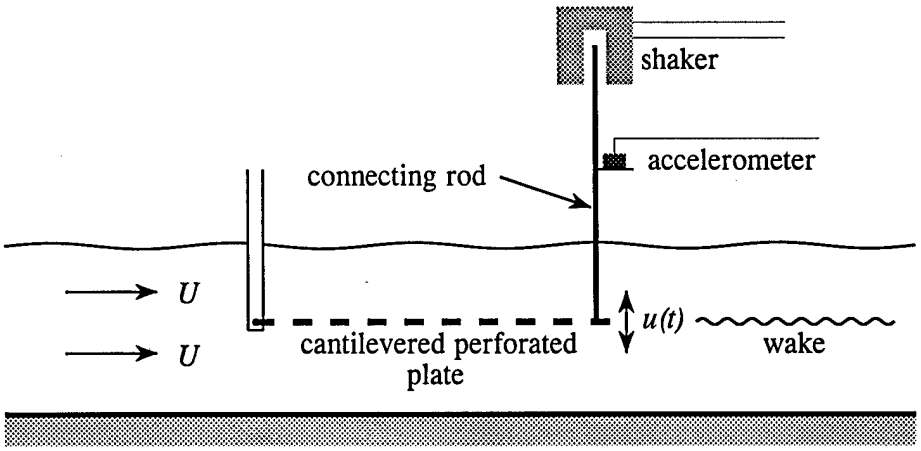

Figure 4. Schematic illustration of the test configuration.

a)

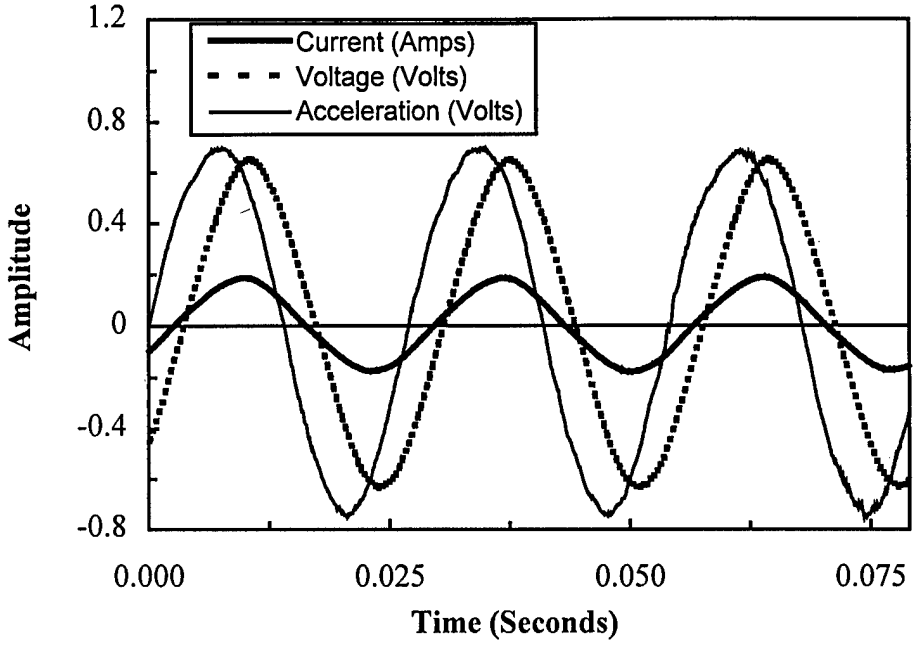

b)

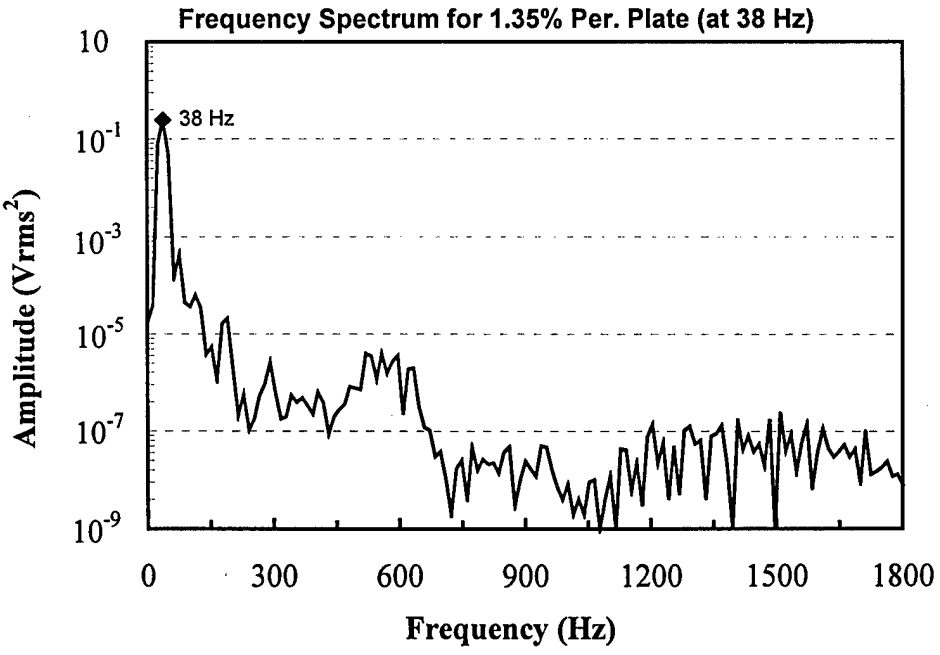

Figure 5. (a) Shaker current and input voltage, and accelerometer voltage for $f = 38$ Hz and $v_0 = 124$mV. (b) Frequency spectrum of the accelerometer reading at a shaker frequency of 38 Hz.

a)

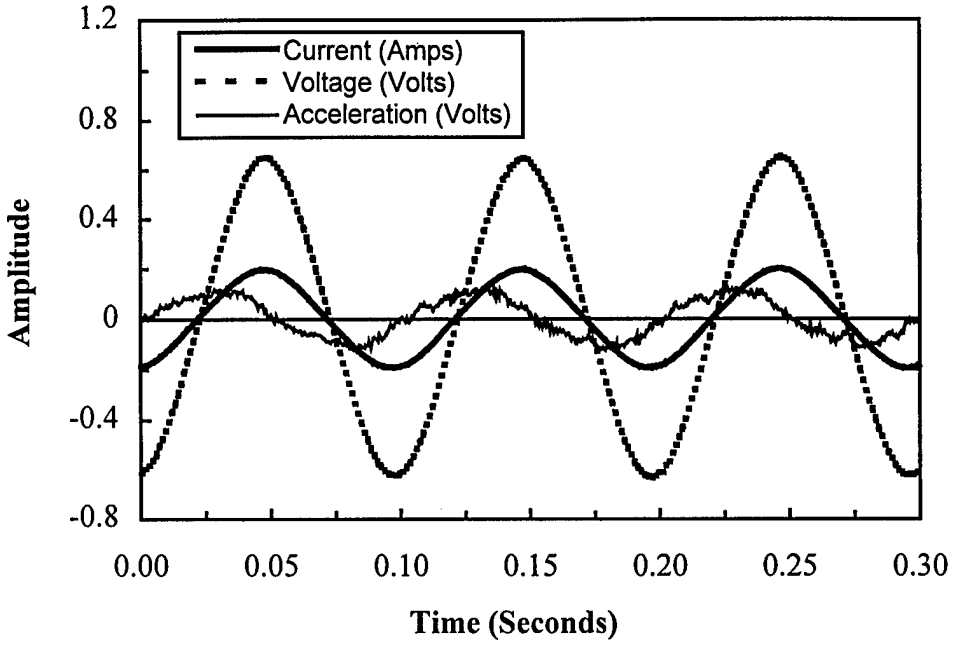

b)

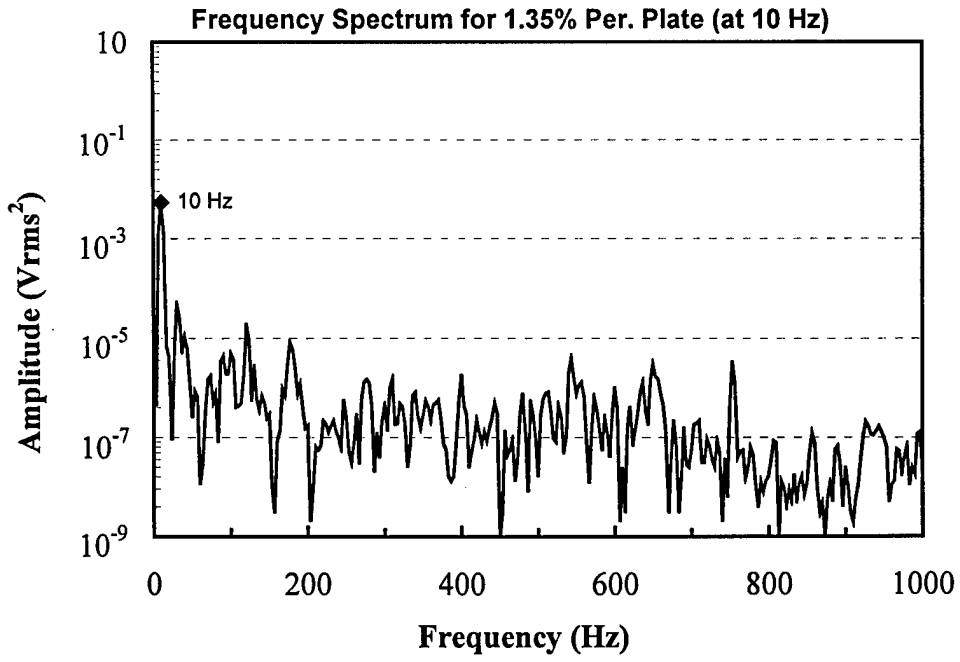

Figure 6. (a) Shaker current and input voltage, and accelerometer voltage for $f = 10$ Hz and $v_0 = 124$mV. (b) Frequency spectrum of the accelerometer reading at a shaker frequency of 10 Hz.

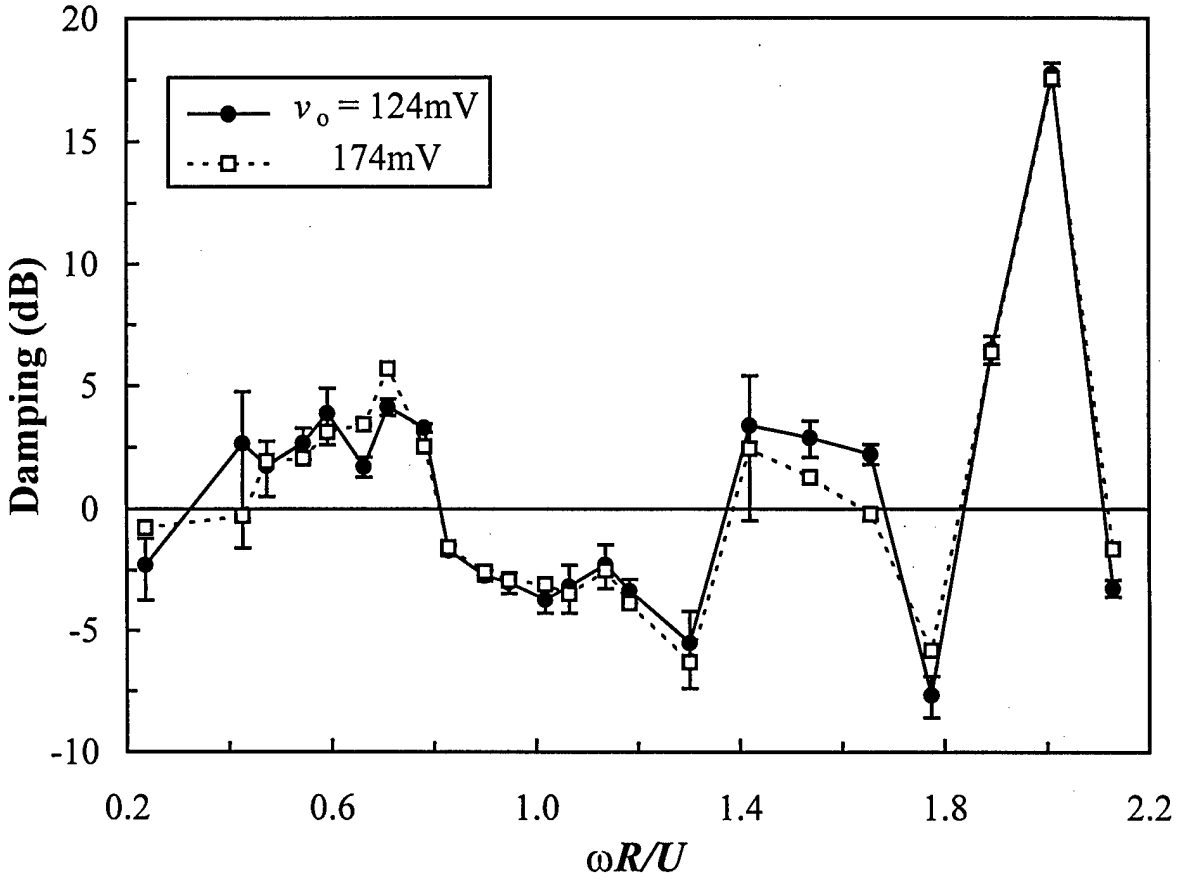

Figure 7. Measured damping (dB) of the 1.35% perforated plate for $v_o = 124$ and 174 mV.

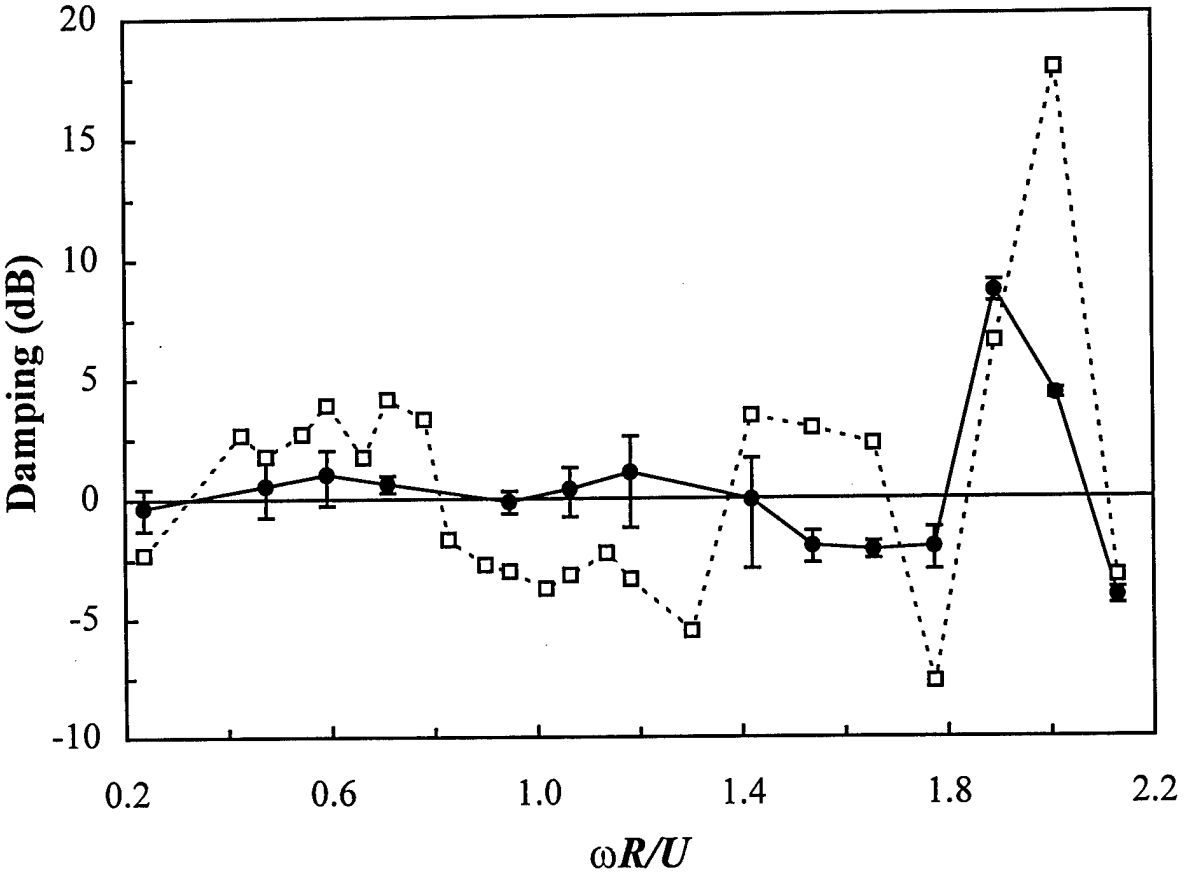

Figure 8. Comparison of the measured damping (dB) of the taped 1.35% perforated plate (solid curve) and the untaped plate (dashed) for $v_o = 124$ mV.

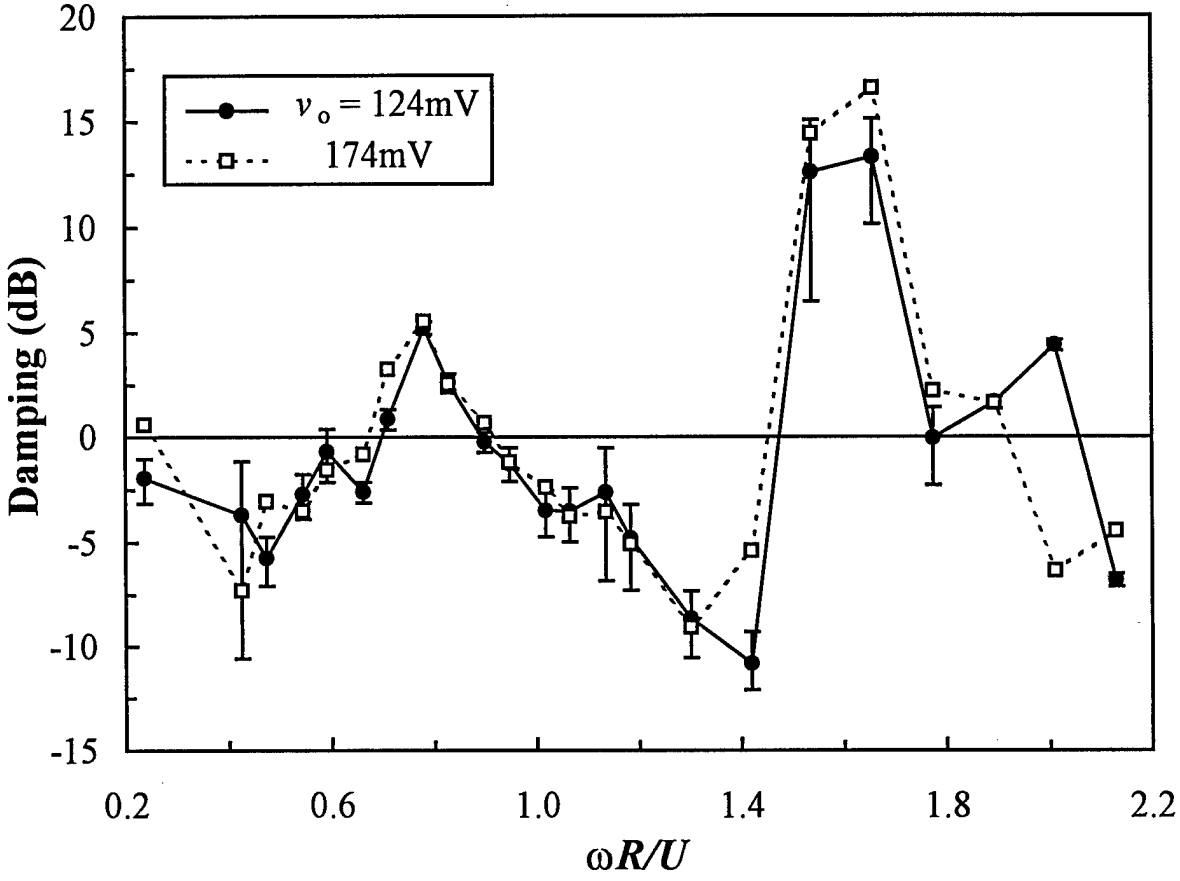

Figure 9. Measured damping (dB) of the 3% perforated plate for $v_o = 124$ and 174 mV.

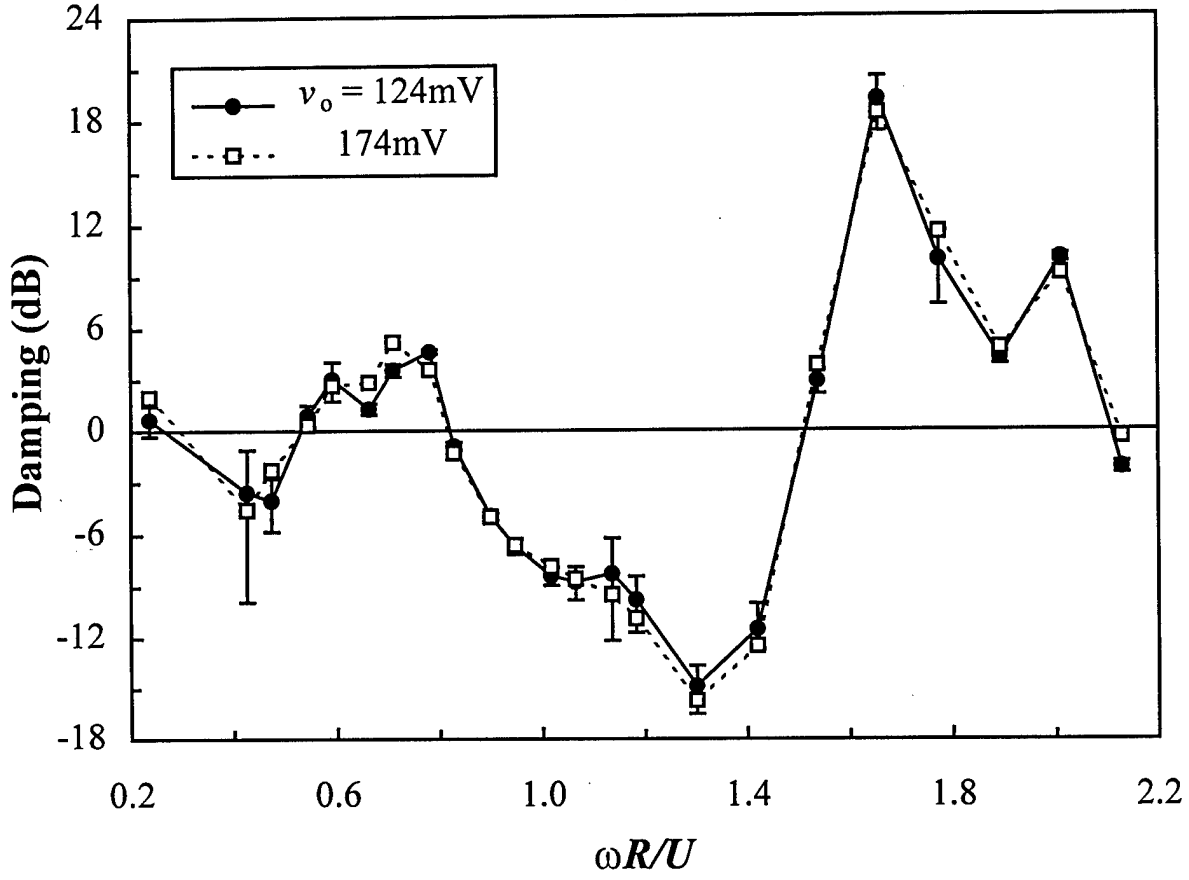

Figure 10. Measured damping (dB) of the 5% perforated plate for $v_o = 124$ and 174 mV.

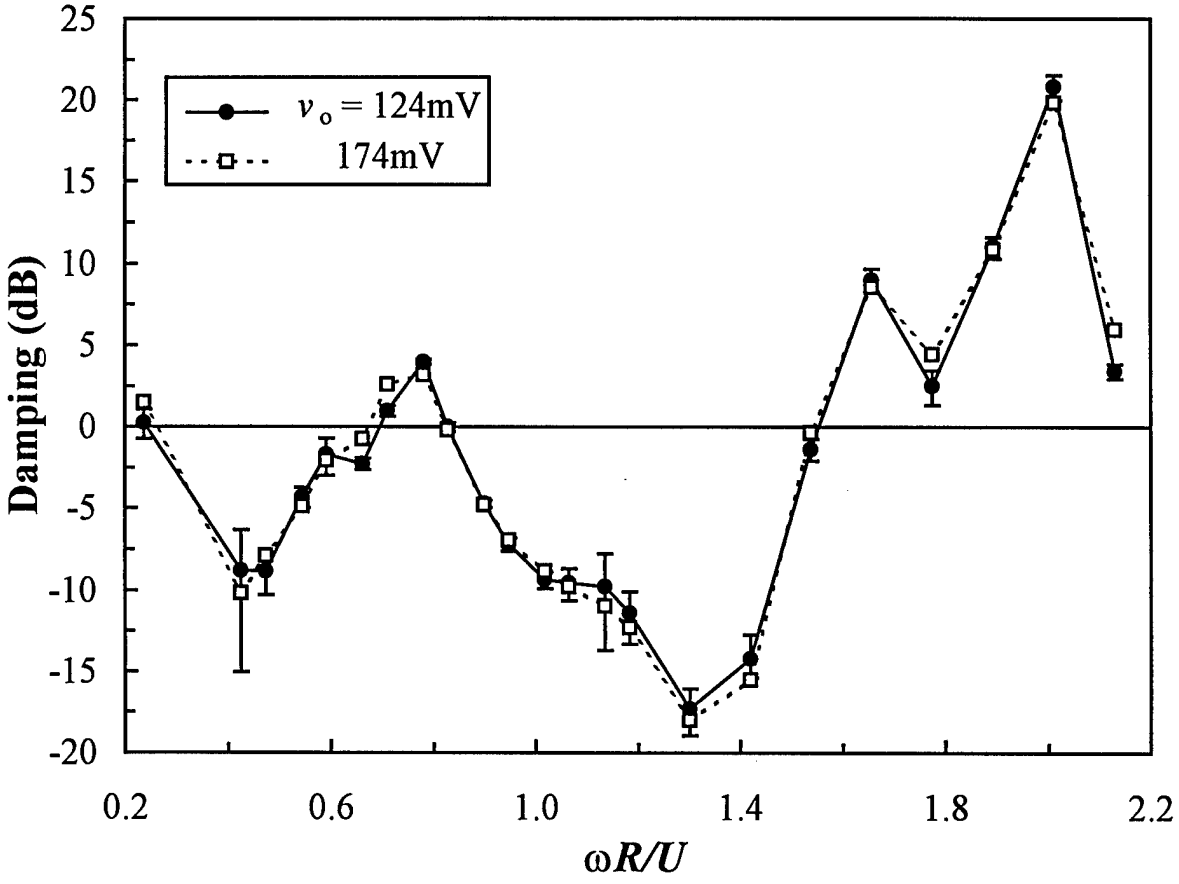

Figure 11. Measured damping (dB) of the 10% perforated plate for $v_o = 124$ and 174 mV.

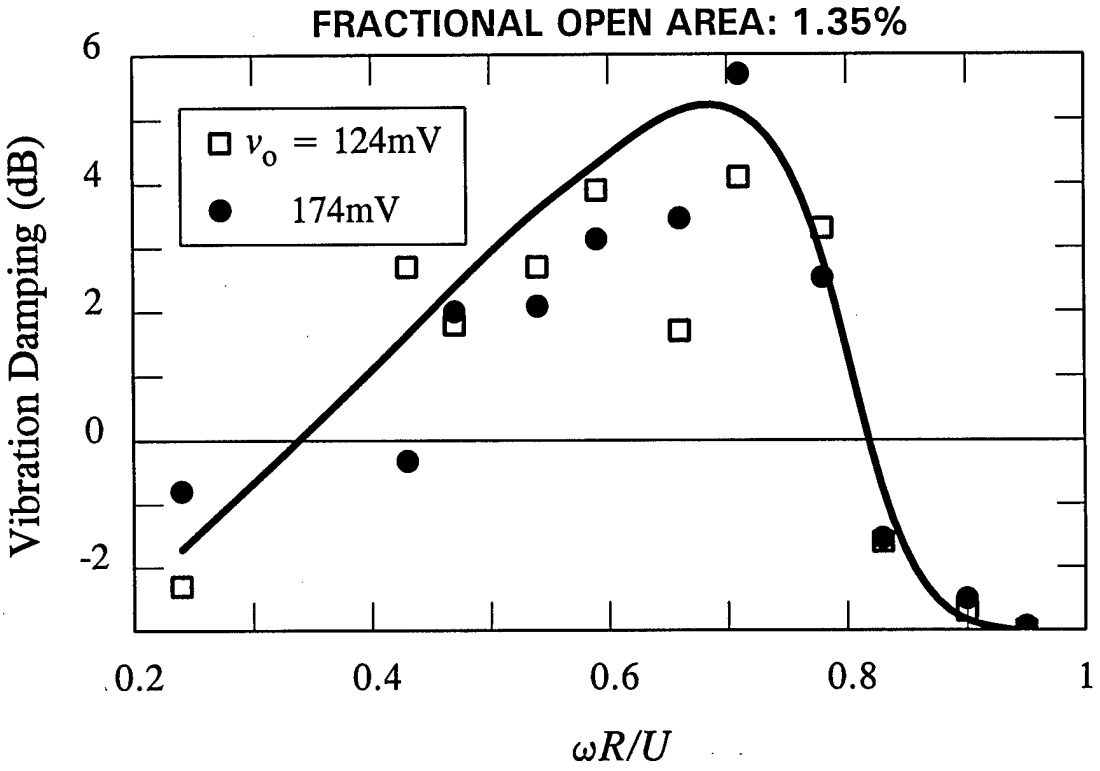

Figure 12. "Best fit" representation of the damping of the 1.35% perforated plate.

CHAPTER 7

DAMPING OF FLAP VIBRATIONS INDUCED BY A TURBULENT WAKE

P. M. Maung and M. S. Howe

SUMMARY

An experimental investigation is being made of the damping of flow-induced vibrations by the controlled production of vorticity by a vibrating body. This is done by suitably perforating all or part of the vibrating structure, and forcing the mean flow to pass either through or over the perforates. It is hypothesized that the kinetic energy of the vortex flow is derived from the vibrating body. A proof of principle test designed to establish the feasibility of the damping mechanism and to yield estimates of the amount of attenuation likely to be obtained in practice was described in Chapter 6. In this chapter an outline description is given of experiments currently being performed using a perforated flap excited by a large scale vortex flow in a wind tunnel; measurements are being made of the vibration damping achieved by vorticity production stimulated by blowing through surface apertures.

1. INTRODUCTION

Aircraft such as the B-1B and F15 are configured with twin engine nacelles, and both have suffered premature failure of external nozzle engine flaps caused by high dynamic pressures. Model tests [1] confirm that the highest dynamic pressures occur where structural damage is observed on full scale aircraft, principally between the nozzles of the twin nacelles. Seiner *et al* [2] have correlated these high pressures with jet screech tones produced by the interaction of turbulence with shock waves in the supersonic jet plumes. In particular, intense surface pressures apparently correspond to a dynamic coupling of the neighboring plumes, a common feature of parallel jets whose separation is less than about four or five jet diameters [3 - 5]. However, more recent wind tunnel tests [6, 7] suggest that the supersonic plume resonance is only important at low flight Mach numbers, typically less than about 0.5. At higher flight speeds the pressures are attributable to large-scale vortex structures impinging from the aircraft forebody. In practice the dominant mechanism is determined by flight profile and aircraft configuration. The jet plume resonance can be eliminated by inserting tabs into the nozzle flow or, more effectively, by means of a small supersonic jet tube within the nozzle [7], but there is currently no effective means of controlling the vortex dominated pressures.

2. THE WIND TUNNEL TEST

Theoretical arguments presented Chapters 1 - 5 of this report suggest that significant damping of structural vibrations is possible by increasing the rate of production of vorticity by a vibrating body. It is known that this mechanism greatly increases the damping of *sound waves* incident on a perforated screen: the presence of a mean flow through the perforates gives enhanced damping when vorticity, *energized* at the expense of the sound, is convected downstream. Appropriately "tuned" devices of this kind have been shown to absorb practically all of the incident sound [8]. Since the production of vorticity in the apertures by sound can be simulated by *vibrating* the screen, it is postulated that the same mechanism will strongly attenuate structural vibrations.

To examine this hypothesis a proof of principle test was first performed in which the vibration damping of a perforated elastic plate immersed a in mean stream is compared to damping in the absence of perforations. This test has been performed in an open water channel (see Chapter 6), where the flow velocity is small and conditions can be

carefully controlled; the heavy fluid loading of water is analogous to the high dynamic loads encountered in high speed flow in air.

The experimental work is currently being extended to situations more relevant to Air Force needs. A porous airfoil (the 'flap' of Figure 1) is elastically supported in the wind tunnel at Harvard University; the natural frequency of vibration can be 'tuned' by adjustment of the supporting sting. The airfoil is mounted close to or within the vortex wake of a cylinder which excites it into vibration. This configuration models the excitation of an engine nozzle flap by vorticity swept over the flap from an aircraft forebody. The vibration damping achieved by 'blowing' air through the surface perforates is being investigated. By proper adjustment of the perforate size and bias flow ('blowing') velocity, it should be possible to tune the optimum damping to selected frequencies that characterise forcing by the turbulent wake.

These tests are currently in progress and the results are expected to be documented towards the end of 1998.

REFERENCES

1. D. E. Berndt, Dynamic pressure fluctuations in the internozzle region of a twin-jet nacelle, 1984 Society of Automotive Engineers Paper No. 841540.

2. J. M. Seiner, J. C. Manning and M. K. Ponton, Dynamic pressure loads associated with twin supersonic plume resonance. 1988 American Institute of Aeronautics and Astronautics Journal 26, 954-960.

3. R. W. Wlezien, Nozzle geometry effects on supersonic jet interaction. 1987 American Institute of Aeronautics and Astronautics Paper No. 87-2694.

4. J. M. Seiner, J. C. Manning and M. K. Ponton, Model and full scale study of twin supersonic plume resonance. 1987 American Institute of Aeronautics and Astronautics Paper No. 87-0244.

5. L. Shaw, Twin jet screech suppression. 1989 American Institute of Aeronautics and Astronautics Paper No. 89-1140.

6. J. M. Seiner, M. K. Ponton, O. C. Pendergraft Jr., J. C. Manning and M. L. Mason, External nozzle flap dynamic load measurements on F-15 S/MTD mode. 1990 American Institute of Aeronautics and Astronautics Paper No. 90-1910.

7. J. M. Seiner, J. C. Manning, F. J. Capone and O. C. Pendergraft Jr., Study of external dynamic flap loads on a 6 percent B-1B model. 1992 American Society of Mechanical Engineers, Journal of Engineering for Gas Turbines and Power 114, 816 - 828.

8. I. J. Hughes and A. P. Dowling, The absorption of sound by perforated linings. 1990 Journal of Fluid Mechanics 218, 299 - 336.

9. P. Maung and M. S. Howe, Vibration damping of jet nozzle flaps by vorticity production. 1997 American Institute of Aeronautics and Astronautics Paper 97-0576.

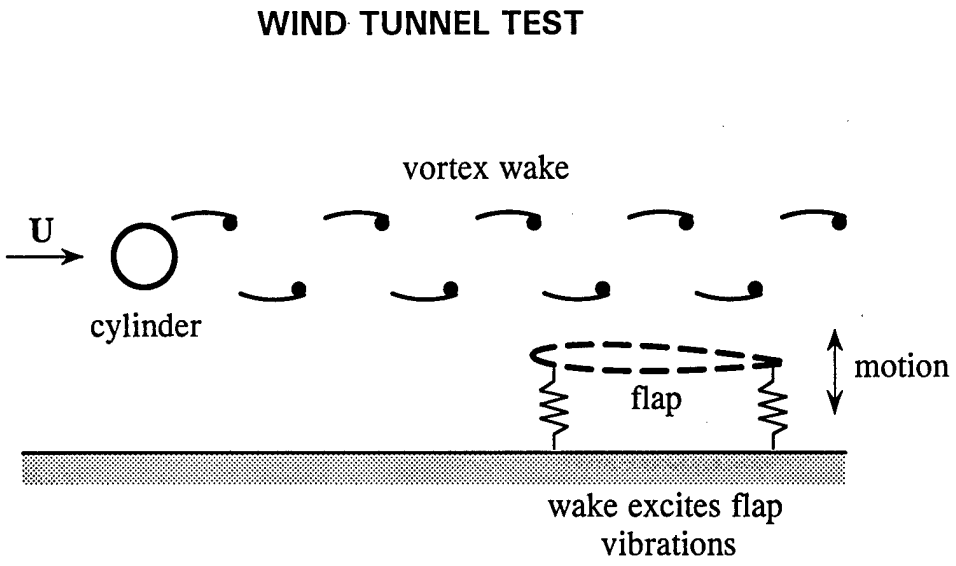

Figure 1. Schematic wind tunnel configuration.

REPORT DOCUMENTATION PAGE

Form Approved
OMB No. 0704-0188

1. AGENCY USE ONLY (Leave blank)	2. REPORT DATE	3. REPORT TYPE AND DATES COVERED
	1 July 1998	Final. 1 Apr. 1996 - 31 May 1998

4. TITLE AND SUBTITLE
Theoretical and experimental investigation of vibration damping by vorticity production

5. FUNDING NUMBERS
F49620-96-1-0098

6. AUTHOR(S)
Michael S. Howe

7. PERFORMING ORGANIZATION NAME(S) AND ADDRESS(ES)
Boston University
College of Engineering
110 Cummington Street
Boston MA 02215

8. PERFORMING ORGANIZATION REPORT NUMBER
AM-98-029

9. SPONSORING/MONITORING AGENCY NAME(S) AND ADDRESS(ES)
Major Brian Sanders
Air Force Office of Scientific Research
110 Duncan Ave, Suite B115,
Bolling AFB, DC 20332-8080

10. SPONSORING/MONITORING AGENCY REPORT NUMBER

11. SUPPLEMENTARY NOTES

12a. DISTRIBUTION/AVAILABILITY STATEMENT

12b. DISTRIBUTION CODE

13. ABSTRACT *(Maximum 200 words)*

Analytical models are formulated and solved to determine the energy transfer between a vibrating perforated plate of finite thickness and a mean shear flow over one or both sides of the plate. Energy transferred to the flow appears as the kinetic energy of vorticity produced in the perforates and swept downstream by the flow. Regions of positive and negative damping are identified as functions of the vibration frequency, and a new, analytic determination is made of the operating stages of self-sustained oscillations of shear flow over apertures (including wall cavities) and validated by comparison with experiment. Numerical predictions are also given that extend the analysis to perforates of arbitrary shape. A water channel experiment has been performed to measure the damping by vorticity production of a vibrating, perforated elastic plate at zero mean angle of attack. An outline description is given of experiments currently in progress in which a porous flap is excited by a large scale vortex flow in a wind tunnel; measurements are being made of the vibration damping achieved by vorticity production stimulated by blowing through surface apertures.

14. SUBJECT TERMS
Damping, sound, structural vibrations, vorticity, bias flow and grazing flow perforated screen, Rayleigh conductivity, Kutta condition.

15. NUMBER OF PAGES
178 + iv

16. PRICE CODE

17. SECURITY CLASSIFICATION OF REPORT	18. SECURITY CLASSIFICATION OF THIS PAGE	19. SECURITY CLASSIFICATION OF ABSTRACT	20. LIMITATION OF ABSTRACT
Unclassified	Unclassified	Unclassified	